Aachener Beiträge zur Akustik

Ingo B. Witew

Measurements in room acoustics

Uncertainties and influence of the measurement position

λογος

IHTA Institute for Hearing Technology and Acoustics | RWTH AACHEN UNIVERSITY

Measurements in room acoustics

Uncertainties and influence of the measurement position

Von der Fakultät für Elektrotechnik und Informationstechnik der
Rheinisch-Westfälischen Technischen Hochschule Aachen
zur Erlangung des akademischen Grades eines

DOKTORS DER INGENIEURWISSENSCHAFTEN

genehmigte Dissertation

vorgelegt von

Dipl.-Ing.
Ingo B. Witew

aus Düsseldorf, Deutschland

Berichter:

Universitätsprofessor Dr. rer. nat. Michael Vorländer
Universitätsprofessorin Ferdinanda Ponci, Ph. D.

Tag der mündlichen Prüfung: 21. Januar 2022

Ingo B. Witew

Measurements in room acoustics

Uncertainties and influence of the measurement position

Logos Verlag Berlin GmbH

λογος

Aachener Beiträge zur Akustik

Editors:
Prof. Dr.-Ing. Janina Fels
Prof. Dr. rer. nat. Michael Vorländer
Institute for Hearing Technology and Acoustics
RWTH Aachen University
52056 Aachen
www.akustik.rwth-aachen.de

Bibliographic information published by the Deutsche Nationalbibliothek

The Deutsche Nationalbibliothek lists this publication in the Deutsche Nationalbibliografie; detailed bibliographic data are available in the Internet at http://dnb.d-nb.de.

D 82 (Diss. RWTH Aachen University, 2022)

Logos Verlag Berlin GmbH 2022

ISBN 978-3-8325-5529-0

ISSN 2512-6008

Vol. 37

Logos Verlag Berlin GmbH
Georg-Knorr-Str. 4, Geb. 10,
D-12681 Berlin

Tel.: +49 (0)30 / 42 85 10 90
Fax: +49 (0)30 / 42 85 10 92
http://www.logos-verlag.de

Abstract

Regardless of the field, measurements are essential for validating theories and making well-founded decisions. A criterion for the validity and comparability of measured values is their uncertainty. The "Guide to the Expression of Uncertainty in Measurement" (GUM) provides a standardized framework for determining and interpreting measurement uncertainty. Still, in room acoustical measurements, the application of these rules is not yet widespread. Firstly, this is due to the fact that well established 2-CH-FFT correlation techniques rely on a complex principle, which is not covered by the classical guide. In addition, the effect of input variables on an individual measurement can only be determined after considerable effort. An example are fluctuations of room acoustical quantities over small distances between measurement locations in concert halls. This variation of the sound field by position is sometimes considerable and can only be predicted in relatively simple boundary value problems. This raises the question of the validity and interpretability of room acoustical measurements.

The goal of this thesis is to provide a GUM-compliant discussion of uncertainties in measuring room acoustical single-number quantities. This starts with a structured search of variables that potentially influence the measurement of room impulse responses. In a second step, this uncertainty is propagated through the algorithm that determines room acoustical single-number quantities.

Further emphasis is placed on the investigation of spatial fluctuations of the sound field in auditoria. The influence of an uncertain measurement position on the overall measurement uncertainty is discussed. To reach general conclusions, the relation between changes in the measurement location and the corresponding changes in measured room acoustical quantities is investigated empirically in extensive measurement series. To this end, a measurement apparatus was designed that allows automatic, high-resolution sampling of sound fields over large areas. The collected data creates the foundation to apply the principle of uncertainty propagation using a Monte Carlo method.

This study shows how precisely a measurement position must be defined to ensure a given uncertainty of room acoustical single-number quantities. The presented methods form a foundation that can be flexibly extended in future investigations to include additional influences on the measurement uncertainty.

Kurzfassung

Unabhängig vom Fachgebiet sind Messungen essentiell für die Validierung von Theorien und für das Treffen fundierter Entscheidungen. Merkmal für die Aussagekraft und Vergleichbarkeit von Messwerten ist unter Anderem deren Unsicherheit. Für die Bestimmung und die Interpretation der Messunsicherheit stellt der *Guide to the Expression of Uncertainty in Measurement* (GUM) einen standardisierten Rahmen bereit. Bei raumakustischen Messungen ist die Anwendung dieses Regelwerks bisher noch nicht grundsätzlich verbreitet. Das liegt einerseits daran, dass mit der weit verbreiteten Korrelationsmesstechnik ein komplexes Messprinzip verwendet wird, das im klassischen Leitfaden nicht behandelt wird. Außerdem ist die Wirkung von Eingangsgrößen, die eine Messung beeinflussen können, nur mit größtem Aufwand im Einzelfall bestimmbar. Beispiel dafür sind Fluktuationen raumakustischer Kenngrößen über kleinste Abstände zwischen Messorten in Konzertsälen. Diese zum Teil beachtliche Änderung des Schallfeldes über den Ort wirft die Frage nach der Aussagekraft und Interpretierbarkeit raumakustischer Messungen auf.

Ziel dieser Arbeit ist eine GUM konforme Diskussion der Unsicherheit beim Messen raumakustischer Einzahlkennwerte. Begonnen wird dabei mit einer strukturierten Suche der Größen, die die Messung von Raumimpulsantworten beeinflussen könnten. In einem zweiten Schritt wird diese Unsicherheit durch den Algorithmus zur Bestimmung raumakustischer Einzahlkennwerte propagiert.

Ein weiterer Schwerpunkt wird auf die Untersuchung von räumlichen Änderungen des Schallfeldes in Auditorien gelegt. Es wird der Einfluss eines unsicher bestimmten Messorts auf die Messunsicherheit diskutiert. Um möglichst allgemeingültige Aussagen treffen zu können wird der Zusammenhang zwischen einer Änderung des Messortes und der korrespondierenden Änderung raumakustischer Kenngrößen in umfangreichen Messreihen empirisch untersucht. Dazu wurde ein Messapparat gebaut mit dem Schallfelder hochauflösend und vollautomatisch über große Flächen abgetastet werden können. Die so gesammelten Daten bilden die Grundlage für die Berechnung der Unsicherheitsfortpflanzung mit einer Monte Carlo Methode.

Die Ergebnisse dieser Untersuchung zeigen, wie genau ein Messort bei raumakustischen Messungen definiert werden muss, um eine zuvor festgelegte Unsicherheit raumakustischer Einzahlkennwerte zu gewährleisten. Die vorgestellten Methoden bilden eine Grundlage, die flexibel erweitert werden kann, um weitere Einflüsse auf die Messunsicherheit in zukünftigen Untersuchungen zu berücksichtigen.

Table of Contents

Acronyms

AWGN	Additive white Gaussian noise
BEM	Boundary element method
$\mathbf{C_{80}}$	Clarity (room acoustic quantity)
Ch	Channel (Information channel)
$\mathbf{D_{50}}$	Definition (room acoustic quantity)
DUT	Device under test
EDT	Early decay time
EDC	Energy decay curve
FFT	Fast Fourier transform
G	Strength (room acoustic quantity)
GUM	Guide to the expression of uncertainties in measurements
HVAC	Heating, ventilation, air-condition
IR	Impulse response
JND	Just noticeable difference
LTI	Linear time-invariant
MLS	Maximum length sequence
RIR	Room impulse response
RMS	Root mean square
SNR	Signal-to-noise ratio
SPL	Sound pressure level
$\mathbf{T_{20}}$	Reverberation time (room acoustic quantity)
$\mathbf{T_{30}}$	Reverberation time (room acoustic quantity)
THD	Total harmonic distortion
THD+N	Total harmonic distortion and noise

1

Introduction

In architecture, concert halls, lecture rooms or open plan offices are designed for different types of communication depending on their specific intended uses. In rooms for speech, it is important that the speaker's loudness is sufficient, but also that individual syllables are clearly intelligible. For music, there are additional aspects such as spatial sound or spectral balance that need to be considered. In some environment, such as offices, distracting communication is unwanted and should be minimized. The acoustician supports the architect in the design to make sure critical limits for good communication are safely met and the room is acoustically suitable for its purpose.

Acoustics is an interdisciplinary field and employs tools and methods from a wide range of other specialized areas. In architectural acoustics, the impulse response has proven to be a very useful concept from system theory. The impulse response, which describes the transmission of information from a source to a receiver also holds in auditorium acoustics since the room in which the sound source and the listener are located can be understood as a transmission channel. The room's response to an impulse is the direct sound that travels from the source to the listener, the sound reflections from the surfaces and the lingering reverberation. Since there is a physical relation between the room's geometry and the sound transmission, it is intuitively evident why the impulse response is so useful for the acoustic design of auditoria. Experts can interpret impulse responses and easily recognize how syllables of a speaker are supported by early reflections or see how a long reverberation blurs successive syllables in time and thus impairs communication.

Room impulse responses can be measured with special equipment and contribute to the acoustic planning process by providing the data to place future design decisions on solid ground and quantify the effectiveness of previous design decisions. In general, measurements are of core importance in science and practice when it comes to proving theories or making well-founded decisions. The suitability of measurements as the basis for a valid argument depends a lot on the data's associated uncertainties. Modern measurement methods (ISO 18233,

2006) to measure transfer functions and their associated impulse responses (IR) using maximum length sequences or swept sine signals are common tools in all areas of acoustics (Müller & Massarani, 2001). In architectural acoustics, room impulse responses are regularly analyzed to determine single-number quantities that serve as predictors for sound perception (see Section 2.1.2). Clarity C_{80}, for example, scales the perceived distinctness of a sound in time from highly detailed ($\approx 7\,\mathrm{dB}$) to blurred ($\approx -5\,\mathrm{dB}$). Provided that the measured environment features the properties of linear time invariant (LTI) systems and that a sufficient signal-to-noise ratio is achieved, acoustical measurements of impulse responses and room acoustic quantities are usually considered to be rather accurate.

This perspective was briefly challenged in a reflex reaction to findings of de Vries, Hulsebos, and Baan (2001). Under quasi-repeatability conditions at Concertgebouw Amsterdam, RIRs were measured every 5 cm along a line following a row of seating. The data de Vries and his team collected shows how room acoustic single number quantities fluctuate over the surveyed distance; Figure 1.1 illustrates this for C_{80} (ISO 3382-1, 2009). In facetious discussions, auditoria were compared with random number generators and the question of explanatory power in room acoustics measurements was raised.

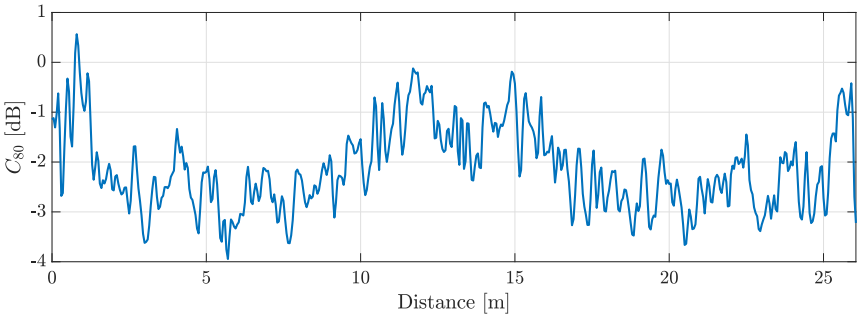

Figure 1.1: Spatial distribution of clarity C_{80} at the 1 kHz octave band along a line measured at a concert hall.

Of course, this fabricated perspective does not appreciate the deterministic character of sound propagation adequately, but the reference to a reproduction problem in measurements is well-founded: If room acoustic quantities change over such small distances, how can measurements be reproduced at another time? How can the acoustic effectiveness of a modification to a building be verified when the expected acoustic change is obscured by strong fluctuations?

At first glance it may seem that de Vries et al. (2001) merely confirm findings

from earlier investigations that were conducted in the advent of the ISO 3382 (1975) revision (e.g., J. S. Bradley and Halliwell (1988); Hidaka, Beranek, and Okano (1995); Pelorson, Vian, and Polack (1992)). After all, these studies also discuss strong variations in room acoustic parameters with relatively small spatial displacements of sources or receivers. The key difference is in the way the collected data was analyzed and interpreted. Prior to de Vries, the determined spread in room acoustic parameters was discussed statistically, such that an adequately large sample size would be sufficient to correctly determine the variance in a statistical population. Consequently, these findings lead to the requirement to measure at numerous positions distributed throughout the auditorium and, hence, provide a sufficiently large sample size to calculate average values (ISO 3382, 1997).

But with growing experience in using the revised standard it soon became more and more evident that the underlying cause-and-effect chain was not fully factored in: J. S. Bradley (1994) demonstrated that calculating hall-spanning parameter averages comes with the potential to flatten out characteristic patterns. This may lead to a point where auditoria, fundamentally different in shape, are no longer distinguishable in their summary statistics. Today, there is a common understanding that averaging over all measurement positions to gain a hall mean value seems (except for the reverberation time) generally unhelpful (Barron, 2005; J. S. Bradley, 2005). This interpretation is justified within the large-scale dimensions of an auditorium, but it does not recognize the parameter variations encountered within smaller distances. Follow-up investigations by Nielsen, Halstead, and Marshall (1998), Sekiguchi and Hanyu (1998) and Okano, Beranek, and Hidaka (1998) indicate that the phenomenon continued to be a target of interest.

In this course of development the initially quoted study by de Vries et al. (2001) marks an important milestone as it provides high-resolution data that shows how the acoustic quantities fluctuate over a wide range of distances, starting from a few cm to the dimensions of a concert hall. This can be interpreted as metrological evidence towards an influence factor of measurement position that seemed "downgraded" by averaging over a number of locations. Taking the *sampling position* as a relevant input quantity it becomes possible to refine the statistical discussion and investigate how this contribution influences the result of acoustical measurements. This approach can create a context for how uncertain room acoustics measurements are and identify the subtleties worth interpreting.

The standardized tools for this discussion are provided by the "Guide to the expression of uncertainty in measurement" (GUM, ISO Guide 98-3 (2008)) that places the original principles of Gaussian *error propagation* on a wider foundation. In the first step a relationship needs to be established that quantifies how a

change in measurement position yields a change in the measured result. This marks an advance to the previous statistical discussion as the sampling position is recognized as an influence quantity. It also moves the discussion away from insulated individual cases to a general discussion of a broad spectrum of sound fields and thus helps to assess how significant the "validity" problem generally is. In light of the raised question of reproducibility in room acoustic measurements, the measurement function marks the foundation to investigate a derived question of practical relevance: How precisely need measurement positions (source and receiver) be defined?

1.1 Defining the scope of this work

Against this background, it is important to discuss the uncertainty of room acoustic measurements. In preparation to determine the measurement model (ISO Guide 98-3, 2008, 4.1.1) empirically, the following questions must be discussed.

- What is the uncertainty of room acoustic impulse response measurements?
- What is the uncertainty of room acoustic ISO 3382-1 (2009) quantities?

In preparing the measurement model this question needs to be answered:

- How do room acoustic quantities change when the measurement position is changed by a given distance?

Based on the answer to the previous question, this problem of practical relevance should be addressed:

- How accurately need measurement positions be defined?

2

Fundamentals and previous work

Discussing these research questions requires a set of tools that will be briefly outlined in this chapter. An initial focus is placed on the theoretical groundwork, as these basics identify the driving forces and the relevant variables; in the next step the measurement uncertainty will be of interest. In this regard it is reasonable to first examine the status quo in room acoustical measurements and then gradually traverse to the framework that permits a uniform discussion of uncertainties in measurements.

2.1 Theoretical principles behind spatial fluctuations

2.1.1 Amplitude distribution due to changes in position

Initial work on spatial fluctuations of the sound field in rooms can be traced back to Kuttruff and Thiele (1954) and Kuttruff (1954). While this work was originally focused on the frequency dependency of the sound pressure in rooms, as part of the investigations that led to what is now known as the "Schroeder Frequency" (Schröder, 1954), the initial empirical study by Kuttruff and Thiele (1954) also discussed the the sound pressure's spatial dependency.

The starting point is the sound field in a rectangular room with the dimensions L_x, L_y, L_z and rigid surfaces. At characteristic eigenfrequencies ω_i for $\forall n \in \mathbb{N}_0$ (here Equation 2.1.1, from Kuttruff (2000), Eq. 3.15) the cartesian components of the respective wave vector k_i meet the scenario's boundary conditions (particle velocity $v_i = 0$ at the room's surfaces) so that the system can oscillate.

$$\omega_i = c\pi \sqrt{\left(\frac{n_{x,i}}{L_x}\right)^2 + \left(\frac{n_{y,i}}{L_y}\right)^2 + \left(\frac{n_{z,i}}{L_z}\right)^2} = ck_{n_x n_y n_z} \tag{2.1.1}$$

At each of the system's ω_i's, standing waves develop. For a single mode the sound pressure at a position $\mathbf{r}_r = (x_r, y_r, z_r)^T$ can be determined through Equation 2.1.2 (Kuttruff, 2000, Eq. 3.16).

$$p_i(\mathbf{r}) = \cos\left(\frac{n_{x,i}\pi x_r}{L_x}\right)\cos\left(\frac{n_{y,i}\pi y_r}{L_y}\right)\cos\left(\frac{n_{z,i}\pi z_r}{L_z}\right) \tag{2.1.2}$$

Based on the principle of reciprocity (Morse & Ingard, 1968, p.134) it can be understood that this relation is valid for the source and the receiver alike. The spatial cosine relationship includes the characteristic nodal points for a standing wave at a given frequency when the cosine's argument is $(2n+1)\pi/2$. At these nodes the sound pressure is naturally zero. Reciprocally, at the same positions the sound field cannot be excited at that frequency. The full relationship is shown in Equation 2.1.3 (Kuttruff, 2000, Eq. 3.10) with the numerator featuring the mathematical representation of the standing wave excited and sampled at the positions $\mathbf{r}_s$ and $\mathbf{r}_r$. This term, thus, shows a dependency on the location and is hence responsible for the spatial fluctuation of the sound field.

$$p(\omega, \mathbf{r}_r) = jQc^2\omega\rho_0 \sum_i \frac{p_i(\mathbf{r}_s)p_i(\mathbf{r}_r)}{(\omega^2 - \omega_i^2 - 2j\delta_i\omega_i - \delta_i^2)K_i} \tag{2.1.3}$$

Obviously, a realistic system requires some damping to balance the source's energy influx and so become stable. This is recognized in the denominator where the ideal dirac-delta-like eigenfrequencies are expanded through the damping constant δ_i to Cauchy-Lorentz functions with characteristic quality factors.

The factors in front of the sum in Equation 2.1.3 recognize the physical properties of the point source. The volume velocity Q includes the harmonic oscillation $e^{j\omega t}$. K_i is a normalization constant for the standing waves (Kuttruff, 2000, Eq. 3.3),

$$K_i = \iiint_V p_i^2(\mathbf{r})dV. \tag{2.1.4}$$

The sigma sign in Equation 2.1.3 indicates that at a given position $\mathbf{r}_s$ and $\mathbf{r}_r$ more than one mode is excited and so the emerging sound pressure level is a result of a sum over i eigenfrequencies. Schröder (1954) argues that when the number of eigenmodes is sufficiently large the Lindeberg-Lévy central limit theorem will take effect and the summary distribution of the real and imaginary parts of the sound pressure will become normally distributed. From there it is only the small step of taking the absolute value of the complex sound pressure to arrive at the Rayleigh distributed (linear) sound pressure amplitude p with a probability density function f_p given in Equation 2.1.5 (Johnson, Kotz, & Balakrishnan, 1994; Rayleigh, 1880). σ_p^2 refers to the variance of the sound pressure's real or imaginary parts $\mathrm{Re}(p)$, $\mathrm{Im}(p)$.

$$f_p(p) = \frac{p}{\sigma_p^2} e^{-\frac{p^2}{2\sigma_p^2}} \tag{2.1.5}$$

The probability density function of the sound pressure level L_p can be determined to be

$$f_{L_p} = \frac{\ln(10)}{2} \frac{p_0^2 10^{L_p/10}}{\sigma_p^2} e^{-\frac{p_0^2 10^{L_p/10}}{2\sigma_p^2}} \tag{2.1.6}$$

by using the *transformation theorem for probability densities* (Johnson et al., 1994, pp. 14-15, Eq. 12.32).

Having considered the central limit theorem and also looking at Equation 2.1.6 can suggest that the resulting SPL is due to a random process over frequency. This perception, however, misses to appreciate Kuttruff's (2000) explanations that recognize the sound field in a room is the result of a deterministic process. As such, once the energy equilibrium is reached, the sound pressure level is stationary and could be determined analytically if all the boundary conditions were known with the required accuracy.

These properties of the sound field can be shown in measurements as in Figure 2.1. At low frequencies, below the "Schroeder Frequency", the sound pressure at a given position is defined by few, individual, sparsely overlapping modes (see Figure 2.1e). At much higher frequencies Figure 2.1a shows how the modes overlap and the characteristic Cauchy-Lorentz functions cannot be identified anymore. The corresponding histogram in Figure 2.1b is a graphical representation of the logarithmic Rayleigh distribution in Equation 2.1.6.

A change in location leads to a change in the contributing resonances according to the cosine terms in the numerator of Equation 2.1.3. For the central limit theorem to take effect, independent samples of contributing modes at the different positions are required. This condition is met as trigonometric functions, oscillating with different integer multiples of a fundamental periodicity, are orthogonal to each other (Bronstein, Semendyayev, Musiol, & Mühlig, 2015, 5.3.6.5-2). This holds for arbitrary geometries since the solutions to Dirichlet and Neumann boundary value problems are always orthogonal (Bronstein et al., 2015, 9.1.3.2-4). As a result, it follows that the resonances/standing waves contributing to the sound pressure at two distant positions are uncorrelated to each other and, hence, are independent samples from the same Rayleigh distribution.

Of course, neighboring positions - $\Delta\mathbf{r}$ apart - are correlated to each other, due to continuously defined standing waves $p_i(\mathbf{r})$. A small change in position will not necessarily lead to a sufficient exchange of the contributing resonances and hence the sound pressure will not immediately show the postulated Rayleigh

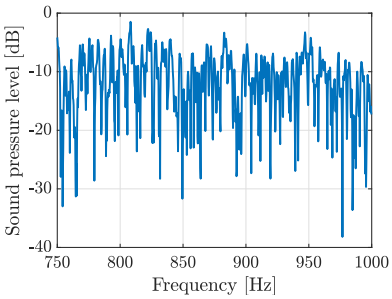

(a) Change in sound pressure level over frequency (*frequency curve*)

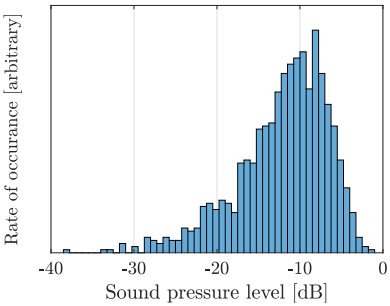

(b) Histogram of the amplitude distribution over frequency based on data shown in Figure 2.1a

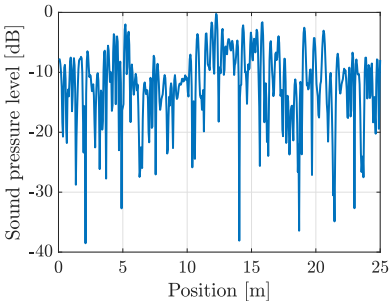

(c) Change in sound pressure level over position at 875 Hz (*space curve*)

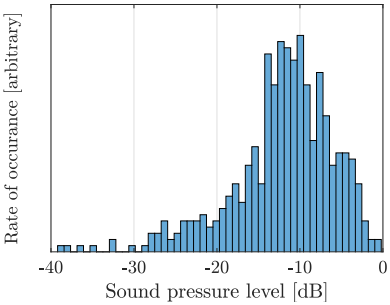

(d) Histogram of the amplitude distribution over space based on data shown in Figure 2.1c

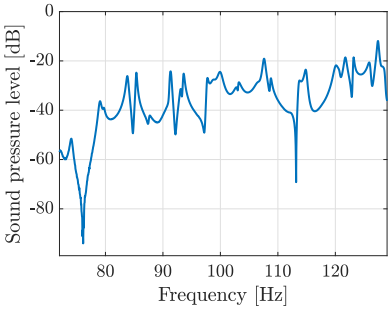

(e) Overlapping modes at low frequencies in a reverberation room.

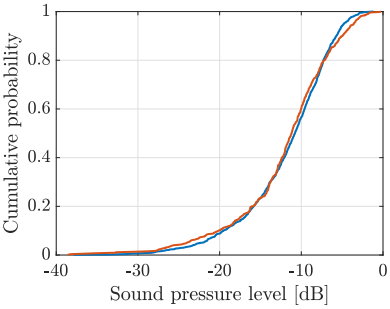

(f) Cumulative density function of the distributions shown in Figure 2.1b (blue) and Figure 2.1d (red).

Figure 2.1: Measured transfer function in a concert hall shown over frequency and space.

distribution. Here, it makes sense to express the "dissimilarity" of the sound pressure along a line (in the diffuse sound field at a single frequency) by the spatial autocorrelation function after Cook, Waterhouse, Berendt, Edelman, and Thompson Jr. (1955) or Bodlund (1977) as

$$\varphi_{pp}(\Delta\mathbf{r}) = \frac{sin(k\Delta\mathbf{r})}{k\Delta\mathbf{r}}. \tag{2.1.7}$$

From Equation 2.1.7 it can be seen that the correlation between contributing modes decreases quickly ($\propto (k\Delta\mathbf{r})^{-1}$) with increasing distance between two sampling positions. A distance between two observation points of a few wavelengths may be sufficient to discuss the sound pressure as completely independent samples from a Rayleigh distribution. Using the data collected by de Vries et al. (2001), Figure 2.1c shows how the sound pressure changes along the surveyed line. The histogram in Figure 2.1d illustrates the underlying distribution. The similarity of the two distributions becomes evident in their cumulative density functions, shown in Figure 2.1f. This is thus an intuitive example that both are samples from the same logarithmic Rayleigh distribution.

Additionally, on closer examination of the discussion by Cook et al. (1955) it can be seen that deriving the spatial autocorrelation function only requires that the discussed spatial sampling points being exposed to the same diffuse sound field. Provided this condition can be met, this is an additional and independent argument that the room's detailed geometry has no influence on the spatial samples of the sound field and its statistic independence.

Based on this understanding, Davy, Dunn, and Dubout (1979), Davy (1980) and Davy (1981) studied the sampling variance of sound field quantities (e.g., SPL) and the variance of derived quantities such as the reverberation time. The Fourier transform of the room's transfer function from Equation 2.1.3 yields the room impulse response in Equation 2.1.8. Even though the explicit evaluation can be quite complicated (Kuttruff, 2000), at high frequencies (Davy et al., 1979), it can be said from acoustical wave theory (Morse & Ingard, 1968) that the solution should be of the general form given in Equation 2.1.9.

$$h(t) = \int_{-\infty}^{+\infty} p(\omega, \mathbf{r}_r, \mathbf{r}_s) \mathrm{e}^{j\omega t} \mathrm{d}\omega \tag{2.1.8}$$

$$= \begin{cases} 0 & : t < 0 \\ \int_{-\infty}^{+\infty} c(\omega) \mathrm{e}^{(-\delta + j\omega)t} \mathrm{d}\omega & : t \geq 0 \end{cases} \tag{2.1.9}$$

In this notation, the impulse response is understood as the infinitesimal sum of responses of individual oscillators, all of which react to the stimulating impulse

with an exponentially decaying sinusoidal oscillation. Since the phase of the oscillators can be considered a random variable the complex and real part of $c(\omega)$ becomes normally distributed.

In numerous applications $h(t)$ is discussed separately in individual frequency bands. The band filtered impulse response $g(t)$ can be expressed through multiplication of the filter's transfer function $H_f(\omega)$ in frequency domain. When the filter's decay is much shorter than the reverberation of the measured room $g(t)$ can be written as in Equation 2.1.10.

$$g(t) \simeq \int_{-\infty}^{+\infty} H_f(\omega) c(\omega) \mathrm{e}^{-\delta t} \mathrm{e}^{j\omega t} \mathrm{d}\omega \tag{2.1.10}$$

$$\simeq \mathrm{e}^{-\delta t} v(t) \tag{2.1.11}$$

$$\text{with } v(t) = \int_{-\infty}^{+\infty} H_f(\omega) c(\omega) \mathrm{e}^{j\omega t} \mathrm{d}\omega. \tag{2.1.12}$$

This representation shows the impulse response of a room as an exponential decay with a function $v(t)$ imposed upon it. The function $v(t)$ features the inverse Fourier transform of the filter's transfer function and the modal amplitude density $c(\omega)$.

2.1.2 The impulse response and other room acoustical quantities

The impulse response of a room plays a central role in auditorium acoustics as it contains all information about the acoustics of a room between a specific source and a specific receiver position (Gade, 2007, Ch. 9.2.1). The significance of the impulse response is also due to its roots in signal and system theory. This background makes a toolkit of helpful methods available.

The different acoustic excitations of a room (e.g., speech or music) are understood as signals and can be represented as a sequence of impulses of different amplitudes. The room impulse response (RIR) describes, in the literal meaning of the word, how an individual impulse is transmitted through the room and arrives at a receiver as the *direct sound*, *early reflections* from the walls and as lingering *reverberation* (see Figure 2.2a). The speech or music heard at the receiver position is thus a sequence of (overlapping) impulse responses. Practical implementations of acoustic impulses are gunshots, or the sound of hands clapping once.

The perspective that Equation 2.1.11 provides on impulse responses is important for the further discussion of spatial fluctuations, but its simple exponential decay term means a pronounced reduction of realistic complexities that may

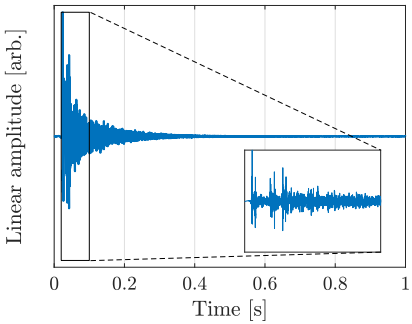

(a) RIR in linear scale and its early part.

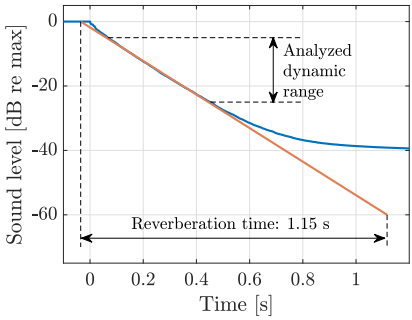

(b) EDC with linear regression.

Figure 2.2: Room impulse response and energy decay curve.

seem detached from what is of practical interest. Referring to Sabine's (1922) initial research, Kuttruff (2000) notes that in room acoustics it is unusual to characterize the decay of the sound field through the damping constant δ rather than the reverberation time T_{xx}.

In his experiment in the Fogg Art Museum, Sabine excited the room with a sound source until a steady state was reached and studied the time T needed for the level to decay by 60 dB after the sound source was switched off. This original definition of the reverberation time remains unchanged (ISO 3382-1, 2009) even with the availability of more sophisticated methods for measuring room impulse responses.

Schroeder (1965) has proven that a backwards integration over the squared impulse response (Equation 2.1.13) leads to the energy decay curve $x(t)$ that is equivalent to the decay Sabine studied in his experiments. This method is a significant advance in reliability and effectiveness as it is based on the room impulse response measured with a deterministic excitation signal. In logarithmic scale, the energy decay curve (EDC) under diffuse field conditions can be parameterized through linear regression. The reverberation time is the time that is covered by the regression's slope over a dynamic range of 60 dB.

$$x(t) = \int_{t}^{+\infty} [h(\tau)]^2 \mathrm{d}\tau = \int_{0}^{+\infty} [h(\tau)]^2 \mathrm{d}\tau - \int_{0}^{t} [h(\tau)]^2 \mathrm{d}\tau \tag{2.1.13}$$

In practice this evaluation can be limited to smaller dynamic ranges (see Figure 2.2b). If, for example, a decay of 20 dB is evaluated, it is usually indicated by the index of the reverberation time T_{20}. Even though this example's regression

curve is established from the EDC between −5 dB and −25 dB, it is still related to a decay of 60 dB to ensure comparability between different reverberation time calculations.

Table 2.1: Overview of studies establishing room acoustical quantities.

Consensus vocabulary	Quantity	Study
Strength	G	Lehmann (1976)
Reverberance	EDT	Jordan (1970)
Definition	D_{50}	Meyer and Thiele (1956)
Clarity	C_{80}	Reichardt, Abdel Alim, and Schmidt (1974)
	t_{center}	Kürer (1969)
Source width	LF	Barron and Marshall (1981)
Envelopment	LG	J. S. Bradley and Soulodre (1995b)

The early part of the impulse response is particularly important for sound perception in rooms. With the direct sound and the early reflections, all being a function of level, direction, frequency and (in the case of reflections also of) time, there is a wealth of information that needs abstraction to provide a view on core concepts that are valid to most people's listening experience. Based on the studies listed in Table 2.1, a consensus vocabulary has been established that leads to room acoustical quantities that can be calculated from impulse responses to predict sound perception. Clarity C_{80} is the logarithmic ratio of the energy in the IR's early and late part. It characterizes how a sequence of music in time is blurred together by reverberant sound components. Definition D_{50} follows a similar concept but targets syllables of running speech. The balance between early and late sound energy can be given with center time t_{c} as the center of gravity of the IR's energy. The contribution of the room to loudness can be quantified with the strength quantity G; its normalization to the source's free field SPL in 10 m distance ensures that G is a characteristic of the room rather than the source. Aspects of spatial hearing (i.e., lateral fraction, lateral strength) are not relevant in this study.

$$C_{80} = 10 \log_{10} \frac{\int_{0}^{80\,\text{ms}} [h(t)]^2 \mathrm{d}t}{\int_{80\,\text{ms}}^{+\infty} [h(t)]^2 \mathrm{d}t} \quad (2.1.14) \qquad D_{50} = \frac{\int_{0}^{50\,\text{ms}} [h(t)]^2 \mathrm{d}t}{\int_{0}^{+\infty} [h(t)]^2 \mathrm{d}t} \quad (2.1.15)$$

$$G = 10 \log_{10} \frac{\int_0^{+\infty} [h(t)]^2 \mathrm{d}t}{\int_0^{+\infty} [h_{10\,\mathrm{m}}(t)]^2 \mathrm{d}t} \qquad (2.1.16)$$

$$t_\mathrm{c} = \frac{\int_0^{+\infty} [h(t)]^2 t \mathrm{d}t}{\int_0^{+\infty} [h(t)]^2 \mathrm{d}t} \qquad (2.1.17)$$

2.1.3 Variance of the reverberation time over space

Algebraic transformations of Equation 2.1.11 allow establishing a term for the energy decay curve $x(t)$. A minor revision of Davy's original formula to recognize the declining need for averaging devices results in

$$x(t) = -2\delta t + \ln[v^2(t)]. \qquad (2.1.18)$$

This expression is pivotal in the line of argument as it shows (based on Equations 2.1.3 and 2.1.8) that $v(t)$ (due to $c(\omega)$) implicitly contains the locations of both the source and the receiver. As a result, the variance of the sound pressure over space can be transformed into a variance of the decay process over space.

Regardless of $c(\omega)$'s distribution, its composition of eigenfunctions or how it is shaped by the filter $H_f(\omega)$, the integration ensures that the Lindeberg-Lévy central limit theorem applies. As a result, $v(t)$ has a mean of zero and is normally distributed (Davy, 1981).

The decay constant m of the reverberation is determined through the least square linear regression of $x(t)$. Hence, the spatial variance of the decay constant, $\mathrm{var}_s\{m\}$, can be related to the spatial covariance of the energy decay curve at different time instances $\mathrm{cov}_s\{v^2(t_1), v^2(t_2)\}$ (Davy et al., 1979). Due to the normality of $v(t)$, $\mathrm{cov}_s\{v^2(t_1), v^2(t_2)\} = 2\mathbb{E}_s\{v(t_1)v(t_2)\}^2$. Through Equation 2.1.12, the latter term can be transformed to $\mathbb{E}_s\{c(\omega_1)c(\omega_2)\}$. Since solutions to Dirichlet or Neumann boundary value problems are orthogonal, the product of $c(\omega_1)c(\omega_2)$ disappears for $\omega_1 \neq \omega_2$ and yields the Dirac delta function $\delta(\omega)$ for all other cases when $\mathbb{E}_s$ is properly normalized[1].

This leads Davy to a rather bulky but closed form expression for the variance of m:

[1] Following Bodlund (1977), $\mathbb{E}_s\{c(\omega_1)c(\omega_2)\} = \delta(\omega_1 + \omega_2)$ is only valid when the spatial autocorrelation function $\varphi_{pp}(\Delta\mathbf{r})$ has dropped to values close to zero. This requires the observation points contributing to the spatial expected value $\mathbb{E}_s$ to be sufficiently far apart from each other. From a practical point of view (Davy et al., 1979), this implies distances greater than $\lambda/2$ between observations points. Secondly, it is important that the sound field is not dominated by the direct sound from the source. Therefore, observation points need to be farther than the critical distance from the sound source, i.e., where the reverberant field has more energy then the direct sound.

$$\mathrm{var}_s(m) = \left(\frac{10}{\ln(10)}\right)^2 \frac{12}{B_1}\left(\frac{m}{D}\right)^3 F\left(\frac{ln(10)}{10}D\right) \tag{2.1.19}$$

with

$$F(x) = 1 - \frac{3}{x}(1 + \mathrm{e}^{-x}) - \frac{12}{x^2}\mathrm{e}^{-x} + \frac{12}{x^3}(1 - \mathrm{e}^{-x}). \tag{2.1.20}$$

In this equation D denotes the change of level of the decaying sound that is analyzed and B_1 refers to the statistical bandwidth of the band-pass filter in Hz with:

$$B_1 = \frac{\left\{\int_0^{+\infty} |H(f)|^2 \mathrm{d}f\right\}^2}{\int_0^{+\infty} |H(f)|^4 \mathrm{d}f}. \tag{2.1.21}$$

In order to gain an overview of the relationship shown in Equation 2.1.20, D is assumed to be set to a fixed value (e.g., 30 dB for T_{30}). With all constants omitted, Equation 2.1.20 becomes:

$$\mathrm{var}_s(m) \propto \frac{m^3}{B_1}. \tag{2.1.22}$$

This expression makes it clear that the variance of the decay rate m increases with longer reverberations by the third power and decreases for larger filter bandwidths. The statistical bandwidth changes by a factor of 0.5 with each doubling of the center frequency. The statistical bandwidth of octaves is thrice that of corresponding third octave filters. This means that the spatial variance is cut half from one octave band to the next higher and is three times as high when the third octave spatial variance is compared to full octave fluctuations.

2.1.4 Reference to the research question

These theoretical principles are directly related to this study's goal, as they indicate important influence quantities of spatial fluctuations of the sound field. Their relation to reverberation times and how their variance depends on the absolute value, the filter center frequency and the filter bandwidth is shown quite clearly by Davy (1980). Apart from a different reference pressure, the sound strength G in concert halls and the steady state sound pressure level are identical. Thus, it is expected that both fluctuate comparably.

These findings, however, cannot be generalized to clearly predict the spatial fluctuations of quantities that target the temporal energy ratios in room impulse responses (i.e., C_{80} or D_{50}). Undoubtedly, global effects may be carried over that motivate a rough expectation, but an exact prediction is not obvious from this theory. Also, the investigation by Gade and Rindel (1985) in 21 Danish concert halls suggests that the basic requirement of the diffuse sound field is not met in many auditoria. All of this motivates empirical studies to investigate how room acoustical quantities (including reverberation times) vary from one measurement position to the next.

2.2 Acoustical measurements in auditoria

2.2.1 Principles and established practice

Measuring acoustical transfer functions or their corresponding impulse responses is part of the standard repertoire in research and practical applications. Müller and Massarani (2001) give a detailed general introduction into today's methods to measure transfer functions using electroacoustic systems. The applicability of these techniques in architectural acoustics is described in ISO 18233 (2006). The systematic structure of a typical measurement chain by today's standard is shown in Figure 2.3: a digital computer with its software marks the starting point. In the most crude of strategies the software serves as a mere signal generator to produce an excitation signal. The signals are converted into the analog domain and amplified to excite the device under test (DUT) with an appropriate transducer. In architectural acoustics the device under test is typically a room that is excited by a dynamic loudspeaker. In order to ensure a uniform sound radiation chassis of regular polyhedron shape (e.g., dodecahedron or icosaedron) are preferred. At the receiving side the sound field is usually measured with a condenser microphone. Through cascaded amplifiers (the first one considered part of the microphone) an analog voltage signal is presented to the analog-digital converter. The loop is closed when the quantized and sampled signal is fed to the software for processing and analysis.

Modern measurement methods recognize the measurement chain and all its parts as a linear time invariant (LTI) transmission system where, according to system theory, all measurement chain properties are included in its impulse response (IR). Under this paradigm an input is linked to the output through convolution with the system's IR. The flow of information in modern measurement methods is shown in Figure 2.4. A deterministic excitation signal $s(t)$ is fed into the acoustic transmission channel and the system's impulse response is determined through deconvolution (two channel FFT method). Output quantities

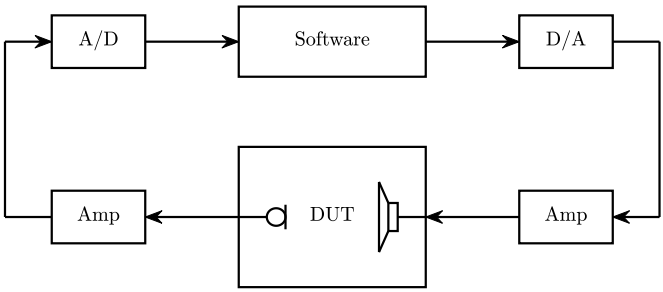

Figure 2.3: Systematic drawing of the acoustical measurement chain.

such as the SPL or other parameters are calculated from the IR using standardized algorithms.

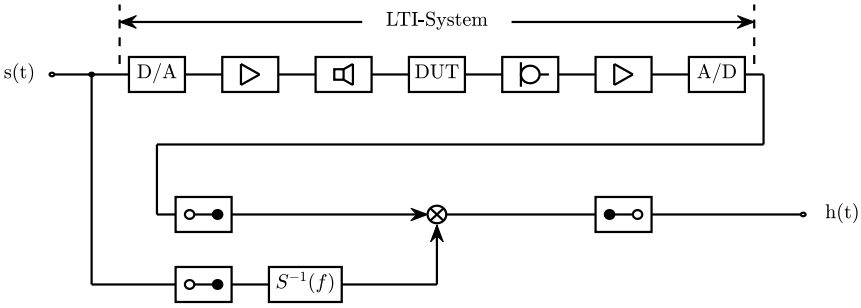

Figure 2.4: Systematic drawing of the measured LTI-System.

The standardization of measurement procedures plays an important role for two reasons. First, international standards represent the consensus on the current state of knowledge, as they are the result of a vote by a committee of leading international experts in the field. Second, such a framework is crucial in regard to uncertainties in measurement as it provides a uniform foundation for better comparability and reproducibility of measured results. In room acoustics ISO 3382-1 (2009) and ISO 18233 (2006) serve as the cornerstones of that foundation.

ISO 18233 (2006) takes a special role in acoustical measurement standards. Unlike other documents which define a measurement procedure to provide a frame for collecting suitable measurement data for a given task, ISO 18233 (2006) provides general information on relatively new correlation measurement methods that can be used in ISO 140, ISO 354 (2003), ISO 3382-1 (2009) and ISO 17497-1 (2004). This is why the provided information provided in ISO 18233 (2006) must

be taken with a grain of salt when determining the uncertainty of a specific measurement procedure that is formally defined elsewhere. Even though ISO 18233 (2006) is an excellent resource to determine where the drafting expert group identified potential sources of problems, the standard avoids clear statements that quantify the point at which deviations are no longer acceptable. Reasons for that are manifold: First, tolerances and uncertainties depend a lot on the context of the measurement procedure. Uncertainties that may be tolerable (insignificant) for one measurement problem may be rated unacceptable for other problems. Second, despite theoretical understanding of the cause and effects uncertainty propagation is widely ramified making it difficult to establish simple guiding rules. Finally, there is evidence that the complexity of system theory exceeds the capabilities of the basic GUM framework (Eichstädt, 2015).

ISO 3382-1 (2009) defines the measurement procedure in performance spaces to determine the reverberation time and other room acoustical quantities. It specifies the required properties of the measurement equipment and procedural aspects directly related to the research question like microphone or measurement positions. Minimum distances need to be maintained to the auditorium's surfaces, the sound source and to nearby measurement positions while ensuring a sufficient sampling relative to the auditorium's size. These requirements are clearly related to the theoretical considerations in Section 2.1 and yet ISO 3382-1 (2009) provides no advice on how accurately measurement positions need to be defined. This open problem is addressed by the research question posed in the introduction.

Compared to other standards in acoustics, ISO 3382-1 (2009)'s discussion of uncertainties appears rather brief. In reference to the work of Davy et al. (1979) and Davy (1980), it notes the variance of measured reverberation times as dependent on on the dynamic range and the bandwidth. Otherwise, the strategy to perform accurate measurements seems to be approached from the standpoint of reproducibility: the standard requires documenting the conditions prevailing during the measurement. The list of information a measurement report should provide includes the state of occupancy, the condition of variable equipment, safety curtains or stage furniture and metrological conditions. With modern auditoria being used for a variety of different performance types and events there can be a staggering amount of detail that needs to documented. This protocol can range from the position of motorized stage elevators to variable absorbing elements, lighting flaps or even stage furniture. The standard leaves unclear what level of detail is necessary to ensure simultaneous reproducibility and practical usefulness, and thus it is difficult to judge whether these specifications are too lenient or overly demanding. The needed minutiae of documentation should be discussed in regard to uncertainties of measurements.

By standardizing the procedure for acoustical measurements in auditoria (i.e.,

ISO 3382-1 (2009)) an internationally accepted method was successfully defined. The standard finds relatively wide use in scientific and applied acoustical measurements and is perceived as both important and helpful to characterize the acoustic conditions in auditoria (Barron, 2005; J. S. Bradley, 2005). Defining a measurement procedure through standardization establishes a necessary prerequisite to make a thorough (GUM-conforming) discussion of measurement uncertainties possible.

2.2.2 Measurement uncertainty in architectural acoustics

The value of standardization as a basis for the uncertainty discussion was described early on. Standards usually represent the state of knowledge from previous studies. These studies thus represent a valuable resource that may provide data to quantify the investigated influences' uncertainty contributions. In this section, a selection of studies are examined to discuss how their findings can shaped and still contribute to the investigation of uncertainties.

The increasing availability of digital measurement technology and the desire to modernize the established measurement standards (ISO 3382, 1975) to recognize these developments have triggered numerous key investigations in the 1990s. At the same time, adding new concepts required some groundwork to confirm the new contents' significance and explanatory power (e.g., J. S. Bradley (1996); Lundeby, Vigran, Bietz, and Vorländer (1995); Pelorson et al. (1992)).

Against this background, the study by Pelorson et al. (1992), with its survey of 14 concert halls, is pioneering as they investigated the general conditions that would need to be met to collect valid data. The authors discuss the general reproducibility of measurements, the type of loudspeaker housing, the microphone and the number of measurement positions that are appropriate for meaningful acoustical measurements. In a second step, the algorithm to calculate room acoustical parameters from the collected data is being investigated. The authors also study the question whether the acoustic conditions in differently shaped auditoria can be distinguished based on the calculated room acoustical parameters. From a present perspective it is evident that many of their findings led to what is now accepted knowledge. Targeting a similar research objective, their investigation of spatial fluctuations is of special relevance. Evidently, investigating the spatial variance of room acoustical quantities is not a newly emerging topic, but a field of research that already received attention in the early 1990s. Today's empiric studies can add to the existing body of knowledge in at least two ways. First, measurement series to investigate influence quantities can be implemented keeping the provisions of the GUM in mind. Making sure the collected data satisfies the principles needed for a standardized uncertainty discussion makes the contri-

bution of different influences comparable. Second, adding further weight to the driving forces identified from theory (Davy, 1980) and recognizing their detailed interplay will permit a more detailed understanding how frequency, bandwidth and changes in the early part of the impulse response contribute to the combined uncertainty of room acoustical quantities. Probably due to limited journal space and due to Pelorson et al. addressing an overwhelmingly large number of influences it is difficult to follow every detail of their conclusions. Thus, the findings are partially supported by the justified confidence in the Pelorson et al.'s experience and reputation. This comes with the drawback that the context of their findings is partially obscured making it difficult to use the data from 1992 to discuss uncertainty of acoustical measurements according to the GUM standard.

J. S. Bradley (1996) conducted a round robin that investigated uncertainties due to different measurement techniques and individual data analysis. It was investigated how a digital reverberator with three preset impulse responses was measured and analyzed by 15 institutions operating a total of 23 different measurement systems. In parallel, J. S. Bradley (1996) conducted repeatability measurements to investigate the variance of measured room acoustical quantities determined by the same observer using the same equipment. His summary findings are shown in Table 2.2

Table 2.2: Standard uncertainty to determine room acoustical parameters under reproducibility conditions for (I) the same measurement system and analysis algorithm and (II) for different measurement systems and analysis algorithms (J. S. Bradley, 1996)

.

Parameter		Reproducibility condition I	II
RT	[s]	4×10^{-3}	1.0×10^{-1}
EDT	[s]	1.3×10^{-2}	0.2
C_{80}	[dB]	8.7×10^{-2}	0.5
C_{50}	[dB]	1.2×10^{-1}	1.2
t_c	[s]	7.0×10^{-4}	6.2×10^{-3}

When discussing the results, J. S. Bradley (1996) identifies two crucial aspects that have a strong influence on the different systems' performance. First, the definition of a RIRs time code (i.e., $t = 0$) is important. Second, at the time the study was conducted the approaches to calculate EDT left room for inter-

pretation. In relation to this study, these findings highlight the importance of reproducibility studies at different scales and the value of clear measurement specifications. Generally, each revision of a measurement standard, e.g., the transition from ISO 3382 (1975) to ISO 3382 (1997), results in a discontinuity, which limits the long-term comparability of results. Thus, it is unclear whether the quantitative findings are still valid today as definitions have since been clarified.

The value of comparative measurements is also highlighted by Lundeby et al.'s (1995) research. They report on a sequence of measurements in which a number of different institutions surveyed acoustical measurement chains that successively grew in complexity. They found that, despite minor caveats, differences in results between highly experienced observers that conducted acoustical measurements under very precisely defined laboratory conditions are in the order range of 1 dB / 10 % or less (depending on the quantity). In a way, Lundeby et al.'s investigation emphasizes and validates the research question posed here, since it is still unclear how the precision in defining the measurement conditions translates to the respective uncertainty.

In a next step, the investigation of Lundeby et al. (1995) picks up a discussion voiced earlier by Barron (1984) and studies how reverberation times can be calculated while ensuring the background noise does not disturb the analysis. Lundeby et al.'s algorithm has attracted some recent attention (Guski & Vorländer, 2015; Jankovic, Ciric, & Pantic, 2016) where it is discussed that different strategies suffice with ISO 3382-1 (2009) but inhere different potential of error and uncertainty. Through this discussion, it becomes clear how a loose definition of the measurement and analysis specification can contribute to measurement uncertainty. For the present study this is taken as an argument to commit to the Lundeby et al. algorithm to determine the clarity index in the presence of background noise.

With the revision of ISO 3382 (1997) almost 25 years ago and the transformation to ISO 3382-1 (2009) introducing only relatively small additions to the measurement procedure. To this present day, many users developed a rich experience using this standard. In this light, Barron (2005) or J. S. Bradley (2005) discuss the context in which measurement results have to be interpreted. The perspective on uncertainties in room acoustical measurements has shifted in the years since the revision of ISO 3382 (1997). Today the measurement procedure can be considered generally accepted and research discusses different influences and their effect on the uncertainty. Among other influences investigations target the directivity of sound sources (Knüttel, Witew, & Vorländer, 2013; Leishman, Rollins, & Smith, 2006; San Martin, Witew, Arana, & Vorländer, 2007; Vorländer & Witew, 2004; Witew, Knuettel, & Vorländer, 2012; Witew, Müller-Giebeler, & Vorländer, 2014), the directivity of receivers (Witew & Behler, 2003; Witew, Lindau, et al., 2013), the position of the receiver (de Vries et al., 2001; Witew,

Behler, & Vorländer, 2004; Witew & Vorländer, 2011) but also the algorithm to analyze impulse responses (Guski & Vorländer, 2015; Katz, 2004; Witew & Behler, 2005).

The study by Witew et al. (2012) on the influence of the source's directivity on measurement uncertainty is addressed separately as it empirically investigates primary and secondary influence quantities. In laboratory conditions a large number of impulse responses were collected in model scale while independently varying the volume of the test room as well as the sound absorbing and scattering properties of the bounding surfaces. Through an ANOVA it was shown that the directivity of a sound source differently influences measured impulse responses (as a function of their running time) when different volumes, absorption, scattering and distances between source and receiver are considered. In addition interaction effects between influence quantities are evident. This approach represents, in regard to the present study, a target to be aimed at. Ideally the combined uncertainty due to potentially interacting influence quantities is investigated where the influences are varied in dedicated experiments. It is uncertain, however, whether this strategy can actually be implemented in auditorium acoustics under real life conditions, given the large number of potential influence factors.

2.2.3 Observations in other fields of acoustics

The discussion of uncertainties in acoustical measurement is a topic that is attracting increasing interest. In particular, measurements that require a sustainability that holds up to judicial dispute uncertainties are of vital interest as they mark the thin border between meeting and violating legal provisions. DIN SPEC 45660-1 (2014) is a technical report that provides a helpful overview of the uncertainty of eight measurement tasks. These measurement problems include uncertainty calculations for (a) one third octave band sound pressure level measurements in anechoic environments, (b) background noise corrections, (c) noise measurements, (d) building acoustical measurements and to (e) sound emission measurements. A detailed discussion of the presented measurement tasks, however, reveals that the stated uncertainties rely on specific assumptions that may be characteristic to the individual measurement conditions. As a result not all of the findings DIN SPEC 45660-1 (2014) reports on can be transferred straightforwardly to this investigation.

Wittstock (2007, 2015) investigates the measurement uncertainty to determine the airborne sound insulation of different types of walls, comparing the uncertainty in theoretical approaches to physical measurements. In theoretical approaches, Wittstock sees the advantage of a clear relationship between input and output quantities. In measurements, however, situations exist where the in-

put quantity cannot be measured directly (e.g., incident sound power). Instead auxiliary quantities are taken (e.g., SPL) that may be inadequate. In Wittstock's (2015) case this defect is traced back to imperfect technical realizations in the supposedly diffuse sound field. Interlaboratory tests are a valid method to quantify this uncertainty contribution. Such a strategy is one way to conform with the ISO Guide 98-3 (2008) framework. The uncertainty determined through such interlaboratory tests is then assigned to all future measurements that are conducted following the same measurement procedure.

This strategy could also be applicable in this study. The assumed diffuse sound field in theory is oftentimes not sufficiently evident in concert halls (Gade & Rindel, 1985). Also, contributing factors such as early reflections that may contribute to spatial fluctuations may not be modeled in simple approaches.

Wittstock's analysis raises the important question of correlation between results determined at different frequencies bands. Evidently in the measured sound reduction index R_i the correlation index spans the full range from uncorrelated to full positive correlation. The uncertainty due to (a partial) correlation between frequency bands is significant. In personal communication he notes that this is a factor he encountered in other measurement tasks as well, for instance in acceptance inspections for anechoic rooms. This factor must therefore also be taken into account in this investigation.

Finally, Eichstädt, Link, Harris, and Elster (2012), Eichstädt (2012) and Eichstädt (2015) bring an additional topic to the table by targeting the uncertainty of so-called dynamic measurements (e.g., 2CH-FFT techniques). He interprets the measurement of dynamic systems as an optimization problem in which the output impulse response of the system is determined to best fit the systems' input and output signals. Due to the involved optimization this approach requires carrying out Bayesian inference. This deviation from the classical Gaussian perspectives brings the GUM-compliant uncertainty discussion to its limits (see Section 2.3.2) and so Eichstädt argues that a detailed discussion of all influence quantities and their correlations may simply be impossible using classical Gaussian perspectives. With regard to this study, this means that the unique features of dynamic measurement systems and their uncertainty discussion are deferred to dedicated future studies.

2.3 Uncertainties in measurements

2.3.1 General metrological terms

The discussion of the previous section shows that incorporating individual results into the big picture requires a framework in which to discuss uncertainties. This begins with the definition of a common terminology. A good point from which to approach metrological concepts are the definitions in JCGM 200 (2012). The "crystallization nucleus", around which other terms will be arranged, is the phenomenon, the body, or the substance of interest, that naturally has properties that are to be measured. A property has a magnitude that can be expressed as a value and a reference. Common references are measurement units that are derived from (or actually are) base units, that in turn are all defined through physical constants (JCGM 200 (2012), 1.1). Properties are referred to as *quantities* in a metrological sense.

This implies that a *measurement* is the process of experimentally obtaining one or more values that can reasonably be attributed to a quantity (JCGM 200 (2012), 2.1). The term "reasonably" accounts for the fact that sometimes properties are not determined directly. Oftentimes it is easier to measure other quantities that are related to the quantity of interest, but other times it is the relation of quantities to each other that permits observing quantities of interest. An example for the first case are microphones where the sound pressure is measured through the capacity of a condenser. Here, a *measurement principle* is introduced to describe a phenomenon serving as a basis of a measurement (JCGM 200 (2012),2.4). The second case can be illustrated considering absorption measurement in reverberation rooms. Here, the sound field's decay constant in a set of measurements under changed conditions yields the absorption coefficient. In contrast to the first case a *measurement method*, as a generic description of a logical organization of operations, is used in a measurement (JCGM 200 (2012),2.5).

Such indirect strategies usually require a conversion between quantities that are known to be involved, presented mathematically through a *measurement model* (JCGM 200 (2012),2.48). The practical implementation of this conversion, be it algebraic or through simulations is referred to as the *measurement function* (JCGM 200 (2012),2.49). The strategy to determine quantities indirectly through the observation of other quantities makes it reasonable to distinguish between *input* and *output quantities*. Input quantities are understood as quantities that must be obtained or measured in order to calculate the *measurand* (i.e., the output quantity intended to be measured)(JCGM 200 (2012), 2.3, 2.50). The *result of a measurement* is summarized as a set of quantity values being attributed to a measurand together with any other available relevant information, such as

their associated uncertainties (JCGM 200 (2012),2.9).

To conclude this section the connective concept of a *measurement procedure*, the detailed description of the steps that are necessary to follow for the practical realization of measurements, is introduced. This sequence of instructions is formulated either according to measurement principles or to a given measurement method, based on a measurement model. This procedure includes all calculations to obtain the measurement result (JCGM 200 (2012),2.6).

2.3.2 The guide to the expression of uncertainty in measurement

Basic concepts

Due to physical laws, the environmental conditions that prevail during a measurement influence the result. While JCGM 200 (2012) distinguishes between *input quantities* (affecting the quantities actually measured) and *influence quantities* (affecting the measuring system), ISO Guide 98-3 (2008) merges both concepts into *influence quantities*. Ideally all conditions and quantities are recorded to the last detail as part of the measurement procedure so that results are accurate and precise. For obvious reasons, most notably practicability, this notion of perfection is unrealistic and unreasonable in a measurement procedure. Consequently the result of a measurement needs to be recognized as an estimate that co-occurs with its uncertainty (ISO Guide 98-3 (2008), 3.1.2).

Using the terminology outlined in Section 2.3.1 as a foundation, the GUM defines the objective of a measurement as determining the value of a measurand that is specified through an appropriate measurement procedure (ISO Guide 98-3 (2008), 3.1.1). This indicates that an uncertainty investigation does not only focus on a measurement process, but also includes how the process is integrated into a measurement procedure. This is because an incomplete definition of a measurand may contribute to the uncertainty as well. The liberties that a measurement procedure leaves determine both the practical usefulness and the uncertainty of the measurement result. A high number of constraints will ensure very precise and accurate measurements but will decrease practicality due to a lack of freedom necessary to serve a variety of conceivable measurement scenarios.

Evaluating the uncertainty of a measurement is generally divided into two main stages, formulation and calculation. In the first stage the information about a measurement is brought together to identify the measurement problem and collect what is known about the measurement principle, method and procedure. This information is compiled to a measurement model which marks the foundation for the following calculation phase. The goal of the calculations is to establish

an expectation of the measurand and its associated uncertainty.

Formulation stage

Defining the measurement problem At first glance the formalism to gather available information on a measurement problem may seem cumbersome and a task of commanded diligence that requires little intellectual work. It may help, however, to understand this review as groundwork for the following modeling phase. There seems to be a good agreement among experts that, for some measurement tasks, establishing a measurement model may turn out to be a challanging endeavor (e.g., JCGM 104 (2008)). Establishing clear borders within which the measurement is discussed is not mandatory from a logical point of view, but should be seen as a provision that helps to confine the model's complexity to a range that can be handled.

Defining the measurement problem is often considered to at least comprise the following information (e.g., PTB: Sommer and Siebert (2004)):

a) Definition of the measurement problem and a clear identification of the measurand.

b) Identification of the measurement principle, i.e., the scientific phenomenon used for the measurement.

c) Formulation of the measurement method, i.e., the logic of how the collected data is used to determine the measurand,

d) Specification of the measurement procedure, i.e., the organizational sequence of steps used to determine the measurand.

In regard to the GUM framework defining the measurand as the model output quantity Y, is the first important contribution to the uncertainty discussion. As an additional qualitative result, the available knowledge and understanding of the measurement is presented.

Identifying influence quantities The available knowledge about the measurement has to be gradually brought into a form so that a GUM-conforming model can be derived. The aspect of interest in this second step is the search for the factors that potentially have an influence on the measurement. Once substantiated, these influence quantities X_i will serve as inputs to the model yielding the output Y.

The Ishikawa-diagram shown in Figure 2.5 is a qualitative way to structure and evaluate these influences. In its generic form it shows the abstract measurand Y on

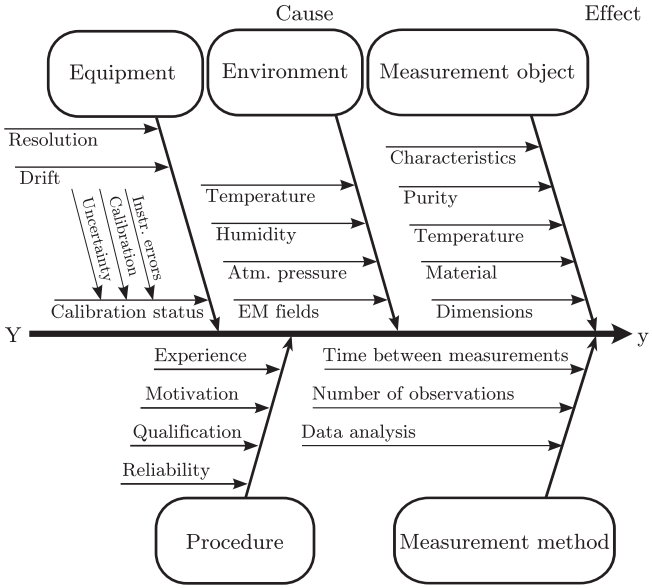

Figure 2.5: Cause-and-Effect diagram of a generic measurement process.

the left and its estimate y as a result of a measurement. The branches pointing to the principle axis are abstract factors that can be found as clusters of influences in many measurement problems. Although the different fields of science span a large spectrum of measurement problems, some five factors can be regularly identified. These are derived from the "5M"-framework of manufacturing quality control Ishikawa (1996). More detailed aspects are assigned to the superior factors. Ideally, influence quantities that need to be considered in the measurement model can be found in the lowest hierarchical level of the cluster. By grouping and arranging the different influence quantities on the cause-and-effect diagram an assessment takes place which allows a targeted discussion of the important uncertainty contributions. Due to its qualitative nature an Ishikawa diagram may also be understood as merely a starting point of a discussion. In many cases the different entries or branches reflect relationships that are thought to exist but cannot be quantified for reasons of complexity or incomplete knowledge at this early stage of the evaluation.

Establishing the measurement model The previous discussion already implies a general measurement model, where a number of influence quantities X_i

serve as inputs, yielding the measurement result Y as the output. In favorable conditions this model can be formed as a mathematical expression which is symbolized by the functional relationship f:

$$Y = f(X_1, X_2, ..., X_N) \tag{2.3.1}$$

In more intricate scenarios, dividing the measurement problem into smaller subsets can help reduce the complexities: different inputs X_i can be interpreted as measurands themselves that may likewise depend on previous subsets. Subdividing the measurement problem is a double-edged sword. On one hand, it allows breaking down a complex measurement problem into smaller chunks that may be easier to handle. On the other hand, this branching out of subordinate measuring processes may lead to an increase in complexity of the higher-ranking process, and thereby develop situations where a closed-form equation for f cannot be found at all (ISO Guide 98-3 (2008), 4.1.2).

In this light the function f needs to be seen as a symbol for the generic relation between the quantities X_i and Y. f may be determined experimentally or through other means, e.g., simulations. In this approach the model function f is sampled through repeated measurements or simulations where a change in Y is related to a controlled change in a particular X_i while the other input quantities are held constant (ISO Guide 98-3 (2008), 5.1.4).

In practice, keeping both known and unknown input quantities constant during the empirical determination of the model function f may not be possible. In this scenario the intrinsic measurement uncertainty of this series of measurements needs to be discussed.

Assigning probability distributions The next step calls the attention to the input quantities again. The goal of this phase is to determine the best estimate x_i of the input quantities X_i and the estimates' respective standard deviation $u(x_i)$. Following the GUM terminology $u(x_i)$ is called the *standard uncertainty*. In line with established statistical notations the variance associated with the influence quantity's estimate is denoted by $u^2(x_i)$ (ISO Guide 98-3 (2008), 3.3.5).

Generally the standard uncertainty and the estimate of the input quantities can be determined empirically (Type A) or from expert knowledge and professional assessments (Type B). Type A uncertainties are determined through repeated measurements under constant measurement conditions whereas type B uncertainties can be determined based on calibration documents, technical specifications, literature, etc.. A second aspect of the uncertainties that needs consideration is the distribution over which the input quantities observations vary. The GUM

provides fixed rules to determine the standard uncertainty based on the input quantity's probability density function (PDF) and its characteristic parameters.

The way this information is processed in the calculation stage depends a lot on the detailed properties and the capabilities of the model. In the most simple scenario the model function f is perfectly linear and is available in closed mathematical form so only very few characteristics of the input quantities' distributions are relevant. Complex models may require detailed properties of the PDFs in order to calculate the output quantity's measurement uncertainty.

Calculation stage In this stage of the GUM framework, the propagation of the previously determined probability distributions through the measurement model is calculated following fixed rules. In its general idea this method is based on the concept of *Gaussian Error Propagation* (Bronstein et al. (2015), 16.4.2.1.2). On the foundation of the underlying model, the GUM offers a significant extension to the classical, Gaussian perspective by including systematic errors or biases, correlated input quantities and (moderately) nonlinear models.

The estimate y of the measurand Y is obtained straightforwardly by inserting the input estimates $x_1, x_2, ..., x_N$ into Equation 2.3.1 (ISO Guide 98-3 (2008), 4.1.4). The notation for the measurement result's standard uncertainty is quite similar to the input quantities' standard uncertainties. When the measurand's uncertainty is determined on the grounds of influence quantities it is termed *combined standard uncertainty* $u_c(y)$ as indicated with the index c.

The combined standard uncertainty $u_c(y)$ can be calculated from the measurement function f and the uncertainties $u(x_i)$ based on a first-order Taylor series approximation of Equation 2.3.1:

$$u_c^2(y) = \sum_{i=1}^{N} \left(\frac{\partial f}{\partial x_i} \right)^2 u^2(x_i) \tag{2.3.2}$$

Due to a change in paradigm regarding the interpretation of errors in the GUM compared to classical error propagation perspectives, Equation 2.3.2 is often referred to as the *Law of Propagation of Uncertainty* (ISO Guide 98-3 (2008), 5.1.2). Figure 2.6 gives a graphical representation of Equation 2.3.2. The output's standard uncertainty $u(y)$ is calculated from the input quantity estimate's standard uncertainty $u(x)$ by multiplication with the *sensitivity coefficient* c. The sensitivity coefficient is the partial derivative of the model function f.

An addition to Equation 2.3.2 recognizes a combined variance of the influence quantities when they are correlated (ISO Guide 98-3 (2008), 5.2.2):

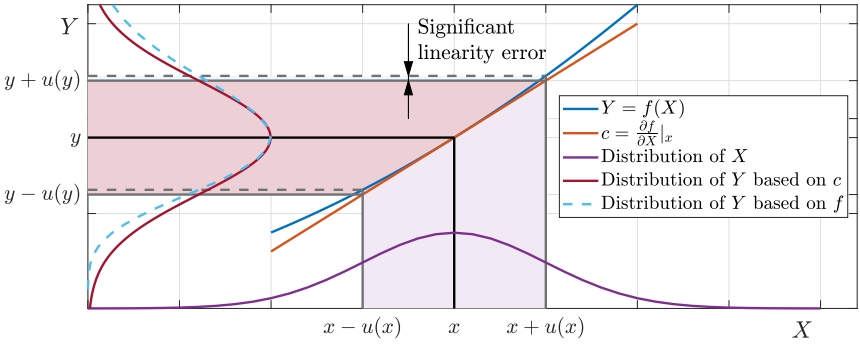

Figure 2.6: The measurement function f and its linearization c. The distribution of the input quantity's estimate x is propagated through the model yielding an estimate of the measurand y and its standard uncertainty $u(y)$; after Sommer et al. (2005).

$$u_c^2(y) = \sum_{i=1}^{N}\sum_{j=1}^{N} \frac{\partial f}{\partial x_i}\frac{\partial f}{\partial x_j} u(x_i, x_j) \tag{2.3.3}$$

$$= \underbrace{\sum_{i=1}^{N}\left(\frac{\partial f}{\partial x_i}\right)^2 u^2(x_i)}_{\text{uncorrelated term}} + \underbrace{2\sum_{i=1}^{N-1}\sum_{j=i+1}^{N} \frac{\partial f}{\partial x_i}\frac{\partial f}{\partial x_j} u(x_i, x_j)}_{\text{mixed terms of covariances}}$$

This notation represents the covariance associated with x_i and x_j as $u(x_i, x_j)$. It is worth noting that the correlation of input quantities in Equation 2.3.3 refers to the correlation of the x_i's probability distribution and not to a correlation of the physical quantities that might be given by linking different quantities through the model function (Mieke, 2014). The random variables of input quantities that are potentially correlated to each other are those that were measured with the same equipment, were calibrated with the same normal or depend on the same reference value. Of course, this list should not be considered as complete as many other sources for correlating quantities are conceivable.

Figure 2.6 also shows how the linearization of the model function may lead to errors when the difference between the nonlinear model function $f(x)$ and its 1^{st}-order Taylor approximation cx becomes significant. In such situations higher-order terms of the Taylor series expansions are added to Equation 2.3.2:

$$\sum_{i=1}^{N}\sum_{j=1}^{N}\left[\frac{1}{2}\left(\frac{\partial^2 f}{\partial x_i \partial x_j}\right)^2 + \frac{\partial f}{\partial x_i}\frac{\partial^3 f}{\partial x_i \partial x_j^2}\right] u^2(x_i)u^2(x_j) \tag{2.3.4}$$

Comparison of Equation 2.3.4 to multivariate Taylor series expansions in mathematical literature (e.g., Bronstein et al. (2015), 7.3.3.3.4) shows that only "leading" terms are considered in the GUM. This creates a situation where dealing with nonlinear measurement functions requires some dexterity that deserves a brief discussion in the last two parts of this section.

Expanded measurement uncertainty Depending on the field of application the level of confidence associated with the combined standard uncertainty $u_c(y)$, namely $p \approx 68\%$, may not be sufficient. Coverage probabilities that differ from the standard deviation can be expressed through the *expanded uncertainty* U by multiplying $u_c(y)$ with an appropriate *coverage factor* k (ISO Guide 98-3 (2008), 3.3.6, 3.3.7, G.1.3). When the distribution of Y is (approximately) normal choosing $k \approx 1.960$ will lead to a confidence interval of 95 % and choosing $k \approx 2.576$ will lead to an interval of 99 % (ISO Guide 98-3 (2008), 6.2.1, 6.3.3). In this regard the concept of approximate normality is supported by the Lindeberg-Lévy Central Limit Theorem (Bronstein et al. (2015), 16.2.5.2) as already a relatively small sum of independent identically distributed (iid) random variables yields an approximately normal distribution.

Choosing the appropriate value for k, however, requires detailed knowledge of the probability distribution over which Y varies.

Statement of results The uncertainty discussion concludes with reporting the uncertainty. Although not explicitly required stating the *uncertainty budget* in tabular form is fairly common. A benefit of preparing an uncertainty budget is the identification of uncertainty contributions that dominate the combined uncertainty. Empirically determined uncertainties (type A) play a special role in the evaluation of individual uncertainty contributions as the standard deviation of the experimental standard deviation of the mean $\sigma[s(\overline{q})]$ may be significant even with a relatively large number of observations. Stating the degrees of freedom helps to rate the accuracy of the uncertainty contribution (ISO Guide 98-3 (2008), G.4).

Limitations of the GUM

A lot of work from the highest-ranking national metrological institutions went into preparing the Guide to the Expression of Uncertainty in Measurement, leading to its widespread acceptance and use as a de facto standard. The challenges

in applying the GUM arise from the rather abstract phrasing of the framework that ensures validity for a wide range of topics. As a result some experience is necessary to handle the details of complex real-world problems. Acquiring this expertise often requires individual interpretations of the Guide that lead to a variety of perspectives that are sometimes difficult to reconcile.

One of the GUM's core assumptions is that the measurement method can be represented through a linear model (JCGM 101, 2008, 5.11.5). Under this premise, the measurement function can be expressed by its first-order Taylor series and the output uncertainty can be determined following the rules of Gaussian uncertainty propagation using Equation 2.3.2. This strategy becomes subject to criticism when the measurement function is nonlinear or possibly even piecewise monotonic. In statistics this is a fairly well-known problem handled using the *transformation theorem for probability densities* (Johnson et al. (1994), pp. 14-15, Eq. (12.32)).

This calls into question whether the basic version of the GUM provides the set of tools necessary to handle complex measurement problems. A processing of influence quantities that goes beyond multiplication with a constant and summing is already outside of the GUM's scope. On the other hand, it must be pointed out that the *Transformation Theorem* is not capable of covering correlated input distributions where the *Law of Uncertainty Propagation* includes the correlation of input quantities.

Mieke (2014) points out that "moderately" nonlinear models can be discussed when significant "leading" 2^{nd}-order Taylor series terms (see Equation 2.3.4) are included in Equation 2.3.3. Upon close inspection of Equation 2.3.2 it is evident that following the GUM framework, variances or coverage intervals instead of full PDFs are propagated. Obviously this reduces the mathematical complexity considerably; however, it highlights two problems: First, an individual interpretation of the term "moderate" is required to assess whether the measurement function nonlinearity is significant. Second, detailed distributions are not considered which may be a significant simplification when numerous individual (potentially elaborate) input distributions act on a model and potentially large coverage factors k need to be determined.

To avoid these limitations, this study resorts to Monte Carlo methods that are added to the GUM framwork through a supplement (JCGM 101, 2008). This method is discussed in the following subsection. For reasons of completeness it is noted that the critical discussion also sometimes includes the missing concept of the *true value* or an inability to include Bayesian concepts (e.g., Grabe (2010); Schmidt (2003)). However, as these concepts do not play a role in this study the reader is referred to the respective references for an in-depth discussion.

Monte Carlo simulations as part of the GUM framework

In order to address two of the core limitations that were discussed in the previous section, JCGM 101 (2008) describes a Monte Carlo method as a practical alternative to the ISO Guide 98-3 (2008) uncertainty framework when the measurement model is significantly nonlinear and the probability distributions of the output (and input) depart appreciably from Gaussian or Student's t-distributions.

Using the Monte Carlo method, a numerical representation of the measurand's probability distribution Y is approximated through repeated sampling from the input quantities' PDF X_i and evaluating the model function for each of these samples. The targeted generation of arbitrary probability distributions that represent X_i can be achieved using the transformation theorem of probability distributions in Equation 2.3.5 or JCGM 101 (2008), C.2. A rectangular distribution $R(0,1)$ is taken as input variable Ψ_{X_n} and the probability density function that is to be generated is $f(x)$. Its inverse function f_k^{-1} can be determined analytically or numerically for each of its k piecewise monotonic sets.

$$\Phi_{Y_n}(y_1,...,y_n) = \sum_{i=1}^{k} \Psi_{X_n}\left(f_k^{-1}(y_1,...,y_n)\right) \left| \frac{\partial f_k^{-1}(y_1,...,y_n)}{\partial(y_1,...,y_n)} \right| \tag{2.3.5}$$

Termination condition for the simulations Based on Y's distribution a multitude of statistics can be calculated for the measurand (JCGM 101 (2008), 5.9). Examples of such statistics are the best estimate, the variance, quantiles and coverage intervals. As these statistics are calculated from a distribution that is sampled from a generally larger population it is clear that the accuracy of the statistics depends a lot on the size of the sampled distribution, i.e., the number of Monte Carlo trials. In order to ensure a sufficiently large number of Monte Carlo trials have been drawn, adaptive procedures generate new sample until a previously set numerical tolerance bound is achieved (JCGM 101 (2008), 7.9). This ensures sufficiently accurate results at the lowest possible cost.

The GUM Supplement 1 (JCGM 101, 2008) provides such an adaptive procedure where Monte Carlo simulations are repeatedly carried out in sets of $\approx 10\,000$ simulations. For each of these sets statistics such as mean, standard deviation and/or quantiles are calculated. Sets of simulations are added to this database until the variance of the calculated statistics falls below the previously defined numeric tolerance.

Properties of Monte Carlo simulations Even though Monte Carlo Methods are a valuable tool to circumvent some of the "basic GUM" limitations there are properties of Monte Carlo simulations that deserve critical discussion as well.

The general suitability and the practical advantage of this class of computational algorithms is a result of its almost certain convergence due to the strong law of large numbers and the central limit theorem (Bronstein et al. (2015), 16.2.5.1+2). On the other side, however, it is sometimes noted that Monte Carlo methods converge rather slowly with a convergence rate of merely $\mathcal{O}(\frac{1}{\sqrt{n}})$ for sample size n (Ballio & Guadagnini, 2004; Mood, Graybill, & Boes, 1974; Müller-Gronbach, Ritter, & E., 2012). Obviously, this aspect needs to be discussed together with the results' accuracy.

Keeping in mind that the basic GUM framework was extended by the Monte Carlo method in order to cope with expanded uncertainties of distributions that deviate from Gaussian-shaped distributions, let's consider sample quantiles and their standard uncertainty (or standard error in statistics literature) to discuss the convergence properties of Monte Carlo simulations. Following the explanations of Wilcox (2005) the variance of the q^{th}-Quantile $\hat{x}_q$ is

$$s^2(\hat{x}_q) = \frac{q(1-q)}{n(\Phi(x_q))^2} \tag{2.3.6}$$

based on n samples of a population with the distribution $\Phi(x)$. Equation 2.3.6 shows that $s^2(\hat{x}_q)$ increases with q approaching the boundaries of its domain $[0, 1]$. In addition to the intuitively expected dependence on n, $s^2(\hat{x}_q)$ also becomes larger for lower values of the probability density function $\Phi(X)$ evaluated at x_q. As a result Monte Carlo methods take especially long to converge in cases they are intended to be used for.

Maritz and Jarrett (1978) suggest a method that estimates the distribution of the quantile $\hat{x}_q$ with a beta distribution

$$s^2(\hat{x}_q) = \frac{x^{\alpha-1}(1-x)^{\beta-1}}{B(\alpha,\beta)} \text{ with } B(\alpha,\beta) = \frac{\Gamma(\alpha)\Gamma(\beta)}{\Gamma(\alpha+\beta)} \tag{2.3.7}$$

This offers a viable path to determine the convergence/accuracy of the Monte Carlo simulations on the grounds of a second method that differs from the original strategy used to generate the data. With Wilcox (2005) stating that all indications are that the Maritz-Jarrett estimator is more accurate than the method based on Equation 2.3.6 there are good reasons to adapt the supplemented GUM framework to a modified termination condition when the sheer amount of data requires efficient calculations.

2.4 The perception of sound in auditoria

In the discussion so far, only physical and theoretical aspects of sound fields and room acoustical single-number quantities have been considered. Of course, this

view is limited as the interpretation of the parameters also has to be seen in light of perception and other influences (Gade, 1982). The literature review of Table 2.1 substantiates that room acoustical quantities are linked to psychoacoustics.

The relevance of the measured spatial variance of room acoustical quantities has to be discussed in relation to the average listener's sensitivity to subtle changes in the sound field and derived parameters. A prominent list of these just-noticeable differences (JND) as a direct quote of data collected earlier by Vorländer (1995) and slightly modified by Bork (2000) (see Table 2.3) can be found in the informative Appendix A of ISO 3382-1 (2009).

Table 2.3: List of just-noticeable differences for terms of the consensus vocabulary.

Consensus vocabulary	Quantity	JND	Study
Strength	G	1 dB	Reichardt and Schmidt (1967)
Reverberance	EDT	rel. 5 %	Seraphim (1958)
Definition	D_{50}	rel. 5 %	J. S. Bradley, Reich, and Norcross (1999)
Clarity	C_{80}	1 dB	Cox, Davies, and Lam (1993)
	t_c	10 ms	Cox et al. (1993)
Source width	LF	rel. 5 %	Cox et al. (1993)
	$IACC$	0.08	Cox et al. (1993)
Envelopment	LG	$\approx$ 5 dB	J. S. Bradley and Soulodre (1995a)

Because the JNDs are noted in ISO 3382-1 (2009), they may seem to carry an authoritative weight. This sometimes obscures that the cited JNDs depend on the experimental methods used in the respective studies (Vigeant et al., 2015). In some cases the perceptual thresholds determined under laboratory conditions are significantly lower than what can be established under more realistic conditions, i.e., in sound fields of real concert halls (Ahearn, Schaeffler, Celmer, & Vigeant, 2009; Höhne & Schroth, 1995; Witew, 2006).

Because perception is the ultimate benchmark for technical findings in auditorium acoustics, it is always important to ensure that the psychological testing conditions are realistic. Thus, in the case of obvious inconsistencies between findings under laboratory conditions and what is experienced in actual concert halls, it may be appropriate to validate suspiciously low JNDs under conditions that match reality.

Additionally there is a fundamental discussion regarding ISO 3382-1 (2009)'s perspective: It is argued that the defined parameters may not entirely reflect

the perception of sound in rooms. As a result, a number of studies are currently being conducted (Lokki, 2013; Neal & Vigeant, 2017; Weinzierl, 2017) to revisit the vector space that perception spans and determine additional features that may be perceived. These studies deviate significantly from the standardized measurements by introducing distributed sound sources to model orchestras that feature clear source directivities. This can be seen as as an invitation to discuss whether ISO 3382-1 (2009) covers the realities of acoustic performance spaces. Unfortunately, however, this trend adds additional, unstandardized complexity to the measurement chain, making it difficult to assess the accuracy and uncertainty of these measurements. Eventually, any newly identified perceptual aspects will be linked to physical properties of sound fields. At this point the question of measurement uncertainty will have to receive closer attention.

3

General Methodology

One of the central research objectives, to determine the measurement uncertainty due to spatial fluctuations of the sound field, was identified in Chapter 1. This section provides the roadmap for the reasoning to answer this question. In the first step, to lay the groundwork, the uncertainty of measured room impulse responses needs to be established, which is closely related to the uncertainty of standardized room acoustical quantities. Based on these findings the target is shifted towards the question of how an uncertain measurement position translates to uncertainty in room acoustical measurements in auditoria.

The tools for this discussion are provided by the GUM framework with the measurement function $Y = f(X)$ as its centerpiece. This function relates input and output quantities to each other (see Figure 2.6), and so sets the foundation for the propagation of uncertainties. The measurement position will serve as the input quantity, while the room impulse response or derived quantities such as clarity can be understood as the output quantities. The limitations of the basic GUM approach and the complexity of sound propagation in rooms (see Section 2.1) suggest an empirical strategy to establish the measurement function.

To keep the complexity of the research question at a manageable level, it makes sense to divide the overall strategy into five subordinate work packages that can be addressed separately.

Determining the uncertainty of acoustical measurements All measurements are subject to uncertain results, and so are measurement series that aim at establishing the measurement function for a specific influence factor. Correctly analyzing the influence of a given uncertainty contribution hence requires knowing the measurement's intrinsic uncertainty. In this first step of the investigation the "baseline" uncertainty of room acoustical impulse response measurements is evaluated. There are numerous studies that have discussed a wide range of possible influence factors, so generic influences can be investigated through a literature review. Factors that are genuine to the used measurement equipment and the pursued strategy require their own, dedicated experiments.

Designing a measurement array The second work package deals with the question of how to collect suitable data to empirically establish the measurement function. To ensure general validity it becomes necessary to sample the sound field in auditoria over sufficiently large areas. Section 5 discusses the requirements and compares different sampling strategies. With the commitment to an automated sampling process, the design of a measurement apparatus is discussed. In the conclusion of this section the properties of the used measurement device are presented and discussed. This includes the influence of the measurement apparatus on the sound field and thus the uncertainty it introduces to the measurement.

Tracking the microphone positions Despite automation, the microphone is placed at its designated position with a finite precision. This, too, is a natural property of any measurement method. As the measurement position plays a rather crucial role in this study's prime research objective, it is appropriate to investigate this aspect in depth. The designated sensor positions are validated by tracking strategies. Based on the time it takes for sound waves to travel from six stationary loudspeakers to the microphones, the actual measurement position and its uncertainty can be determined using multilateration strategies. In Section 6.3 the properties of the used multilateration method are discussed and the uncertainty of the determined measurement position is evaluated.

Establishing the measurement function After these preceding steps the foundation is set to discusses the central aspect of the research question. The measured impulse responses and the available position information are combined to derive the measurement function f. The analysis is based on the comparison of a large number of microphone pairs, and investigates how the sound field changes as a function of distance between compared sensor positions. In line with the GUM framework, the distance between any of the two microphones will be recognized as the primary influence quantity. The output quantity will be the average change in room acoustical single number quantities.

How accurately must a measurement position be defined? With the measurement function established in the previous step it is possible to investigate practical uncertainty aspects. The starting point is the general fact that an established measurement position always features an uncertainty. This leads either to a mismatch between the intended and the actual position in a single measurement or a difference in positions in reproduced measurements. Since this discrepancy implies a range of possible deviations, the resulting uncertainty in acoustical measurements cannot be read directly from the measurement function. Instead, the principle of uncertainty propagation needs to be complied with so

that and the uncertainty in room acoustical measurements can be established based on the measurement position's uncertainty. To address this question, proven strategies such as Monte Carlo methods will be used.

4

Uncertainty of room impulse response measurements

4.1 Introduction

This entire study relies on auditorium impulse response measurements that are analyzed to investigate spatial fluctuations of the sound field. This leads directly to the question of uncertainty in these measurements due to the acoustical measurement chain used and due to other influences on the acoustic conditions that have an effect on the uncertainty.

The discussion in Sections 2.2.2 and 2.2.3 supports the idea that to this day measurement uncertainty in architectural acoustics is addressed mainly from a pragmatic point of view. In room acoustics, the question of validity was the focus of interest when new measurement methods became available. In building acoustics, factors of legal robustness play a role in measurements for quality management and accreditation, which are ultimately met by achieving accepted limits of uncertainty. The underlying studies must be placed in the context of the state of the art (available at the time) and the investigated measurement task. Not all results can be adopted to other measurement methods without targeted customization.

In this chapter, the uncertainty budget of room acoustical impulse response measurements is presented based on a detailed evaluation outlined in the "Guide to the expression of uncertainty in measurement" (GUM) ISO Guide 98-3 (2008) and its introductory document JCGM 104 (2008). Even though a clear focus is placed on the equipment used in this study, the presented method may serve as a blueprint for other studies to evaluate the capabilities of their own measurement chains.

For reasons of brevity, the reader is referred to Appendix A for an organized search for potential uncertainty contributions and for the detailed discussion leading to the combined uncertainty in room acoustical measurements. Although this uncertainty discussion may well contribute to scientific innovation in archi-

tectural acoustics the final result is most important because it provides the basis for the next chapters' line of argument on spatial fluctuations of sound fields.

4.2 Uncertainty budget for room impulse response measurements

The combined uncertainty is determined according to ISO Guide 98-3 (2008), using Equation 2.3.2. Based on the discussion in Appendix A, the influences given in Table 4.1 are considered. The uncertainty inventory is sorted, starting with the largest uncertainty contribution.

Table 4.1: Measurement uncertainty budget for room acoustical impulse response measurements.

Symbol b_i	Uncertainty source	Knowledge base	Uncertainty contribution $u(b_i)$ [dB]
$b_{\text{LS-dir}}$	Directivity	Behler and Vorländer (2018)	0.38
$b_{\text{LS-level}}$	Calibration measurement	Wittstock and Bethke (2005) with revised contributions	0.26
$b_{\text{Mic-cal}}$	Pistonphon calibration	Wittstock and Bethke (2005)	0.21
b_{LTI}	Long term repeatability	Measurements in two auditoria	0.2
$b_{\text{LS-spec}}$	Equalization measurement	Revised contributions based on Wittstock and Bethke (2005)	0.16
$b_{\text{Mic-spec}}$	Flatness of microphone freq. response	32 measurements (LAS)	0.15
b_{Filter}	Octave-band filtering	Wittstock and Bethke (2005) with revised contributions	0.12
$b_{\text{Meteo-}\vartheta}$	Change in temperature	Payne (2004)	0.12

Table 4.1: (continued)

Symbol b_i	Uncertainty source	Knowledge base	Uncertainty contribution $u(b_i)$ [dB]
$b_{\text{Meteo-p}}$	Change in athm. pressure	Payne (2004)	0.07
$b_{\text{Mic-dir}}$	Directivity	measurements in 3° resolution (MMT)	0.07
$b_{\text{Mic-field}}$	Sound field distortion	Payne (2004)	0.011
$b_{\text{Meteo-rh}}$	Change in rel. humidity	Payne (2004)	7.5×10^{-3}
$b_{\text{LS-THD}}$	Loudspeaker nonlinearities	Behler and Vorländer (2018)	$\approx 1\times10^{-3}$
$b_{\text{Amp-THD}}$	Power amplification	Manufacturer's specifications	$\approx 1\times10^{-4}$
$b_{\text{Mic-amp}}$	Amplification linearity	Payne (2004) with revised contributions, own experience	$\approx 1\times10^{-4}$
$b_{\text{Amp-SNR}}$	Amplification noise	Technical documentation	$\approx 1\times10^{-6}$
$b_{\text{Mic-SNR}}$	Microphone noise	Technical documentation	$\approx 1\times10^{-6}$
$b_{\text{D/A-SNR}}$	D/A noise	Technical documentation	$\approx 1\times10^{-8}$
$b_{\text{D/A-THD}}$	Digital-Analog distortion	Manufacturer's specifications	$\approx 1\times10^{-8}$
$b_{\text{clock jitter}}$	clock jitter	Neu (2010)	$\approx 1\times10^{-8}$
$b_{\text{Mic-THD}}$	Microphone nonlinearities	Manufacturer's specifications	$\approx 1\times10^{-9}$

Table 4.1: (continued)

Symbol b_i	Uncertainty source	Knowledge base	Uncertainty contribution $u(b_i)$ [dB]
$b_{\text{A/D-THD}}$	Analog-digital conversion	Manufacturer's specifications	$\approx 1{\times}10^{-9}$
$b_{\text{quant-SNR}}$	Quantization noise	Havelock, Kuwano, and Vorländer (2008), specifications	$\approx 1{\times}10^{-12}$
$u_c(b_{\text{Equip}})$	Combined uncertainty		0.62
$U(b_{\text{Equip}})$	Expanded uncertainty	k=2	1.24

The combined uncertainty given in the last row of Table 4.1 can be calculated according to Equation 4.2.1 with all significant (larger than $1{\times}10^{-2}$ dB) contributions included. Influences that introduce a background noise to the measurement are not recognized.

$$\begin{aligned} u_c(b_{\text{Equip}}) = [&u^2(b_{\text{LS-dir}}) + u^2(b_{\text{LS-level}}) + u^2(b_{\text{LTI}}) + \\ &+ u^2(b_{\text{LS-spec}}) + u^2(b_{\text{Mic-spec}}) + \\ &+ u^2(b_{\text{Mic-cal}}) + u^2(b_{\text{Filter}}) + \\ &+ u^2(b_{\text{Meteo-}\vartheta}) + u^2(b_{\text{Meteo-p}}) + \\ &+ u^2(b_{\text{Mic-dir}}) + u^2(b_{\text{Mic-field}})]^{\frac{1}{2}} \end{aligned} \tag{4.2.1}$$

This leads to a combined standard uncertainty of

$$u_c(b_{\text{Equip}}) = 0.62\,\text{dB}, \tag{4.2.2}$$

which reduces to

$$u_c(b_{\text{Equip}}) = 0.56\,\text{dB} \tag{4.2.3}$$

when not considering the sound power calibration, and to

$$u_c(b_{\text{Equip}}) = 0.52\,\text{dB} \tag{4.2.4}$$

when neither the sound power nor the pistonphon calibration are taken into account.

4.3 Discussion

The direct comparison of the different influences contributing to the measurement uncertainty is quite helpful, since it permits distinguishing between significant and less relevant factors. The hierarchy of significance can be read from Table 4.1. Since the combined uncertainty is strongly determined by the largest individual contributions, it makes sense to focus uncertainty reduction discussions on the top entries such as the loudspeaker.

At the same time, the view can be inverted to address the following argument: Lower ranking elements of the measurement chain in Table 4.1 like amplifiers or AD/DA converters have hardly any significant influence on the combined uncertainty, so their requirements can be reduced without significant effects on the overall uncertainty.

Which influences are to be considered, i.e., which of the combined uncertainty in Equations 4.2.2 to 4.2.4 is relevant, is context-dependent and varies with the discussed research question or how the results are used.

For a detailed discussion regarding individual influences or the strategy pursued the reader is referred to Appendix A.

4.4 Conclusions

This chapter presents the intrinsic uncertainty of room acoustical measurements. To follow an organized approach, quality management principles using a cause-and-effect perspective were used in Appendix A to identify and group different uncertainty contributions. Based on the GUM framework, some 20 influence factors were discussed quantitatively and reasonable uncertainties were determined that characterize the properties of the measurement environment.

As a result, the expected uncertainty of individual time samples in measured room impulse responses due to the used equipment is

$$u_c(\mathrm{b_{Equip}}) = 0.52\,\mathrm{dB}. \tag{4.4.1}$$

This uncertainty will be used in this study's main line of argument to determine the uncertainty of room acoustical single number quantities (see Section 6.2).

5

Design of a measurement array

5.1 Introduction

The theoretical discussions led by Kuttruff and Thiele (1954); Schroeder (1962) and Davy (1981) (see Section 2.1) indicated how the sound field in rooms changes from one position to the next. These discussions exposed the profound reasons for the spatial variance of decay rates. So far, these theoretical findings are not put into practice in auditorium acoustics on a regular basis. This is probably due to two main reasons: First, the findings from theory generally address the quasi-stationary sound field or the reverberant decay and rely on a number of assumptions (i.e., the diffuse sound field) that are not always met in practical situations (Gade & Rindel, 1985). Second, in architectural acoustics the early part of the sound field carries information that is significant for sound perception. This early part of the impulse response depends on the detailed geometry of the auditorium and is hence difficult to predict with general theory.

This is why an empirical investigation is needed to collect a suitable sample with the capacity of showing how all room acoustical quantities vary over space. Such a study must meet specifications from two sides: On the one hand, experiences from previous studies about surveying the acoustic conditions in auditoria should be recognized. On the other hand, it is necessary to collect data that allows a standardized discussion in line with the GUM framework.

In this section, a measurement device is presented that is capable of automatically sampling the sound fields in auditoria. Its design is discussed in three steps: first, establishing the requirements that a measurement device needs to meet in order to collect data that is suitable to target the central research objective; second, presenting the rationale of the design and the apparatus' practical use and, finally, discussing the nature of the collected data.

Parts of this chapter have been published before. As a result, the line of argument shown here features some overlap with previous publications, namely Witew, Vorländer, and Xiang (2017) and Witew and Vorländer (2018). Some of the following ideas are paraphrased from these publications.

5.2 Methodology

5.2.1 Requirements for the measurement setup

Conclusions drawn from previous investigations

The study of de Vries et al. (2001) is this study's starting point, as it was the first to vividly show the spatial fluctuation of room acoustical metrics in a concert hall. Their measurement apparatus, shown in Figure 5.1, consisted of a roughly 3 m-long rail along which a single microphone was moved automatically by pulley. This setup allowed a precise positioning of the microphone. In repeated measurements, the entire structure was moved along a row so that the measured segments of approximately 3 m length could be joined to form a total covered distance of more than 26 m.

Figure 5.1: Measurement setup used by de Vries et al. (2001) in Concertgebouw Amsterdam. Image courtesy of Diemer de Vries and TU Delft.

This measurement strategy skillfully combines two aspects: The relatively small setup achieves precise and automated microphone positioning through motorization, while moving the entire structure allows measurements to be conducted over a wide range. The spatial fluctuations shown in Figure 1.1 highlight the need for a spatial sampling in resolution of about one measurement position every 5 cm. This matches the spatial Nyquist-Shannon sampling theorem as well.

Engaging in a critical discussion sets the stage to develop possible improvements to de Vries et al.'s groundbreaking measurement strategy. Findings by Vorländer and Kuttruff (1985), shown schematically in Figure 5.2, raise a point in illustrating that the room acoustical quantities vary along all spatial dimensions in different room shapes. As a result, sampling along a single straight line may not show the full variation of changes encountered over entire listening areas.

Akama, Suzuki, and Omoto (2010) shows that the process of acoustical measurements in auditoria can be streamlined to a point where it becomes feasible

Figure 5.2: Lateral fraction in rooms with different shapes (the sound source is represented by the white circle; dark areas indicate a high lateral fraction)(after Vorländer and Kuttruff (1985), from Vorländer and Witew (2020)[p.523], Copyright: Verlag Wilhelm Ernst & Sohn GmbH & Co. KG. Reproduced with permission).

to measure the impulse response at every seat. These findings are impressive, as they show that it is not necessary to rely on simulation results when discussing the acoustic conditions in an entire auditorium; it is possible to measure this data. To position the microphone, Akama et al. (2010) used a clamping fixture that was attached to the backrest of a seat, and moved manually in repeated measurements from one position to the next.

Using a similar sampling strategy (Witew et al., 2004), some pittfalls can be pointed out that have to be recognized. When conducting measurements at individual seats, there is always the question of positioning accuracy: Placing a microphone relative to a reference object, such as a seat, that is approximately 50 cm wide will permit a limited accuracy of perhaps 5 cm - especially when the measurement procedure is streamlined in order to measure a comprehensive set of positions within a limited time. Furthermore, in complex geometries (e.g., the auditorium floor rising according to constantly changing slopes), it is rather difficult to determine the absolute position of the reference object when relevant data (i.e., from cross sections) is unavailable. Also, in view of the findings by de Vries et al. (2001) in Figure 1.1, it can be argued that this strategy will not feature the resolution necessary to survey spatial fluctuations in sufficient detail. For all these reasons, impulse responses collected at individual seats are not suitable to discuss the uncertainty in measurements due to spatial fluctuations.

The challenges arising from having to cover large dimensions while maintaining a high resolution can be met with measurements in model scale, as Xiang, Escolano, Navarro, and Jing (2013) have shown. In their study on the acoustic

coupling of two-room volumes, they investigated the sound field using a 1:8 scale model. A motorized microphone was moved automatically in two dimensions with high accuracy. Using this setup, Xiang, Alamuru, Witew, and Vorländer (2018) were able to show the sound propagation in coupled volumes in great detail. Here, too, perspectives arise from the author's own experience (Witew et al., 2012) that should be taken into account. Measurements in model scale often require some form of abstraction as the transition from the natural scale to the reduced model requires a simplification - this can concern the absorption properties of the walls, but also the room geometry. Even though the math to transform measured impulse responses in model scale to natural scale is understood rather well, this conversion between different scales will introduce additional influence factors to the uncertainty budget of Section 4. The benefit of further inflating the uncertainty budget seems unnecessary when measurements in existing rooms are also feasible.

In a pilot study, Witew and Vorländer (2011) investigated how the sound field in a room could be sampled using a measurement array with 24 microphones. Figure 5.3 shows the setup: The heart of the system is an xy-table, which allows a mounted central support and two extension arms to move freely in two dimensions. The 24 microphones are attached to the horizontal arms at regular distances. Tracing an S-shaped pattern with the xy-table resulted in the coverage of a 2.1 m x 2.4 m area with a 5 cm sampling resolution. Obviously, this raises the question of whether this small sampling area can be representative for entire concert halls that may easily have hundreds of square meters of audience area. The collected acoustical data also show that the proximity of the supporting structure to the microphones can lead to disturbed sampling of the sound field.

Figure 5.3: Robot to sample the sound field over an area of 2.1 m x 2.4 m.

While Chapter 7 discusses the measurement function more completely, some aspects about the sampling distribution should be considered here. When introducing the central research question in Chapter 1, the distance between two measurement positions was identified as the input quantity to be examined. This relation can easily be determined from a pairwise comparison of any two sensor positions and their coordinates. To ensure that this comparison is balanced across all two-sensor combinations, the sampling grid needs to have a spatially constant sampling density and be isotropic in the comparison of different measurement positions.

The first requirement suggests a homogeneous and regular sampling grid. The second requirement, however, cannot be achieved with finite and discrete sampling. In a two-dimensional regular Cartesian grid, adjacent sampling points that are closest to each other have one of just four directional relations (i.e., $\pm x, \pm y$) to each other. With larger distances the directional resolution becomes finer. Despite these limitations, a regular, rectangular sampling grid may still be the best choice from a practical perspective. Cartesian sampling can be implemented with relative ease. From theory there is no indication that spatial fluctuations could be anisotropic when the room's geometry features similar dimensions along orthogonal coordinate axes and the discussed frequency is above the Schroeder frequency.

Rectangular sampling could in future studies permit a sound field synthesis to derive a low-pass filtered, continuous representation of the sound field. This sampling strategy, combined with the appropriate analysis, could provide the foundation to discuss the change of the sound field without salient sampling directions (as they exist in the discrete case).

From these experiences the following specifications for the measurement setup emerge:

- Measurements should cover a sufficiently large surface area.
- Large fixtures of the measurement device should to be far away from the microphones. Suspension of the microphones should present a small disturbance to the sound field.
- Microphones must be positioned accurately at known coordinates.
- Measurements should be in a regular but arbitrary high-resolution sampling grid.

(a) Overview of the apparatus.

(b) Carbon truss.

(c) Rolling carriage with actuators.

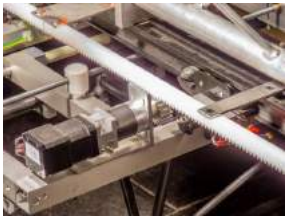

(d) Actuator along the hall's front-rear dimension.

(e) Actuator along the hall's left-right dimension.

Figure 5.4: Measurement device to sample the sound field in auditoria.

5.2.2 Design of a measurement device

Based on these specifications, the device, shown in Figure 5.4, has been designed. It is capable of automatically sampling the sound field in rooms over a surface of 5.30 m × 8.00 m. Its main body consists of standardized aluminum trusses that are commonly used in stage equipment to support lights. The trusses' profile has a triangular cross section of 220 mm width and 195 mm height. The three load-carrying tubes along the length of each truss have a diameter of 35 mm. These trusses form a load-carrying frame structure that is elevated at a 2 m height and supported by a pedestal in each of the four corners. Figure 5.4a shows an overview of the entire device. To enable easy movement on flat surfaces, small rollers are mounted under the structure's supports.

The central truss, running along the hall's front-rear dimension, supports a black double-T beam that is mounted underneath. A rolling carriage is attached that can travel along the rail's full length of 5.30 m (see Figures 5.4c). The carriage is driven through a motorized pinion that acts on a fixed rack mounted parallel to the track of the guide rail and the central cross beam (see Figure 5.4d).

The carriage in turn holds an 8 m carbon truss, running along the hall's left-right dimension. At its ends, the carbon truss is supported by the aluminum frame through a roller bearing and a slide bearing (see Figure 5.4b). This mounting allows the carbon truss and the trolley to move together along the front-rear axis. At the same time, a second stepping motor drives a spindle with a shaft joint which permits moving the carbon truss from left to right over a distance just short of 30 cm (see Figure 5.4e).

The carbon truss carries 32 KE-4-type electret microphones that are held in place through fixtures every 0.25 m. These fixtures consist of thin, 1 m-long carbon tubes with adjustable collars so that the microphones can be lowered to the sampling area about 1.2 m above the floor.

In this setup, the microphones are aligned linearly in fixed steps of 0.25 m and can be moved freely over a surface of 0.25 m × 5.30 m; this composes a coherent sampling area of 8.00 m × 5.30 m in any desired resolution.

5.2.3 Acoustical measurements

Due to the size of the entire apparatus, it takes a trained team of at least four people about 2 h to assemble and 2 h to disassemble the device. In 530 individual measurement runs using 32 microphone channels, the sound field is sampled over a surface of 8.00 m × 5.30 m in a rectangular 5 cm-grid. In between each measurement run, the robot travels from one position to the next. Conducting a measurement series that covers the entire surface at this resolution yields 16 960 impulse responses of the FFT-degree 17. Such a session takes a grand total of about 8 h to complete, including 4 h measurement time and provisions for mounting and demounting.

After setting up the system's hardware and before starting the acoustical measurement series, the proper functioning of the measurement chain is ensured through calibration measurements. Electrical components are equalized through short circuit measurements and calibrated to a voltage reference. The microphones are calibrated through pistonphone measurements, repeated three times to ensure the calibration yielded consistent sensitivity coefficients. The excitation's stop margin and the amplification of the microphone are adjusted to meet the acoustic conditions of the reverberation length and background noise encountered during the measurements.

Measurements in different auditoria

The discussion of analytical approaches in Section 2.1 (i.e., Davy et al. (1979); Kuttruff and Thiele (1954); Schröder (1954)) identifies the superposition of individual modes as the central contributing factor to spatial fluctuations. This

provides important references as to which factors have to be recognized in the measurement series. Importantly, it would have to be ensured that the diffuse sound field dominates the measured sample. In theory this could be achieved by limiting the distance between the microphones and the sound source to ranges larger than the critical distance, i.e., making sure that the direct sound's energy is less than the energy in the diffuse sound field.

When broadening the perspective to include quantities beyond reverberation time and discuss early reflections, the situation becomes a bit more complex. On the one hand, it can be argued that the spatially changing composition of early reflections contributes to a natural large-scale spatial change in the acoustic conditions that has little to do with the phenomenon of fluctuations. On the other hand, however, due to room acoustical quantities that rely on rectangular time windows, it is plausible that isolated, bandpass filtered reflections fluctuate spatially due to the decaying oscillation of the filter. This effect may contribute to spatial fluctuations and, thus, the auditorium's geometry may have an influence. Generally speaking, it seems reasonable to investigate sound fields with different compositions of early reflections.

Over the course of the entire study, numerous measurements were conducted in different auditoria. Although all of this collected data ultimately serves the goal of answering the central research questions, subordinate questions were examined based on the data from individual measurement sessions.

The first measurements were carried out in RWTH Aachen University's *Aula 2* general assembly (see Figure 5.5b) hall as part of Thevissen's (2015) master thesis to prove the concept of such array measurements. Based on an existing mechanical design, a software infrastructure for the control of the stepper motors and the acoustical measurement procedure was developed (Thevissen, 2015).

In a following series of measurements in collaboration with J. Hartl, many conditions were tested. First, measurements were carried out in *Aula 2* under similar conditions (compared to Thevissen (2015)) to investigate the reproducibility of the measured data (see Figure 5.4b). In a separate setup in the large hall of *Eurogress Aachen* (see Figure 5.5c), the repeatability of measurements was investigated through two measurement sets conducted in immediate succession (see Figure 5.4a). In a third set of measurements in *Eurogress*, chairs were removed from underneath the array to investigate how significantly those changes affected the surveyed sound field. In the final measurement session, measurements were conducted in the large hall of the historic town hall of Wuppertal (see Figure 5.5d) to investigate whether the entire processes had matured enough to allow measurements at distant auditoria under strict time constraints.

(a) Aula 1.

(b) Aula 2 (see also Figure 5.4b).

(c) Eurogress Aachen (see also Fig. 5.4a).

(d) Historische Stadthalle Wuppertal.

(e) Rehearsal room of *Aachen Symphony Orchestra*.

(f) Concertgebouw Amsterdam.

Figure 5.5: The auditoria surveyed in this study.

In a following episode, measurement series were conducted in both general assembly halls of RWTH Aachen University, i.e., *Aula 1* (see Figure 5.5a) and *Aula 2*, as documented by Reich (2018). In both halls, four measurement sets were collected, each with the array covering a different section of the room, so that the entire audience area was surveyed. In between these sets the entire array was moved to cover the entire audience area. This series of measurements was designed to investigate whether spatial fluctuations change throughout the room.

The last series of measurements was done in collaboration with H. Hasti, and added measurements of two new rooms to the database. First, *Aachen Symphony Orchestra*'s *rehearsal room* (see Figure 5.5e) was studied. To accommodate orchestras of different sizes and music for different styles, this auditorium features adjustable acoustic panels that were varied between measurements to change the reflection pattern and the room's absorption. These variations set the foundation to investigate congruence with theory (see Section 2.1), i.e., how a change in reverberance and reflection pattern influences spacial fluctuations. Second, *Concertgebouw Amsterdam*'s large hall (see Figure 5.5f) is a renowned landmark in architectural acoustics, and studying its acoustic conditions added to the practical relevance of this study. These measurements also offer a reminiscence to the work of de Vries et al. (2001) and permit comparison between the two different sampling approaches.

5.2.4 Data analysis

From the measured raw impulse responses, some elementary processing is necessary to recognize the sampling strategy and to ease the visual display. At this point, the analysis it not yet targeted at generating the data that will eventually be subject to a discussion of measurement uncertainties; instead, the objective of the analysis is to foster a tangible understanding of the data's properties and evaluate the device's merits.

In a few rare cases, equipment issues occurred during the measurements. Due to frequent movement of the measurement setup, fatigue phenomena became obvious for individual microphone cables. Due to repeated bending of the cables in the flexible duct, cable breaks sometimes occurred, which led to individual microphone dropouts. Such defects occurred in roughly a dozen of the collected impulse responses and only became apparent in the post-measurement analysis through algorithmic and visual inspection. This is regrettable, but in relation to the almost 17 000 flawlessly collected RIRs in each measurement series, it is of little concern.

Even though impulse responses were measured over a frequency range including the octave bands from 125 Hz to 8 kHz, a sampling grid of 5 cm introduces an

upper frequency limit of 3400 Hz while observing the spatial sampling theorem. This yields a reasonable frequency range including the octave bands from 125 Hz to 2 kHz without being subject to spatial aliasing.

5.3 Results

The core goal of the measurements with the array is still, of course, to collect data for the uncertainty discussion. At the same time, this new measurement tool requires experience, which can emerge when new measurement results can be related to the existing body of knowledge. Visualizing measured sound fields can do just that when the collected data is related to the informed expectation of sound propagation phenomena.

5.3.1 Visualization of sound fields

The additional benefit of measurement data collected with microphone arrays is due not only to the larger amount of available data to analyze, but also to the geometric relations the measurement positions have to each other. The RIRs collected with the device described here mark no exception in this regard. The graphical presentation of four-dimensional data (two spatial dimensions and the amplitude of the impulse response over the running time), however, poses known challenges with presentation modalities resulting in only three dimensions for simultaneous display. The microphone data (i.e., RIR at a given time) over the spatial dimensions of the measurement array's sampling area can be shown effectively so that each presented pixel refers to a corresponding sampling position. The energy of the impulse response can be coded in color for a given time, leading to graphical representations such as the ones shown in Figures 5.6 and 5.7. Here, blue colors are used to show low amplitudes and yellow colors high amplitudes, all in logarithmic scale.

In Figure 5.6, the propagation of the first wavefront through a completely empty auditorium (Figure 5.6a) and the same auditorium with chairs (Figure 5.6b) is illustrated. The differences in both measurement scenarios are particularly evident immediately after the direct sound. Amplitudes, spatially behind the direct sound are relatively low in the empty hall. In contrast, the right image (with chairs) shows how the chairs influence sound propagation. The major difference compared to the empty hall is the additional wave pattern that can be seen in the upper part of the right image. From the shape of this pattern (also in time), it is evident that this is the sound that is scattered back from the chairs. The color coding indicates that the scattered sound is of relatively low amplitude.

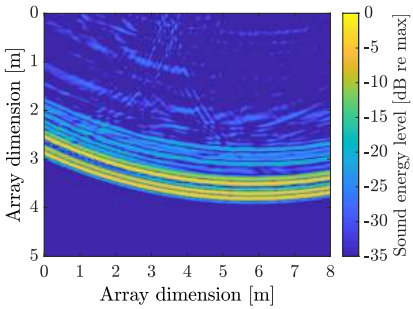

(a) Without chairs.

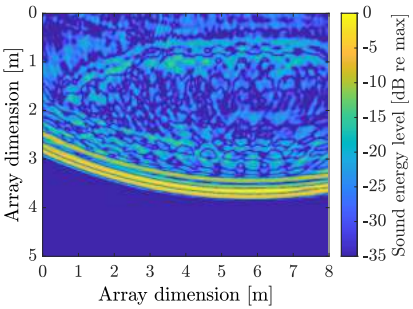

(b) With chairs.

Figure 5.6: Direct sound in *Eurogress Aachen*.

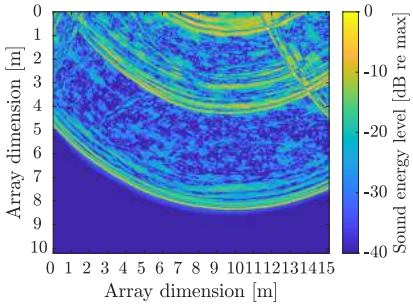

(a) Direct sound.

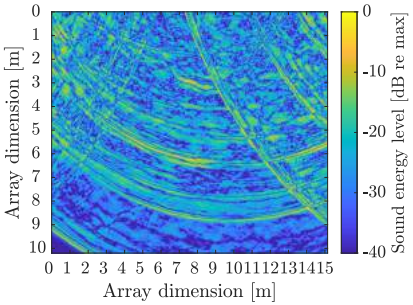

(b) Early reflections.

Figure 5.7: Sound propagation in *Aula 2*.

Figure 5.7 shows how four individual sets of measurements at different positions in a hall can be merged to form a larger and coherent sampling area. These images are intended to provide an intuitive and graphic understanding of the measurements' stability. Although the individual measurement sets are separated by four to 12 hours, they can be combined rather well to form a broader account of the sound field in the room. A detailed discussion of the sound propagation is referred to Witew and Vorländer (2018); Witew et al. (2017).

The next paragraphs discuss specific results relevant to the adequacy of the measurement setup. Obviously, the suitability of the device is determined through its ability to collect data to answer the central research questions.

Influence of the device's structure

Just as microphone properties were discussed as part of the "intrinsic measurement uncertainty" in Chapter 4, the structure's influence on the measurand needs to be evaluated. Looking at Figure 5.6a can provide an idea of how this factor contributes to the measurements. This illustration shows how the direct sound propagates through the measurement device in the otherwise empty auditorium. Apart from the ground reflection immediately following the direct sound, the large blue areas indicate that the room does not feature surfaces that reflect or scatter sound (with short delays) into the sampling area.

This makes this scenario ideal for investigating scattering from the array's structure. Considering Figure 5.4a, the two circular wave fronts concentric to the upper left and right corners of the sampling area can be traced back to scattering from the supporting pillars at the front. A detailed investigation, based on analyrical and empirical considerations, of how the measurement apparatus contributes to the combined uncertainty of the measurements can be found in Appendix B. This discussion concludes with the assessment that the influence of the measurement setup on the measurand can be determined to be

$$u(b_{\mathrm{Setup}}) = 0.35\,\mathrm{dB}. \tag{5.3.1}$$

The uncertainty contribution of the measurement setup's disturbance of the sound field increases the combined uncertainty from 0.62 dB (Equation 4.2.2) to

$$u_{\mathrm{c}}(b_{\mathrm{Equip}}) = 0.71\,\mathrm{dB}. \tag{5.3.2}$$

Precision of the sampling position

One of the preceding paragraphs described how the apparatus positioned the microphones along a rail system. Figure 5.8a shows a detailed perspective of how the carbon truss is held in place along a rail using a roller bearing. To facilitate flexible use in different measurement locations the device needs to be portable and designed to allow easy setup and takedown. By dividing large parts into smaller modules, this requirement is achieved at the price that small discontinuities may form at the connecting joints (see Figure 5.8b). This would not be noteworthy if manufacturing tolerances did not complicate the bearings' ease of movement ever so slightly. When the roller bearing passes the discontinuity in the rail, a sightly greater force is required to move the wheels over the obstacle. At the point when this resistance is not in perfect symmetry at both outer rails, the carbon truss will twist until all forces are equal or the pulleys can pass the obstacle.

(a) The carbon truss is held in place by a roller bearing that can traverse along a rail.

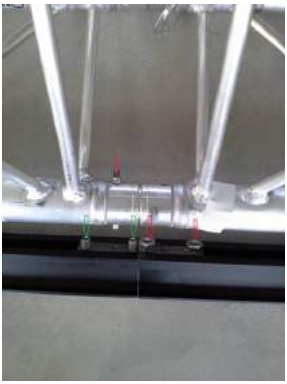

(b) Connecting joints of the rail.

Figure 5.8: Detailed views of the measurement system.

Thus, at these joints there there is a chance of small discrepancies, say 3-4 cm, between the intended and the actual sampling positions. Observing this "jitter" in sampling positions requires a very close examination of the color maps. The jitter appears in Figure 5.6 as a discontinuity along the x-axis, e.g., at the y-intersections of approximately 2.5 m.

5.3.2 Data for the uncertainty discussions

Deriving the measurement function f is of central importance for the discussion of measurement uncertainties. That's why it is important that the collected data be suitable for this analysis. Previously, pilot studies (Witew, Dietrich, de Vries, & Vorländer, 2010; Witew, Dietrich, Pelzer, & Vorländer, 2013) showed how the collected data from regularly sampled sound fields could be processed to determine the model function f. The rationale to establish f is discussed in detail in Section 7.

5.4 Discussion

In general, the presented device is capable of sampling the sound field in rooms over relatively large areas and in relatively high resolutions. The shown images (Figures 5.6 and 5.7) and the calculated animations (Witew & Vorländer, 2018; Witew et al., 2017) allow an intuitive illustration of sound propagation in rooms and present a new perspective on wave field phenomena such as sound scattering

and reflections. In particular, the sampling of merged areas that jointly cover surfaces on the order of 15 m x 10 m with more than 60 000 measured impulse responses (see Figure 5.7) seems to be beyond the scope of previous publications.

The spatial relation between the microphones allows identifying subtle features of measured impulse responses that can be associated to structures in the room in a way that has not been possible before. This is particularly evident when comparing the propagation of the direct sound in *Eurogress Aachen* with and without chairs (Figure 5.6), or the detailed analysis of the sound field in *Aula 2* or *Concertgebouw Amsterdam* in Figure 5.7 or in Witew and Vorländer (2018).

Problem awareness

Due to the design of the measurement apparatus, only auditoria with flat, planar audience areas have been surveyed. From a statistical point of view, this limits the diversity of the collected sample and, hence, should be recognized. From the discussed fundamentals (see Section 2.1 and Davy (1981); Kuttruff (2000)), it can be seen that the modal density is the main factor influencing the spatial fluctuations. For its part, the modal density is independent of the detailed room geometry as long as the auditorium's general size and the surfaces' absorption properties remain unchanged. Furthermore, special cases that feature focal points or room dimensions with integer multiples of each other have to be excluded. On these grounds, it is unlikely that this limitation in sampling has any appreciable impact on the collected data.

Figure 5.6a shows that the measurement device affects the measurand via back-scattering of sound from the array's supporting structure. The detailed discussion of this disturbance is deferred to Section B, where the back-scattering is treated as a regular uncertainty contribution and its magnitude is investigated using Kirchhoff's diffraction formula and empiric approaches. This leads to a result that quantifies the uncertainty due to the measurement device's influence on the sound field.

The restricted capability to move and position microphones, due to design-related manufacturing tolerances, raises the question of whether the validity of the collected data is diminished. To place this discussion on a solid foundation, steps were taken to determine the actual microphone positions using a multilateration strategy. Details of this concept are discussed in Section 6.3. Knowing a microphone's actual position provides the means to faithfully assess the significance potential problem. On the one hand, this limitation in the position accuracy can be interpreted as imperfections of the sampling grid that introduce a positional jitter to the measurement. This uncertainty can be assessed according to the known rules (see Section 4) that have already worked rather

well for clock jitter. On the other hand, the actual knowledge of the measurement position may well enhance and increase the accuracy of the analysis compared to the alternative assumption that a planned sampling location was probably attained.

Figure 5.7 shows the merged sampling areas of *Aula 2*. Discontinuities seem subtle; however, they can be identified when specifically sought after. It is clear that this is due to the relatively long duration of some 4 h it takes to complete a single set of measurements. This perspective may be seen as an additional take on LTI uncertainty as a contributor to the intrinsic uncertainty of Chapter 4: The fact that neighboring sampling fields align quite closely is an argument that time invariances may not be severe problems after all. Whether this attitude can persist when discussing the measurement function will be examined in Chapter 8, based on reproducibility and repeatability measurements.

Finally, the technical failure of microphones during the sets of measurements should be addressed. These "dropouts" introduce gaps into the sampling area that are detrimental to the graphical representation. In regard to the uncertainty discussion, however, such voids in the data space seem tolerable although regrettable. This assessment is based on the observation that isolated and sparse microphone dropouts mean that individual pairs of compared sensors can no longer be evaluated. With $n = 16960$ microphones, each microphone can be compared to $n-1$ microphones, leading to a total number of $n(n+1)/2$ comparisons (Bronstein et al., 2015, 1.2.4). In this order of magnitude the change in sample size due to "losing" a few microphones is not critical as the distribution of distances between microphones remains generally unchanged.

5.5 Conclusions

- The previously described measurement system provides a method capable of sampling the sound field in auditoria covering large areas in high resolution. This section discusses the general properties of the collected data.
- Through the graphical representation of this data, the sound propagation in rooms was impressively visualized. Covering individual and combined sampling areas that span entire auditoria is unprecedented.
- Despite minor flaws, the collected data is relevant and suitable to investigate spatial fluctuations of sound fields in rooms.
- Based on the detailed investigation of a measurement series, the influence of the measurement setup on the measurand was determined to be

$$u(b_{\mathrm{Setup}}) = 0.35\,\mathrm{dB}. \tag{5.5.1}$$

- The uncertainty contribution of the measurement setup's disturbance of the sound field increases the combined uncertainty of individual time samples in measured room impulse responses from 0.62 dB (Equation 4.2.2) to

$$u_{\mathrm{c}}(b_{\mathrm{Equip}}) = 0.71\,\mathrm{dB}. \tag{5.5.2}$$

The revised combined uncertainty in Equation 5.5.2 serves as the input quantity for the uncertainty discussion of room acoustical quantities (Chapter 6). The acoustical data collected with the array forms the foundation to establish the measurement function (Chapter 7).

6

Uncertain input quantities of the measurement function

6.1 Introduction

The most important prerequisite for a GUM conforming uncertainty discussion is the measurement function (or model function) that maps the input quantities of a measurement to the final result. If this transfer function cannot be determined analytically, empirical methods are also valid.

Because a potentially large number of individual measurements are taken to sample the model function, the ability to reduce the data is importantant, so permitting a clear view on the essentials. In the statistical analysis of measured data, it is a common practice to fit and summarize the results, i.e., through (nonparametric) regression. It is well known that the absence of error-in-variables models can lead to incorrect estimates of the consolidated curves (Carroll, Ruppert, Stefanski, & Crainiceanu, 2006, Ch.1). In the simplest case of linear regression, the slope of the regression line is systematically underestimated by the so-called regression dilution (Carroll et al., 2006, Ch.3). In nonlinear regressions, Griliches and Ringstad (1970) expect even greater errors.

Determining the measurement function is essentially a nonparametric regression (see Section 7), making it important to know the uncertainty of the input data, when aiming to obtain an unbiased model function. In this study, the measurement function maps the distance between two measurement locations to a change in room acoustical quantities. As a result, both the measurement positions and the room acoustical parameters are candidates of uncertain input variables that will be discussed in this chapter.

Section 6.2 investigates the uncertainty of room acoustical parameters is investigated by propagating intrinsic measurement uncertainty determined in Sections 4 and B through the functional definition of the room acoustical parameters. This yields their output uncertainties according to the rules of the GUM.

Section 6.3 addresses a method to determine the microphones' position dur-

ing the measurement and its positional uncertainty based on a multilateration paradigm.

6.2 Uncertainty of room acoustical quantities

The uncertainty of room acoustical quantities, i.e., strength and clarity, has already been discussed by Vorländer (2013) in regard to room acoustical simulations. Although the presented method is also valid for acoustical measurements, there are some particular differences that warrant an independent discussion: In simulations, uncertainties are due to the implemented physical (sound propagation) model and the input data of the calculated scenario, whereas in measurements inadequacies of the measuring equipment play a prominent role. Additionally, for measurements, the uncertainties of the input quantities are available in logarithmic scale. Also, the findings of Vorländer's (2013) fundamental investigation are extended by the uncertainties of other room acoustical quantities that have not been discussed before.

6.2.1 Methodology

To discuss the uncertainty of room acoustical quantities, the standardized GUM framework, whose core concept is given in Equations 2.3.2 and 2.3.3 and requires the partial derivatives of the measurement function in respect to all uncertain input variables, can be used. Since this chapter addresses the uncertainty of the input variables, the concept of the measurement function here refers to the propagation of the RIR's uncertainty to room acoustical quantities. The measurement function is, hence, the calculation formula to determine metrics such as reverberation time, clarity and the like.

The starting points of this study are the influence quantities determined as part of the intrinsic measurement uncertainty (Section 4) and the measurement setup (Appendix B). The intrinsic measurement uncertainty budget leads to a combined standard uncertainty of 0.71 dB.

Handling random and systematic uncertainty contributions.

A closer look at the uncertainty contributions in Table 4.1 makes it clear that the individual factors do not contribute in the same way to the uncertainty of the individual samples of an impulse response. While the pistonphone calibration of the microphone has a systematic effect on all samples due to the same correction term, the uncertainty contribution of the loudspeaker's directivity is random from sample to sample.

In ISO Guide 98-3 (2008)[E.3], the introduction of (uncertain) correction factors β_r and β_s permits recognizing random and systematic effects as shown in Equation 6.2.1. In this view, $p_x(s_j)$ represents the impulse response's raw (uncorrected) sound pressure at the sampling time s_j. Both βs are linked to the correction term b through Equation 6.2.2. β_r has an expected value of one, while b_s may be nonzero based on a calibration measurement. $p_y(s_j)$ is the corrected sound pressure at the sampling time s_j.

$$p_y(s_j) = p_x(s_j)\beta_\mathrm{s}\beta_\mathrm{r} \tag{6.2.1}$$

with

$$\beta = 10^{0.1b} \tag{6.2.2}$$

The intrinsic uncertainties of Table 4.1 can be sorted into Tables 6.1a to indicate systematical and random effects. The combined uncertainties given at the bottom of their respective tables reflect the statistic properties of both effects and thus βs' variance. Influence factors that are not recognized in Table 6.1a lead to an uncertainty $u(p_x)$. As these contributions are individually less than 0.01 dB, it is reasonable to assume that they are insignificant (ISO Guide 98-3, 2008, 3.4.4). The variance of β_r has to be considered for each sample s_j individually, whereas the variance of β_s is global.

Discussing room acoustic quantities

Energy decay curve The basis for determining the reverberation time is the backward integrated impulse response (Schroeder, 1965), which leads to the energy decay curve $E(t)$.

$$E(t) = \int_t^\infty p^2(\tau)\mathrm{d}\tau = \int_0^\infty p^2(\tau)\mathrm{d}\tau - \int_0^t p^2(\tau)\mathrm{d}\tau \tag{6.2.3}$$

Because the running variable of the energy decay curve (EDC) is the integration limit, it can be supposed that the uncertainty $u\,(E(t))$ is not the same for all t, but increases with longer integration intervals. The definition of the energy decay curve as a single integral suggests a maximum uncertainty at $t = 0$. This would be detrimental, since the earliest part of the EDC is evaluated to determine the early decay time (EDT), and it would be beneficial if this segment could be determined as accurately as possible. In a slightly mitigated form, this argument holds for the technical reverberation times as well.

Table 6.1: Uncertainty contributions to impulse response measurements.

Symbol b_i	Uncertainty contribution $u(\mathrm{b}_i)$ [dB]
$\mathrm{b}_{\text{LS-level}}$	0.26
$\mathrm{b}_{\text{Mic-cal}}$	0.21
$\mathrm{b}_{\text{LS-spec}}$	0.16
$\mathrm{b}_{\text{Mic-spec}}$	0.15
$\mathrm{b}_{\text{Filter}}$	0.12
$\mathrm{b}_{\text{Meteo-}\vartheta}$	0.12
$\mathrm{b}_{\text{Meteo-p}}$	0.07
Combined uncertainty $u_{\mathrm{c}}(\mathrm{b_s})$	0.44

(a) Systematic effects.

Symbol b_i	Uncertainty contribution $u(\mathrm{b}_i)$ [dB]
$\mathrm{b}_{\text{LS-dir}}$	0.38
$\mathrm{b}_{\text{Setup}}$	0.35
b_{LTI}	0.2
$\mathrm{b}_{\text{Mic-dir}}$	0.07
$\mathrm{b}_{\text{Mic-field}}$	0.011
–	–
–	–
Combined uncertainty $u_{\mathrm{c}}(\mathrm{b_r})$	0.56

(b) Random effects.

Expressing the decay process as the difference of two integrals, in which the first part serves as a normalization, may indicate a solution. By normalizing the EDC to 0 dB at $t = 0$, the first integral and thus the associated uncertainty is dropped. The uncertainty of $E(t)$ now rises steadily as t increases. Equation 6.2.3 can be expressed as a sum of discrete samples, yielding

$$E(s_j) = 10 \log_{10} \left(1 - \frac{\sum_{k=1}^{j} p^2(s_k)}{\sum_{k=1}^{\infty} p^2(s_k)} \right). \tag{6.2.4}$$

The sound pressures p in Equation 6.2.4 contain the correction factors β for random and systematic effects. β_{s} can be separated from both sums and thus canceled from the fraction entirely. As a result, only random effects are relevant for the uncertainty of the energy decay curve. The energy of the sound pressure in Equation 6.2.4 therefore depends on the correction term b_{r} as follows:

$$p^2(s_j) = p_x^2(s_j) 10^{0.2 b_{\mathrm{r}}}. \tag{6.2.5}$$

Based on the step-by-step procedure in Appendix C, the uncertainty of the energy decay curve is given through:

$$u^2\left(E(s_j)\right) = 4\left(\frac{1}{\sum_{k=j+1}^{\infty} p^2(s_k) \times \sum_{k=1}^{\infty} p^2(s_k)}\right)^2 \times$$
$$\times \left[\left(\sum_{k=j+1}^{\infty} p^2(s_k)\right)^2 \sum_{k=1}^{j} p_x^4(s_k) + \left(\sum_{k=1}^{j} p^2(s_k)\right)^2 \sum_{k=j+1}^{\infty} p_x^4(s_k)\right] \times$$
$$\times\, u^2\left(b_\mathrm{r}\right). \tag{6.2.6}$$

The first factor's denominator decreases as k increases which makes the overall result of Equation 6.2.6 larger, thus confirming the introductory hypothesis. On closer inspection, however, it becomes clear that this is not due to the notation of the integral in Equation 6.2.3, but to the fact that the logarithm has a very large slope for very small values. Uncertainties of small sound pressures are thus greatly amplified.

Reverberation Times The energy decay curve is approximated by a linear regression (Bronstein et al., 2015, 16.3.4.2), and the reverberation time is reciprocal to the regression's slope m:

$$T_\mathrm{RT} = \frac{60}{m}. \tag{6.2.7}$$

Linear regression is a common analysis tool in research and technology. The uncertainty discussion of both regression parameters is sometimes considered an introductory problem in metrology (Wiese and Wöger (1999)[Ch. 5], Squires (2001)[App. C]). Therefore, the reader is referred to Appendix C, in which the uncertainty of reverberation times is discussed with respect to acoustical particulars. This leads to the following expression, in which l refers to half the number of samples that fit into the reverberation time's evaluation period and the EDC's evaluated dynamic range ΔL.

$$u^2(T_\mathrm{RT}) = \left(\frac{2l-1}{2l}\frac{360}{\Delta L(l+1)(2l+1)}\right)^2 \sum_{j=1}^{2l} (j-l)^2\, u^2\left(E(s_j)\right) \tag{6.2.8}$$

Equation C.2.9 identifies some of the factors that influence the reverberation times' uncertainty. The sum contains the weighted uncertainty of the EDC curve, which becomes more and more uncertain as the running time of the decay progress

increases. The squared weighting causes the early and the late decay to have a stronger effect on the reverberation times' uncertainty. The squared fraction can be interpreted as a sensitivity coefficient that amplifies the result of the sum. The variables in the fraction's denominator are inversely proportional to the reverberation times' uncertainty, i.e., larger dynamic ranges ΔL and longer reverberation times ($\widehat{=}$ larger l) reduce the uncertainty.

Clarity The starting point for the uncertainty discussion of the clarity metric is its definition based on the works of Reichardt et al. (1974), its standardization in ISO 3382-1 (2009) and its equivalent for discretely sampled impulse responses $p(s_i)$ as shown in Equation 6.2.9.

$$C_{t_\mathrm{e}} = 10\log_{10}\frac{\int_0^{t_\mathrm{e}} p^2(t)\mathrm{d}t}{\int_{t_\mathrm{e}}^{\infty} p^2(t)\mathrm{d}t} \widehat{=} 10\log_{10}\frac{\sum_{j=1}^{n_\mathrm{e}} p^2(s_j)}{\sum_{j=n_\mathrm{e}}^{\infty} p^2(s_j)} = 10\log_{10}\frac{\sum_{j=1}^{n_\mathrm{e}} p^2(s_j)}{\sum_{j=n_\mathrm{e}}^{n_\mathrm{cp}} p^2(s_j) + E_\mathrm{comp}} \tag{6.2.9}$$

$$= 10\log_{10}\frac{E_\mathrm{early}}{E_\mathrm{late} + E_\mathrm{comp}}$$

Lundeby et al. (1995) add a compensation term to recognize the influence of background noise. Comparable approaches to tackle the noise problem may exist, but this reference is intended to point to a specific definition of an algorithm to avoid making the uncertainty discussion ambiguous.

For the calculations that lead to the uncertainty, the reader is again referred to Appendix C. Due to the way the input quantities are related to each other in Equation 6.2.9 and due to the relatively complex algorithm to determine Lundeby et al.'s compensation energy E_comp, the mathematical expressions become convoluted quickly. Presenting a closed-form expression for the uncertainty of the clarity metric hinders the flow of the arguments and does not aid understanding. For the sake of brevity the solution is given in the Appendix C.

Definition - Deutlichkeit The definition metric as developed by Meyer and Thiele (1956) is closely related to the clarity parameter through Equation 6.2.10.

$$D_{t_\mathrm{e}} = \frac{1}{1 + 10^{-0.1 C_{t_\mathrm{e}}}} \tag{6.2.10}$$

Using Equation 2.3.2, this yields the uncertainty for the definition metric:

$$u^2\left(D_{t_\mathrm{e}}\right) = \left(\frac{\partial D_{t_\mathrm{e}}}{\partial C_{t_\mathrm{e}}}\right)^2 u^2\left(C_{t_\mathrm{e}}\right) = \left(\frac{\log_\mathrm{e}(10)}{10}\frac{10^{-0.1C_{t_\mathrm{e}}}}{\left(1+10^{-0.1C_{t_\mathrm{e}}}\right)^2}\right)^2 u^2\left(C_{t_\mathrm{e}}\right) \tag{6.2.11}$$

Strength To determine the uncertainty of the strength parameter as introduced by Wilkens (1977), the required tools are already available. The starting point is the standardized formula from ISO 3382-1 (2009) that is re-written to recognize the discretely sampled impulse response. Identical to the strategy pursued in the clarity metric's uncertainty discussion (see Appendix C), the numerator in Equation 6.2.12 can be understood as a sum of the energy components.

$$G = 10\log_{10}\frac{\int_0^\infty p^2(t)\mathrm{d}t}{\int_0^\infty p_{10}^2(t)\mathrm{d}t} = 10\log_{10}\frac{\sum_{i=1}^\infty p^2(s_i)}{E_{10\mathrm{m}}} = 10\log_{10}\frac{E_\mathrm{early}+E_\mathrm{late}+C_\mathrm{comp}}{E_{10\mathrm{m}}} \tag{6.2.12}$$

The denominator features the source's free field energy at a 10 m distance. The denominator's uncertainty is, hence, identical to the uncertainty of the loudspeaker level $u(\mathrm{b_{LS\text{-}level}})$ discussed in Section 4. Using Equation 2.3.2, the derivative of Equation 6.2.12 with respect to each of the four variables leads to the following uncertainty for the strength parameter

$$u^2(G) = \left(\frac{10}{\log_\mathrm{e}(10)}\right)^2\left(\frac{u^2\left(E_\mathrm{early}\right)+u^2\left(E_\mathrm{late}\right)+u^2\left(C_\mathrm{comp}\right)}{\left(E_\mathrm{early}+E_\mathrm{late}+C_\mathrm{comp}\right)^2}+\frac{u^2\left(E_{10\mathrm{m}}\right)}{E_{10\mathrm{m}}^2}\right). \tag{6.2.13}$$

This notation suggests that the uncertainty of the early, late and compensated energies, that were a result of the clarity discussion, can be readily applied here, too. While mathematically correct, it needs to be recognized that unlike in the clarity discussion, the correction term for systematic effects β_s cannot be factored and removed from Equation 6.2.12. Consequently, systematic effects have to be recognized in Equation 6.2.13.

In this study, however, systematic effects still do not have to be recognized, as differences in room acoustical quantities are evaluated to determine the primary measurement function. Based on elementary properties of the logarithm

(Bronstein et al., 2015, 1.1.4.3), the difference in strength ΔG can be represented as a simple fraction. In this notation, the free field normalization $E_{10\mathrm{m}}$ and the correction for systematic effects β_s can be factored and canceled. This simplifies Equation 6.2.13 to the point where the uncertainty of the free field reference can be omitted and the uncertainty of the energies can be calculated according to Equations C.3.3, C.3.4 and C.3.13.

Center time The uncertainty discussion of the center time metric follows the sucessfully adopted path of the previous uncertainty discussion. First, Kürer's (1969) originally time-continuous definition is transformed into its time-discrete equivalent. Next, to simplify the handling of the GUM's Equation 2.3.2, the arbitrarily chosen sample s_k is isolated from the t_c definition.

$$t_\mathrm{c} = \frac{\int_0^\infty t p^2(t)\mathrm{d}t}{\int_0^\infty p^2(t)\mathrm{d}t} = \frac{\sum_{j=1}^{\infty} s_j p^2(s_j)}{\sum_{j=1}^{\infty} p^2(s_j)} = \frac{s_k p^2(s_k) + \sum_{j\neq k} s_j p^2(s_j)}{p^2(s_k) + \sum_{j\neq k} p^2(s_j)} = \frac{s_k p^2(s_k) + \gamma_k}{p^2(s_k) + \delta_k} \tag{6.2.14}$$

This leads to the following expression for the uncertainty of the center time:

$$u^2(t_\mathrm{c}) = \sum_{\forall k} \left(\frac{\partial t_\mathrm{c}}{\partial p^2(s_k)} \right)^2 u^2(p_k^2) \tag{6.2.15}$$

with

$$\frac{\partial t_\mathrm{c}}{\partial p^2(s_k)} = \frac{s_k\delta_k - \gamma_k}{\left(p^2(s_k) + \delta_k\right)^2} = \frac{\sum_{j=1}^{\infty} (s_k - s_j) p^2(s_j)}{\left(\sum_{j=1}^{\infty} p^2(s_j) \right)^2}. \tag{6.2.16}$$

For a complete uncertainty discussion, the partial derivatives of Equation 6.2.15 must be determined with respect to all uncertain variables. As this should generally include the sampling times s_k, Equation 6.2.15 should also feature a sum of the partial derivatives with respect to all s_k. Since the uncertainty associated with the sampling times $u(s_i)$ is regularly regarded as insignificantly small, this step can be waived.

As a first side note, the partial derivatives of the center time in Equation 6.2.16 differ significantly from the derivatives of the other quantities, as the coefficients of the numerator's sum are different for each k. Although these coefficients (as

a function of k) differ from each other only by a simple shift operation, this variation increases the memory requirement/computing time to determine $u^2(t_c)$ immensely. In light of the large number of collected impulse responses, this analysis requires high performance computing.

As a second side note, the compensation energy was not considered when calculating the center time. This is due to the scaling by s_j of the impulse response's individual samples $p^2(s_j)$. Since the compensation energy only contributes minimally to the uncertainty, more comprehensive calculations have been avoided for the sake of simplicity.

Validating through redundancy

In view of the seemingly complex formulas for the single-number quantities and their uncertainties, there is a need for thorough quality control: this validation has been carried out in two stages. First, all equations have been independently developed by two researchers, namely David Kliesch (as part of his supervised master thesis) and Ingo Witew. Second, the analytic findings were compared to Monte Carlo simulations.

This second validation stage is motivated by concerns that the relatively simple standard GUM strategy (first-order Taylor approximation) may not be sufficient to propagate the uncertainties correctly. After all, the extensions to the GUM JCGM 101 (2008) provide alternatives for calculating error propagation with Monte Carlo methods. These alternatives are significantly more costly to calculate, but they should be preferred if the standard GUM method yields significant errors.

From the large number of impulse responses in a given measurement series (i.e., 16 960 RIRs), a smaller sample of almost 1 %, chosen to uniformly cover the entire survey area, was taken. The uncertainty of the various room acoustical parameters is available using the standard GUM method based on the previously derived formulas. Additionally, the uncertainties for the validation subgroup were determined using a Monte Carlo Method (JCGM 101, 2008). The validation procedure used, however, was simplified to the point that a fixed number of 2000 Monte Carlo trials were carried out, in contrast to stopping after reaching a dynamic termination criterion. Ideally, both strategies lead to the same results. Thus, if the uncertainties determined with the standard GUM method are plotted against the Monte Carlo uncertainties, the sample under investigation would have to be located along the bisecting line between the coordinate axes.

Due to the random nature of the Monte Carlo method and the fixed trial size, a residual dispersion of results is to be expected. However, when the results of both calculation methods are sufficiently similar, this can be considered proof

that the standard GUM method is sufficiently accurate. Such a result would also suggest that the algorithms to calculate the GUM uncertainty were implemented correctly and that they provides valid results. Conversely, however, it is not conclusive to suspect an implementation error when both results differ greatly. Instead, it must then be discussed whether the first-order Taylor approximation is sufficiently accurate for the uncertainty discussion pursued here.

The calculation of the room acoustical quantities was also verified with two independently implemented routines (i.e., the author's own implementation and the ITA-Toolbox for Matlab). Results of this comparison do no need a further discussion, as both algorithms lead to identical results.

6.2.2 Results

Energy decay curve

The starting point for calculating the reverberation times is the energy decay curve according to Formula 6.2.4. Figure 6.1 shows the EDC for an arbitrarily chosen impulse response in blue. The uncertainty of the decay curve can be determined from Equation 6.2.6, and is shown as the interval between the red and the blue curves. Based on the assumed sample uncertainty of the input impulse response of $u(\mathrm{b}_r) = 0.56\,\mathrm{dB}$, the EDC is subject to an uncertainty of about 0.03 dB. Since the relatively large dynamic range of the decay curve cannot be reasonably displayed along with the relatively small uncertainty, the standard uncertainty is amplified by a factor of 100 in the figure.

The dashed yellow line indicates the standard uncertainty determined using Monte Carlo simulations with 2000 trials. Both calculations are based on the same assumptions regarding the uncertainty of the individual samples of the impulse response. The red and the yellow uncertainty curves are in very good agreement.

On closer inspection, there is evidence that the standard uncertainty of the EDC is not constant with 0.03 dB, but instead increases moderately with the running time of the impulse response. This confirms the algebraic findings, but the effect is very small and only becomes significant at very small amplitudes when uncertainty rises above all limits. This can be seen in Figure 6.1 at around 3 s. Apart from such singularities, it seems to be helpful to have a single value at hand to indicate the uncertainty of the EDC with about 0.03 dB.

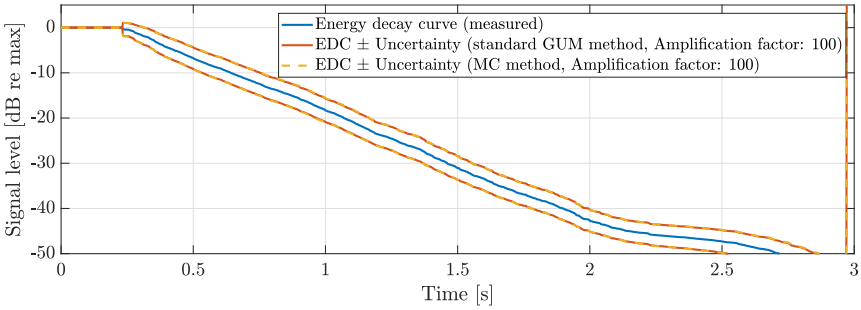

Figure 6.1: Measured energy decay curve (blue) and its 100-fold-amplified uncertainty (dashed orange and yellow).

Reverberation time

The different reverberation times EDT, T_{10}, T_{20} and T_{30} are determined from the energy decay curve. While the drop in level between 0 dB and −10 dB is evaluated to determine EDT, the level drop starting at −5 dB is analyzed for the technical reverberation times T_{xx} (ISO 3382-1, 2009).

Figure 6.2 shows the distribution of the measured early decay times and their associated standard uncertainties for all of the surveyed auditoria. In general, the early decay times fully cover a range from just above 0.5 s to just short of 3 s. This value range emphasizes the validity of the collected data set. Section 2.1 shows the significance of the modal quality factor on the variance of the sound field over space and time. By covering a full range of reverberation times that can be encountered in auditoria, the collected data set, hence, covers modal quality factors over the full range as the driving force of spatial fluctuations.

With a standard uncertainty determined to be less than 1 ms, the EDT can be calculated with sufficient accuracy for the vast majority of applications. In a direct comparison of the EDTs' uncertainty in *Concertgebouw* (orange) and *HSH Wuppertal* (black), it can be seen that the uncertainty differs significantly in both rooms. It is also noticeable that the uncertainties of the determined reverberation times are not the same across locations in an auditorium: In both *Aula 1* (red) and *Concertgebouw* (orange), the uncertainty at the different sampling fields differs. In order to identify the cause of these differences, a more detailed investigation beyond the scope of the present study would be required. An ad hoc investigation leads to the hypothesis that impulse responses with high signal amplitudes (direct sound and isolated reflections) tend to yield larger uncertainties in the reverberation time.

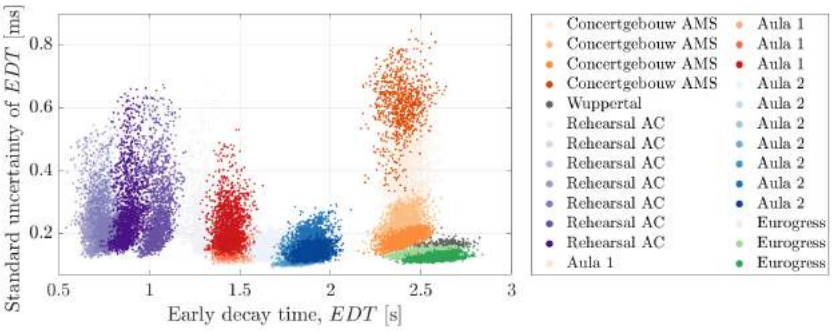

Figure 6.2: Broadband early decay times and the associated standard uncertainty in different auditoria.

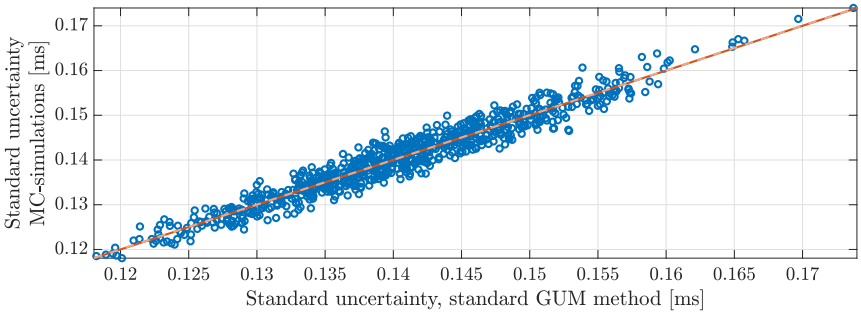

Figure 6.3: Comparison of uncertainties for EDT determined with different methods. The red line marks the identity between both methods.

The validity of the uncertainty calculation can be discussed for EDT by considering Figure 6.3. In this figure, the uncertainties calculated using both valid GUM methods are plotted against each other. Apart from the stochastic noise of the Monte Carlo method, the results are identical, since they are clustered around the red line that denotes the identity of both strategies.

For additional perspective, Figure 6.4 shows the range of T_{30} as measured in the different auditoria. In principle, the data shows a similar pattern to Figure 6.2 for the EDT. Nevertheless, differences are evident, too: the uncertainty for T_{30} is much smaller than that of the EDT, and the range of T_{30}s measured in individual auditoria is smaller. This makes the gaps in the covered range of values across all auditoria slightly larger, but the basic argument regarding the suitability of

the measurement results remains valid.

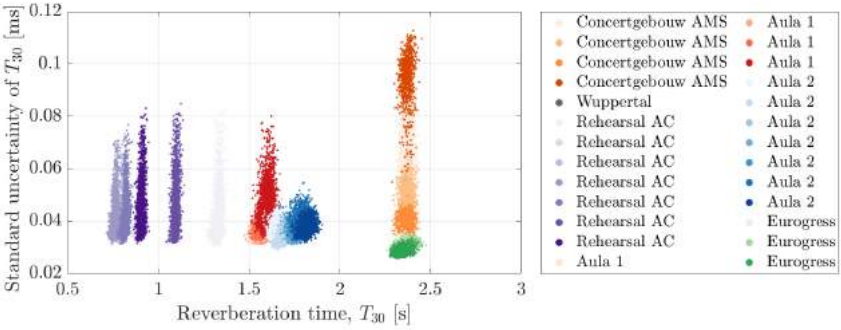

Figure 6.4: Broadband reverberation times T_{30} and the associated standard uncertainty in different auditoria. The color palettes are the same as in Figure 6.2.

Clarity

The range of values spanned by the measurements and their associated uncertainty can also be reported for the clarity parameter. Figure 6.5 illustrates that the auditoria for orchestral music (*Concertgebouw Amsterdam*, *Historische Stadthalle Wuppertal* and *Eurogress Aachen*) show the lowest clarity values, whereas lecture rooms and the *rehearsal room* feature successively higher values. Here, too, it can be seen that the full spectrum of the reasonable clarity range is covered without gaps. As before, these results underline the suitability of the data set.

To check the validity of the standard GUM method for the uncertainty discussion of the clarity quantity, the results of the independent uncertainty calculations are plotted against each other in Figure 6.6. The solid red line marks the identity of both methods. Apart from the stochastic noise, a clear agreement of the results is evident. This observation can be expressed more precisely through the broken line that denotes to the linear regression. The similar slope of both lines indicates that both methods lead to similar results. A small offset of 0.0008 dB [unit $u(C_{80})$] between the two curves indicates that Monte Carlo simulations tend to lead to higher uncertainties. A close examination of the uncertainty propagation reveals that this difference is due to the approximation of the logarithm by a first-order Taylor series. In light of the significantly higher computational costs of the Monte Carlo method, this discrepancy of 0.0008 dB appears to be small enough to be tolerated.

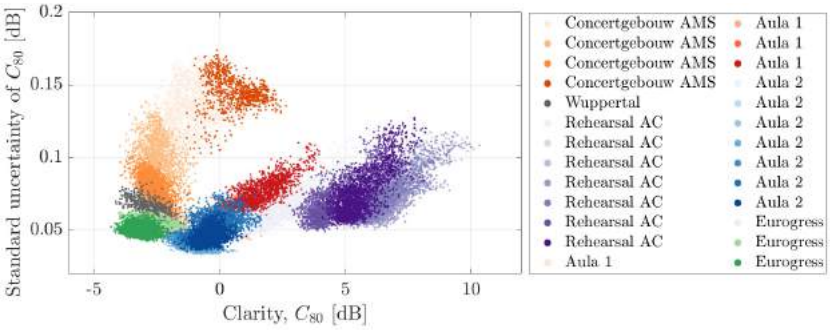

Figure 6.5: Broadband clarity index C_{80} and the associated standard uncertainty in different auditoria. The color palettes are the same as in Figure 6.2.

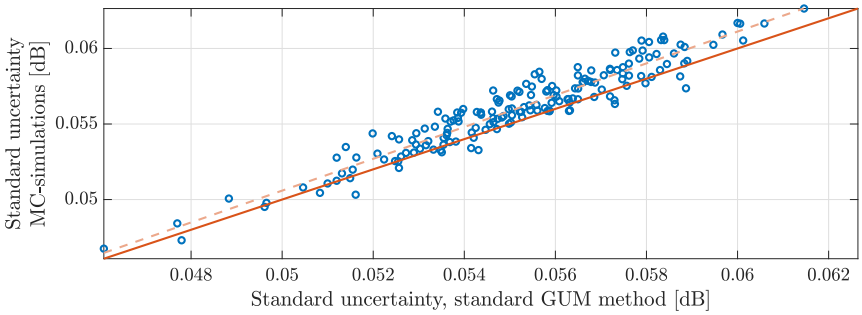

Figure 6.6: Comparison of uncertainties for C_{80} determined with different methods. The solid red line marks the identity between both methods. The dashed line marks the linear regression of the data points.

Definition

The results for the clarity parameter are by nature similar to the results of the clarity quantity. For this reason, it is not particularly surprising that the distribution of D_{50} shown in Figure 6.7 is similar to the distribution shown in Figure 6.5. Since clarity can only assume values between 0 % and 100 %, Figure 6.7 shows very clearly that the collected measurement data cover the possible value range quite well. The collected measurement data are thus suitable for answering the research question.

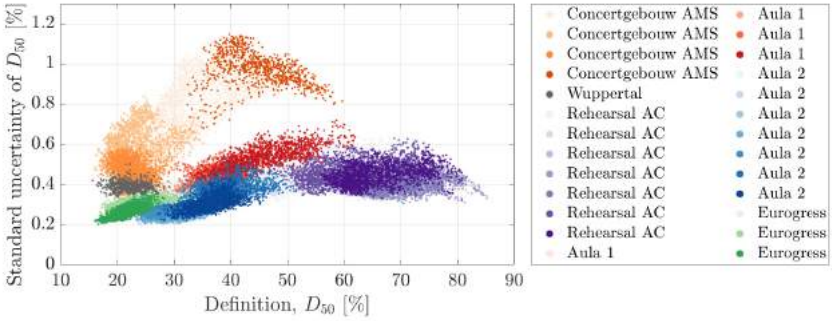

Figure 6.7: Broadband definition index D_{50} and the associated standard uncertainty in different auditoria. The color palettes are the same as in Figure 6.2.

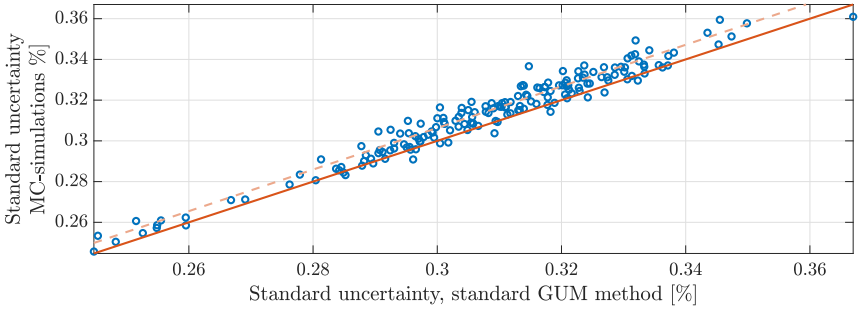

Figure 6.8: Comparison of uncertainties for D_{50} determined with different methods. The red line marks the identity between both methods. The dashed line marks the linear regression of the data points.

At this point it should be noted that, for algorithmic reasons, definition was calculated directly from the impulse response, whereas its uncertainty was determined based on Equation 6.2.11 using clarity's uncertainty as the input quantity. Although this reduces the computational effort, it has the side effect that the determined uncertainty is slightly larger. As with the clarity measure, Figure 6.8 shows that the Monte Carlo simulations lead to an uncertainty for the definition quantity that is slightly higher compared to the uncertainty from the standard GUM method. Just as before, the origin is found in the back-and-forth transformations into and out of the logarithmic level domain, which is represented inaccurately by the partial Taylor series. With a difference of just 0.0052 % [unit $u(\mathrm{D}_{50})$], however, the advantage of the significantly lower computational cost makes it worthwhile to use the standard GUM method.

Strength

In general, the strategy pursued for the previously discussed room acoustical quantities can be applied to the strength parameter, G, as well. Getting the amplitude of G right, however, requires measurements with a calibrated sound source. This additional effort was deliberately omitted because it was already clear at the time of the measurements that this normalization factor would be eliminated in the intended analysis. After all, in a pair comparison of strength values at different measurement locations, the calculation rules for the logarithm allow omitting common terms.

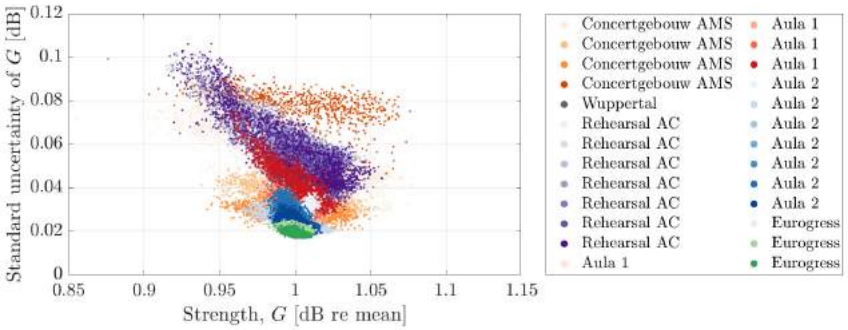

Figure 6.9: Range of the broadband strength index G and the associated standard uncertainty in different auditoria. Strength is normalized to the respective mean value of the measured sampling area denoted by the different colors. The color palettes are the same as in Figure 6.2.

For the sake of completeness and continuity, Figure 6.9 shows the distribution of strength relative to the sampling area's mean. A little more relevant are the results presented in Figure 6.10, since the comparison of the independent uncertainty calculations is compared. On the grounds of the regression analysis, a difference of 0.0004 dB [unit $u(G)$] is detectable in the uncertainty calculation. This difference appears to be tolerable without limiting the validity.

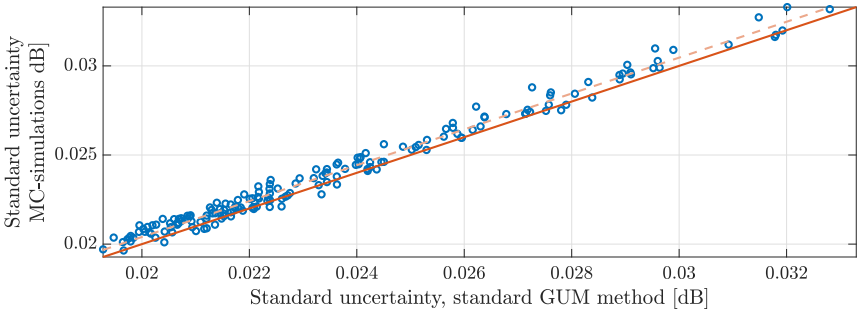

Figure 6.10: Comparison of uncertainties for G determined with different methods. The red line marks the identity between both methods. The dashed line marks the linear regression of the data points.

Center time

Figure 6.12 shows the range of values and the associated standard uncertainty of the center time. Here, too, it can be seen that with the measurements in the various auditoria, it was possible to cover a very large range of values that can all be expected in practice. Figure 6.11 shows that Monte Carlo simulations yield an uncertainty for center time that is 0.0002 ms [unit $u(t_c)$] higher than to the standard GUM uncertainty. This discrepancy appears tolerable for the present investigation.

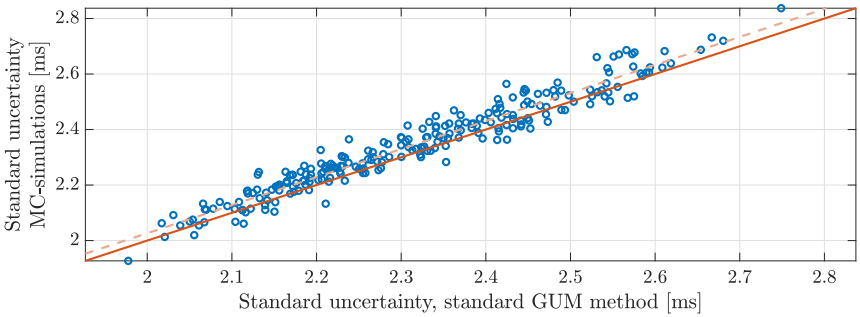

Figure 6.11: Compared uncertainties of t_c for different methods.

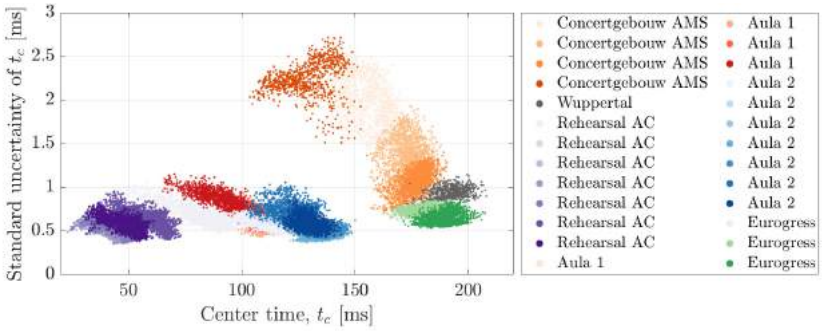

Figure 6.12: Range and standard uncertainty of broadband t_c in different auditoria.

6.3 Uncertainty of the sampling location

6.3.1 Introduction

For mechanical reasons of manufacturing tolerances, for economic reasons of trying to limit the number of drives and for technical reasons of not being able to control two actuators in Matlab at the same time, it is not possible to position the microphones to within millimeter accuracy. This translates to uncertainties regarding the measurement locations at which the room impulse responses were recorded. This problem became apparent early in the design of the array. As it was not possible to precisely control the microphones in the first place, steps were taken to determine the measuring position as accurately as possible.

Out of an affinity to acoustical solutions, and since electromagnetic tracking methods for all 32 microphones did not represent an economically viable strategy, the acoustical multilateration method was chosen to determine the actual microphone position during the room acoustical measurement. As seen in Figure 6.13, a total of six small loudspeakers were mounted in the aluminum frame of the measurement array. In addition to the primary room impulse responses to determine room acoustical quantities at the 16 960 sampling locations, $6 \times 16\,960$ secondary impulse responses were collected to determine the direct sound's "time of flight" between the small loudspeakers and the microphones.

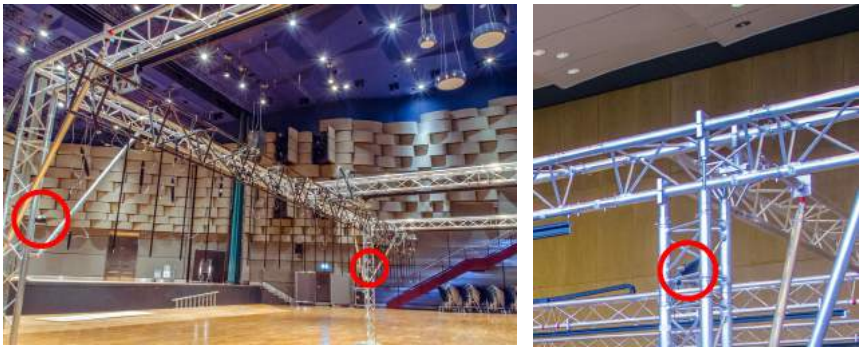

Figure 6.13: Detailed view of small loudspeakers mounted in the measurement setup's frame structure.

Background - Multilateration

The first application of multilateration (in combination with triangulation) can be traced back to the 1910s. Reportedly this technology was developed independently by the Russians, Germans, French, Americans and very successfully by the British to detect hostile artillery during World War I. From the time delay of the firing boom between two microphones, the bearing to firing sites was determined. The most common present day applications of multilateration are the *NAVSTAR* or the *Galileo* global positioning systems. The topic is widely investigated with a large number of different approaches and dialects. As an example, three investigations from the same year can be cited: Schau and Robinson (1987) describe a procedure based on intersecting hyperboloids, Carter (1987) publishes about the application of the PHAT algorithm and Smith and Abel (1987) report on a closed-form least-squares solution. Acoustical applications cover a wide range as

well, including the detection of aircraft and submerged vehicles (Torrieri, 1984), video camera steering (Huang, Benesty, & Elko, 2000) or animal bioacoustics (Militello & Buenafuente, 2007).

Against the background of the numerous research activities and the technical maturity of the applications, it is not obvious whether and how an innovation could be developed without long experience in this particular field of research. At the time of implementation, however, literature review gave no indication that such strategies had previously been implemented as (quasi) blind methods (i.e., without exact knowledge of the sensor positions) or in room acoustical applications.

6.3.2 Initial methodology

The principle of multilateration is based on the measurement of a wave's arrival times at a number of sensors under the assumption that the wave's propagation speed is constant and that the clocks at the receivers are synchronized. In the case discussed here, the measured data can be interpreted after the deconvolution as if the small distributed loudspeakers had emitted an impulse in their own respective measurements. Due to the (constant) latency of the measurement system, this impulse is delayed by t_{latency} before it propagates in a spherical wave through the medium and eventually passes the microphones at the time t_{em}. This relation is expressed in Equation 6.3.1 and is visualized in Figure 6.14 through the red circles.

$$t_{\mathrm{em}} = \frac{R_{\mathrm{em}}}{c} + t_{\mathrm{latency}} \tag{6.3.1}$$

with

$$\begin{aligned} R_{\mathrm{em}} &= |\vec{x}_m - \vec{x}_e|_2 \\ c &= 331.3 + 0.606\vartheta \end{aligned}$$

R_{em} denotes the distance between the emitter at $\vec{x}_e$ and the microphone at $\vec{x}_m$. c is the speed of sound as a function of temperature ϑ.

Equation 6.3.1 can be set up for each combination of the six "position loudspeakers" and the 16 960 microphones. This system features 101 760 equations with 50 900 unknown variables, i.e., three position coordinates for each of the microphones and the loudspeakers and the temperature and latency. The unknowns can be determined (see Equation 6.3.2) by a Levenberg-Marquardt nonlinear least-squares optimization approach (Marquardt, 1963).

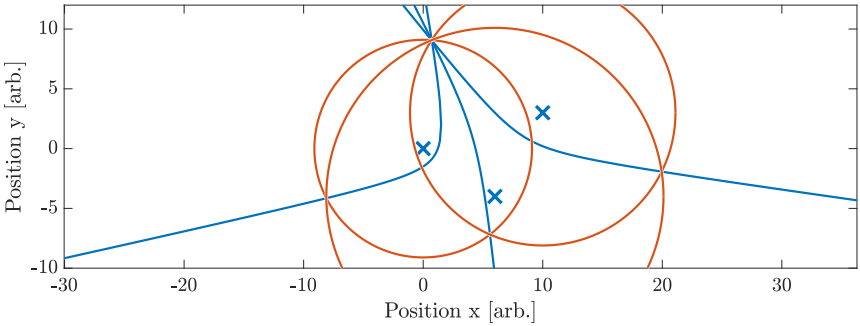

Figure 6.14: Comparison of time-of-arrival (red) and time-difference-of-arrival (blue) approaches to detect a source's position. The emitter positions are marked by blue X (after Kaune (2012)).

$$\min_{\substack{\vec{x}_m \in \mathbb{R}^3 \setminus \vec{0} \\ \vec{x}_e \in \mathbb{R}^3 \setminus \vec{0} \\ t_{\text{latency}} \in \mathbb{R}^+ \\ \vartheta \in \mathbb{R} \setminus \infty}} |\vec{t}_{\text{em,measured}} - \vec{t}_{\text{em}}| \tag{6.3.2}$$

This formulation raises the problem that for $\vec{x}_m, \vec{x}_e = \vec{0}$ and $\vartheta \to \infty$, there is a singular solution that is not particularly reasonable, and that the solution space is indifferent to rotations and scaling. These challenges can, however, be avoided by choosing an iterative method through which the speaker and the microphone positions cannot be optimized at the same time. In addition, the solution space is subject to a rotation normalization by minimizing the variance of the microphone positions along the z-axis.

For a good optimization of the problem it is important to have an accurate measurement of the arrival times of the direct sound. Here, the time of arrival of the direct sound is defined as the time sample of the highest amplitude's absolute value. Alternative definitions that rely on the first rising of the signal amplitude above a pre-defined level (e.g., ISO 3382-1 (2009)) were not proven to be very effective, as the coincidental detection of local extrema would introduce a significant variation in the detected time-of-arrivals. Establishing the absolute maximum leads to much more accurate results, but the measured times are still uncertain by $\pm 0.012\,\text{ms}$ because of the sampling rate of 44.1 kHz. What may not appear at first glance to be problematic corresponds to an uncertainty of the distance measurement of some 7 to 8 mm depending on the prevailing speed of sound. However, since the band-limited signal can be perfectly reconstructed

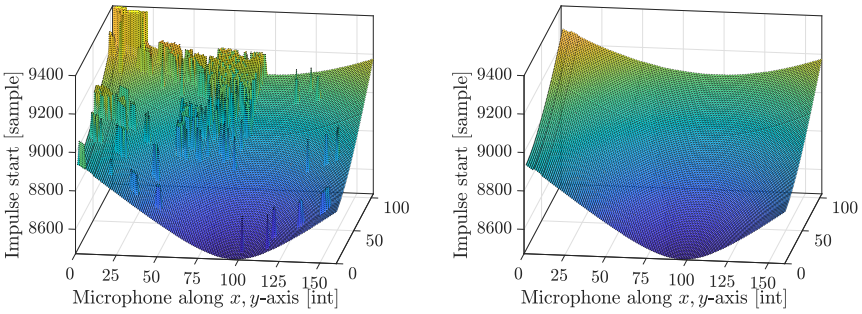

(a) With outliers.

(b) Corrected.

Figure 6.15: Detected arrival of the direct sound.

below Nyquist and Shannon's cutoff frequency, there is no good reason to reduce the accuracy of the optimization due to uncertain input data.

Through trial and error, it was determined that by applying up to a 100-fold upsampling to determine the time-of-arrival, the accuracy of the optimization could be improved. The upsampling results in a theoretical accuracy of $\pm 0.11\,\mu\text{s} \widehat{\approx} \pm 39\,\mu\text{m}$ for the arrival time measurement. This may be a limitation due to the clock jitter, which the manufacturer of the hardware quantifies as "less than 5 ns". In contrast to the discussion before, however, the uncertainty in the time-of-arrival measurement is very small compared to the time it takes for the sound wave to travel through the entire array. This difference in orders of magnitude constrains the uncertainty of the output to very small and potentially negligible values (Carroll et al., 2006, Ch. 2).

Another aspect that is detrimental to the accurate determination of the arrival time is the false detection of reflections. Due to the high directivity of the small loudspeaker diaphragms and due to nearby surfaces, there is the occasional problem that a later reflection features a higher amplitude than the (off-axis) direct sound. In such situations, the measured arrival times are far too late. This large time difference between adjacent measurement locations and the knowledge that the earlier arrival time is the "better" time makes it relatively easy to adjust the search interval for the direct sound maximum. Figure 6.15 shows a particularly error-prone example in which the initial falsely detected times-of-arrival, on the left, have been identified and corrected, yielding the distribution shown in the right.

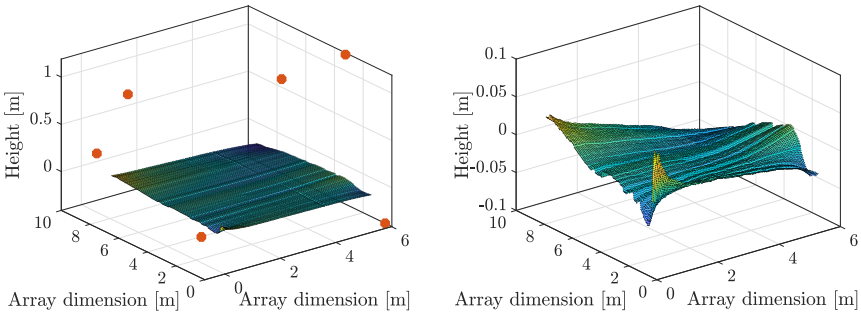

(a) Overview with loudspeakers (red).

(b) Detailed view with expanded z-axis.

Figure 6.16: Multilateration results: Microphone and loudspeaker positions.

6.3.3 Results

The results of the multilateration can be seen exemplarily in Figure 6.16. The left picture shows how this approach can be used to determine generally plausible microphone positions: the red dots mark the detected positions of the loudspeakers. On closer examination of the identical results shown in the right-hand image, it becomes clear that the z-dimension follows a position-dependent systematic trend. Even when this wave pattern does not appear to be particularly large relative to the dimensions of the sampling area, these results fall short of the author's initial expectations.

Accuracy of the estimation

Considering the working principle of the measurement robot, the wide range in z-coordinates shown in Figure 6.16 feeds the suspicion that not all positions were estimated with the same accuracy. On the assumption that the normality of the involved uncertainty distributions can be maintained, Donaldson and Schnabel (1987) present a strategy that permits quantifying the confidence region of a nonlinear optimization's result (i.e., the determined microphone positions) based on the equation system's Jacobian matrix. Considering that the Jacobian is the first-order partial derivative of a vector-valued function (Bronstein et al., 2015, 12.8.2), the analogies to the multi-dimensional standard GUM method become obvious. Consequently, the normality prerequisite of the Donaldson and Schnabel (1987) method coincides with the fundamental assumption of this investigation, and can be justified for the same reasons.

The uncertainties of the determined microphone positions (as the ℓ^2-norm) are shown in Figure 6.17 through the color of the position markers. In addition, the

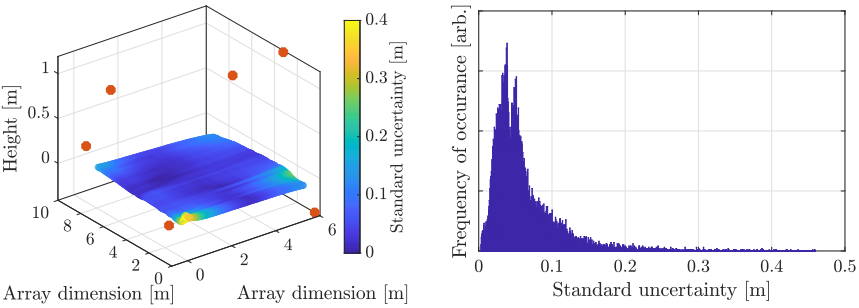

(a) Spatial distribution.

(b) Uncertainty histogram.

Figure 6.17: Uncertainty of the detected microphone positions.

uncertainty histogram plotted in the right image permits a second perspective. These images show two aspects: First, the initial suspicion that the wave pattern in Figure 6.16 is a (general) indication of estimation's uncertainty is confirmed by Figure 6.17. Second, it can be seen that standard uncertainties of up to 40 cm can hardly be interpreted as sufficient for the intended purpose.

6.3.4 Revised methodology

These results support the wish to modify the optimization strategy to increase accuracy. The observation of the measurement process (see Section 5) provides a useful starting point: The design of the measurement setup features a carbon truss from which the 32 microphones are lowered on rigid carbon tubes. This implies that each of the microphones may have individual elevations (z-coordinates): however, along the path each microphone travels, all of the respective 530 measurement positions must have the same z-coordinate. This reduces the degrees of freedom from 50 900 to only 33 972. By exploiting this additional boundary condition, the underlying system of equations is significantly better conditioned, and thus yields much smaller uncertainties.

6.3.5 Results

For the same data discussed in Figure 6.16, the uncertainty of the microphone positions based on the revised conditions are shown in Figure 6.18. The confidence intervals are now more evenly distributed over the sampling areas that the different physical microphones cover. Additionally, the color coding and the histogram data give evidence that the standard uncertainty has been significantly reduced to less than 1 cm. Changes of several orders of magnitude are no longer

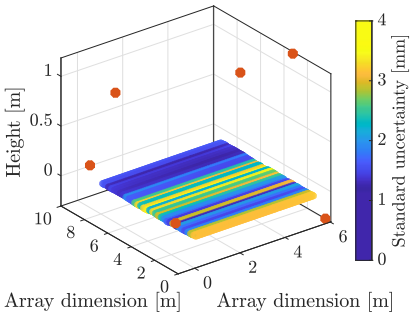

(a) Spatial distribution.

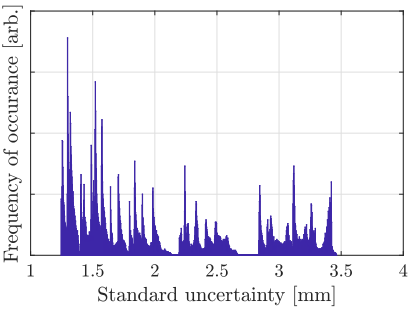

(b) Uncertainty histogram.

Figure 6.18: Uncertainty of the detected microphone positions for the revised optimization approach. Compared to Figure 6.17, the color coded display range has been reduced by a factor of 100.

very easy to display graphically on a linear scale; therefore, the color scaling has been changed by a factor of 50 when comparing Figures 6.17 and 6.18.

Validation

Since it is not automatically guaranteed that over-determined optimization problems converge towards the absolute minimum when they are solved, an independent validation is appropriate. The data collected in some auditoria, through repeated measurements with relative loudspeaker and microphone positions essentially unchanged, offer the opportunity to determine whether the independent multilateration yields comparable results. For the sake of brevity, a representative and average case is discussed here.

In the *rehearsal room* seven measurement series were run in which neither the loudspeaker positions nor the z-coordinates of the 32 microphones were changed. For each of the series, the microphone and loudspeaker positions were determined based on independent measurement data and respective optimizations. Figure 6.19 shows in blue the standard deviation of the seven determined z-coordinates for each of the microphones. As a comparison, the average over seven 68 % confidence intervals based on Donaldson and Schnabel (1987) is displayed in red. The z-coordinates from the 7 multilaterations exhibit a standard uncertainty of about 0.51 mm, whereas Donaldson and Schnabel's algorithm predicts an average standard uncertainty of 0.37 mm.

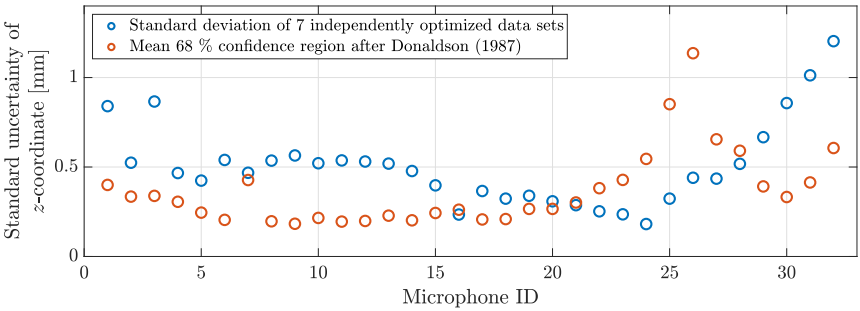

Figure 6.19: Comparison of different methods to determine the uncertainty of the multilateration.

6.4 Discussion

The discussion of the results presented here is divided into the uncertainty of room acoustical quantities and the uncertainty of determining the microphone positions.

As far as the uncertainty of room acoustical metrics is concerned, the methodology of the standard GUM procedure appears appropriate compared to the Monte Carlo procedure. Although there are differences in both methods, especially for logarithmic quantities, the differences are so small that the higher costs associated with stochastic simulations are disproportionate.

The uncertainty of measured room acoustical quantities (Section 6.2) is relatively low compared to the quantities' absolute values, the variations within a room and the variations between different rooms. The presented results depend on the properties of the measurement chain discussed in Chapter 4. When using a measurement chain with other elements, the elements' respective uncertainties must be taken into account.

Considering the wide range of contexts in which measurements are taken, in some conditions greater uncertainties in determining room acoustical quantities could be tolerated. Based on the considerations presented here, these reduced uncertainty requirements could be translated into less rigorous demands on the measurement equipment. In such scenarios, room acoustical metrics could be determined with rather simple measurement equipment.

Since the uncertainty of the room acoustical parameters has not yet been investigated with the methodology discussed here, there is, unfortunately, a lack of references against which to compare these results. Clearly, the uncertainties associated with measuring room acoustical quantities seem low enough for the

intended discussion of the central research question.

The second part of this discussion focuses on the multilateration's uncertainty. The determined microphone positions show that the sampling is not perfectly regular over the covered area. Since the knowledge of the sampling locations is of central importance to determining the measurement function, it is reasonable to go through the efforts described here to determine the measurement locations as precisely as possible.

With the approach described here, the relative measurement position can be determined to a few millimeters. In acoustics, this uncertainty seems almost unheard of and absurd, since it is already on the order of magnitude of the microphone's capsule and membrane, and even the acoustic wavelength. The latter aspect in particular should encourage caution in considering such (low) uncertainties. It is probably due to the three-fold overdetermination of the system of equations, and the associated averaging effects, that the measurement locations can be determined so precisely when wave effects would not initially support this.

Because the influence of the measurement position on room acoustical measurements is precisely the target of the investigation pursued here, it is promising that the sampling locations can be determined with an accuracy that is significantly higher than that of the sampling grid, and also more accurately than the underlying driving forces, i.e., decorrelation of the sound field over space (Bodlund, 1977). Compared to other investigations (Akama et al., 2010; Barron, 1984; J. S. Bradley, 1996; Lokki, 2013, and others), where measurement positions are given relative to reference objects such as numbered seats, the accuracy determined here appears absolutely adequate.

It can be summarized that the methods described here allow determining the expected value, and the associated standard uncertainty, of both room acoustical quantities and measurement positions with a precision that allows setting up the measurement function in the following section.

6.5 Conclusions

- The uncertainty of room acoustical quantities due to uncertainties of the acoustical measurement equipment was determined.

- The relative uncertainty of room acoustical quantities is low enough for most applications.

- Measurement positions can be determined with an uncertainty of a few millimeters using an acoustical multilateration approach.

- This position uncertainty is sufficient for the general purpose of this investigation.

With these findings, the uncertainties of the sampled sound field data are fully known, and can be processed in the next chapter to establish the measurement function.

7

Measurement function

7.1 Introduction

This chapter discusses the measurement function and how it is established. In regard to the central research question, this function shows how the sound field changes based on a given distance between two sampling positions. This provides the essential relationship required for an ISO Guide 98-3 (2008) compliant discussion of uncertainties in room acoustical measurements. In this framework, the distance between the measurement positions is understood as the input variable and the average change of room acoustical quantities (over this distance) as the output variable. For a summary of the rationale behind the uncertainty discussion, the reader is referred to Chapter 2.3.2.

On a smaller scale, a discussion on the uncertainty of room acoustical parameters was performed in Chapter 6. With the various room acoustical quantities defined in ISO 3382-1 (2009), the measurement function was available there as an analytical expression. Here, in contrast, due to the numerous boundary conditions that define the sound field in rooms and the boundaries' complex relationships, an analytical expression for the measurement function is not to be expected. In accordance with the GUM procedure, however, it is also a valid alternative to determine the measurement function empirically (ISO Guide 98-3, 2008, 5.1.4).

In the analytical case, measurement uncertainties can act on the uncertainty propagation only if input variables of GUM type B are considered. In the empirical case, however, the input and the output to the system are both surveyed in (uncertain) measurements. Since the measurement function depends entirely on uncertain data, it is uncertain, too. In order to avoid a bias (Carroll et al., 2006, Ch.3) when assuming model variables have been measured exactly, subtle adjustments to the reasoning behind measurement functions are required. This section is, thus, to discuss the processing that transforms the measured raw data into a suitable measurement function.

Available raw data from measurement series

The foundation for the experimental approach is the data collected through 26 series of measurements in 6 different auditoria (see Section 5). Figure 7.1 provides an example and shows the broadband distribution of room acoustical quantities measured across the sampling area in *Eurogress Aachen*. This particular scenario shows that the measured quantities vary over a range indicated by the color bar in the respective images. Depending on the room acoustical quantity, fluctuations are evident both on a local scale of a few decimeters and on a larger scale (of a few meters) through gradients from front to back or left to right. In ideal cases, each set of these measurements consists of 16 960 RIRs that were uniformly measured over a sampling area of 5.3 m × 8.0 m in a rectangular 5 cm resolution grid. Deviations from this ideal case exist as a result of the inevitable impediments in practical measurements of this complexity. These shortcomings manifest in a few invalid impulse responses and in the uncertainties of both the determined measurement locations and the calculated room acoustical quantities (see Section 6).

7.2 Establishing the measurement function

7.2.1 Methodology

Identifying influence quantities and output measurand

The central research question of this entire study is to investigate how the sound field changes from one position to another. To make this target both measurable and quantifiable, suitable variables need to be identified that can serve as ISO Guide 98-3 (2008) conforming input and output quantities (see Figure 2.6 in Section 2.3.2). Quantifying the "sound field" based on room acoustical quantities Q (ISO 3382-1, 2009) is straightforward and relatively easy. The "change from one position to the next", however, refers to an aspect that cannot be obtained from the collected measurement data directly. As a solution, a difference in position between two locations A and B can be expressed reasonably well through the distance $d = |\vec{d}| = |\vec{r}_A - \vec{r}_B|$. This distance can be recognized as the input quantity (that would be displayed along the x-axis in Figure 2.6). The associated change in room acoustical quantities ΔQ is then the output quantity (shown along the y-axis in Figure 2.6).

It may seem that this interpretation exceeds the capabilities of the standard GUM framework: Although the sound field property Q can only take a single value at each position, a given distance between two sampling points is not unique. As a result the sound field can change over a given distance in different ways. Statistically, this range of possibilities can be represented by a probabil-

ity distribution. The model function f then no longer represents a real-valued transform, but rather a continuous probability density function $f_{\Delta Q}(d)$, in which the probability of a change in the sound field ΔQ is given as a function of the distance d.

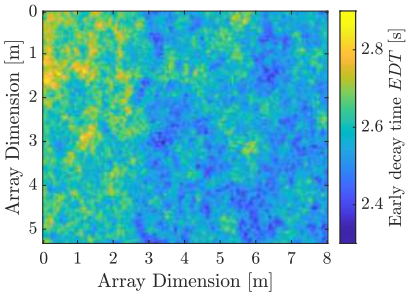

(a) Early decay time EDT.

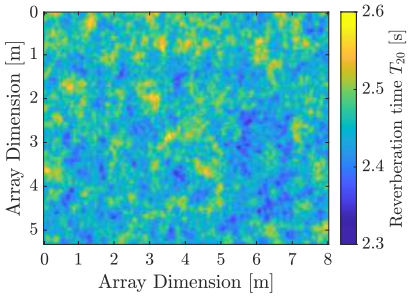

(b) Reverberation time T_{20}.

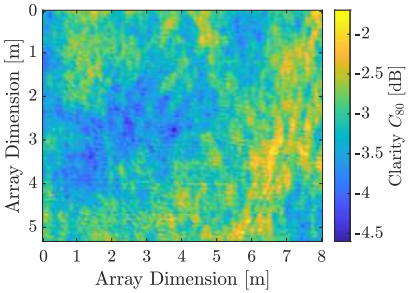

(c) Clarity C_{80}.

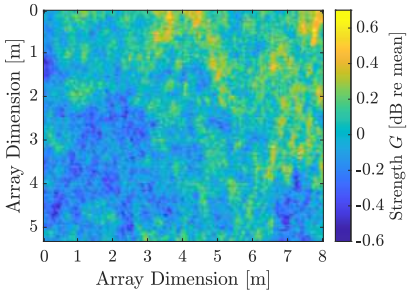

(d) Strength G.

Figure 7.1: Broadband distribution of room acoustical quantities at *Eurogress Aachen*.

This abstraction comes at the price of a sound field's global (or larger scale) properties being represented with a loss of information. Taking the example of Figure 7.1a, it is evident that EDT systematically exhibits higher values in the left part of the sampling area than in regions in the center or in the right. Such patterns appear in $f_{\Delta Q}(d)$ as wide distributions and indicate that, at a given distance, there is a relatively high probability for large ΔQ and small ΔQ at the same time. This means $f_{\Delta Q}(d)$ preserves the information that characteristic spatial trends occur in the sampled sound field even though the details of the exact location are discarded. To permit the most general possible discussion as possible and to cover the widest possible range of applied scenarios, this abstractions

seems justifiable.

Introducing a PDF to characterize a measurement process presents a view that needs to be reconciled with the GUM framework's basic take on measurement functions and the propagation of uncertainties. Although not stated specifically in the GUM, the principle of uncertainty propagation implies a function that maps the input to a unique output. Such a requirement would seem to contradict f being a probability density function that maps a singular input value to a (probable) range of output values. The discussion by Kacker, Sommer, and Kessel (2007), however, relates Bayesian statistics to JCGM 101 (2008)[2] and thus to ISO Guide 98-3 (2008). Today, Monte Carlo methods are an accepted (GUM conforming) tool to propagate uncertainty distributions through measurement functions. In order to avoid probabilistic measurement functions, $f_{\Delta Q}(d)$ can be seen as a likelihood function $\mathcal{L}(d|\Delta Q)$ that represents the probability of a change in room acoustical quantity ΔQ based on the parameter (‚true or given value) d. Kacker et al. argue that a likelihood function can be interpreted as the input variables' PDFs sampled through the Monte Carlo method (JCGM 101, 2008), and is thus in line with ISO Guide 98-3 (2008). This perspective recognizes the Monte Carlo method as a statistical (Type A) evaluation of data to arrive at an estimate x_i of the input quantity X_i. In this discussion, the measurement function is a straight line with slope $c = 1$ that maps ΔQ to ΔQ.

Degrading the measurement function to a neutral element may seem like a harsh cut on interpretative leeway and not very descriptive from a room acoustics standpoint. For this reason, the original interpretation of a probabilistic measurement function is preferred. The considerations by Kacker et al. (2007) serve as evidence that GUM conformity is provided.

The introduction to this chapter highlighted the need to recognize the inherent uncertainties of observed input and output variables when the measurement function is to be determined empirically. The uncertainties of the room acoustical quantities and the measurement positions were determined in Chapter 6.

Comparing two individual measurement positions

To start, two arbitrary microphone positions A and B in the sampled sound field are considered. Both measurement locations are characterized by their Cartesian coordinates r_1, r_2 and r_3 and their respective uncertainties $u(r_1)$, $u(r_2)$ and $u(r_3)$. In the acoustical domain, both positions are defined through their impulse responses, the derived room acoustical quantities and the associated uncertainties.

[2] At the time of publication, Kacker et al. (2007) were refering to the final draft version of JCGM 101 (2008).

The input quantity of the measurement function is the distance between the two microphones given through the ℓ^2-norm

$$d = \sqrt{\sum_{k=1}^{3} (r_{k,\mathrm{A}} - r_{k,\mathrm{B}})^2} \tag{7.2.1}$$

and the associated variance

$$\begin{aligned} u^2(d) &= \sum_{k=1}^{3} \left(\left(\frac{\partial d}{\partial r_{k,\mathrm{A}}} \right)^2 u^2(r_{k,\mathrm{A}}) + \left(\frac{\partial d}{\partial r_{k,\mathrm{B}}} \right)^2 u^2(r_{k,\mathrm{B}}) \right) \\ &= \sum_{k=1}^{3} \left(\frac{r_{k,\mathrm{A}} - r_{k,\mathrm{B}}}{d} \right)^2 \left(u^2(r_{k,\mathrm{A}}) + u^2(r_{k,\mathrm{B}}) \right) \end{aligned} \tag{7.2.2}$$

The measurement function's output quantity is the difference of the room acoustical quantities ΔQ determined at the positions A and B. Based on Equation 2.3.2, ΔQ's variance is the sum of the individual parameters' variances at the respective measurement positions:

$$u^2\left(\Delta Q\right) = u^2\left(Q_{\mathrm{A}}\right) + u^2\left(Q_{\mathrm{B}}\right). \tag{7.2.3}$$

Following the considerations in Section 6 and the standard GUM method (ISO Guide 98-3, 2008, 4.3.4), both $u(d)$ and $u(\Delta Q)$ are assumed to be normally distributed. In this initial step, for a single pair of microphones, the parameter-distance relation that forms the measurement function can be set up as a two dimensional Gaussian distribution:

$$p\left(\vec{x}; \vec{\mu}, \Sigma\right) = \frac{1}{2\pi\sqrt{|\Sigma|}} \exp\left(-\frac{1}{2} (\vec{x} - \vec{\mu})^T \Sigma^{-1} (\vec{x} - \vec{\mu}) \right) \tag{7.2.4}$$

with

$$\begin{aligned} \vec{x} &= \begin{pmatrix} |d| \\ |\Delta Q| \end{pmatrix} \\ \vec{\mu} &= \begin{pmatrix} |\overline{d}| \\ |\overline{\Delta Q}| \end{pmatrix} \\ \Sigma &= \begin{pmatrix} u^2(d) & 0 \\ 0 & u^2\left(\Delta Q\right) \end{pmatrix}. \end{aligned}$$

Equation 7.2.4 takes the distance d and the change in the sound field ΔQ in absolute value. Fundamentally, omitting the algebraic sign is due to the original

sample's finite statistical degree of freedom. Considering a given microphone pair more than once, perhaps by discussing the change of the sound field from position A to B and vice versa, cannot add new information and would only result in $p\left(\vec{x};\vec{\mu},\Sigma\right)$ being reflected on the coordinate axes. Recognizing the magnitude alone suppresses this redundant part of the probability density function without affecting its shape.

Generalizing to compare numerous measurement positions

Discussing a single pair of microphones only serves as the initial step to demonstrate an elementary relation. It is obvious that the additional microphone pairs have to be evaluated in order to establish a more generally valid relationship. This can be achieved using the $m = 16\,960$ sampled microphone positions in each data set and the resulting

$$\sum_{k=1}^{m-1} k = \frac{m(m-1)}{2} = 143\,812\,320 \tag{7.2.5}$$

possible pair comparisons (Bronstein et al., 2015, 1.2.4). To the extent that these individual draws contribute equally to the total population, the total probability density function results from the sum of the individual probability densities and a normalization according to Equation 7.2.6.

$$p_c\left(\vec{x}\right) = \frac{\sum\limits_{\forall d \setminus 0} p\left(\vec{x};\vec{\mu}_d,\Sigma_d\right)}{\left\|p_c\right\|} \tag{7.2.6}$$

Numerical handling of the probability density functions

With the high number of possible pair comparisons, it quickly becomes clear that an analytical expression to describe the combined distribution (i.e., Equation 7.2.6) is not very practical, as it is costly to evaluate at a large number of observation points. Both the computational cost and the complexity can be reduced by spatially sampling the contributing two-dimensional Gaussian probability distributions. This approach replaces computational complexity with memory requirements, but also introduces sampling and truncation errors. The conditions under which these defects can still be tolerated need to be investigated.

The investigations by Genz (1992) and Genz and Kass (1997) raise doubts that the numerical integration over infinitely extended functions with dominant peaks (e.g., normal distributions) is not a trivial problem that readily converges. To address this sampling and truncation question, this study uses Genz's notion

that the numerical integration over a sampled normal distribution is a Riemann sum. In simulation series, which are not reported further here, it was observed that the error falls below $2{\times}10^{-15}$ when the standard normal distribution was sampled at a resolution of at least 2 samples per standard deviation and to a width of at least 8 standard deviations (see also Bronstein et al. (2015),8.2.5-5). Errors due to deviations from classical Riemann sums through nonsymmetrical sampling of the Gaussian distribution are taken into account, and the presented remaining error is considered negligible in the context of this study.

Normalizing probability densities

In the context discussed here, the measurement function is a probability density function. As such, its full integral must equal 1, as shown in Equation 7.2.7.

$$\int_0^{+\infty}\int_0^{+\infty} f(d, \Delta T_{\mathrm{EDT}})\,\mathrm{d}d\,\mathrm{d}\Delta T_{\mathrm{EDT}} \stackrel{!}{=} 1 \tag{7.2.7}$$

7.2.2 Results and discussion

Due to the methodology of the previous section, the measurement function is the two-dimensional probability density function (PDF) showing the probability of a given change in room acoustical quantity at a given distance between sampling points. Figure 7.2a is as an example of the PDF for the early decay time as measured in *Eurogress Aachen* (set 6). The figure illustrates the statistical properties of the analyzed data through color coding, marking likely changes in the sound field in yellow and rare combinations of d and ΔEDT in blue.

These data's suitability for more global conclusions depends on them not being statistically distorted by the sampling. Potential distortions can be studied by looking at Figure 7.2b, which shows the distance distribution between sampling points as they occur in the surveyed 5.3 m × 8.0 m area. Thus, the distance distribution is a sum of many single-variate Gaussian distributions. The shown "probability of occurrence" along the y-axis is qualitative as it depends on the number of samples that contribute to the distribution. The vertical broken lines in Figure 7.2b mark the dimensions (and the halves) of the sampling area. It can be seen that the shape of the distance distribution changes at these distances.

Influence of the finite sampling area

The shape of the curve shown in Figure 7.2b and the significance of the characteristic distances can be understood by realizing that the number of contributing

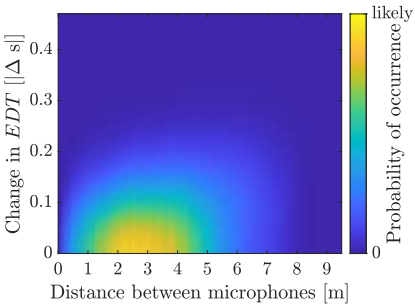

(a) Likelihood of a change in EDT at a given distance between microphones.

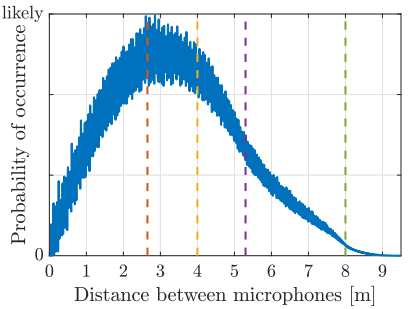

(b) Distance distribution between sampling points.

Figure 7.2: Raw data of the pair comparison in EDT at Eurogress Aachen.

data points is based on a simple complete pairwise comparison of all microphones. Figure 7.3 illustrates important relations between microphone pairs under the paradigm that the comparison pattern is run sequentially from top to bottom and from left to right: For a fixed distance d, when comparing microphone A with B, B can only be located on the semicircle around A. As a result, the number of microphones B at a distance d from A increases linearly with the circumference of the drawn semi-circle. Figure 7.2b shows this very clearly for pairs of microphones at very short distances. Due to the spatial quantization, the directional distribution of the distance vector $\vec{d}$ is discrete, but uniformly distributed over the angle around A.

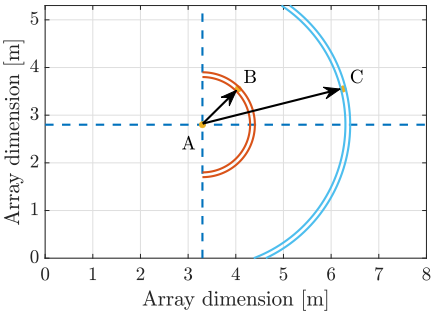

Figure 7.3: Pairwise comparison of the microphones in the sampling field.

For microphone positions A close to the sampling area's upper or lower boundary, the red semicircle in Figure 7.3 can be truncated. When A is closer than

d to the upper boundary, the directional distribution of $\vec{d}$ features a truncated number of "back-front" pair comparisons and is thus imbalanced. The same happens inversely to horizontally symmetric microphone positions A' close to the lower boundary. In sum, both truncations compensate each other, leading to an overall uniform directional distribution of $\vec{d}$.

For microphones A that are close to the right boundary there is no complement to the truncated distribution, as the pair comparison is simple (, illustrated through the right semicircle in Figure 7.3). At very small distances d, the imbalance due to "missing" complements is negligible. With increasingly longer distances, the skewedness becomes more and more significant and can be seen in the gradual flattening of the distance distribution in Figure 7.2b as the curve approaches the red vertical line from the left.

As d exceeds 2.65 m, the blue semicircle in Figure 7.3 is simultaneously truncated at the top and the bottom. This reduces the number of possible pair comparisons and skews the directional distribution of $\vec{d}$. As d approaches the violet line at 5.3 m in Figure 7.2b, there are increasingly more "left-right" comparisons relative to "front-back" or "back-front" pairs.

At even larger distances, the directional distribution of $\vec{d}$ becomes more and more restricted. All these observation also hold for the probability density function in Figure 7.2a, as the PDF shows higher probabilities at distances between pairs of microphones that are particularly likely in the sample. The finite size of the sampling area thus comes with negative side effects that need to be compensated.

Sampling-induced cluster points

Both in the distance distribution and the PDF in Figure 7.2, structures at regular intervals of about 5 cm are visible along the x-axis. An extensive root cause investigation identified two contributing factors.

First, the design and operation of the measuring system (see Chapter 5) permits placing the microphones at positions of different accuracies along individual coordinate axes. As the 32 microphones are rigidly linked together, relative measurement positions along the carbon truss can be controlled very accurately. In the perpendicular direction, the truss' position is only partially controlled by the roller bearing.

In the grid of microphone positions, distances along the carbon truss occur very regularly and accurately, which leads to local maxima in the PDF at multiples of the sampling resolution. Along the perpendicular dimension, the sampling positions are arranged on average just as densely; however, the distances between any two samples are distributed much more widely. This phenomenon is particularly

evident in the distance distribution in the 7-8 m range. The distances plotted here are mainly composed of components along the carbon truss. Due to their relatively high precision, these distances cluster in particular regions. At smaller distances in the interesting range, below 5.3 m, the effect is still recognizable but far less pronounced. This phenomenon can be recognized in the probability density distribution because the sound field changes differently along the two sampling dimensions. This shortcoming cannot be corrected. Its significance is discussed in Chapter 8, along with the general properties of the measurement function.

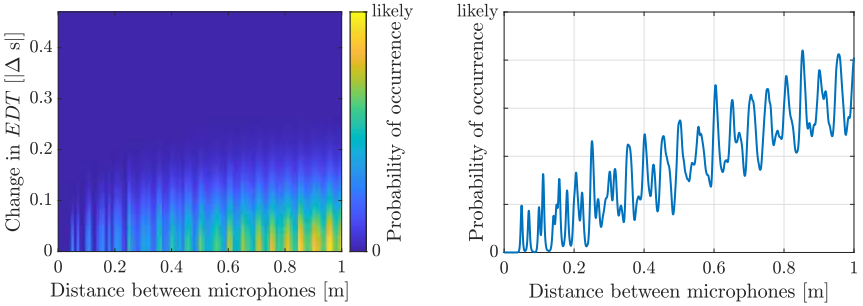

(a) Likelihood of a change in EDT at a given distance between microphones.

(b) Distance distribution between sampling points.

Figure 7.4: Close-up of the raw data of the pair comparison for EDT at *Eurogress Aachen*.

The second factor becomes evident at very small distances, near the origin, as shown in the close-ups in Figure 7.4. Both tiles show potential voids in the distribution density. These gaps in the curve occur at distances that are covered by particularly few pairs of microphones. Distances between microphones other than 5 cm, $\sqrt{2} \cdot 5$ cm, $2 \cdot 5$ cm, ..., cannot theoretically be achieved in a perfectly equidistant sampling grid. Deviations from the ideal positions evidently occurred for the reasons just discussed; however, they apparently occurred at a much lower frequency than anticipated. This leads to a low number of data points at small distances that fall between the perfect sampling grid. This phenomenon is almost identical to the modal density of sound fields in rooms at low frequencies (Schröder, 1954). The consequences are discussed at the end of Section 7.3.2.

7.3 Compensating the effect of a finite sampling area

7.3.1 Methodology

The previous section discussed how the finite sampling area leads to a nonuniform distribution of distances d between microphone pairs and a skewed directional distribution $\vec{d}$. To illustrate the compensation strategy, it is helpful to consider Figure 7.5. In this diagram, two equidistant pairs of microphones are marked by the red and blue vector arrows. The overall sampling area is shown by the graph's boundary.

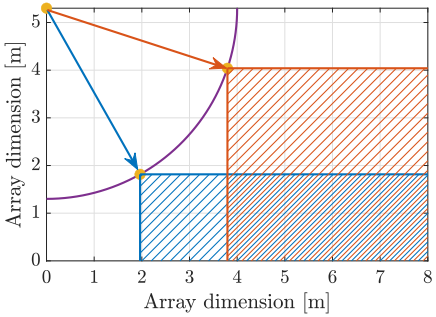

Figure 7.5: Systematic drawing of the sampling area to illustrate the distribution of distances between compared microphones.

Based on an ideal rectangular sampling pattern, there are many pairs of microphones that have the same spatial relation $\vec{d}$ to each other. For the indicated red and blue arrows respectively, the number of such "identical pairs" is proportional to the hatched areas. A comparison of the blue and red areas suggest that there are more "red" than "blue" microphone pairs leading to a bias towards left-right comparisons rather than front-back relationships. This bias can be compensated by introducing to the elementary Gaussian distribution in Equation 7.2.4 a weighting factor w_{dir}, that is reciprocal to the number of pairs with the same relative spatial relationship $n_{\vec{d}}$.

This line of argument holds for distances between microphones of up to 5.3 m. Beyond this point, the shorter edge of the sampling area is smaller than the observed distance between microphones which leads to preferential directions of $\vec{d}$. This distortion of the directional distribution cannot be corrected. Consequently, distances greater than 5.3 m must be excluded from the discussion.

The remaining "nonuniformity" of the distance distribution in Figure 7.2b, due to the linearly rising number of pairs with a given distance to each other, can

be compensated using Bayes' Theorem (Bronstein et al., 2015, 16.2.1.3). The probability density of the change in a room acoustical quantity, based on the prior condition that two sampling points have a given distance between each other, can be calculated by normalizing the probability density function according to Equation 7.3.1.

$$\int_{0}^{+\infty} f(d, \Delta T_{\mathrm{EDT}})\, \mathrm{d}\Delta T_{\mathrm{EDT}} \stackrel{!}{=} 1 \tag{7.3.1}$$

The resulting probability density function serves as the measurement function in line with the GUM framework.

7.3.2 Results and discussion

Figure 7.6 shows the probability density of a change in EDT when the effects of the finite sampling area are compensated. Compared to the original PDF in Figure 7.2, the revised distribution no longer shows the skew towards larger distances.

Figure 7.6a is a visual display of the likelihood function for the distance parameter $d < 5.3\,\mathrm{m}$ plotted along the x-axis. The y-axis shows the change in EDT that can occur in the sampling field. The color coding indicates whether a change in EDT at a given distance between microphones is relatively likely (yellow) or improbable (blue). For the presented range of distances, the yellow color tones indicate that it is most likely that the sound field between two sampling points does not change, and that both points exhibit the same decay time. Changes in EDT between sampling points are evident, but they occur less frequently as $|\Delta s|$ increases. For the chosen parameter of $d = 1\,\mathrm{m}$ and $d = 5\,\mathrm{m}$, the vertical "slices" through the likelihood function in Figure 7.6a are shown as separate curves in Figure 7.6b. It can be seen that the distribution for the short distance (blue) is narrower than the distribution for $d = 5\,\mathrm{m}$ (red). This means that large changes in EDT are less likely at shorter distances than they are at longer distances.

Both curves in Figure 7.6b are very similar and show a great visual resemblance to a half-normal distribution. With this similarity it is clear that wider distributions have a lower maximum at $\Delta EDT = 0$. The same trend is visible in Figure 7.6a, where the color tone for the maximum probability of occurrence changes from yellow to orange as the distance increases. At the same time, it is evident that the color gradients are distributed over a wider Δs range as d increases.

This trend is indicated a bit more clearly by the red line in Figure 7.6a. Building on the similarity to the half-normal distribution, the red curve shows the 68.3 %

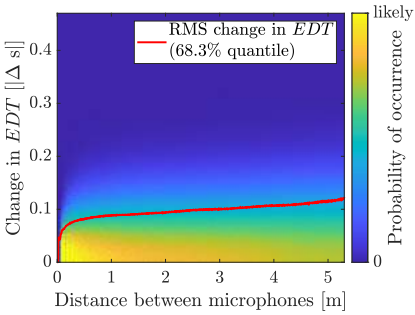

(a) For distance parameter: $0 < d < 5.3\,\mathrm{m}$.

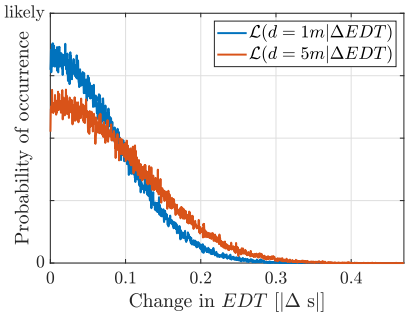

(b) For distance parameter: $d = 1\,\mathrm{m}, 5\,\mathrm{m}$.

Figure 7.6: Likelihood $\mathcal{L}(d|\Delta EDT)$ of a change in EDT at *Eurogress Aachen*.

quantile for each of the sliced distributions as a function of distance d. Starting from the origin, the quantile function (red) makes it evident that the distribution widens rapidly even for very small distances. After this *initial rise*, the curve flattens for larger distances and shows only a very moderate increase in its *extended trend*.

Other room acoustical quantities show a very similar trend when plotted like in Figure 7.6. The main target in this chapter, however, is to discuss the procedure that leads to the measurement function. For the connection between room acoustical quantities and the validity of the measurement function, the reader is referred to Chapter 8. There, Figures 8.2 to 8.9 show the 68.3 % quantile function for different room acoustical parameters in different auditoria.

When looking at smaller distances (of less than 5 cm), it becomes noticeable that individual and isolated areas exhibit very high probabilities of occurrence (single yellow pixels). In contrast, the distribution at larger distances extends continuously over a whole range of room acoustical quantities. This is clearly related to the previous observation (Figure 7.4) that at some distances there are relatively few pairs of compared sampling positions that contribute to the PDF. This sparse sampling of the sound field may lead to implausible predictions about how the acoustics change at the shortest distances ($d \lesssim 5\,\mathrm{cm}$) between two measuring points. At larger distances ($d > 5\,\mathrm{cm}$), the continuous trend of the 68.3 % quantile function suggests that the distributions of distances overlap to an extent that the impairment is no longer significant.

7.4 Reducing the complexity

7.4.1 Methodology

Transition to the quantile function

Although the color gradient in Figure 7.6 completely represents the available information of the given example, this visualization has disadvantages in a quantitative discussion because the colors can only be compared inaccurately. In statistics, it is a common strategy to parametrize probability densities and thus compare characteristic quantities. Specifically, when normality can be assumed in all likelihood, attention can be shifted from the PDF's characteristic shape to the respective change in variance σ^2.

This line of argument is pursued for the present data set, too. For each of the data sets and each of the distances, it was investigated whether the average change in room acoustical quantities follows a half-normal distribution (i.e., $\left|\mathcal{N}(0,\sigma^2)\right|$). Based on a Kolmogorov-Smirnov-test (Massey, 1951) using a 5 % significance level, it was found that, in most of the tests, the hypothesis of normality could not be rejected. For EDT, T_{20}, G and C_{80}, the percentages of distances where it is reasonable to assume half-normality are shown in Table 7.1.

Table 7.1: Most of the probability densities describing the expected changes in room acoustical parameters are normally distributed. Based on the examination of 1061 examined distance intervals.

Parameter	Percentage of normally distributed distances
EDT	92 %
T_{20}	93 %
G	71 %
C_{80}	75 %

These statistics suggest that, for the vast majority of distances between sampling points, it is sufficient to describe the distribution through the standard deviation σ. Since this point of view cannot be maintained for the few remaining cases while preserving mathematical rigor, calculating the 68.3 % quantile is a valid alternative, because quantiles in general can be calculated for arbitrary distributions. Furthermore, the 68.3 % quantile of the half-normal distribution corresponds to the standard deviation of the (full) Gaussian distribution and thus indicates the root mean square of changes in room acoustical quantities. The 68.3 % quantile is shown as the red curve in Figure 7.6a.

Behavior of the quantile function at the origin

In Figure 7.6a, it can be observed on close inspection that near the origin the color-coded probability density function shows a grain at individual distances, and that the quantile function exhibits discontinuities. At distances shorter than 5 cm the blue color suggests generally low probabilities of occurrence, while the quantile function shows a singularity.

In order to put these observations in perspective, it is first worthwhile to note that there is no reason to assume that the statistical properties change abruptly between adjacent distance intervals. Discontinuities in the quantiles as a function of distance should thus be interpreted less as an abruptly changing sound field property but rather as an indication that the global probability density function might have been sparsely sampled at the discontinuities. This interpretation is also consistent with the observation that the color coded probability density is displayed granularly at these distances.

This provides evidence that at distances below the spatial sampling rate of 5 cm there are indeed too few valid sample pairs, and thus neither the PDF nor the quantile function is meaningful. At distances beyond the spatial sampling rate sparse sampling does not appear to be a significant problem, which makes the quantile function a valid summary metric of the global probability density function.

With this in mind and recognizing the need for a fully defined measurement function (in Chapter 9), a decision must now be made about how to deal with the missing information between $0\,\text{cm} < d < 5\,\text{cm}$. It is intuitively clear that at the origin, at $d = 0$ between two sampling points, no change in the room acoustical quantities is to be expected. As a result the following must hold:

$$P(\Delta T_{\text{EDT}}|d = 0) = \delta(0). \tag{7.4.1}$$

Since theory provides no obvious answer about expected changes for distances between 0 and 5 cm, a pragmatic solution seems appropriate. For lack of better knowledge, a simple linear interpolation of the quantile function between the interval boundaries is applied. Since the 68.3 % quantile is the suitable defining parameter of the semi-normal distribution in the vast majority of distances, this approach is used to determine the probability density function for distances smaller than 5 cm.

7.4.2 Results

The just discussed methodology yield measurement functions as shown in Figure 7.6. Even a superficial comparison with the model functions shown in the next

section (i.e., Figures 8.2 to 8.9) indicates that the quantile function discussed here is representative for the functions discussed later. Thus, the example in Figure 7.6a can be used to point out some key features of the quantile function that will be crucial for further discussion.

Starting at small distances between microphones, Figure 7.6a shows that the average change in room acoustical quantities is very small. The root mean square (rms) change in EDT increases rapidly with moderately increasing distance. This pattern will be referred to as the *initial rise* of the quantile function in the following discussion of the results. Above a clearly identifiable distance between the sensors, however, the curve flattens as the rate of the rms change in room acoustical quantities over distance decreases. This part of the quantile function will be referred to as the *extended trend*.

The careful observer notices that the quantile functions are affected by some sort of noise, which causes the curves to fluctuate around their general profile in a repetitive pattern with a period of about 5 cm. Since this coincides with sampling-induced cluster points, these fluctuations provide evidence of the perseverance of this measurement artifact.

7.5 Discussion

In this chapter, the data analysis is presented that leads to the measurement function that is needed for the uncertainty discussion in Chapter 9. The way the sound field changes from one position to the next does not provide for a unique, real-valued measurement function but suggests a probabilistic interpretation instead. Although, strictly speaking, this view is incompatible with the GUM framework, this form of the measurement function was preferred to facilitate an intuitive acoustical viewpoint. This perspective does not limit the uncertainty discussion, as the measurement function can be interpreted in a GUM-compliant manner based on Bayes' Theorem when Monte Carlo methods (JCGM 101, 2008) are applied.

The general shape of the quantile curves discussed here appears plausible in light of the findings of de Vries et al. (2001) and Vorländer and Kuttruff (1985). The *initial rise* refers to fluctuations of room acoustical quantities over relatively short distances, and the *extended trend* maps global trends of room acoustic properties as they occur over larger distances or in comparison of different room shapes. So far, the curves' division into these two parts is based only on the curves' visual appearance, and is not yet backed up by theory.

Discussing small changes in sound fields of one tenth of a dB usually is not very meaningful in acoustics for reasons of measurement uncertainty that were discussed in Chapter 4. The analysis described in this chapter, however, is based

on about 17 000 impulse responses. Their even larger number of pair comparisons reduces the uncertainty significantly and theoretically make it possible to discuss nuances that would not make sense otherwise. The small superimposed ripple on the quantile function that was related to anisotropic sampling of sound field changes is an example of very small effects that become apparent with the availability of a large sample size. This property of the data implies a reduced explanatory power when discussing isolated and singular distances between microphones. Similarly, very small changes in room acoustical quantities along the y-axis should not be interpreted. In the presence of this measurement artifact, discussing differences in the quantile functions of $< 0.001\,\mathrm{s}$ for EDT/T_{30} or $< 0.01\,\mathrm{dB}$ for G/C_{80} is not justified. In a broader context, however, discussing such nuances can be waived since they are relatively small compared to the larger trends of the *initial rise* or the *extended trend*. Should the results of this investigation later be used to discuss the uncertainty of singular or few measurements, other much larger uncertainties will dominate the uncertainty budget. The author is thus inclined to note that there is no significant limitation on the data's informative value.

Discussing the influences of the finite and discretely sampled sound field is multifaceted, and it is difficult to weigh the various arguments against each other. When making pairwise comparisons of different sampling locations, it is clear that the equidistant sampling of a finite region results in both preferred directions, and distances clustered at multiples of the spatial sampling rate. The main effects such as the nonuniform distance distribution can be compensated by appropriate weighting of the samples and truncation of distances beyond 5.3 m. For the smallest distances, however, the sparseness of the data leading to the quantile function is due to discrete sampling positions that cannot be overcome. Even if there is no proof in the literal sense, this is a phenomenon that occurs in a comparable form with any type of discrete sampling.

The decision to fill the gap between the origin and the smallest sample in the measurement function is necessary to allow the Monte Carlo sampling at distances below 5 cm that occurs in Chapter 9. Nonetheless, the approach to linearly interpolate the gap may seem crude. From the theoretical considerations, however, there is no argument that promotes a different functional expression. In the absence of a substantive justification, all that remains is the visual inspection of the graphs to bridge the first 5 cm gap of the measurement function. As new evidence becomes available, this decision should be readily reviewed.

7.6 Conclusions

- The presented analysis shows spatial fluctuations as a function of distance between observation points. This perspective is novel in the existing body of knowledge.
- A GUM-compliant measurement function was established that allows drawing a picture of spatial fluctuations that is more differentiated than is possible with global summary statistics that were used in initial studies (de Vries et al., 2001; Pelorson et al., 1992). The probabilistic approach looks beyond the pure existence of large spatial fluctuations in the sound field and also introduces the likelihood at which they occur. In this context, it becomes possible to focus on dominant phenomena and discourages distraction by rare and particular cases.
- The probabilistic measurement function can be well parameterized by a quantile function, which enables good comparability.
- Characteristic features such as the *initial rise* or the *extended trend* can be clearly identified in the discussed case and for other quantities and scenarios (see Chapter 8). For reasons of plausibility, the *initial rise* can be related to spatial fluctuations over shorter distances and the *extended trend* to broader patterns that extend across entire auditoria.

The measurement function presented here marks an important base result of this study. Since this analysis reveals a hitherto uncommon perspective on spatial fluctuations, the validity of the measurement function is examined in the following chapter. In Chapter 9, the measurement function established here becomes the core for the GUM-compliant discussion of the research question.

8

Validity of the measurement function

8.1 Introduction

The previous chapter (Chapter 7) described the analysis procedure that transformed the collected array data into the measurement function (ISO Guide 98-3, 2008, 4.1) that is necessary for the uncertainty discussion. Formally, the measurement function has the properties of a likelihood function that shows the distribution of differences in the sound field between two sampling positions at a given distance d apart from each other. To ease the display and facilitate comparability, the details were tapered down to the (68 %) quantile function. Given the justified normality assumption, this function represents the root mean square difference of room acoustical quantities as a function of the distance d.

In room acoustics, a solid understanding in array measurements can be built upon (Berzborn & Vorländer, 2019; de Vries et al., 2001; Klein, 2020; Lokki, 2013; Neal & Vigeant, 2017; Witew et al., 2017). However, for the here presented method of analysis (Chapter 7) and its application in measurement uncertainty, examples of similar approaches are sparse. The absence of appropriate sources suggests a lack of experience in the field of architectural acoustics that would otherwise permit assessing the validity and significance of the method. Against this backdrop, it is not sufficient to simply establish the quantile function, but it is also necessary to investigate how susceptible it is to changes in the measurement conditions. This chapter targets the validity of the established measurement function under repeatability conditions and under a variety of practical reproducibility conditions. The investigation pursued in this chapter is intended to create the foundation for identifying significant and marginal differences when comparing the novel measurement functions to each other.

8.2 Methodology

To investigate the spatial change of the sound field in different environments, measurements were performed in different auditoria and collected in Table 8.1

were collected. Some of these measurement series have special commonalities, which enables comparisons to address validity aspects. Formally, this discussion is closely related to the question of repeatability and reproducibility as outlined in the GUM framework (ISO Guide 98-3, 2008, B.2.15 and B.2.16). It is to be investigated whether establishing the measurement function is in general repeatable, and under which conditions its determination is reproducible.

The reproducibility conditions may comprise aspects of "principle of measurement", "method of measurement", "observer", "measuring instrument", "reference standard", "location", "condition" and "time" (ISO Guide 98-3, 2008). Due to the fact that this study uses a highly specialized measurement system for which no practicable alternatives exist, the influence of changes in the principle or the method of measurement were not investigated. Furthermore, factors such as the "measurement instrument" or the "reference standard" have already been discussed in the context of intrinsic measurement uncertainty in Chapter 4. No new findings are expected in this regard.

8.2.1 Repeatability

The measuring system has already been described in detail in Chapter 5. To recap, it takes about 4.5 h for the robot to survey the sampling area. Even though the long-term stability of measurements was already touched on in Chapter 4, it is not self-evident that acoustic conditions remain sufficiently constant over relatively long time periods so that results are repeatable. Due to its automation, the measurement sets 4 and 5 of Hartl and sets 7 and 8 of Reich (see Table 8.1) were carried out in immediate succession under the GUM repeatability conditions (ISO Guide 98-3, 2008, B.2.15). The similarity of these results permits discussing the degree of repeatibility of measurements in a large lecture room and in a large multi-purpose auditorium.

8.2.2 Reproducibility

Ideally, the uncertainty is investigated in measurement series in which deliberate changes in conditions are compared to the resulting change at the system's output. However, when all possible combinations of input variables are considered, investigating complex measurement tasks can quickly become so extensive that generally available resources may not suffice. In reproducibility measurements, influences are grouped logically and left uncontrolled under realistic conditions to investigate the variance of the results. In another perspective, the aim is to solidify experience with this relatively new type of measurement function.

Table 8.1: List of measurements conducted in different auditoria.

Set ID	Auditorium (Operator)	Description
1	Aula 2 (Thevissen)	Rows of loose chairs underneath array Position in room: center
2	Aula 2 (Hartl)	Similar to set 1, new setup at different day
3	Hist. Stadthalle Wuppertal (Hartl)	Reduced sampling area due to time constraints
4	Eurogress (Hartl)	Empty room with loose chairs underneath array
5		Immediate automated repeat of set 4
6		Immediate repeat of set 5 without chairs
7	Aula 2 (Reich)	Classroom-style seating with chairs and tables Position in room: rear, left (facing stage)
8		Immediate automated repeat of set 7
9		Position in room: rear, right (facing stage)
10		Position in room: front, right (facing stage)
11		Position in room: front, left (facing stage)
12	Aula 1 (Reich)	Loose chairs underneath Position in room: front, left (facing stage)
13		Position in room: rear, left (facing stage)
14		Position in room: rear, right (facing stage)
15		Position in room: front, right (facing stage)
16	Rehearsal room	Source: back right, doors closed (reverberant)
17	(Hasti)	As set 16, doors 45° open
18		As set 16, doors 90° open
19		As set 16, doors 135° open
20		As set 16, doors fully open (absorptive)
21		Source: back left, doors alternating open and closed
22		As set 21, doors 45° open
23	Concertgebouw Amsterdam	Position in room: 2^{nd} quarter from front left center audience area (facing stage)
24	(Hasti)	Position in room: 3^{rd} quarter from front
25		Position in room: 4^{th} quarter from front (rear)
26		Position in room: 1^{st} quarter from front (front) Reduced sampling area due to time constraints

Changed condition: Time and observer

The first question that needs to be approached is whether results can be reproduced independently at a different time or by a different observer. In formal GUM terms, this refers to reproducibility measurements (ISO Guide 98-3, 2008, B.2.16) with the changed conditions "time" and "observer".

This can be investigated when comparing the measurements in the large lecture room *Aula 2* that were carried out at two independent occasions by Thevissen and Hartl (sets 1 and 2 in Table 8.1). Both series required a complete setup and dismantling of the measurement apparatus. The aspects of "location" and "condition of use" were loosely held constant: in both measurements, the microphone array was placed in the center of the room with rows of loose chairs underneath it. These two measurement sets mirror the situation in which two measurement teams wish to independently survey the acoustic conditions in a given auditorium. In consequence, no special effort was made to reproduce the measurement location (source and receiver) with the utmost precision ($\approx \pm 1\,\mathrm{m}$), nor to place the chairs in identical positions ($\approx \pm 0.5\,\mathrm{m}$).

The detailed planning and implementation of the two measurement sets was carried out relatively independently by the two operators, although preparations were always done under the advice and supervision of the author of this study. This can be interpreted as a limitation to the ideal uncontrolledness of reproducibility measurements under the condition "observer". In a more benign mindset, however, this supervision could also be viewed as "professional development" to qualify personnel to operate the measurement robot. The influence of the conditions "time" and "observer" were investigated simultaneously based on the available two data sets and, thus, it may not be possible to strictly separate the two factors.

Changed condition: Location

The next step of reproducibility studies targets the question of how the measurement location affects the measurement function. The relevance of this reproducibility condition becomes clear when considering two aspects: On the one hand, based on the theoretical principles and the properties of the ideal diffuse sound field, there is an expectation that spatial fluctuations should be more or less the same across an auditorium. On the other hand, however, it is evident that ideal diffuseness cannot be achieved in reality - especially in acoustic environments where early reflections are crucial to a room's proper functioning. This dichotomy raises the question of which parts of the determined measurement functions are characteristic for the auditorium as a whole and which parts depend on the detailed measurement location.

Here, the measurement series of Reich and Hasti (sets 8-11, 12-15 and 23-25 in Table 8.1) are suitable to study the changed reproducibility condition of "location". In these series, the measurement apparatus was placed on wheels and quickly moved between measurements from one location to the next in the same room. Measurements at different locations were conducted in almost immediate succession, with some 5-10 minutes between the end of the previous run and the start of the subsequent run. As a result, the condition of "time" is closely in line with the repeatability conditions and may hence be seen as constant under reproducibility conditions. In the measurements in *Aula 1* and *Aula 2*, the sound field was documented in four quadrants over the entire audience area. In *Concertgebouw Amsterdam*, the sound field at the middle-left audience area was surveyed. The apparatus was subsequently moved in four steps from the front to the very back of the hall, making it possible to investigate how the acoustic conditions change with increasing distance to the sound source.

Changed condition: Conditions of use

In ISO Guide 98-3 (2008) the "condition of use" is listed as a reproducibility condition to be changed. The generality of this term allows a versatile projection to many measurement applications, but makes it difficult to identify the exact aspect meant in a specific measurement task. In regard to the ISO 3382-1 (2009) measurement standard, this aspect can be interpreted as the setup of the test object (i.e., the room). This aspect is very relevant for two practical considerations: On the one hand, the acoustic conditions in multipurpose rooms are regularly modified in a targeted manner to accommodate the widest possible range of event types. These changes are usually perceivable and must therefore also be distinguishable in suitable measurements. On the other hand, it is often a question of what level of detail must be documented in measurements. Marginal changes to the room should not alter measured data to a point where a new situation arises. Exploring this boundary is also an objective of investigating this reproducibility condition.

The measurement series by Hartl (sets 5-6), Hasti (sets 16-22) and to some extent the comparison between measurements by Hartl and Reich (sets 2, 7-11) may provide some insights in this regard. Hartl conducted repeated measurements in *Eurogress Aachen*, first with chairs placed underneath the sampling area in the initial set 5, and later without in set 6. Hasti's measurements in the *rehearsal room* of the *Aachen Symphony Orchestra* were performed with ever so slight changes in the variable acoustic panels of the space so that the acoustic condition of the room changed in between measurements. In particular, in set 16 the reflective side of the wall panels was exposed to the sound field, creating a relatively

reverberant environment, whereas in set 20 the absorptive side of the panels was fully exposed. As these changes in the conditions have a significant influence on the absorptive properties of the space (see Figures 6.2 and 6.4), these series offer a good foundation to investigate how these changes in the reverberation time affect spatial fluctuations (Davy, 1981; Kuttruff & Thiele, 1954).

Changed condition: Frequency and bandwidth

The theoretical principles discussed in Chapter 2.1 identify both the frequency and the bandwidth as having a significant effect on the spatial fluctuations: Bodlund (1977) targets the spatial correlation of modes and Davy (1981) addresses the fluctuation's amplitude as a function of frequency and bandwidth. Davy's discussion of the decay's variance is closely related to this study's rationale of the measurement function, but they are yet to proven equivalent. To qualify the validity of the measurement function, it is necessary to investigate whether it matches Davy's theoretical predictions.

To do so, the measured impulse responses are analyzed in broadband and filtered in octaves and third-octave bands. The simple comparison of the different cases permits investigating the changed conditions of frequency and bandwidth. From the data of the 26 measurement series a set collected in *Eurogress*, set 5 was picked as an arbitrary example to discuss this effect.

Changed condition: Auditorium

In the final abstraction stage, the measurement functions determined in different auditoria are compared. Measurements in lecture halls, concert halls, a multipurpose hall and an orchestra rehearsal room with variable acoustics cover a wide range of acoustic environments. As before, these data will be compared to investigate which properties of the measurement function are meaningful. The theoretical considerations (Bodlund, 1977; Davy, 1981; Kuttruff & Thiele, 1954) give raise to the strong expectation that (at least parts of) the measurement function makes it possible to distinguish between different spaces. In discussing this last reproducibility condition, the focus is not so much on similarity as it is on targeting differences that support recognizing the measurement function as a valid indicator of spatial fluctuations (varying between rooms). To discuss this question, for each of the six surveyed auditoria, representative measurement sets are selected and compared to each other.

8.3 Results

Acoustic properties of the different rooms

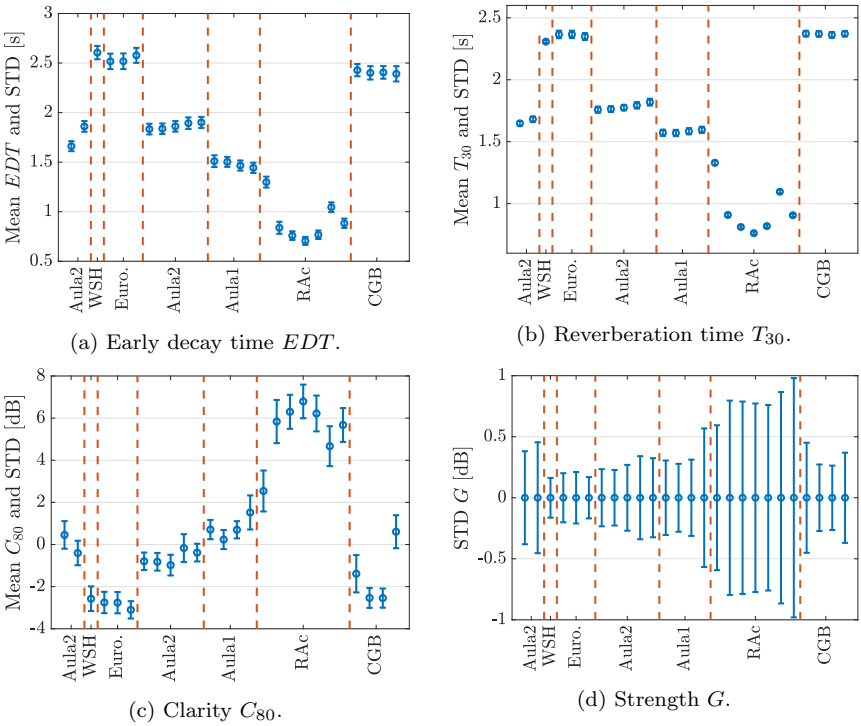

(a) Early decay time EDT.

(b) Reverberation time T_{30}.

(c) Clarity C_{80}.

(d) Strength G.

Figure 8.1: Distribution of room acoustical quantities in different halls. The sequence along the x-axes coincides with the listed sets in Table 8.1.

Under the umbrella term of validity, this chapter seeks to identify the driving factors that influence the properties of the measurement function. The background provided in Chapter 2.1 highlights that the general acoustic properties of the surveyed rooms play a role. Figure 8.1 shows a simple statistical summary of the room acoustical quantities collected in each of the 26 sets. The detailed properties of the sets' measurement conditions are listed in Table 8.1. To allow better interpretation of the data, the acoustic properties in the subplots of Figure 8.1 are identified by the room names even though they are presented in set order. Images of the different auditoria can be found in Figure 5.5. The shown

mean and standard deviations are generally determined based on the 16 960 room impulse responses that were collected in each set's sampling area.

Across all surveyed auditoria both EDT and T_{30} show generally similar results, which suggests a rather homogeneous decay and a relative small influence of the direct sound. In line with general experience, EDT shows a slightly larger variance compared to the T_{30} values. Auditoria used for the performance of symphonic music (i.e., *Concertgebouw Amsterdam*, *Wuppertal Stadthalle* and *Eurogress Aachen*) show (without an audience) relatively long reverberation times, just short of 2.4 s - 2.5 s. Meanwhile, the surveyed large lecture rooms feature reverberation times around 1.5 s - 1.8 s, and the reverberation times measured in the *rehearsal room* are shortest of all the 26 sets. The orchestra *rehearsal room* is equipped with variable acoustic wall elements that make it possible to change the acoustic conditions and alter the reverberation times. Most of the investigated setups yielded decay times around 0.8 s, but in the two most reverberant scenarios the measured decay (T_{30}) lasted for 1.3 s and 1.1 s respectively.

Mean values of clarity in the surveyed auditoria confirm the negative correlation to reverberation times. One data set in *Aula 1*, *Aula 2*, *Concertgebouw*, as well as the data from the orchestra *rehearsal room* (i.e., sets 10, 15, 16 - 22 and 26) exhibit a slightly larger variance in C_{80}. This larger variance is a common property of measurement series that sample the sound field in relative close proximity to the sound source. In these cases, the sound field changes considerably over the sampled area, which manifests in a larger variance. This phenomenon is also quite pronounced for strength (G).

8.3.1 Repeatability

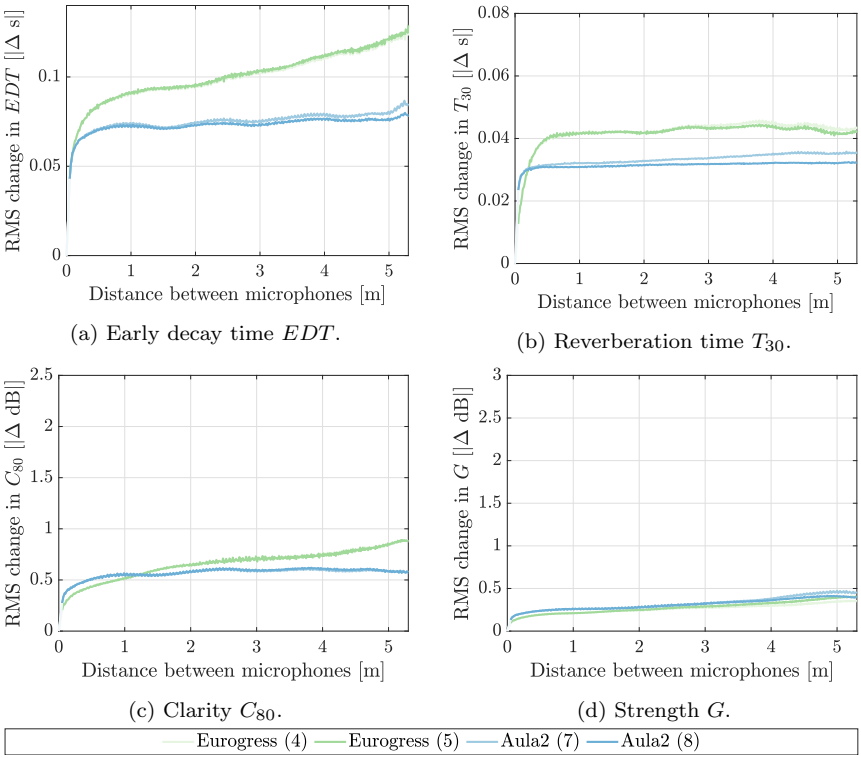

(a) Early decay time EDT.

(b) Reverberation time T_{30}.

(c) Clarity C_{80}.

(d) Strength G.

Figure 8.2: Measurement function under repeatability conditions in two halls.

Based on the two measurements in *Eurogress Aachen*'s main hall (green in Figure 8.2) and in *Aula 2* (blue), each conducted in immediate succession, it is possible to investigate how the quantile function changes over relatively short periods of time. The juxtaposition of these repetitions is shown in Figure 8.2. The two measurements taken in the same room are shown in the same color but can be differentiated through their hue.

The four tiles show the measurement functions for EDT, T_{30}, C_{80} and G. Along the x-axis, the distance between microphones is plotted. The y-axis shows the rms change in the respective room acoustical quantity. To permit comparability between different conditions, the presented range across both axes is held constant throughout the remainder of this chapter. The quantile functions follow the

general pattern of the *initial rise* and the *extended trend* discussed in Section 7.

Comparing the curves of the same color but different hue, it is evident that they are in very close agreement. Here, close agreement means that the curves of the repeated measurements cannot be distinguished over wide ranges in the shown scaling. Regardless of the room acoustical quantity, the *initial rise*s measured in the same rooms run in almost perfect congruence. Small differences become evident when contrasting the *extended trend* of repeated measurements in *Aula 2* for EDT and T_{30} (Figures 8.2a and 8.2b) against each other. With longer distances between microphones, the differences under repeatability conditions in reverberation times increase but remain smaller than 0.006 s. Differences between repeated measurements in clarity (Figure 8.2c) are hardly detectable for both the *initial rise* and the *extended trend*. In regard to strength G (Figure 8.2d), differences between measurements are generally less than 0.07 dB.

Interim discussion

The observation that the curves from repeated measurements overlap almost perfectly shows that the determined quantile functions are not the results of random changes in the sound field. Maximum differences of less than 0.006 s or 0.07 dB are still very small compared to the absolute value of the shown curves. Without anticipating too much, it can already be said that the differences under repeatability conditions turn out to be significantly smaller than differences due to any of the upcoming reproducibility scenarios. Differences between repeated measurements are just above the noise due to the anisotropic sampling density (for background see Chapter 7). In any case, such subtleties are beyond the scope of a reasonable evaluation.

8.3.2 Reproducibility

Changed condition: Time and observer

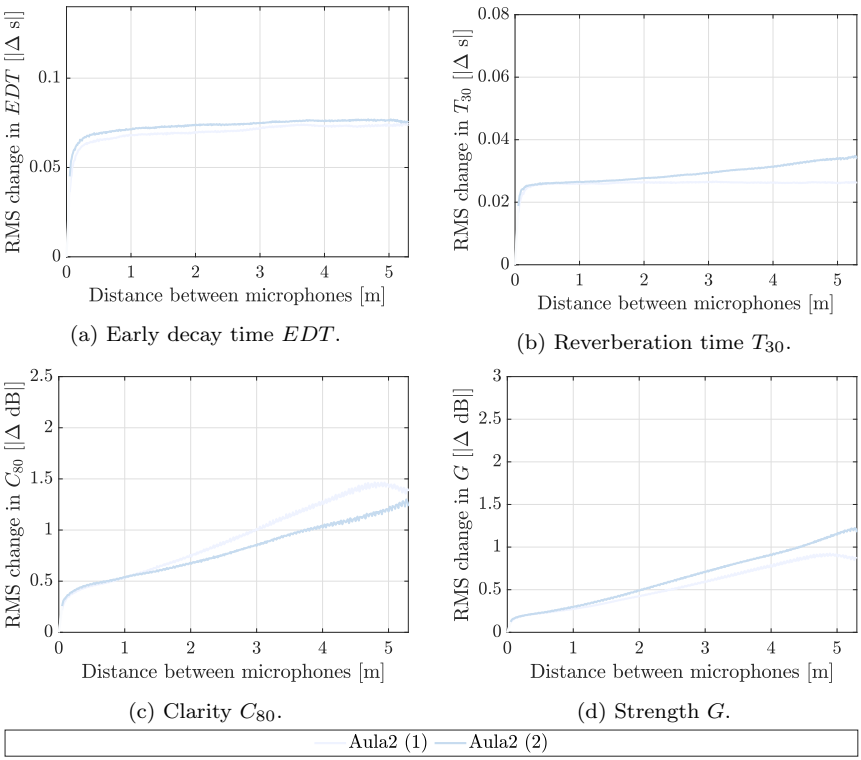

(a) Early decay time EDT.

(b) Reverberation time T_{30}.

(c) Clarity C_{80}.

(d) Strength G.

Figure 8.3: Measurement function under reproducibility conditions at different times.

The differences resulting from independently repeated measurements on different days (including complete setup and dismantling of the measurement setup) can be investigated through sets 1 and 2 that were collected in *Aula 2*. The rms change of room acoustical quantities as a function of distance between sensors is shown in Figure 8.3.

When comparing the *initial rise* between sets across all of the four room acoustical quantities, both curves run in close agreement. Differences can be detected upon very close inspection, but these are small compared to the curves' covered range (in amplitude) over a wider trend.

Focusing on EDT (Figure 8.3a), it can be seen that in set 2 the *initial rise* terminates at slightly higher amplitudes than in set 1. This difference remains over the entire *extended trend*. At the same time, Figure 8.1a shows that the mean early decay times differ between both sets, with set 2 having considerably longer decay times. Shifting attention to T_{30} (Figure 8.3b), a similar picture emerges with nuanced contrasts. While the curves of both sets exhibit close similarity at shorter distances, the lines diverge as the distance between sampling points increases. The larger rms change in T_{30} for set 2 relative to set 1 over the *extended trend* coincides with slightly longer mean reverberation times (Figure 8.1b).

The general trend and the differences in the other parameters discussed (Figures 8.3c and 8.3d) are characterized by two noteworthy distinctions. The quantile functions for C_{80} and G show a continuous rise throughout the *extended trend*, and the curves for both sets diverge under the studied repeatability condition. At very large distances the difference becomes most prominent with 0.2 dB for both quantities. The continuous slope evident under this reproducibility condition was not seen under repeatability conditions (Figures 8.2c and 8.2d). In reference to the generally prevailing conditions (Figure 8.1c), it can be seen that clarity is generally higher in the first set.

Interim discussion

Compared to repeatability measurements, the differences in reproducibility measurements under the changed condition "time" are slightly greater but still appear rather small compared to the range of amplitudes covered in the *initial rise* and the *extended trend*. This is a fundamental result when discussing spatial fluctuations. Even though they still appear small, the EDT and T_{30} differences in the fluctuation's amplitude can be related to simultaneously prevailing differences in the reverberation times. Consequently, these differences in fluctuations are in line with qualitative theoretical predictions (Davy, 1981).

Differences in the *extended trend* of the quantile function with regard to clarity and strength deserve a nuanced and careful discussion. In general, variations in the results should not be particularly surprising, given that some conditions were deliberately uncontrolled in this reproducibility measurement. The upcoming discussion targets some of the several factors that may play a role; however, the uncontrolledness aggravates the unique identification of possible causes from the data shown in this pair comparison.

The observation that the *extended trend*s of the strength and clarity quantile functions cover a wider range (Figures 8.3c and 8.3d compared to Figures 8.2c and 8.2d) is evidence that the sound field under both reproducibility conditions changed considerably over larger distances (i.e., $d \gtrsim 2\,\mathrm{m}$). The most ob-

vious cause seems to be a closer proximity to the sound source of the sets 7 and 8 than sets 1 and 2. Even if, through reference to the critical distance, the RIRs' main energy contribution can be attributed to the diffuse reverberation, the direct sound still plays a relevant role for C_{80} and G. Thus, if a continuous increase in G and C_{80}'s *extended trend*s can be related to an influence of the direct sound, this is true not only in the joint comparisson of sets 1 and 2 to sets 7 and 8, but also in the comparison of sets 1 and 2. Thus, it is up for discussion whether the sampling position "middle of the room" was reproduced exactly. This doubt is justified by the fact that the measurement region could not be marked in the lecture hall as the time between measurements was several months. As a result, the measurement location is not known exactly.

Other factors to consider are the generally prevailing acoustic conditions (i.e., differences in mean EDT and T_{30}) during the different measurement series. Figure 8.1a suggests a clear difference in EDT between sets 1 and 2. This difference could be explained quite well by the sampling areas' distances to the sound source, but the consistent difference in Figure 8.1b suggests that a fundamental difference in the sound fields' damping existed simultaneously. Differences in the sound field's decay are a plausible explanation for the differences in quantile functions' extended trend in Figures 8.3a and 8.3b.

Despite these differences and their potential explanations, the curves' overall similarity in Figure 8.3 indicates a fairly good reproducibility ($\Delta EDT < 0.005\,\mathrm{s}$, $\Delta C_{80} < 0.02\,\mathrm{dB}$) in the parts of the measurement series that contribute to the *initial rise* and, thus, to spatial fluctuations. The differences found appear plausible within the scope of the previous discussion's explanatory power. There are first indications that the *extended trend* depends on the measurement location in the room. This is also plausible in light of Vorländer and Kuttruff's (1985) findings (see Chapter 5.2).

Changed condition: Location

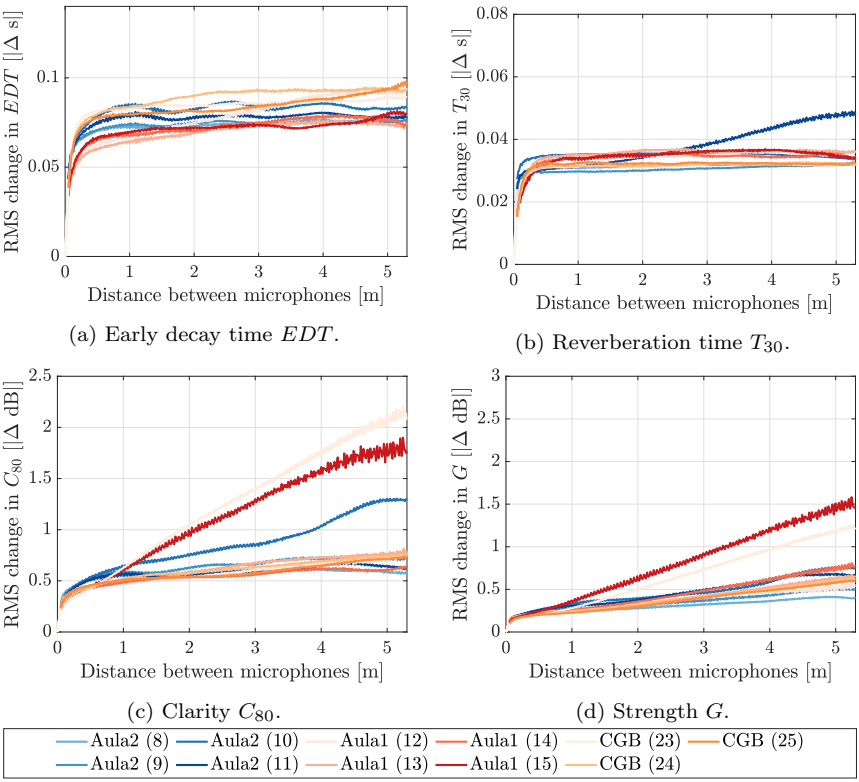

(a) Early decay time EDT.

(b) Reverberation time T_{30}.

(c) Clarity C_{80}.

(d) Strength G.

Figure 8.4: Measurement function at different locations under reproducibility conditions in different halls.

To test the changed condition of "location", measurements were taken in three spaces in immediate succession at different locations in the room. This data, featuring a total of eleven curves, is shown in Figure 8.4. The blue curves show results from *Aula 2*, red from *Aula 1* and orange from *Concertgebouw Amsterdam*.

In a first step, the EDT curves in Figure 8.4a are investigated. It is noticeable that the curves from the same rooms (same color, different hue) follow a similar pattern in terms of the niveau and the general slope in the *extended trend*. Curves from different rooms (different color) can be distinguished by the same traits. When considering T_{30} in Figure 8.4b, the same trend generally seems to be valid; however, more sublte differences do excist. Curves 10 and 11 in *Aula 2* stand out,

as the former's *extended trend* runs on a noticeably higher level and the latter's features a fairly steep slope.

Focusing on the *initial rise* of EDT in Figure 8.4a, great similarities in all curves' slopes starting at the origin are evident. Differences can only be observed when the curves bend at different amplitudes to transition to the *extended trend*. The transitions, albeit occurring at different levels, appear to have a similar pattern and shape. A similar observation does not seem valid for T_{30}'s *initial rise* in Figure 8.4b. Different rooms exhibit different T_{30} slopes, while T_{30}s from the same rooms show similar behavior. Visual inspection suggests that *Aula 1* (red) shows the highest average quantile function at short distances. According to the same visual criterion, *Concertgebouw*'s quantile functions run slightly above *Aula 2*'s sets 8, 9 and 11 and show a successively steeper slope at the *initial rise*.

Shifting attention to C_{80} and Figure 8.4c, it becomes evident that most of the curves follow a similar pattern in their *initial rise* and *extended trend*. Differences exist, but they are small compared to the rms change in clarity range covered by of all curves. From each of the three auditoria there is one set (i.e., 10, 15 and 23) that shows a diverging *extended trend* with a significantly steeper slope. Referring to Figure 8.1c, it can be seen that each of these three sets feature a higher mean clarity index and a larger standard deviation than the other sets collected in the same room.

Regarding the strength data presented in Figure 8.4d, a situation emerges similar to that of the clarity results. The only notable difference is that set 10 from *Aula 2* does not stand out as before, and instead follows a relatively flat *extended trend*.

Interim discussion

Comparing the trends across the four discussed room acoustical quantities, there seems to be a distinction between reverberation times and the other two quantities. With respect to the reverberation times (EDT and T_{30}), curves from the same room show similar *initial rise*s and *extended trend*s. When discussing EDT's and T_{30}'s spatial fluctuations, this means that the measurement location plays a minor role. This confirms findings by Davy (1981) and thus increases the validity of the measurement function.

Similar findings are so far not available for other room acoustical quantities. The similar pattern of the strength and clarity curves shows, in broad terms, that there are no significant differences in spatial fluctuations across location. The outliers from this general assessment (i.e., sets 10, 15 and 23) deserve a closer look as part of a differentiated discussion to further investigate why their *extended trend*s exhibit a relatively steep rise. Figure 8.5 shows the spatial distribution of

broadband C_{80} in two of the surveyed sampling areas: one each in *Aula 2* and *Concertgebouw Amsterdam*. The data from *Aula 1* is not shown, but exhibits a similar trend as in Figure 8.5b.

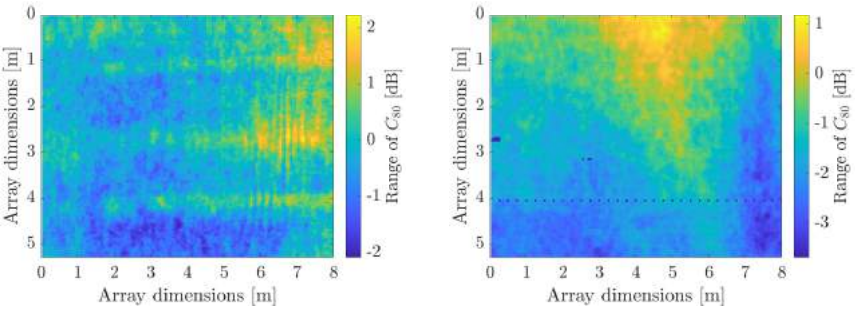

(a) Aula 2 (10).

(b) Concertgebouw Amsterdam (23).

Figure 8.5: Distribution of broadband C_{80} in two sampling areas.

The most prominent feature of the sampling areas shown in Figure 8.5 is that, apart from local fluctuations, clarity follows an overarching trend. Possible reasons may be a strong early reflection from a surface that exposes only parts of the sampling areas (Figure 8.5a), or a relatively close proximity to the source that causes the direct sound to be strongly distance-dependent (Figure 8.5b). This distance dependence is obviously to be seen in relation to the energy in the diffuse reverberation.

Noteworthy, but only relevant as a side note, are the horizontal lines in Figure 8.5a, which originate from the direct sound's reflection off the table surfaces (in classroom-style seating). This regular pattern is also found in *Aula 2*'s quantile functions (particularly obvious in Figure 8.4a).

The ability to relate special properties of the sound field to the quantile function through clear causal relationships is a very strong argument for the validity of the measurement function. Given that Davy's fluctuations occur independently of location, it can be deducted that an *extended trend* with a significant slope results from the superposition of an overarching trend.

Changed condition: Conditions of use

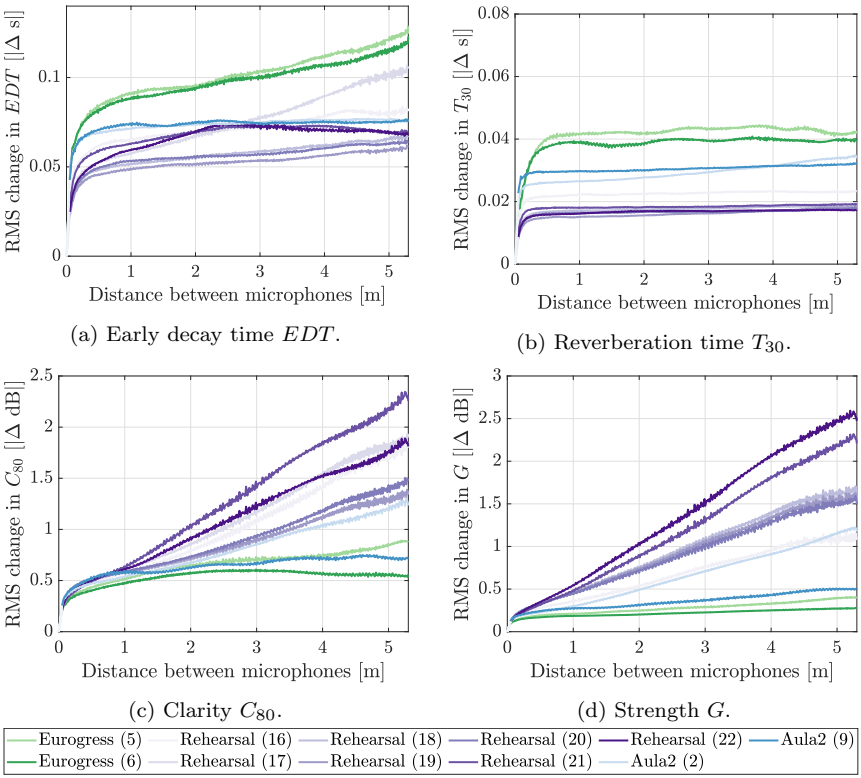

(a) Early decay time EDT.

(b) Reverberation time T_{30}.

(c) Clarity C_{80}.

(d) Strength G.

Figure 8.6: Measurement function in three halls under different conditions of use.

For some measurement series, the acoustic conditions of the space were changed between the measurements. In *Eurogress*, measurements were first conducted in a completely empty room. Then, for the immediately following series of measurements, rows of stackable chairs were placed underneath the array. *Aachen Symphony*'s *rehearsal room* features flexible wall elements that can be turned. At different positions, these elements expose either a reflective or an absorptive surface to the sound field. It is thus possible to change the absorption and the reflection pattern in the room. In seven subsequent measurement series the condition of the room was changed in small steps from a relatively reverberant environment to its most absorptive setup. Measurements in *Aula 2* were taken on different days with rows of seating in set 2 and classroom-style seating in

set 9. The results of these comparisons are shown in Figure 8.6. The collected data from the different rooms is shown in different colors: green for *Eurogress Aachen*, violet for the *rehearsal room* and blue for *Aula 2*.

From Figure 8.6a, it can be seen that EDT quantile function curves from the same room are clustered. In *Eurogress* and *Aula 2*, differences due to the changed condition of use in the same room are smaller than the differences between the two rooms. In contrast, the violet curves of the *rehearsal room* exhibit a relatively large variance that is most evident through the amplitude at which the *initial rise* transitions into the *extended trend*.

The T_{30} data in Figure 8.6b permits observations similar to those made for EDT. The most significant difference relative to Figure 8.6a is the *extended trend* running in mostly flat curves. Of the curves showing data from the *rehearsal room*, sets 16 and 21 have the largest rms change in EDT and T_{30} in the *extended trend*.

Shifting the focus to C_{80} and Figure 8.6c, it is evident that the *initial rise* is quite similar (relative to the covered rms change in C_{80}) across all of the presented curves. All data from the *rehearsal room* exhibits a continuously rising *extended trend*, but also features a large variance between different acoustic conditions. The green curves from *Eurogress* are very similar in their flat *extended trend*s. This is in contrast to the blue quantile functions from *Aula 2* that follow a diverging pattern throughout the *extended trend*. Qualitatively, the same observations made for C_{80} can also be made for G in Figure 8.6d.

Interim discussion

Even if the term "conditions of use" were to correctly summarize the scope of the discussed reproducibility conditions, a joint analysis of all presented measurement series might not be justified. This is because the changes in the surveyed acoustic environments are different in extent and nature. Removing chairs from underneath the sampling area between two successive series of measurements apparently has a relatively small effect on the sound field compared to changing the absorption properties and orientation of wall elements. Further considering that the changes in the acoustic conditions in *Aula 2* are intricate, the insight emerges that the various influences cannot be reduced to a single factor. Instead, a differentiated discussion is necessary.

Across all tiles in Figure 8.6, it can be seen that the green curves of *Aula 2* show a very similar pattern. This is evidence that chairs underneath the sampling area have a limited influence on the sound field. The only quantitative difference can be identified in Figure 8.1b. The diagram shows that the chairs reduce the average reverberation time and thus increase the room's average absorption ever

so slightly. According to Davy (1981) this should lead to a reduced variance in reverberation times, which can be confirmed in Figure 8.6b. Since the added chairs did not alter any of the sound's main propagation paths (including via the hall's floor), the influence of this changed condition of use is rather small.

The changes in the *rehearsal room*'s wall elements have (at least) a twofold influence on the sound field. The first notable change is absorption of the sound, which reduces the reverberation (see Figure 8.1b) and thus the amplitude of the *extended trend* in Figure 8.6b. The same data suggests that not all changes in settings lead to notable changes in reverberation. As a result, the violet curves in Figure 8.6b cluster according to their associated reverberation time.

The second notable change to the *rehearsal room*'s setup is that the orientation of the wall panels changes the distribution of early reflections. This effect cannot be shown directly in the presented data, but is hinted at by the change in clarity, and is plausible from contemplation and general experience. These changes to the sound field likely manifest in the divergence of the violet curves' *extended trend* in Figures 8.6c and 8.6d.

Detailed comparison of sets 2 and 9 from *Aula 2* reveals that many conditions have changed simultaneously. Table 8.1 indicates that the measurement date, the location in the room and the condition of use changed: in set 2 the room was surveyed at a central sampling area with rows of seating set up, whereas in set 9 the sampling area was located towards the left-rear of the hall with classroom-style furniture in place. In this intricate situation and based on the available data, it is not possible to show clear correlations. The only conclusion that can be drawn is that the changes to the room discussed here are sufficient change the quantile function notably.

These facts and arguments lead to a situation that makes it difficult to identify new findings robustly. The influencing factor of reverberation can be identified (again) and is in line with the theoretical findings of Chapter 2.1 and Davy (1981). In regard to existing knowledge, the validity of the measurement function is supported. To other discussed changes influence the overarching gradient of the sound field that appears in the measurement function's *extended trend*. Again, this supports the validity of the measurement function.

Unfortunately, however, it has to be realized that describing the room's condition of use with a single quantity and mapping this to a change in the sound field, and by further extension the quantile function, is not a unique line of reasoning. Thus, the available data is too sparse to unambiguously reveal subtle relationships. This leads to the assessment that the measurement function appears valid based on a sense of proportion and general experience.

Against this backdrop it is evident that an auditorium's condition of use can have a significant influence on spatial fluctuations. Although not all of the in-

fluences discussed here are of the same significance, some cause and effect relationships could be made plausible, and this notion supports the validity of the measurement function. Additional, more targeted investigations can shed new light on the driving driving forces.

Changed condition: Frequency and bandwidth

Since all phenomena in acoustics are due to wave effects, frequency dependencies are considered common knowledge and may therefore not seem particularly interesting as a focus of investigation. The study by Davy (1981) already paints a rather clear picture as it proves that the reverberation time's spatial variance is proportional to the statistical filter bandwidth's reciprocal value (Equation 2.1.19). Since the statistical bandwidth of IEC 61260-1 (2014) filters changes

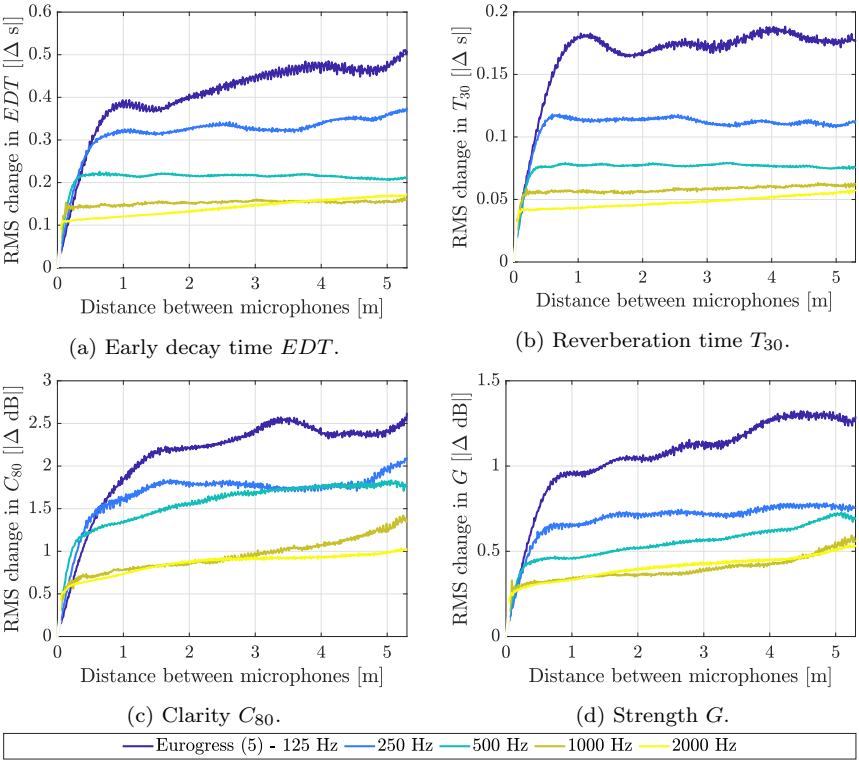

(a) Early decay time EDT.

(b) Reverberation time T_{30}.

(c) Clarity C_{80}.

(d) Strength G.

Figure 8.7: Measurement functions at different frequencies.

with center frequency and fractional octave bandwidth, spatial fluctuations are predicted to vary in amplitude when analyzed at different frequencies with different bandwidths. Quantitatively, the statistical bandwidth changes from one octave to the next higher by a factor of 2. Octave filters' statistical bandwidths are three times larger than third-octave filters.

This background provides an opportunity to empirically replicate the predictions from theory and so discuss the validity of the measurement function. The changed condition of frequency and bandwidth is investigated using the data set collected in *Eurogress Aachen* (set 5) as a representative example. The results are shown in Figures 8.7 and 8.8.

Figure 8.7 shows the quantile functions for different room acoustical quantities at different frequencies of full octave band filtered data. It is a unison result

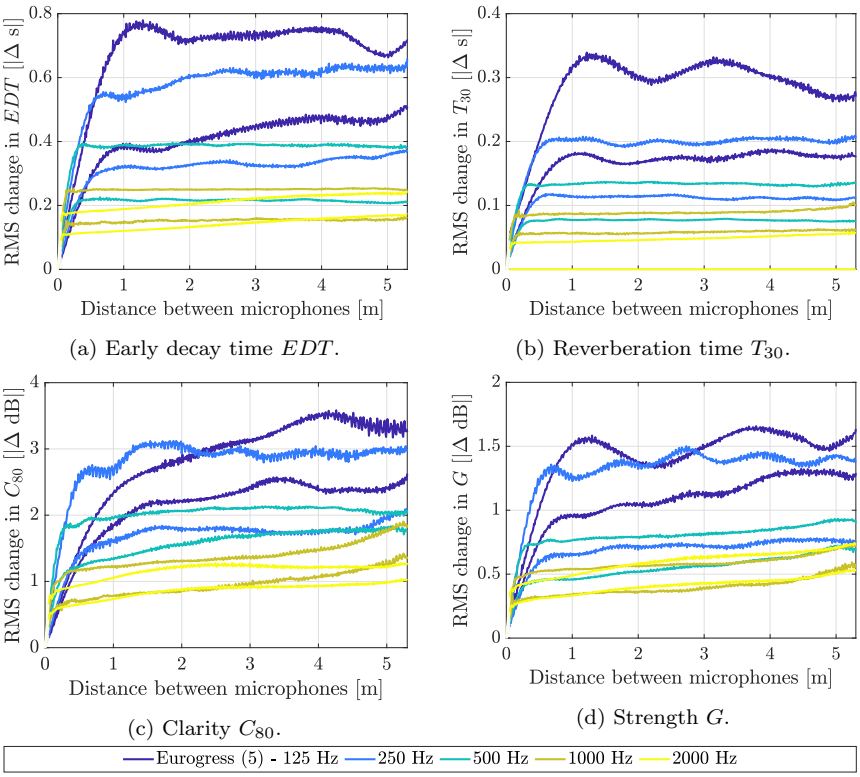

(a) Early decay time EDT.

(b) Reverberation time T_{30}.

(c) Clarity C_{80}.

(d) Strength G.

Figure 8.8: Measurement function at different frequencies in different bandwidths.

that the *initial rise* is steeper at higher frequencies. For the reverberation times EDT and T_{30}, the transition to the *extended trend* occurs at higher amplitudes for lower frequencies. At the same time, it can be observed that at lower frequencies the transition from the *initial rise* to the *extended trend* extends to larger absolute distances between microphones. Referencing the common acoustical knowledge mentioned before, the transition occurs at roughly the same wavelength-related distance (i.e., $k\Delta\mathbf{r} \approx 2.2$). Looking at the C_{80} and G data, both trends are similar; however, there are some curves in the 1 kHz to 2 kHz octave bands with similar amplitudes in spatial fluctuations.

When the additional factor of bandwidth is introduced, the graphs shown in Figure 8.8 become relevant. For the center frequencies given in the legend, the quantile function was determined both in full and in third-octaves. Curves of the same center frequency are drawn in the same color. Regardless of the room acoustical quantity, it can be seen that the spatial fluctuations are significantly greater with narrow-band evaluation. In addition, it can be observed that the *initial rise* is steeper when discussing the data in third-octave bands.

Table 8.2: The ratios of spatial fluctuations at different bandwidths and frequencies

Room acoustical quantity	Octave band fraction	Mean rms change in quantity ($1\,\mathrm{m} < d < 5.3\,\mathrm{m}$)					Ratio
		Frequency band					
		125 Hz	250 Hz	500 Hz	1 kHz	2 kHz	
EDT	1/1	0.440	0.335	0.215	0.155	0.148	0.60
	1/3	0.738	0.610	0.388	0.251	0.220	
T_{30}	1/1	0.176	0.112	0.077	0.059	0.050	0.59
	1/3	0.304	0.201	0.134	0.090	NaN	
Ratio			0.72	0.66	0.70	0.89	

To permit a quantitative comparison of the spatial fluctuations, Table 8.2 lists the rms change for EDT and T_{30} at different center frequencies and octave band fractions. The presented values show the quantile functions' mean amplitudes over the distances between 1 m and 5.3 m (Figures 8.7 and 8.8). At these distances the spatial fluctuations are fully pronounced, and the curves run into the *extended trend*'s domain. Following Davy's (1981) discussion the spatial variance of reverberation times, conversion to rms requires taking the variance's squareroot:

$$\sqrt{\frac{1}{n-1}\sum_{i=1}^{n}(x_i-\bar{x})^2} = \sqrt{\mathrm{Var}(x_i)}. \tag{8.3.1}$$

Reference to theory is given in two stages. First, the absolute comparison shows that the rms changes in Table 8.2 over all frequencies are on average almost 75 % higher than Davy's model prediction (Equation 2.1.19). Second, comparison indicates that relative rms changes between octave band fractions or neighboring center frequencies are in agreement with theory's suggested influence of the statistical filter bandwidth. The values in Table 8.2 associated with the curly brackets provide the empirical data to this comparison. It can be seen that the quantile function's amplitude is 0.59–0.60 times lower for full octaves compared to third-octaves. Davy's theory suggests the ratio should be $1/\sqrt{3} \approx 0.58$. Similarly, the quantile function is on average lower by a factor of about 0.74 when comparing data from one octave band center frequency with the next higher. This ratio can be juxtaposed to theory (Equation 2.1.19; Davy (1981)) that predicts a factor of $1/\sqrt{2} \approx 0.71$.

Interim discussion

The collected data clearly shows that both the filter's center frequency and its bandwidth have particularly strong influences on the spatial fluctuations. As a mater of fact, none of the previously investigated conditions have a similarly strong effect on the amplitude of spatial fluctuations. Thus, these are the most important factors influencing spatial fluctuations so far.

The notion of the filter properties "influencing" a measurement result may seem unjustified when subscribing to a perspective that recognizes filtering as a multiplication in frequency domain that has little to no effect on the transfer function in the passband interval. Although this view is certainly justified for many applications, it neglects the filter's impulse response. The reason that filters are discussed as influence factors in the context of this study can be illustrated by the following example:

The starting point is an arbitrary room impulse response with homogeneous characteristics over the entire frequency range. Evaluating the reverberant decay will lead to identical reverberation times across frequencies and bandwidths as long as the reverberant decay is long compared to the filter decay. In contrast, however, despite the RIR's homogeneity in the frequency domain, spatial fluctuations will be different when analyzed at different frequencies and bandwidths.

The quoted average difference of 75 % between the model prediction and empirical data may seem large at first. These differences have to be put into perspective

with respect to Davy et al.'s 1979 measurements in reverberation rooms that intended to validate their theory. In their validation study, Davy et al. (1979) indicate in their Figure 4 that empirical standard deviations can differ from model predictions by factors of 0.5 to 2 The spatial variances measured in *Eurogress Aachen* are thus within the upper range of Davy et al.'s original validation. Thus, the results shown for the reverberation times indicate a moderate agreement with the theoretical predictions.

Davy et al.'s predicted change in variance in the spatial fluctuations' amplitudes from one octave to the next higher (i.e., 1/2) and the change in variance when comparing full octave with 1/3 octave bandwidths (i.e., 1/3) is in very close agreement with the empirically determined rms ratios shown in Table 8.2. Even when this agreement is expected, it is not guaranteed in the presence of other factors (e.g., reverberation) that may have changed simultaneously over frequency. These contributions may also be the reasons for the differences relative to the absolute model predictions.

These results are very important for the validity assessment of the measurement function. Apart from the conversion needed to transform Davy et al.'s spatial variance of reverberation times to the rms change discussed here (Equation 8.3.1), the *extended trend* discussed in Figures 8.7 and 8.8 targets the same aspect. Qualitative agreement can be claimed based on the *extended trend* for the reverberation times running in flat lines. The ratios shown in Table 8.2 indicate that the changes in bandwidth are in almost perfect agreement with theory, while changes over frequency are in fair agreement (less than 6 % deviation), due to larger differences at higher frequencies.

Even though theory does not permit direct predictions about the spatial fluctuations of other room acoustical parameters, it can be seen in Figures 8.8c and 8.8c that the factors of "frequency" and "bandwidth" are driving forces for these quantities in a very similar way. This represents a new finding of this study that is consistent with the other results and with theory.

Changed condition: Auditorium

When comparing the quantile functions of various room acoustical quantities in different auditoria, the situation shown in Figure 8.9 emerges. The concepts of *initial rise* and *extended trend* can be observed here as well.

Starting with Figure 8.9a and EDT data, it can be seen that the *extended trend* of curves from different rooms generally run in parallel with a moderately rising slope. Two measurement series (i.e., *Eurogress*(5), *rehearsal room*(17)) stand out as they show a slightly steeper rise throughout the *extended trend*. Starting at the origin, the *initial rise*s of all curves run in unison. Differences become evident

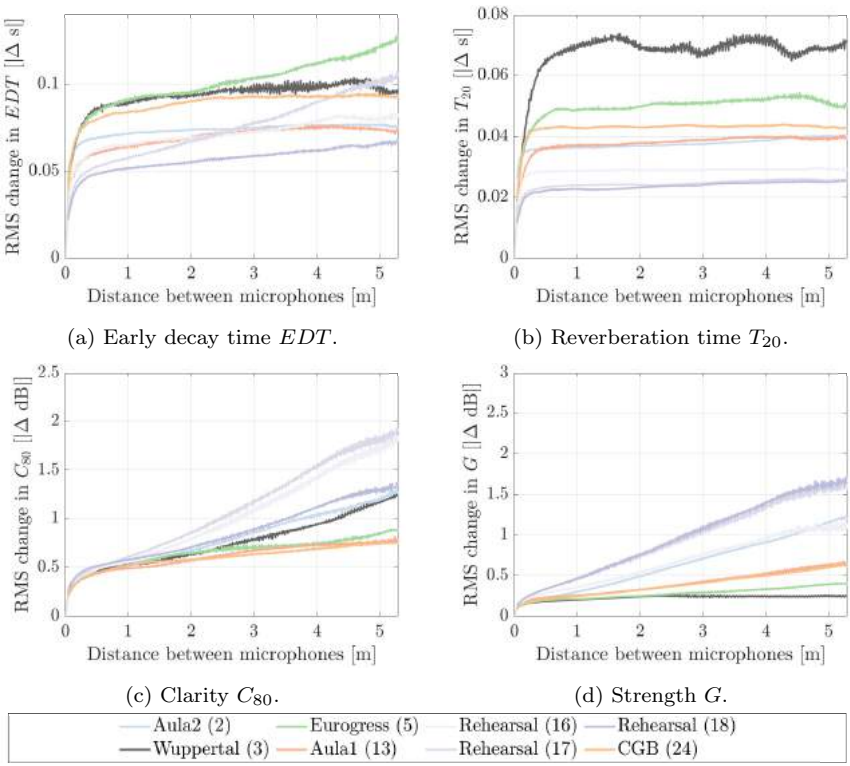

(a) Early decay time EDT.

(b) Reverberation time T_{20}.

(c) Clarity C_{80}.

(d) Strength G.

Figure 8.9: Measurement function in different auditoria.

at the rms change amplitude when the curves take a turn to join the *extended trend* that runs at individual levels.

Shifting over to Figure 8.9b and T_{20}, a generally similar picture emerges except that in all cases the *extended trend* runs in flat, parallel lines. The different types of rooms are clustered in different groups: curves measured in the *rehearsal room* feature the lowest rms change in T_{20}, the large lecture halls show a similar *extended trend* at a medium amplitude, just below 0.04 s, and the concert halls exhibit the largest spatial fluctuations. For reasons of lacking SNR in *Wuppertal* measurements, Figure 8.9b shows curves for T_{20} rather than T_{30}. In light of Equation 2.1.19, the only difference to be expected is a slightly higher amplitude of the shown rms changes in reverberation time, due to the smaller dynamic range of $D = 20\,\text{dB}$. In Figure 8.9b, the *initial rise* of T_{20} shows a similar behavior to that of EDT. The transition between the two domains appears to occur at the

same distance between microphones.

Shifting attention to the G and C_{80} data in Figures 8.9c and 8.9d, it can be seen that there are a few sets where the *extended trend* shows a continuous rise. These curves mainly represent data collected in the *rehearsal room*. To establish a sense of proportion, it can be seen that the continuous trend to longer distances spans larger rms changes in room acoustical quantities than does the *initial rise*. Compared to curves for EDT or T_{30}, there are finer differences in the G and C_{80} curves' that shape how the *initial rise* transitions into the *extended trend*. While

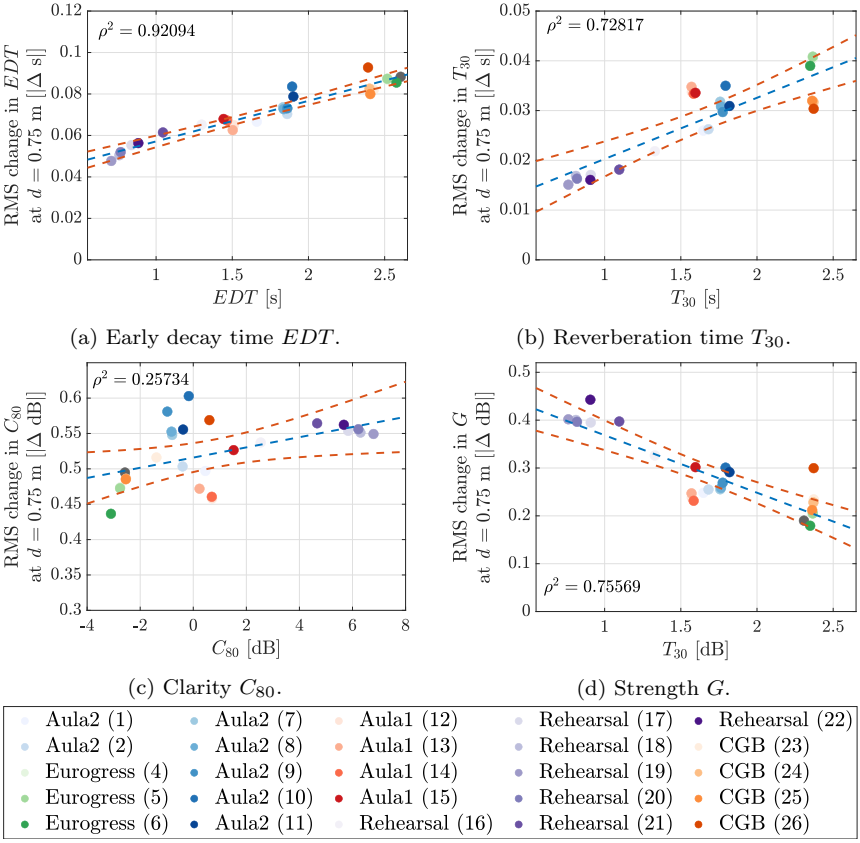

(a) Early decay time EDT.

(b) Reverberation time T_{30}.

(c) Clarity C_{80}.

(d) Strength G.

Figure 8.10: Spatial fluctuations as a function of the absolute value of room acoustical quantities. The blue line marks the linear regression with its 95 % confidence interval shown in red.

curves for EDT or T_{30} data show a very similar pattern in this transition, there does not seem to be a clear trend for how the C_{80} or G *initial rise*s flatten off at short distances.

To investigate how spatial fluctuations over shorter distances depend on the investigated quantity's absolute value, Figure 8.10 was prepared. All of the 26 collected sets (from Table 8.1) are marked in each of the subplots as colored points. For EDT, T_{30}, C_{80} and G, the y-axis indicates the quantity's rms change at a distance of 0.75 m between observation points. With the exception of G, the x-axis shows the quantity's mean value (from Figure 8.1). Since the absolute value of G was not measured (due to the absence of the source's sound power calibration), the T_{30} is used instead, as a simplified and conditional predictor for G (Barron, 2009, Ch. 2.9). The linear regression is plotted as a dashed line and the goodness of fit is measured through Pearson's ρ^2.

It can be seen quite clearly that the fluctuations are much more pronounced with longer reverberation times. In the surveyed rooms, the rms change in reverberation times (at least) doubles over the covered range in reverberation times of 0.7 to 2.5 s. Especially for EDT, the linear model's goodness of fit is "very strong" (Evans, 1996) with $\rho^2 = 0.92$.

Figure 8.10c suggests a slight trend towards larger fluctuations as C_{80} increases. With $\rho^2 = 0.26$, however, the goodness of fit is "weak". Figure 8.10d indicates a trend of decreased fluctuations in G with longer reverberation times. The goodness of fit of $\rho^2 = 0.76$ is "strong" and comparable to that of T_{30}. In the mid-range of values across T_{30} and C_{80}, a few outliers emerge that stem from sets collected in the large lecture halls.

Interim discussion

The differences between the various curves across rooms are a very important, if unsurprising, result. Almost all of the previously investigated conditions (time, observer, location, condition of use) have changed incoherently between measurements series, and as a result the shown data displays a considerable variance, too. Compared to other repeatability conditions (except frequency and bandwidth), the range seen in spatial fluctuations is largest. For this measurement function to have merit as a new tool in the uncertainty discussion, it must be capable of distinguishing between different acoustic conditions. The versatility of the shown quantile functions in Figure 8.9 proves that, thus making this measurement function a valid metric.

Linking the rms change in EDT and T_{30} at short distances to the generally prevailing reverberation times in the respective auditoria is in line with theoretical predictions (Davy, 1981). It is a bit surprising, however, that EDT shows a

higher goodness of fit compared to T_{30}, when EDT is more affected by early reflections and less by the decay of the diffuse sound field. Possible causes cannot be determined with certainty, but it seems sensible to consider whether the assumed diffuse sound field actually prevails to a sufficient degree. Thus, there is a possibility that other factors contribute to spatial fluctuations in auditoria, further underscoring the need for this empirical study. Given the range of variance spanned in the existing results, the presented data set is very well-suited for the following uncertainty discussion. However, should it be the goal to understand some of the nuanced observations in more detail, a larger sample of targeted measurement series would be helpful.

Theory and measurements suggest a clear rise of spatial fluctuations with longer reverberation times. Although there are no studies on the factors contributing to spatial fluctuations in clarity and strength, one might be inclined to extrapolate the findings that are valid for reverberation time to these room acoustical quantities. When longer reverberation times correlate with lower C_{80} and higher G values, due to the exponential decay, there may be the expectation that spatial fluctuations also increase as clarity decreases or strength increases. This expectation is not consistent with the data shown in Figures 8.10c and 8.10d.

A closer look at Figure 8.10c reveals that the goodness of fit for the clarity regression is not particularly high, suggesting merely a "weak" correlation with $\rho^2 = 0.26$. This, along with the visual inspection of the shown data points, may lead the observer to wonder how much the regression is shaped by the measurement results from the orchestra *rehearsal room*. Leaving the violet points out of consideration, the remaining data in Figure 8.10c form a relatively homogeneous cluster whose visual impression does not imply a clear regression line. This gives raise to a cautious suspicion that the seven sets of measurements from the *rehearsal room* pose a risk of bias in the sample.

As a counterargument, however, it must be noted that the Pearson ρ^2 correlation coefficient is significantly higher in Figure 8.10d for the regression over the strength data. In this plot it does not appear obvious that the violet markers affect the regression one-sidedly. Instead, a potential bias would more likely come from the outlier measurement series in *Aula 1*, *Aula 2* and *Concertgebouw Amsterdam* (i.e., sets 10, 11, 15, 26) that feature higher fluctuations in G compared to their peer sets from the same auditorium. These salient sets result from sampling areas where the sound field was measured relatively close to the source. Also, in light of the large dynamic range that G exhibits in the *extended trend* of Figures 8.9c and 8.9d, it seems reasonable to ask whether the fluctuations of G and C_{80} are subject to a single driving force. It is conceivable that in addition to the factors that reverberation theory suggests, the change of the direct sound and the early reflections over space may contribute to the spatial fluctuations.

In the absence of additional data, it can be summarized that the fluctuations of C_{80} cover a range from 0.43 dB to 0.6 dB and do not show a clear dependence on the measured absolute value. The fluctuations of G range from 0.2 dB to 0.45 dB. Therefore, here too, the covered value range provides a suitable basis for the following uncertainty discussion. In order to identify deeper causalities regarding the question of additional factors driving spatial fluctuations, further series of measurements would be helpful.

8.4 Discussion

This chapter focuses on the practical validity of the measurement function, i.e., the quantile function. Validity was discussed on the grounds of three arguments, namely the repeatability and reproducibility of measurements and the agreement with theoretical predictions. Many of these points have been addressed in the interim discussions. Even though the analysis gives raise for a confident use of the measurement function in the following line of argument, it should not be ignored that there are some challenges that the critical reader should be aware of.

Theoretical predictions cover only a part of the aspects to be modeled by the measurement function. The most prominent example may be the goal to include the spatial fluctuations of C_{80} and G. In subject areas where the theoretical foundation can still be improved, the evaluation of the measurement function depends on an expectation which is ultimately fed by experience, and thus cannot yet be confirmed quantitatively. Against this backdrop, a quantitative relation can only be established from targeted measurement series, in which individual variables are varied in a deliberate manner. Not only is the systematic control of a single variable in complex subject matters an enormous challenge, but this would also go far beyond the scope required for an uncertainty discussion. In the simplest case, to investigate uncertainties, it is sufficient to cover the range of values that reasonably occur. This perspective is comparable to the GUM's Type B evaluation of uncertainties (ISO Guide 98-3, 2008, 4.3.7), i.e., assigning a uniform distribution to an input variable in the absence of specific knowledge other than the variable's bounding limits. Consequently, if there were a desire to show possible causalities beyond the target of this study, a further series of measurements and a separate investigation would be required.

In discussing spatial fluctuations as a function of distance between observation points not only for T_{30} but also for EDT, C_{80} and G, the results of this chapter mark a novel perspective. Including room acoustical quantities that target early reflections adds to the theoretical foundation that relies on concepts like the diffuse sound field. Since the early part of the RIR is inaccurately captured in

statistical steady state models, this chapter's findings address the need for the empirical studies that have been established in the groundwork of this thesis (see Chapters 1, 2 and 3).

Investigating measurements under repeatability conditions in controlled conditions is a core GUM concept to establish uncertainties. It needs to be kept in mind, however, that in complex measurements it is unclear whether the ideal of quick measurements in immediate succession can actually be reached. In the measurement method discussed here, it takes a significant period of time to complete a full series of measurements. This raises the question of whether, in addition to the controlled condition, other factors may have also changed. Eventually, this leads to the conclusion that the shown curves have to be associated with an unknown variance. Whether these potential secondary influences have been controlled to a sufficient extent depends in parts on the experimenter's experience.

This chapter's examination of a wide variety of quantile functions from the 26 measurement sets (Table 8.1) allows solidifying some of the concepts introduced in Chapter 7 (Measurement function). All of the shown curves can be divided into the domains of *initial rise* and *extended trend*. The *initial rise* marks the interval of distances between sampling locations where the sound field becomes increasingly uncorrelated as the distance between observation points gets larger. At a fixed, wavelength dependent distance around $kd \approx 2.2$, the *initial rise* flattens out and transitions into the *extended trend*. In terms of reverberation times (e.g., T_{30}), the *extended trend* generally resembles a horizontal line indicating that spatial fluctuations (spatial variance after Davy (1981)) are constant across the investigated rooms. Based on the discussion on the changed reproducibility condition of "location", it was found that an *extended trend* with a rising slope is an indication that the sound field changes according to an overarching pattern. As such larger trends are not related to spatial fluctuations, it was discussed that the rising slope of the *extended trend* is a superposition of a baseline flat *extended trend*, (solely due to spatial fluctuations), and a rising slope (due to overarching patterns). Differences in conditions "time", "observer", "location" and "condition of use" are (generally) small compared to the baseline amplitude of spatial fluctuations.

Comparing the data collected under the various reproducibility conditions highlights the factors of frequency, bandwidth and prevailing reverberation as the most significant influences to spatial fluctuations. This coincides exactly with the points Davy (1981) already identified as driving forces. Relating the predicted spatial variance to the measured rms change in reverberation time anchors the results collected here to the existing body of knowledge, and thus supports the data's validity. This is especially evident for the influences of "frequency" and "bandwidth". Based on the concept of explained variance, differences between

Davy's prediction and the measured rms changes suggest that additional factors contribute to spatial fluctuations. Early reflections may play a role in this regard, but the analysis performed is not able to quantify this contribution precisely.

Even when subtle differences in the various quantile functions cannot be explained in full detail, the collected data must be recognized as a valid sample of a common range in acoustic conditions. It thus provides a suitable foundation for the following propagation of uncertainty in Chapter 9.

8.5 Conclusions

- The measurement function for the following uncertainty discussion is valid as it shows very little change in immediately repeated measurements.
- Frequency, bandwidth and reverberation are an important influence factor for spatial fluctuations. This is in line with previous findings (Davy et al., 1979), and thus supports the validity of the measurement function.
- Measurements under reproducibility conditions vary depending on different factors. The "condition of use", the "location" in the surveyed room or the "time/observer" generally result in less significant differences compared to factors of the previous item.
- Room acoustical quantities that place a strong weight on the early part of the impulse response (e.g., clarity, EDT or strength) are especially susceptible to the distance between the source and the receiver and lead to large average changes in the measurement function (at larger distances between sampling points). Such findings are a novel contribution to the existing body of knowledge.
- The surveyed rooms cover a wide range of acoustic conditions and are thus a suitable sample to investigate the uncertainty due to spatial fluctuations. The rooms' classification into the categories of *concert hall*, *lecture hall* and *rehearsal room* highlights that several acoustic environments have been surveyed for each type of use.
- The concepts of *initial rise* and *extended trend* are helpful in discussing the changes of room acoustical quantities as a function of distance between observation points.
- The *initial rise* characterizes relatively short distances between observation points between which the sound field has not become uncorrelated to a degree that spatial fluctuations are fully pronounced.

- The *extended trend* characterizes longer distances between observation points where spatial fluctuations have reached a base level amplitude and are thus fully pronounced.

- In diffuse sound fields, the *extended trend* represents a horizontal line denoting the base level amplitude of spatial fluctuations. For reverberation times this amplitude can be determined based on Davy (1981) and Equation 2.1.19.

- Overarching trends in the acoustic conditions that manifest in larger-scale changes of room acoustical quantities lead to an *extended trend* with a rising slope. This can be understood as the superposition of an overarching trend to the base level amplitude of spatial fluctuations.

- Differences in spatial fluctuations between changed conditions of "time", "observer", "location" and "condition of use" are (generally) small compared to the base level amplitude of spatial fluctuations.

Now that the properties of the measurement function are understood, it is justified to turn the attention to addressing the central research question.

9

How accurately must a measurement position be defined?

9.1 Introduction

In this chapter the data collected so far and the findings from the analysis will be put to practical use: The consequences of an uncertain measurement position will be investigated under realistic conditions.

The starting point is the understanding that uncertainties arise from the measurand's incomplete definition or imperfections in realizing the measurement definition (ISO Guide 98-3, 2008, 3.3.2). In room acoustical measurements, this statement becomes tangible when measurements under repeatability and reproducibility conditions are compared to each other (see Chapter 8). Small differences in reproduced measurements already lead to observable changes in their results. In complex metrological scenarios, it can be quite difficult to characterize the influence factors, even more so to state how their uncertainty propagates to the output quantity. In such elusive situations, the only remedy is to describe measurement scenarios as precisely and meticulously as possible.

In auditorium acoustics, based on results by de Vries et al. (2001), the measurement position (source and receiver) is such an influence, which, if not precisely controlled, leads to a considerable variance in measured results. At the same time, the measurement location is a measurand like any other that can only be determined inaccurately. Consequently, a mismatch between the assumed and the actual source and receiver positions may exist. A discrepancy between sampling locations in reproducibility measurements presents the same situation in a different way.

In the acoustical domain, it is intuitively clear that the impulse responses determined at the actual and the assumed measurement position differ from each other. Since neither the differences in sampling positions nor the differences in impulse responses can be established by the observer, an uncertainty must be assumed for the impulse response. With room acoustical quantities being

derived from impulse responses, the same need to assume an uncertainty applies regardless. Since impulse responses are significantly more complex than room acoustical quantities, this investigation will only consider the uncertainties of ISO 3382-1 (2009) parameters. The presented methods can be applied in future studies to RIRs with marginal modifications.

This chapter investigates how exactly the measurement location must be documented or reproduced. Since the threshold where uncertainties can no longer be tolerated depends on the situation, a single-value result is not very meaningful. Instead, a functional relation is aimed at that shows how the uncertainty in room acoustical quantities changes as the uncertainty in the measurement location increases. Based on the reciprocity principle, this uncertainty discussion is equally valid for source and receiver positions alike.

9.2 Methodology

The strategy that permits addressing the research question is the *law of propagation of uncertainty* (ISO Guide 98-3, 2008, 5.1.2): The uncertainty distribution of the input quantity is propagated through the measurement function which leads to the uncertainty distribution of the output quantity (i.e., the measurand).

In the situation discussed here, the measurement position is understood as the input quantity. The corresponding distribution results from the distance between the sensor position's best estimate and its actual position as expressed in the introduction to this chapter. In the equivalent scenario of reproducibility measurements, the input quantity is the distance between the positions in the original and the second measurement.

The input quantity is transformed into the output quantity through the measurement function established in Chapter 7. Since the measurement function is not available in analytical form, it is not possible to calculate the measurement uncertainty based on the first-order Taylor approximation as the simplest method. Additionally, the measurement function's characteristic *initial rise* and *extended trend* suggest a nonlinear relationship between the inputs and outputs, which also contradicts an analytical solution. In precisely such cases, Monte Carlo simulations can serve as alternatives to determine the measurement uncertainty.

This method (see Chapter 2.3.2 or JCGM 101 (2008)) samples the input quantity by drawing random numbers. For each of the drawn samples, the corresponding result is determined based on the measurement function. After a sufficient number of repetitions, a distribution for the output variable emerges that yields the output uncertainty. Figure 9.1 provides a graphical representation of the method. The standardized adaptive method allows determining the measurement uncertainty with a minimum calculation effort while ensuring a previously

determined level of accuracy in the results.

From the classical GUM method's point of view, a challenge arises because the measurement function of this study is not a binary relation that maps the input to a unique output. Instead, it relates the input to a distribution of possible outputs, as illustrated in Figure 9.1. To establish a summary statistic for the output that is in agreement with the JCGM 101 (2008) Monte Carlo method, however, it is necessary for each Monte Carlo trial to lead to a definite result that contributes to the output distribution (JCGM 101, 2008, 7.9.4.d). This definiteness can be easily established by a small extension to the standardized procedure based on a second (independent) Monte Carlo draw from the distribution of possible outputs. This approach can be understood as a nested two-step process. Its relation to a Bayesian approach to measurement uncertainties and its validity has been discussed previously in Chapter 7.2.1.

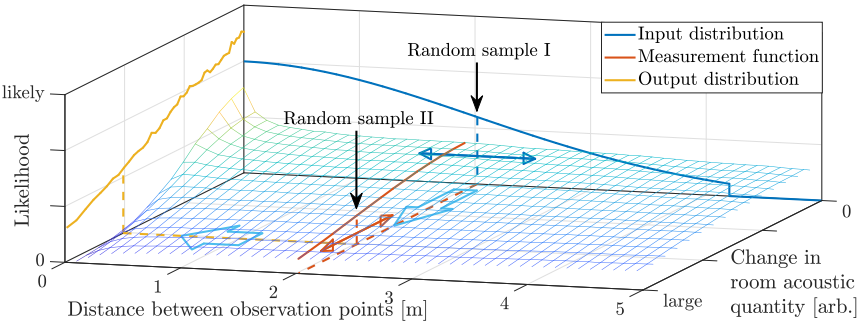

Figure 9.1: Scematic drawing of the two-stage Monte Carlo method. The measurement function is interpreted as a likelihood function $\mathcal{L}(d|\Delta Q)$. In each trial, the first random sample determines the parameter d, and the second sample evaluates the resulting PDF. The sum of all trials form the output distribution.

9.2.1 Establishing the input quantity distribution

The foremost prerequisite to apply the *law of uncertainty propagation* is assigning a distribution to the input quantity (ISO Guide 98-3, 2008, 4.1.6). For the scenario of positioning a microphone, no empirical data and no reference from literature seems to exist regarding an appropriate distribution that can reasonably be assumed. As a result, a plausible *GUM-Type B* distribution must be aimed for (ISO Guide 98-3, 2008, 4.3).

Even though the indefiniteness of this specific scenario does not suggest a preference towards a specific probability distribution, the normal distribution plays a prominent role in the GUM framework. This is due to the central limit theorem, according to which the summary distribution of an increasing number of contributing distributions approaches normality (Bronstein et al., 2015, 16.2.5). Normality, however, may not seem an intuitive choice to describe the distances that occur between sampling points as the distribution extends into the negative half-space. Negative distances make little sense and can thus be excluded through truncation, yielding a half-normal distribution (Johnson et al., 1994, Sec. 13.10.1). From practical experience, the $|\mathcal{N}(0, \sigma^2)|$ distribution seems to be a plausible representation of the distances that occur in the considered situations. The shape of the Gaussian distribution reflects the expectation that small discrepancies in the compared locations are somewhat more likely than larger deviations. Larger distances are supposed to occur increasingly less frequently, and thus have a lower probability.

The infinite extent of the half-normal distribution introduces disadvantages that need discussion. First, determining extreme quantiles using Monte Carlo simulations requires relatively large random samples to converge and thus relatively high computational power. This aspect can be addressed with patience or brute force.

Perseverance, however, may not be sufficient for the second point: as Monte Carlo simulations require large samples, large distances will eventually be drawn. For the uncertainty propagation to work, the measurement function must be defined at these distances and feature a valid transformation into the room acoustical quantity space. Due to the finite size of the measurement setup's structure, the evaluation of the measurement function is limited to distances smaller than 5.3 m between sampling locations. This constraint may defeat the original intent to resemble normality when large parts of the distribution are trimmed off. Against this backdrop the Gaussian distribution can be seen as an ideal, and its truncation is merely a concession to practical necessities that just have to be made. The coverage factor $k = 1.96$ to determine expanded uncertainties finds regular recognition in the uncertainty discussion as it represents a 95 % level of confidence. This can be understood as an argument to include this range after truncation and avoid trimming off "large" parts of the normal distribution.

Setting the input distribution's cutoff limits is, to some extent, an act of arbitrariness. To the author, limiting the normal distribution to a $[0 \quad 2.1\sigma]$ interval maintains a resemblance to the starting point of this discussion, as it only removes the largest 3.57 % from the ideally (half-)normally distributed distances. As the domain of the measurement function limits distances to a maximum of 5.3 m, the underlying normal input distribution (before truncation) is limited to

a maximum standard deviation of $\sigma = 2.5\,\mathrm{m}$. An illustration of the input's PDF is shown in Figure 9.1 in blue.

Strictly speaking, the input's normality is thus no longer given. As a result, the previous discussion of normal coverage factors is rendered obsolete. If one were to consider the truncated 3.57 % to be relatively small, one could still regard the exploited relationships between confidence levels p and coverage factors k as roughly valid. In practical measurements, other sources of error are conceivable, such as simply mixing up measurement positions. Such mistakes could lead to a large position mismatch that may not be supported by the suggested input distribution. It is estimated, however, that such lapses happen on very rare occasions and are, due to their nature, best attributed to the observer.

9.2.2 Implementing the measurement function

The measurement function derived in Chapter 7 plays the central role in the rationale of this investigation. In Chapter 8 some of the measurement function's influencing factors and its relation to theory were identified. Also, a common general shape of the measurement function became evident through its *initial rise* and *extended trend*.

To recall, the measurement function is available in a minimally-processed data set as an empirical likelihood function showing the 2D probability of a change in room acoustical quantity based on a given distance between observation positions (Mesh grid in Figure 9.1). To facilitate the interpretation and comparison of different measurement functions, the 2D-distribution was parameterized through the 68.3 % quantile. This abstraction is valid due to its significant similarity to a half-normal distribution (see Table 7.1).

From all of the measurement series, 26 different measurement functions (likelihood functions) are available. A further data reduction could help reduce the complexity of this wealth of data. To avoid a bias due to prematurely tapering down the data, all measurement functions of the 26 sets are used to investigate how the spatial fluctuations affect the room acoustical quantities' uncertainty as a function of distance between two sampling locations. Once experience with this type of measurement function and the new perspective it allows on spatial fluctuations has reached a profoundness to identify core influences, further data reduction may be warranted.

9.2.3 Determining the measurement uncertainty using Monte Carlo simulations

In its first step, each Monte Carlo trail consist of a draw from the $[0, |2.1\sigma|]$ truncated $|\mathcal{N}(0, \sigma^2)|$ distribution. This random sample serves as the distance d between implied measurement positions, which is the input quantity that will be propagated through the measurement function. The measurement function is a $\mathcal{L}(d|\Delta Q)$ likelihood whose properties depend on the parameter d. In Figure 9.1, the measurement function is illustrated through the mesh grid. Once d is established, only the red "slice" through the mesh grid needs to be considered.

Here, two cases need to be distinguished: In the first case, the initial draw from the input distribution results in a distance $d \geq 5\,\text{cm}$. For these distances the measurement function is available based on empirical data, and the distribution of changes in room acoustical quantities at a particular distance is an infinitesimal slice of the measurement function. Due to its discrete nature, the drawn distance may not coincide with the grid of the measurement function. Thus, the needed distribution is determined through linear interpolation along the distance axes.

Theoretically, the second Monte Carlo sample ought to be drawn from the so determined slice of $\mathcal{L}(d|\Delta Q)$. Since this PDF may not be similar to known distributions, a detour based on the *transformation theorem for probability densities* (Johnson et al., 1994, pp. 14-15, Eq. 12.32) has to be considered. This theorem requires establishing a transformation function that is the inverse of the target's cumulative distribution function. In a practical implementation, the random variable of the second Monte Carlo step is a sample from the uniform $\mathcal{U}(0, 1)$ distribution that is appropriately distorted by the transformation function to yield the required definite sample of the "sliced" measurement function. Just as before, the transformation function is discrete, and so the required sample is determined through linear interpolation. The resolution of the measurement function is fine enough that error due to interpolation along both dimensions is negligible.

In the second case, the sample drawn for the first Monte Carlo step corresponds to distances $d < 5\,\text{cm}$ where the measurement function was identified as potentially unreliable. This is due to the 5 cm resolution at which the sound field was sampled. As discussed in Chapter 7, the linear interpolation of the 68.3 % quantile function was found to be the best estimate of the measurement function in the $[0\,\text{cm}, 5\,\text{cm})$ interval (see reasoning that lead to Table 7.1). Thus, when the sample from the first Monte Carlo step yields distances below 5 cm, the change in room acoustical quantity in the second Monte Carlo step is based on a draw from a $\mathcal{N}(0, \sigma^2)$ distribution. σ is the result of the 68.3 % quantile function's linear interpolation between 0 cm and 5 cm, and thus is a function of d.

Table 9.1: Termination criteria for the adaptive Monte Carlo procedure.

Room acoustical quantity	Numerical tolerance δ	Smallest resolvable value z
EDT	$0.5{\times}10^{-4}$ s	0.001 s
T_{xx}	$0.5{\times}10^{-4}$ s	0.001 s
C_{80}	$0.5{\times}10^{-3}$ dB	0.01 dB
D_{50}	$0.5{\times}10^{-2}$ %	0.1 %
t_{center}	$0.5{\times}10^{-5}$ s	0.1 ms
G	$0.5{\times}10^{-3}$ dB	0.01 dB

Reliable results require a sufficiently large sample that is ensured by the implementation of an adaptive procedure (JCGM 101, 2008, 7.9). In line with the standardized method, this process is repeated in sets of 10^4 trials until the standard deviation of the estimates of Y over all sets have stabilized below half the numerical tolerance δ given in Table 9.1. The quantities' required tolerances are deliberately chosen to be one order of magnitude below what would be considered meaningful on the grounds of metrological and perceptual experience (see Table 2.3).

Generally, JCGM 101 (2008) recognizes the mean value y and the standard uncertainty $u(y)$ as valid estimates of Y. Consequently, the simulations are continued until these estimates have stabilized sufficiently between the sets of Monte Carlo trials. In this study, quantiles are recognized as valid estimates of Y, too. As a result, the termination criterion is extended to also include the integer percentiles from 5 % to 95 % of the output distribution. Including quantiles as target values permits a more accurate understanding of the resulting output distribution.

To ensure that the results carry meaning for the most general range of applications, the Monte Carlo simulations are not only based on a single input distribution. Instead, the simulations are repeated in series while the standard deviation of the input distribution is increased with each successive repetition. The truncated half-normal $|\mathcal{N}(0, \sigma^2)|$ distribution used in the first Monte Carlo step is varied over the range $1\,\mathrm{cm} \leq \sigma^2 \leq 250\,\mathrm{cm}$ in steps of 1 cm. This range makes best use of the measurement function's full domain.

The final step to conclude the Monte Carlo simulations that leads to establishing the measurement function is due to the simple pair comparisons. In Chapter 7.2.2 it was discussed that a bidirectional pair comparison between any

two microphones (i.e., a with b and vice versa) would not add information. As a result, the measurement function only shows the unsigned change in room acoustical quantities. Regardless, since changes in the sound field can have both positive and negative signs, the stabilized unsigned output distribution must be mathematically reflected at the coordinate axis and appropriately normalized. The resulting output distribution is thus symmetric.

The GUM's Monte Carlo supplement addresses fundamental conditions that need to be met to determine elementary uncertainty parameters such as the standard uncertainty (JCGM 101, 2008, 5.10). One of these prerequisites is the measurement function's unimodality. While this aspect bears some relevance for coverage intervals and standard uncertainties, is not of highest concern in regard to individual quantiles. Visual inspection and the KS-Test for normality that led to Table 7.1 establishes overall unimodality of $\mathcal{L}(d|\Delta Q)$, but very small secondary modes (similar to added noise) cannot be completely ruled out.

9.3 Results

This section presents the results of Monte Carlo simulations for the different room acoustical quantities. All of the graphs used are structured in the same way to make them easier to read and compare. The x-axis shows the expanded uncertainty of the microphone position. Since the input distribution after truncation is no longer genuinely normal, the expanded uncertainty refers to the $d = [0\ x]$ distance interval which accounts for 95 % of the contributing distance samples. The expanded uncertainty determined for the respective room acoustical quantity is plotted along the y-axis. Although the output distribution is symmetric around the origin, normality cannot be assumed. Accordingly, the shown 95 % interval is also based on the 2.5 %, 97.5 % quantiles.

In Section 7.2, it was pointed out that the measurement function was linearly interpolated for very small distances between microphones. A broken red line has been drawn on Figure 9.2 to 9.8 to indicate results that are based on this compromised solution by more than 68.3 % (two standard deviations if normality were assumed). The corresponding results (to the left of this line) are drawn semitransparently. The uncertainties from different sets of measurements are displayed in color coded form.

Important answers can be derived from the graphs shown. If, for example, the situation arises that a microphone has been placed with an expanded uncertainty of 50 cm (i.e., the dimension of a seat in an auditorium), Figures 9.2 to 9.8 indicate the corresponding expanded uncertainty for the different room acoustical quantities.

9.3.1 Uncertainty of room acoustical quantities

Early decay time

Starting with the smallest uncertainties of the sensor position $u(d)$, the uncertainty of the early decay time increases rapidly with even slightly larger distance uncertainties (see Figure 9.2). For larger $u(d)$, the uncertainty of the quantity $u(EDT)$ quickly reaches an almost constant plateau, which changes only marginally with larger distance uncertainties. The graphs representing the individual rooms/sets rarely cross each other, and the sequence of rooms scaled in the order of parameter uncertainty remains essentially unchanged for different $u(d)$. The differences of $u(EDT)$ in the different rooms lead to the hypothesis that $u(EDT)$ correlates with core properties of the prevailing sound field (e.g., reverberation time). This question is examined in Section 9.3.2.

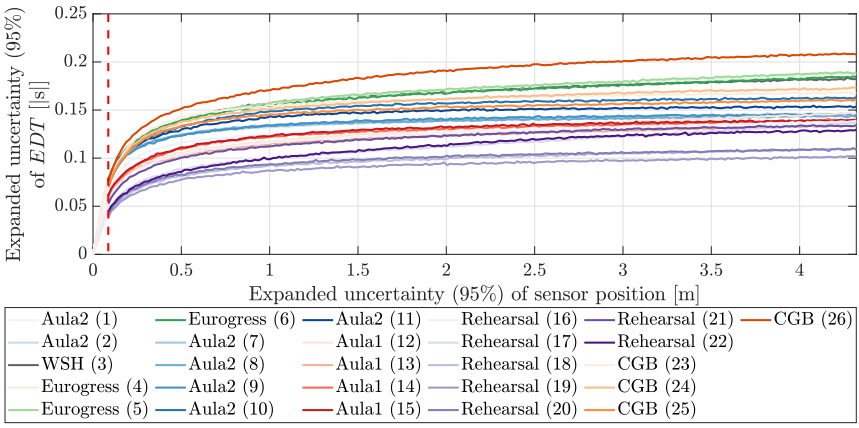

Figure 9.2: Expanded uncertainty of EDT (broadband) as a function of uncertainty of the sensor position in different auditoria.

Reverberation time

Figure 9.3 shows the uncertainty curves for the reverberation time T_{30}. Compared to the early decay time, the increase in $u(T_{30})$ is even steeper for small $u(d)$. For larger distance uncertainties, the curves' trends are even flatter. The uncertainties of EDT and T_{30} can be easily compared: the uncertainty of EDT, with about $\pm 0.1\,\mathrm{s}$, is about twice as large as that of T_{30}. Again, this promotes the hypothesis that the generally prevailing reverberation time correlates to the uncertainties shown in Figure 9.3. This will also be investigated in Section 9.3.2.

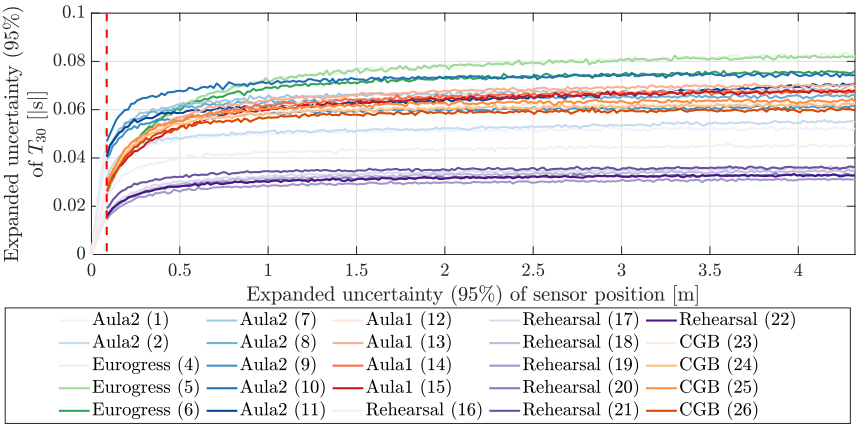

Figure 9.3: Expanded uncertainty of T_{30} (broadband) as a function of uncertainty of the sensor position in different auditoria.

Clarity

In terms of clarity, Figure 9.4 generally shows a rapid increase and flat plateau for the uncertainty, as was found for the reverberation times. For some auditoria (e.g., curves 12, 15, 21 or 26), however, it is noticeable that $u(C_{80})$ increases even more with larger distance uncertainties. At the same time, in these cases the quantity's uncertainty is slightly lower for smaller $u(d)$.

In order to identify possible causes for the different shapes of curves, two extreme cases from Figure 9.4 are compared. Curve 6 and curve 21 are respectively the flattest and the steepest curves. Figure 9.5 shows for both cases how C_{80} was measured at different locations in the sampling fields. The left tile shows the spatial distribution in *Eurogress Aachen* (set 6), while the right image features the data collected in the *rehearsal room* (set 21). Even though the color bar in each of the tiles represents different values, the covered range in both scenarios is the same, i.e., the difference between C_{80} represented in blue and yellow is in both cases about 5.3 dB. It is obvious that the sound field in set 6 is much more homogeneous, whereas the sound field in set 21 changes strongly with increasing distance from the source (outside, to the top left of the graph).

This data provides indications that other effects, such as the influence of the direct sound, may be superimposed on the basic uncertainty due to local fluctuations. Such added effects may be smaller for curves that run flatter at longer distances.

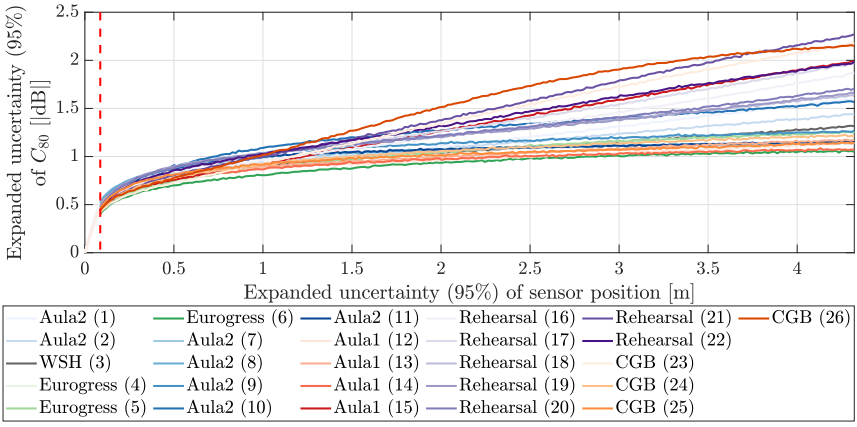

Figure 9.4: Expanded uncertainty of C_{80} (broadband) as a function of uncertainty of the sensor position in different auditoria.

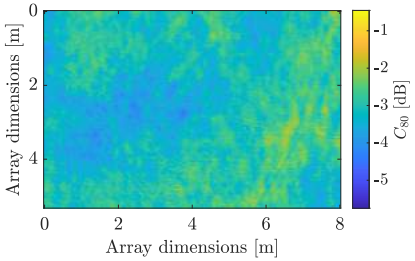

(a) Distribution in *Eurogress*.

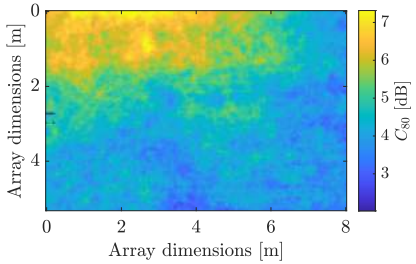

(b) Distribution in the *rehearsal room*.

Figure 9.5: Comparison of C_{80}'s spatial distribution.

Definition

The definition curves shown in Figure 9.6 are quite similar to what was shown for clarity in Figure 9.4. The two previously highlighted extreme cases stand out here for the same reasons.

A detailed comparison of D_{50} to C_{80}, however, is difficult for three reasons. First, the evaluated time intervals are different with their respective limits of 50 ms and 80 ms. Secondly, the ratios are formed differently: while for C_{80} the energy in the early and the late part of the impulse response are compared to each other, for D_{50} the ratio of the early to the total energy is formed. Finally, the comparison of an absolute and logarithmic ratio is not readily possible.

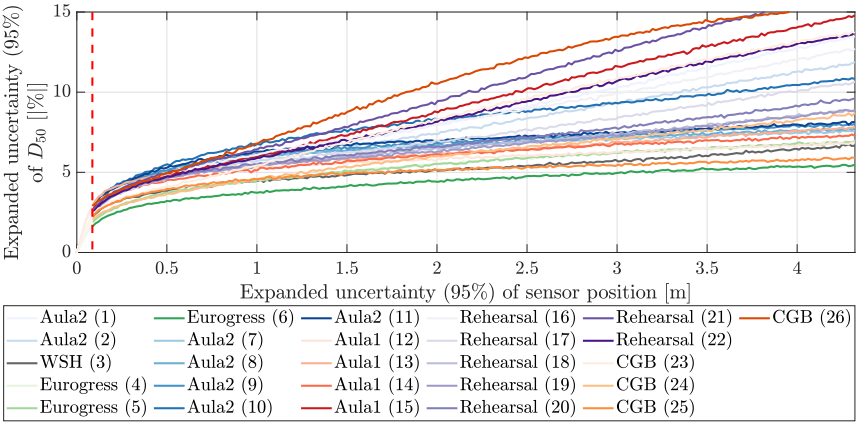

Figure 9.6: Expanded uncertainty of D_{50} (broadband) as a function of uncertainty of the sensor position in different auditoria.

Center time

In the original discussion on spatial fluctuations (de Vries et al., 2001), the question was raised of whether the rectangular time window functions of clarity and definition were the cause of the discovered phenomena. In this light, the curves for center time in Figure 9.7 are particularly informative, since they show the same general trend of a sharp rise and a flattening curve for larger distance uncertainties, despite the absence of a finite time window in the algebraic definition of center time.

In contrast to previous observations regarding clarity and definition, small differences emerge when inspecting two extreme sets of measurements. While

set 21 still features data with a particularly steeply rising curve in center time domain, the set 6 data is no longer prominent as an example for small amplitudes. In addition, when inspecting Figure 9.7 at small position uncertainties, it can be seen that the 26 curves form clusters that correspond to the different rooms: series collected in the *rehearsal room* (violet) have the lowest amplitude, data from *Aula 1* exhibits a medium amplitude and the other series show the highest t_c uncertainty. In the *extended trend* towards larger position uncertainties, this order remains generally unchanged except for series that are already known for their relatively strong dependence on the direct sound (i.e., sets 10, 12, 15, 21, 22 or 26)

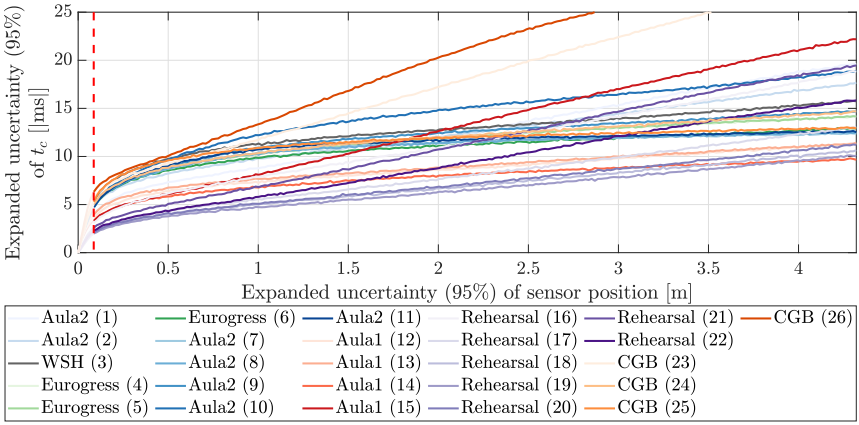

Figure 9.7: Expanded uncertainty of t_c (broadband) as a function of uncertainty of the sensor position in different auditoria.

The differences between the three temporal clarity quantities (C_{80}, D_{50}, t_c) give reason to examine the possible causes in more detail. The question arises of whether the different time windows of the impulse response (i.e., 0 ms to 50 ms vs. 80 ms), the different terms in the numerator and denominator or the absolute vs. the logarithmic ratio are affected differently by the spatial fluctuations, i.e., whether the uncertainty of definition compared to clarity or center time differs independently of the unit (dB, % or s) used. This aspect is examined separately in Section 9.3.3.

Strength

Looking at the strength parameter, essentially the same picture emerges. As with all previously discussed quantities, a rapid increase in uncertainty can be

observed for small distance uncertainties. At larger distances, the already known contrast between the two types of data sets can be seen. On the one hand, there are auditoria where the uncertainty is nearly independent of the sensor position uncertainty, and on the other hand, data sets exist where the sound field changes strongly as a function of source-receiver distance.

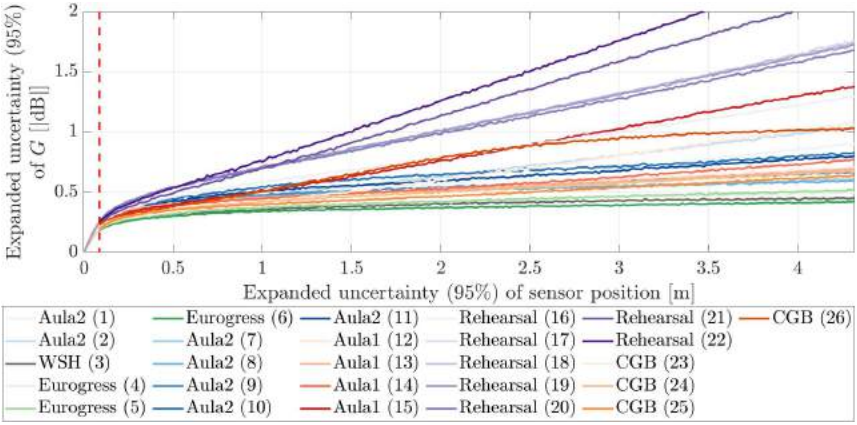

Figure 9.8: Expanded uncertainty of G (broadband) as a function of uncertainty of the sensor position in different auditoria.

9.3.2 Effect of the auditorium's reverberation

When presenting the uncertainties of the different quantities (especially regarding the reverberation times), the hypothesis was introduced that the amplitude of the spatial fluctuations depends on the room's generally prevailing reverberation time. In light of the theoretical discussion in Section 2.1 or the examination of the measurement function (Figure 8.10), this notion appears valid.

First, this question will be investigated for the early decay time of the results in Figure 9.9. The horizontal axis shows the mean broadband EDT based on 16 960 sampling area data points for each of the 26 sets. The vertical axis shows the expanded uncertainty of EDT (due to spatial fluctuations). This y-axis value is based on the 95 % expanded uncertainty of the microphone position with $u_{95\%}(d) = 0.5\,\mathrm{m}$ in Figure 9.9a and $u_{95\%}(d) = 2.5\,\mathrm{m}$ in Figure 9.9b.

The exact values of the position uncertainties are to some extent arbitrary. The small uncertainty of 0.5 m serves as a sample of distances between measurement locations, where fluctuations are obviously evident but usually not perceivable

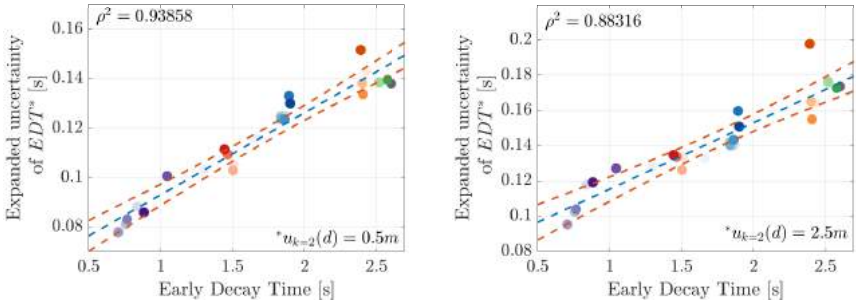

(a) Small distance uncertainty.

(b) Large distance uncertainty.

Figure 9.9: Correlation between the absolute value of EDT and its uncertainty. The color code is identical to that used in Figure 9.8.

for listeners. At a distance of 2.5 m there is some potential that macroscopic changes to the acoustic conditions add to the existing spatial fluctuations. All too-large differences between these two scenarios may indicate how strongly early reflections contribute to the spatial change of the sound field.

The mean EDT and the corresponding uncertainties show a "very strong" correlation (Evans, 1996) to each other, namely $\rho^2 = 0.94$ for $u(d) = 0.5$ m and $\rho^2 = 0.88$ for $u(d) = 2.5$ m. The dashed lines show in blue the linear regression and in red the $\alpha = 0.05$ confidence intervals of the regression model.

The same analysis was performed for the T_{30} reverberation time. Again, there is an apparent correlation between the prevailing reverberation time and the uncertainty induced by the fluctuations (Figure 9.10). In contrast to EDT, however, the correlation is not quite as strong ($\rho^2 = 0.77$), which is due to the red and blue measurement points of *Aula 1* and *Aula 2*, respectively, that do not match the trend of the regression very well. It is not obvious which acoustic features of these rooms contribute to their "outlier" position.

On the basis of the previous results, where longer reverberation times correspond to more pronounced spatial fluctuations (Figures 9.9 and 9.10), one might expect a similar relation for clarity as well. In fact, however, Figure 9.11 does not show this intuitive trend. Instead, for C_{80} shorter reverberation times are associated with slightly greater C_{80} uncertainties.

At the same time, with $\rho^2 = 0.39$, the correlation is "weak" (Evans, 1996) for small position uncertainties. For larger position uncertainties, the correlation is "very weak" (Evans, 1996) ($\rho^2 = 0.08$) and, thus, it is even more difficult to claim a robust relation between the decay and clarity's uncertainty.

Interestingly, this lack of distinctness does not hold for center time. For small

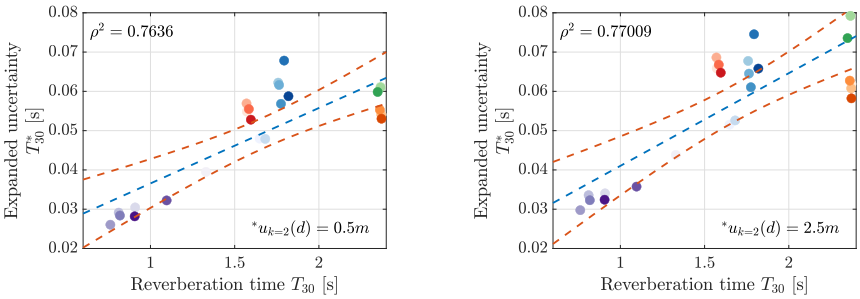

(a) Small position uncertainty.

(b) Large position uncertainty.

Figure 9.10: Correlation between the absolute value of T_{30} and its uncertainty.

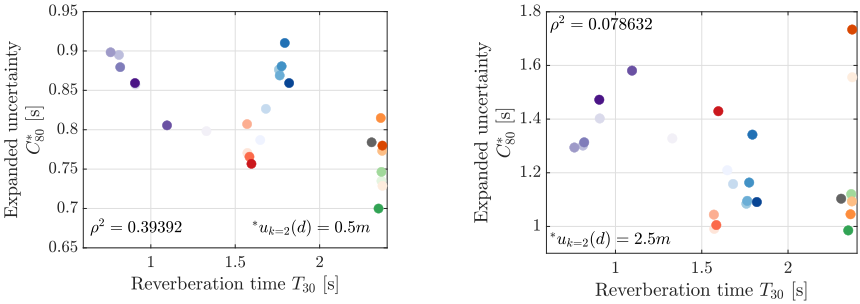

(a) Small position uncertainty.

(b) Large position uncertainty.

Figure 9.11: Correlation between the absolute value of T_{30} and the uncertainty of C_{80}.

position uncertainties there is a clear, "very strong" trend ($\rho^2 = 0.88$) towards larger uncertainties for longer reverberation times. With greater position uncertainties the picture is less clear again, but the correlation is still "moderate" with $\rho^2 = 0.54$. The data points from *Aula 2* turn out to be outliers again, deviating rather clearly from the regression line. As far as one is inclined to recognize the regression in Figure 9.11a (C_{80}) as meaningful, it is worth noting that the trends shown in Figures 9.11a and 9.12 (t_c) are exactly opposite, although both quantities are supposed to predict similar properties of the sound field.

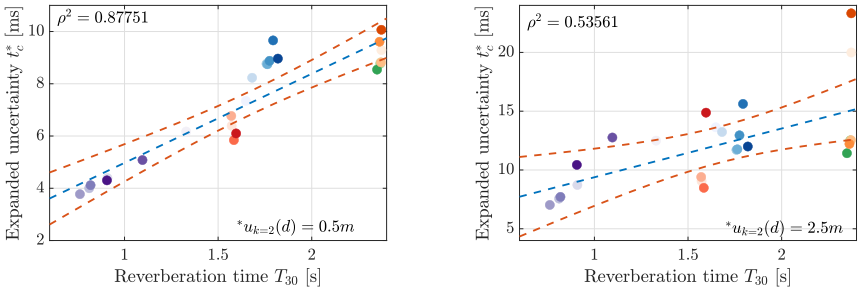

(a) Small position uncertainty.

(b) Large position uncertainty.

Figure 9.12: Correlation between the absolute value of T_{30} and the uncertainty of t_c.

9.3.3 Effect of the evaluation interval (time)

Reverberation times

The results shown so far have indicated that the spatial fluctuations of the two reverberation times differ in detail. This is interesting because EDT and T_{30} evaluate similar properties of the decay, and therefore the question arises of whether impulse responses are influenced by the fluctuations in the same way throughout the running time. In addition, Davy (1981) suggests that the variance of evaluated dynamic ranges contributes to the differences in the fluctuations. In order to draw a more precise picture, the different quantities and their spatial fluctuations are examined in detail.

Figure 9.13 shows as a box chart the fluctuations of the different reverberation times that were determined according the following scheme: For each of the 26 sets, the expanded uncertainties of the reverberation times (EDT, T_{10} - T_{30}) were calculated for the sampling position's expanded uncertainty of $u_{95\%}(d) = 0.5\,\mathrm{m}$ in blue and $u_{95\%}(d) = 2.5\,\mathrm{m}$ in red. The line inside each box is the sample median of the distribution, the top and bottom edges of each box are the 25 % and 75 % quantiles and the whiskers indicate the maximum and minimum of the spatial fluctuations. There were no outliers based on a 1.5 interquartile range criterion.

When looking at Figure 9.13, it is immediately obvious that a greater position uncertainty (red) leads to greater fluctuations than those that occur with more precisely defined positions (blue). At the same time, it is evident that reverberation times with larger evaluated dynamic ranges exhibit less fluctuation, and thus feature a lower expanded uncertainty of reverberation time. This general trend is almost perfectly consistent with findings by Davy (1981), except for a

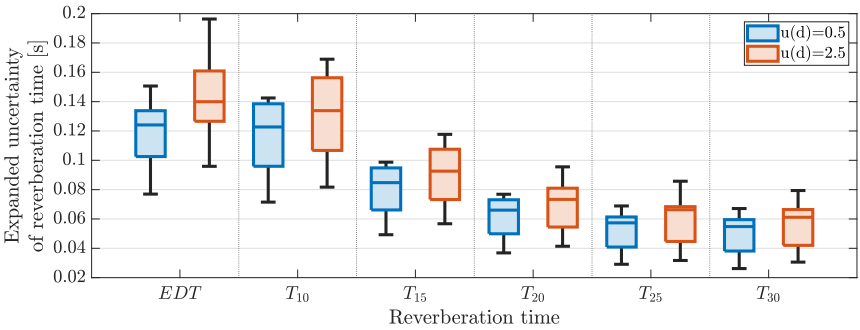

Figure 9.13: Comparison of the uncertainty of different reverberation times.

proportionality factor. A perfect, one-to-one, agreement cannot be reasonably expected because Davy's variance is calculated differently from the Monte Carlo uncertainty presented here.

The comparison of the expanded uncertainties of EDT and T_{10} are very similar. In this light, there is little evidence that would suggest that the early part of the RIR is affected differently or more strongly by the spatial fluctuations than by the late part of the RIR.

Temporal energy distribution

Clarity, definition and center time are three parameters that evaluate the temporal distribution of signal energy in room impulse responses. They differ from each other in the length of the time windows, but also in how the energy intervals are related to each other. These differences raise the question of whether all these energy ratio quantities are affected by spatial fluctuations in the same way.

Investigating this question is delicate, as the three quantities are difficult to compare simply because of the different units (dB, %, s) that the energy ratios are given in. To reach this comparability, a common ground is established that resorts to diffuse field theory and the propagation of uncertainties depicted in Figure 2.6.

The starting point is a hypothetical diffuse sound field with a perfectly exponential decay that matches the mean T_{25} reverberation time across all 26 measured scenarios of 1.73 s. This agreement in reverberation time is chosen to ensure an appropriate operating point for the propagation of uncertainties, and does not imply a diffuse sound field that may possibly exist in the surveyed auditoria. The hypothetical exponential decay $E(t) = E_0 \exp(-\lambda t)$ corresponds to a clarity of -0.47 dB, a definition of 32.99 % and a center time of 125 ms.

Based on the methodology in Section 9.2, the uncertainties for D_{50}, C_{50}, D_{80}, C_{80} and t_c are calculated for $u_{95\%}(d) = 0.5\,\mathrm{m}$ and $u_{95\%}(d) = 2.5\,\mathrm{m}$ (see Figures 9.4, 9.6 and 9.7). Using the principle of uncertainty propagation, these energy ratio uncertainties can be converted into uncertainties of the decay constant λ. To avoid errors due to the first order Taylor approximation, a nonlinear least squares optimization was used to calculate $u_{95\%}(\lambda)$. Provided that the transform from C_{xx},D_{xx} or t_c to λ is monotonic and the uncertainty distributions of the room acoustical quantities are each unimodal, the uncertainty of the decay constants determined through the different quantities are now comparable to each other. The results of this comparison can be found in Figure 9.14. For the room acoustical quantities listed along the horizontal axis, the expanded uncertainty of the decay constant λ is shown on the y-axis.

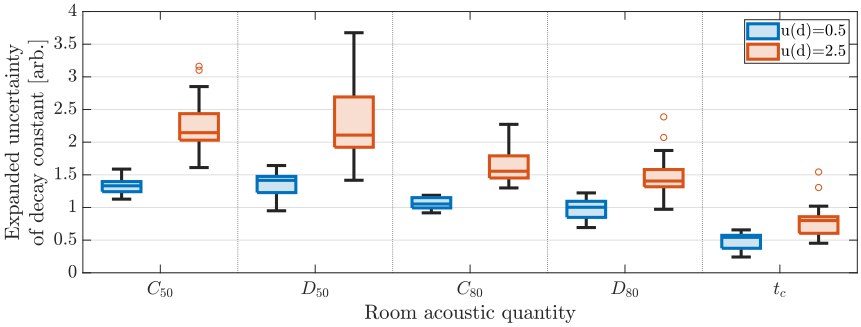

Figure 9.14: Comparison of the decay constant for different room acoustical quantities.

The first and most obvious finding is that the uncertainty is significantly lower with a more precise measurement position (blue). This confirms the trend already observed in all situations before.

Somewhat more subtle, but still quite clear, is the observation that the decay constant has less variance for parameters with an 80 ms time window compared to corresponding quantities with a 50 ms time window. If the basis of comparison is extended to include the center time, it becomes clear that this parameter is least affected by spatial fluctuations.

When examining the quartiles of clarity and definition, it can be seen that in about three out of four direct comparisons the box plots for definition generally exhibit marginally smaller uncertainties in the decay constant.

9.3.4 Effect of the center frequency

It is already clear from Davy's study and the discussion in Sections 2.1 and 8.3.2 that spatial fluctuations change with the (center) frequency of the filter. To illustrate that this is valid in auditoria, too, the expanded uncertainty of EDT as a function of uncertain sensor position at different 1/1-octave band frequencies is shown in Figure 9.15. In general, the results show a pattern that is quite similar to what was previously discussed. It is therefore no loss that the complete presentation of curves from all sets has been forgone, when little new insight was to be gained. All curves feature a steep *initial rise* and a flatter *extended trend*. Towards higher frequencies the *initial rise* steepens. while, at the same time, the *extended trend* exhibits lower levels. This is consistent with the observations on the measurement function in Section 8.3.2.

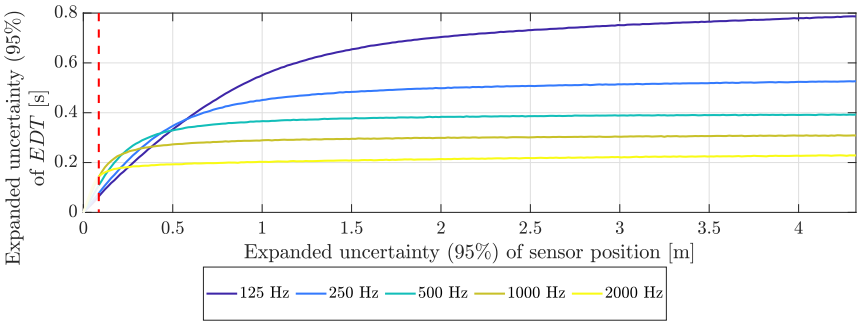

Figure 9.15: Expanded uncertainty of EDT for different 1/1-octave bands as a function of uncertainty of the sensor position in a concert hall.

Based on the theoretical discussion in Chapter 2.1, and especially in light of Equation 2.1.7, a discussion in the context of wavelength is appropriate. Figure 9.16 shows one tile for each of six room acoustical quantities and illustrates the parameters' expanded uncertainty as they change with increasing sensor position uncertainty in $ku_{95\%}(d)$.

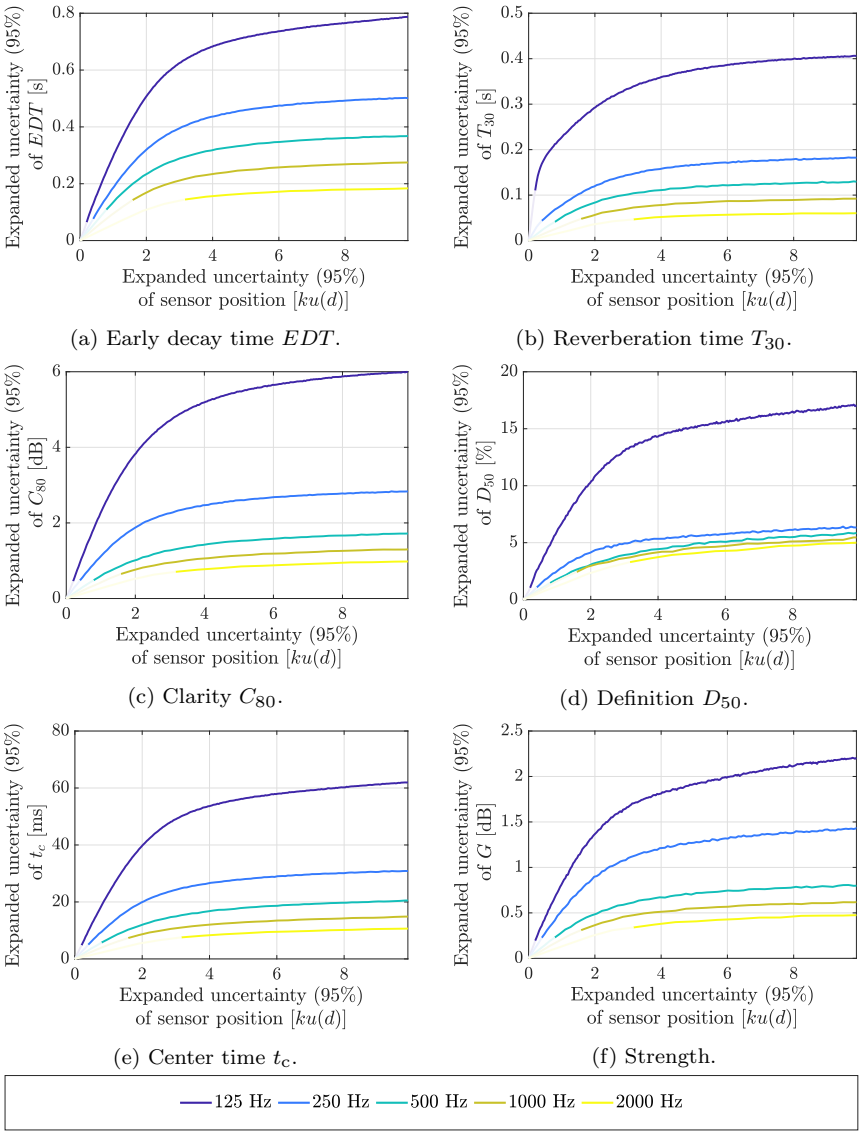

(a) Early decay time EDT.

(b) Reverberation time T_{30}.

(c) Clarity C_{80}.

(d) Definition D_{50}.

(e) Center time t_c.

(f) Strength.

Figure 9.16: Expanded uncertainty of different room acoustical quantities for different 1/1-octave bands as a function of uncertainty of the sensor position in wavelengths in a concert hall.

9.3.5 Effect of the bandwidth

For the same reasons given in the previous section, it is already clear that spatial fluctuations depend on the bandwidth of the filter. To illustrate that this is also true in practical measurement scenarios, the expanded uncertainty of room acoustical quantities as a function of uncertain sensor position at different 1/3-octave band frequencies is shown in Figure 9.17.

The results shown in Figure 9.17 are very similar to the data shown in Figure 9.16 except for the frequency resolution. All curves show a rapid increase in the uncertainty of room acoustical quantities as position uncertainty increases. Towards relatively large position uncertainties the curves flatten out. The main difference - that the uncertainties (or fluctuations) of room acoustical quantities analyzed in third-octave band are significantly greater than the uncertainties occurring in full octaves - becomes apparent when visually comparing Figure 9.16 to Figure 9.17. At both bandwidths, the same general trend can be observed: spatial fluctuations show the highest amplitudes at lower frequencies and decrease towards higher frequencies.

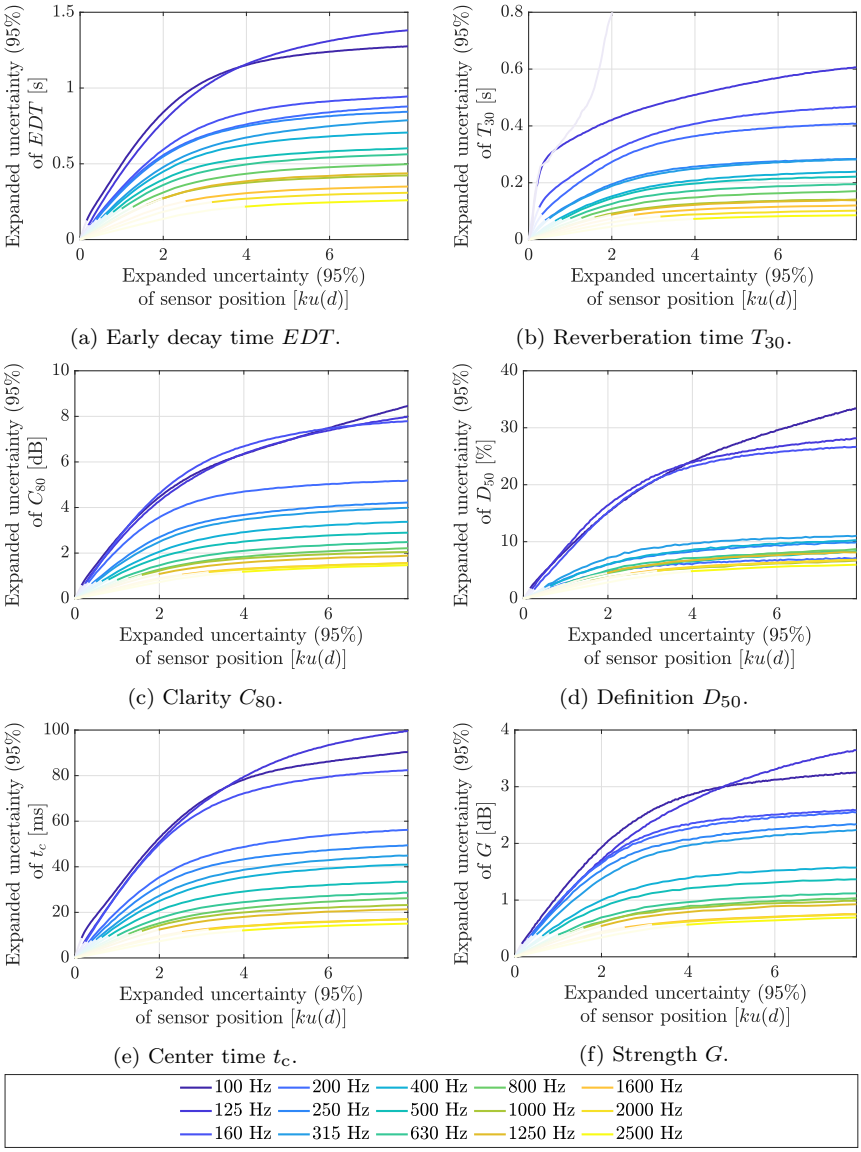

Figure 9.17: Expanded uncertainty of different room acoustical quantities for different 1/3-octave bands as a function of uncertainty of the sensor position in wavelengths in a concert hall.

9.4 Discussion

9.4.1 Uncertainty of broadband measurements

Figures 9.2 to 9.8 show the uncertainty of room acoustical quantities determined in broadband as a function of the measurement position's uncertainty. These curves provide the foundation for answering the central research question. A summary of these findings is shown in Figure 9.18 as the mean of the 26 measured sets. The red curves shows the 68 % coverage interval (standard uncertainty) while the blue curves identifies the 95 % coverage interval (expanded uncertainty). The dashed horizontal line highlights the just noticeable differences (JNDs; from Table 2.3). Along the x-axis, the expanded uncertainty of the sensor position is shown. As the underlying distribution is closely related to the normal distribution, the sensor position's standard uncertainty can be approximated by dividing the axis scaling by two.

Since the red curve of the mean 68 % confidence interval consistently runs well below the dashed just noticeable differences, there are no requirements for the measurement position's uncertainty that can be justified in this (standard) uncertainty class. Up to the maximum standard uncertainty covered by the x-axis (i.e., 2.1 m), the probability that repeated measurements differ from each other by more than the perceptual thresholds due to spatial fluctuations is (on average) less than 68 %. However, if the expanded measurement uncertainty is discussed with the 95 % coverage interval, occasionally a different situation emerges: the blue curves of (mean) expanded uncertainties exceed the just noticeable differences for almost all room acoustical quantities. This means that for larger position uncertainties, it is - in a repeated measurement - no longer 95 % certain that the difference in the two results, due to spatial fluctuations, is smaller than the threshold of perception.

Using the example of C_{80}, it can be read from Figure 9.18c that, on average, the measurement location needs to be described accurately enough to ensure that it can be reproduced with a precision of better than ± 1.2 m. The blue shaded area in this figure shows the values covered by the different measurement series. From this it can be seen that in the most extreme cases (C_{80}, set 10 in *Aula 2*), the measurement position must be documented even more precisely, namely to within ± 0.75 m.

The discussion of the clarity metric offers yet another perspective. While the JND determined under laboratory conditions (Cox et al., 1993) is plotted at 1 dB, other investigations suggest that changes in auditoria are not perceptible until differences exceed levels of 3 dB (Höhne & Schroth, 1995). The latter threshold would greatly relax the accuracy requirements of the measurement location. This

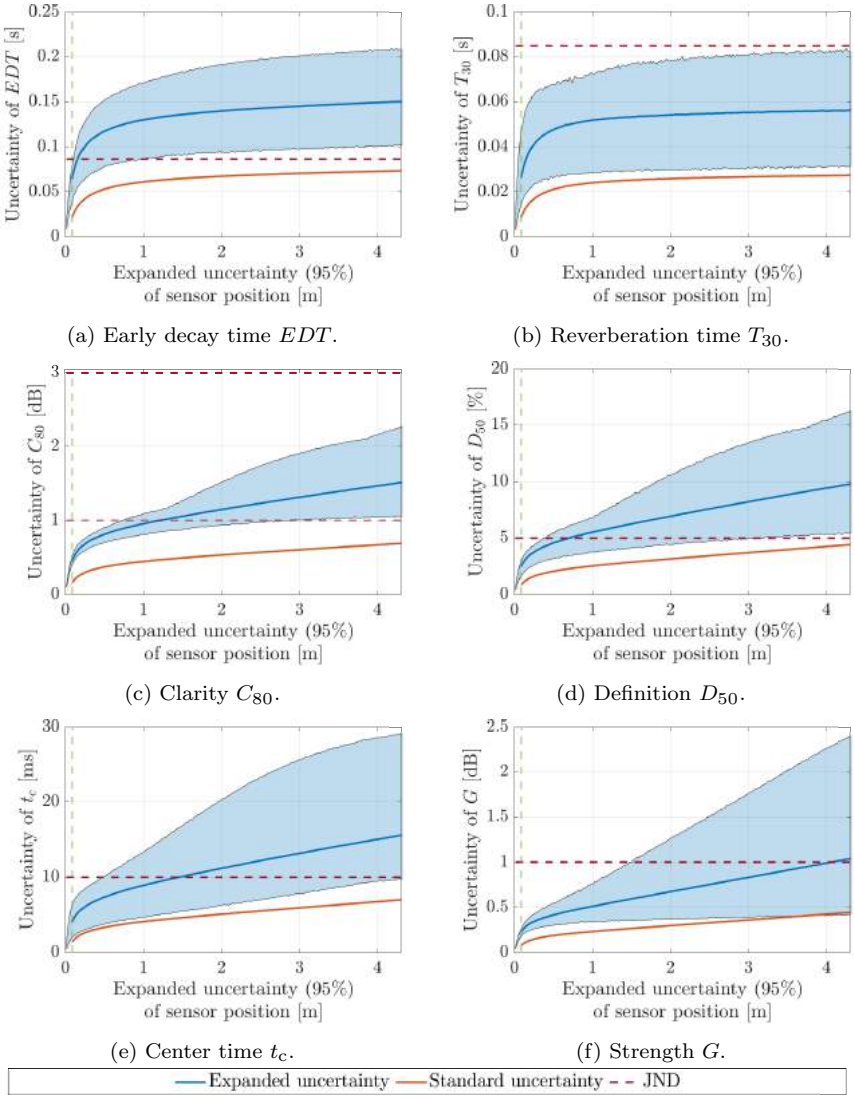

(a) Early decay time EDT.

(b) Reverberation time T_{30}.

(c) Clarity C_{80}.

(d) Definition D_{50}.

(e) Center time t_c.

(f) Strength G.

Figure 9.18: Standard (68 %) and expanded (95 %) uncertainty of different room acoustical quantities as functions of the sensor position's (expanded) uncertainty. The broken red line indicates the just noticeable difference. The solid blue area marks the range covered by the 26 sets.

contradiction offers great potential for future investigations in which frequently quoted JNDs are put to the test of real sound fields.

From the comparison of different room acoustical quantities, it can be seen that a T_{30} reverberation time measurement can be reproduced sufficiently well even with the measurement position only rudimentarily documented. This is, on the one hand, because reverberation times with large dynamic ranges fluctuate relatively little, and, on the other hand, because technical reverberation times change very little from one region to another in an auditorium.

These arguments do not hold for EDT at all: Figure 9.18a indicates that spatial fluctuations for the early decay quickly rise to amplitudes that are quite similar to the JND. Consequently, in particularly adverse conditions, position uncertainties of some 10 cm can already mean that uncertainties due to spatial fluctuations exceed just noticeable differences. The maximum coverage intervals of the sensor position's uncertainty under both critical and under average conditions can be taken from Table 9.2

Table 9.2: Maximum expanded uncertainties of the sensor position to ensure the expanded uncertainty of room acoustical quantities is below JNDs.

Room acoustical quantity	Coverage interval (95 %) sensor position	
	average conditions	critical conditions
EDT	15 cm	10 cm
T_{30}	> 4.3 m	> 4.3 m
C_{80}	121 cm	73 cm
D_{50}	69 cm	36 cm
t_{center}	145 cm	48 cm
G	406 cm	150 cm

9.4.2 Reference to theory

Driving Factor: Reverberation time

In Chapter 8, the properties of the measurement function were successfully matched with theoretical predictions (Davy et al., 1979). It was found that for EDT and T_{30}, the amplitude of spatial fluctuations depends on the prevailing reverberation time. In view of Figures 9.9 and 9.10 and the shown regression, it can be seen that the general relation holds equally for uncertainties and the main research question.

It is interesting to see how C_{80} and t_c behave in different ways. While center time follows a "moderate" to "very strong" trend that exhibits greater uncertainties at longer reverberation times, the trend for clarity is much less pronounced and shows (at best) a weak, opposite relation. The potential reasons for these different properties are examined in more detail below.

Driving Factor: Frequency

Amplitude The data presented in Figures 9.15 to 9.17 shows that the magnitude of the spatial fluctuations increases greatly with lower frequencies. This observation is consistent with the discussion on reverberation times in Chapter 8, specifically Table 8.2. What is new, however, is the finding that this trend applies not only to reverberation times but to all the room acoustical quantities discussed here.

To move towards a more quantitative comparison, the curves shown in Figures 9.16 and 9.17 were parameterized with a simple model of two straight lines that meet at an inflection point a:

$$f(x) = \begin{cases} bx & : x < a \\ cx + (ba - ca) & : x \geq a \end{cases} \tag{9.4.1}$$

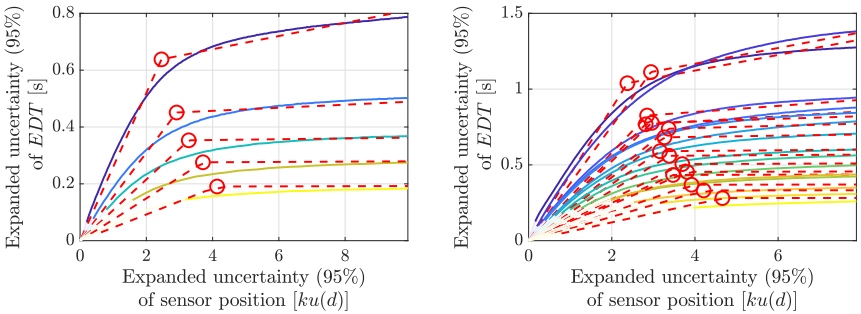

(a) 1/1-octaves. (b) 1/3-octaves.

Figure 9.19: Expanded uncertainty of EDT in a concert hall as a function of uncertainty of the sensor position in wavelength, with parameterized curves in red.

In Figure 9.19, EDT data and the fitted model are shown through red dashed lines. The inflection point is marked by the red circle. To counteract the risk of misunderstanding, it is necessary to clearly indicate that this parameterization

does not imply a physically motivated model. Instead, Equation 9.4.1 should be seen as a mathematical expression of the visually motivated concepts of the *initial rise* and the *extended trend*. In this light, the parameter b refers to the slope of the *initial rise* and c to the slope of the *extended trend*. The inflection point at $ku_{95\%}(d) = a$, where both lines intersect, can be understood as a transition between the domains. These parameters permit comparing the many curves (for EDT and other quantities) with each other regardless of whether they accurately represent a physical or theoretical property down to the last detail. The limits of the linear regression model are discussed in further detail in Section 9.4.3. Although only shown for EDT, such curves can be prepared for any of the room acoustical quantities.

To discuss the frequency-dependent amplitude of spatial fluctuations, and thus Davy's theory, Figure 9.20 shows ratios of the inflection points at neighboring frequency bands. The amplitude ratio at different frequencies (color coded) is plotted for different room acoustical quantities ("shape coded") along the y-axis.

Quantitatively, Davy et al. (1979) reports a linear proportionality that suggests a change in the fluctuations' variance by a factor of 2 (or 0.5 respectively) from one octave band to the next. Since Figure 9.19 shows uncertainties and since these are determined by the square root of the variance, a ratio of $\sqrt{2} \approx 1.41$ is to be expected between neighboring frequency bands. The amplitude ratio in Figure 9.20 confirms this expectation up to the second decimal digit.

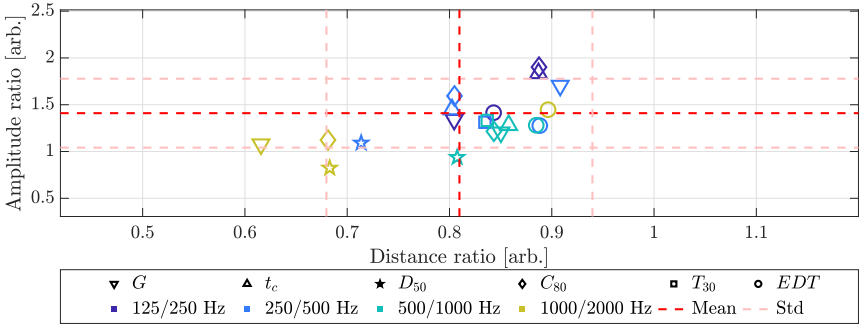

Figure 9.20: Ratio of the inflection points when neighboring frequency bands are compared to each other. The x-axis shows the distance ratio. The y-axis shows the amplitude ratio. The colors represent the compared center frequencies. The shape of the marker represents the room acoustical quantity.

Even though the demonstrated relationship is in perfect agreement with theory,

this finding is particularly noteworthy since, strictly speaking, Davy's theory is valid only for the diffuse sound field. Although many of the room acoustical quantities quantify the contribution of the early (nondiffuse) part of the RIR, the relative change of the fluctuation's magnitude over frequency is well predicted by diffuse field theory.

Spatial extent There is a second expectation that is based on Bodlund's (1977) theoretical considerations. They suggest that spatial fluctuations increase up to a wavelength-dependent distance of $d = ka = \pi$ as the sound field's spatial autocorrelation function rapidly decays to zero with increasing distance.

Even though the inflection points shown in Figure 9.19 cluster around 3 $[ku(d)]$, it is also evident that there is a trend shifting the inflection points to slightly shorter distances (in wavelength) as the frequency decreases. This pattern can be observed for all room acoustical quantities, and, with marginal differences, in any of the rooms.

This aspect relates to the spatial extent of the *initial rise* domain and can therefore be explored with the segment-wise linear regression model and the associated inflection point. Looking at Figure 9.19a, for full octaves some goodwill may be required to recognize a cluster point at the predicted distance of π. The third-octave analysis in Figure 9.19b shows this possible accumulation point a bit more pronouncedly, at least at frequencies below 630 Hz.

These observations cannot be reconciled with Bodlund's (1977) predictions beyond doubt. Instead, the transition from the *initial rise* to the *extended trend* seems to shift to larger distances (relative to wavelength) at higher frequencies. The quantitative evaluation in Figure 9.20 reveals that this is not an optical illusion but a quite solid trend: When the distances of inflection points at neighboring frequency bands are compared to each other (along the x-axis), the ratio is on average 0.80, with a small overlayed trend of larger differences towards higher frequencies. This illustrates why there appear to be clustering points at low frequencies that continuously shift to greater distances at higher frequencies.

Possible causes cannot be substantiated by targeted observations, but there are a number of arguments that come into play. First, at higher frequencies the limits of the sound field's spatial sampling grid are reached. As a result, the fluctuations were sampled at a lower resolution in ka scaling. Second, caveats against the regression analysis (discussed below) could be cited. Third, it should be kept in mind that the fluctuations of the sound field that Davy or Bodlund discuss are not synonymous with Monte Carlo uncertainties discussed here.

Despite these particular differences, there is the qualitative perception that the general results can still be aligned reasonably well with theoretical expectations. The transition from the domains of the *initial rise* to the *extended trend* occurs

at around $3 \approx \pi$ wavelengths which translates to a potential mismatch of some 5 %.

Driving Factor: Bandwidth

The influence of the filter bandwidth on the uncertainty due to spatial fluctuations is best discussed by considering Figure 9.21. The figure's structure is quite similar to Figure 9.20, and also represents a compressed display of the curves shown in Figures 9.16 and 9.17. The distance ratio $u(d_{1/3\text{-octave}})/u(d_{1/1\text{-octave}})$ (along the x-axis) is plotted against the amplitude ratio of the quantity's uncertainty, e.g., $u(EDT_{1/3\text{-octave}})/u(EDT_{1/1\text{-octave}})$ (along the y-axis). Just as before, the shape of the marker indicates the quantity and the color represents the center frequency.

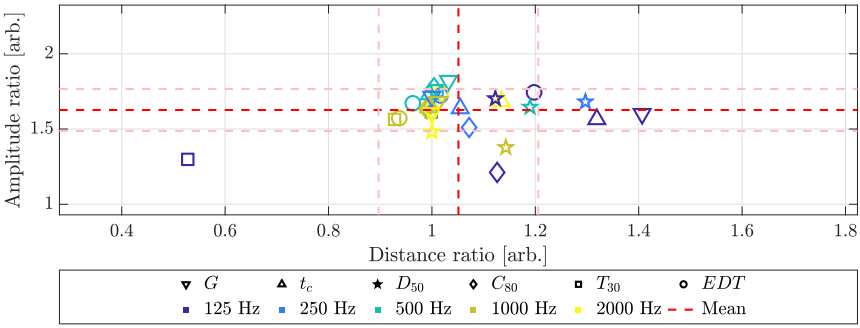

Figure 9.21: Ratio of the inflection points determined in 1/1-octave and in 1/3-octave bands. The x-axis shows the distance ratio. The y-axis shows the amplitude ratio. The colors represent the center frequencies. The shape of the marker represents the room acoustical quantity.

Amplitude From Davy's theory (Davy et al., 1979) and Equation 2.1.22, it can be taken that the variance of the spatial fluctuations depends linearly on the inverse of the statistical bandwidth. With the uncertainty being the square root of the variance and the ratio between third and full octave statistical bandwidths being 3 , there is the expectation that the uncertainty analyzed in both bandwidths should differ by a factor of $\sqrt{3} \approx 1.73$. The empirical analysis in Figure 9.21 yields an average amplitude ratio of 1.62. Though not quite as accurate as in the previous discussion, this deviation of less than 7 % still represents a reasonably good agreement with theory. A possible reason is the SNR-related

outlier of T_{30} in the 125 Hz band. Again, it is remarkable that Davy's prediction holds for reverberation times as well as for other quantities.

Spatial extent A second step investigates whether the fluctuation's spatial extent depends on the filter's bandwidth. The x-axis in Figure 9.21 shows the distance ratio of the inflection points in third- and full octaves. The vertical dashed lines show the mean and the standard deviation of ratios. Since these ratios are very close to unity (i.e., 1.05), it can be seen that the transition between the *initial rise* and the *extended trend* at third and full octaves occurs at almost identical distance uncertainties. Thus, the investigated bandwidth has no detectable influence on the areal extent of the spatial fluctuations.

9.4.3 Appropriateness of regression models

The calculation of the uncertainty propagation through a Monte Carlo method makes it possible to evaluate the empirical measurement function in the first place, and thus to answer the research question. Since the uncertainty curves of the different room acoustical quantities exhibit a visually similar characteristic trend, a breakdown into the two domains of the *initial rise* and the *extended trend* was made in Section 9.3.1. This basic idea along with a segment-wise linear parameterization of the curves was pursued to allow a limited quantitative comparison of the numerous different results.

It can be argued that the explanatory power of such a comparison may be limited for a number of reasons. First, a solely visual fitting suggests a model that lacks a physical rationale and thus comes with the risk of obscuring underlying concepts. Second, as pointed out, there is little reasonable justification as to why the shapes of the empirically determined curves can be reasonably approximated by a simple linear regression. Third, the quantitative comparison of any two curves may not be fully robust since there is no proof of validity that shows how the linear regression parameters correlate to the underlying physical principlest.

As a counterargument, due to its complexity it is unreasonable to perform the nonuniform sampling of the empirical measurement function by the Monte Carlo simulations with the expectation that the result will miraculously obeys a simple functional relationship. Quite the opposite: It would even be surprising if the output distribution followed simple laws. Consequently, resorting to a basic linear regression is rather to permit some limited comparability without the intention of suggesting a curve's shape for which there is no evidence.

On these grounds, one can consider the concepts of *initial rise* and *extended trend*. It seems that both domains map the properties of the impulse response, i.e., early reflections and reverberant decay, to changes of the sound field in space.

In the case of a perfectly diffuse sound field, the stochastic superposition of uncorrelated standing waves (Section 2.1) leads to spatial fluctuations that are generally independent of the location in the room. Thus, the *extended trend* runs as a flat line at an amplitude suggested by Davy et al.'s theory; a linear regression model would be a valid parameterization. The T_{30} uncertainty curves in Figure 9.3 provide empirical confirmation.

For shorter distances between two observation points ($ka < \pi$) the modes are not fully uncorrelated, which manifests in smaller fluctuations described by the *initial rise*. When the *extended trend* continues to increase to larger distances, it is an indication that the sound field is not (particularly) diffuse and that the direct sound and the early reflections significantly influence the spatial profile. For these parts, the linear regression serves well as an initial approach.

9.4.4 Influence of early reflections

The contribution of early reflections to spatial fluctuations is best discussed by considering Figure 9.14, which illustrated the uncertainties of clarity, definition and center time. To lay the foundation, two factors are central to investigate the influence of early reflections. First, converting the uncertainties of room acoustical temporal clarity quantities into the uncertainty of the exponential decay constant λ provides a common ground that all room acoustical metrics relate to. In line with the previous discussion in Section 9.3.3, this transition does not assume the investigated sound fields to be diffuse or to have any other specific property. Second, contrasting the same quantity calculated using different time windows against each other, i.e., C_{50} to C_{80} or D_{50} to D_{80}, eliminates the influence of the algorithm (Equations 2.1.14 and 2.1.15) from the comparison and thus highlights the influence of the time window.

Comparing the quantities relying on a 50 ms time window with those derived from an 80 ms time window in Figure 9.14, it is evident that C_{80} and D_{80} have slightly lower uncertainties compared to C_{50} and D_{50}. In this analysis, particular significance is attached to the clarity metric: In this quantity, only the numerator of Equation 2.1.15 depends on the varying time window, while the denominator remains unchanged with the energy of the full decay. This indicates that the early part of the impulse response also contributes to the spatial fluctuations.

The significantly lower uncertainty of center time compared to other temporal quantities is worth discussing as well. The question arises of whether this is due to time windowing of the impulse responses or the weighting of the RIR energy with its running time t (see Equation 2.1.16). This contrast cannot be resolved on the basis of the available data; however, the weighting of the RIR's energy over time provides a plausible explanation for why t_c's uncertainty increases with

longer reverberation times.

As far as the uncertainty due to spatial fluctuations is concerned, center time appears be the quantity best-suited to accurately discuss the temporal energy distribution in room impulse responses. It appears, however, that t_c is the least commonly used quantity among peers (compared to clarity and definition), which may imply that general experience in its interpretation is also more limited.

9.4.5 Necessity for measurements

In the discussion so far, the good agreement of the results with theoretical predictions has been emphasized so strongly that one may wonder whether the efforts for the measurements and Monte Carlo simulations were justified after all. This sentiment would ignore that, to the best knowledge, so far there is little known about spatial fluctuations of room acoustical quantities other than reverberation times. As general theoretical approaches do not consider early reflections, there is a clear need for empirical studies. Even though other simulation tools are available to calculate sound propagation (e.g., ray-tracing models), these methods do not consider modal effects and thus it is uncertain whether these strategies are suitable to discuss the spatial variance of sound fields.

Previous measurement surveys have been designed to investigate uncertainties and spatial fluctuations from different perspectives. As a result, the data collected here permits a new view on spatial fluctuations. The inverse trend between C_{80} and t_c as a function of prevailing reverberation time in Figures 9.11 and 9.12 may serve as evidence that contributions to spatial fluctuations exist that have not been discussed before. This is why this study can contribute to understanding spatial fluctuations.

9.5 Conclusions

In this section, the relationship between an uncertain measurement position and the resulting uncertainty in reproduced room acoustical measurements was presented. Based on the empirically determined measurement function and an assumption about the measurement positions distribution, the resulting uncertainty distribution of room acoustical quantities was determined using a Monte Carlo method.

Based on the results shown and the discussion, the following conclusions emerge:

- The uncertainty in reproduced measurements of room acoustical quantities due to spatial fluctuations in the sound field when the receiver (or the source) position is uncertain was determined

  - in broadband (see Figure 9.2 to 9.8),
  - filtered in different bandwidths (see Figures 9.16 and 9.17), and
  - at different center frequencies (see Figures 9.16 and 9.17).

- Based on published just noticeable differences, it was determined how accurately measurement positions need to be documented and reproduced to ensure the uncertainty due to spatial fluctuations does not exceed thresholds of perception.
  - To ensure the standard uncertainty of room acoustical quantities (68 % coverage interval) remains below the just noticeable difference, the results indicate that the maximum standard uncertainty of the measurement position can exceed the surveyed range of 2.1 m.
  - To ensure the expanded uncertainty of room acoustical quantities (95 % coverage interval) remains below the just noticeable difference, the results indicate that the maximum expanded uncertainty of the measurement position should not exceed a range of approximately 0.40 m. For EDT the requirements are more stringent (for details see Table 9.2.

- The findings are in good agreement with theoretical predictions (Davy et al., 1979) in regard to their dependency on
  - the mean prevailing reverberation time,
  - the filter's center frequency and
  - the filter's bandwidth.

- Based on empirical results and Monte Carlo simulations, the uncertainties of clarity, definition, center time and strength due to spatial fluctuations were determined, which could not previously be predicted based solely on diffuse field theory.

- A two-segment linear regression model was used for a quantitative discussion of uncertainties due to spatial fluctuations.
  - For very small uncertainties, in position an *initial rise* indicates that the uncertainty of room acoustical quantities increases quickly as the position uncertainty increases.
  - At position uncertainties of about $ka \approx \pi$, the uncertainty of room acoustical quantities reaches a plateau and grows much more slowly as the position uncertainty continues to increase. There is a small

frequency dependency towards larger position uncertainties at higher frequencies.

  - For position uncertainties beyond $ka \approx \pi$, an *extended trend* is defined by a base level due to spatial fluctuations (Davy et al., 1979) and a moderate rise towards larger distances that is related to the change in room acoustical quantities due to the geometry of the room.

- The uncertainty in reproduced measurements due to uncertainties in the measurement position is not only due to spatial fluctuations of the reverberant decay, but also (albeit to a smaller extent) due to changes in early reflections from one position to the next.

- Not all room acoustical quantities of temporal clarity (C_{80}, D_{50}, t_c) are affected by spatial fluctuations in the same way.
  - Quantities without time windows (t_c) are affected least,
  - quantities with time windows for music are affected moderately and
  - quantities for speech are affected most.

- Based on the reciprocity principle, the effect of uncertain source and receiver positions on the uncertainty of room acoustical quantities needs to be introduced twice: once due to the source, and once due to the receiver (when both positions are independent from each other).

10 General results

In this study, the uncertainty of room acoustical measurements in auditoria is investigated. An emphasis is placed on the contributions due to spatial fluctuations of room acoustical quantities. Partial results towards this goal are the listing of uncertainty contributions affecting impulse response measurements. Furthermore, it is examined how the uncertainties of these influence factors propagate to the output uncertainty of room acoustical quantities. These results are summarized in this section.

10.1 Uncertainty of measured impulse responses

Based on studies performed at a number of national metrological institutes, the uncertainty budget shown in Table 10.1 was established. Along the way, each individual contribution was scrutinized and adjusted to properly characterize the performance of the measurement system used here. Thus, the uncertainty budget presented here needs to be adjusted to represent the properties and capabilities of other systems. The combined uncertainty refers to the amplitude of the individual samples in a measured impulse response. The type of uncertainty (random vs. systematic) indicates whether each sample is affected independently or whether all of them are affected in the same way. The exact details that lead to this result can be found in Section 4.

Table 10.1: Uncertainty budget for room impulse response measurements.

Symbol b_i	Probability distribution	Type	Sensitivity coefficient c_i	Standard uncertainty $u(b_i)$ [dB]
$b_{\text{LS-dir}}$	Normal	Random	1	0.38
b_{Setup}	Normal	Random	1	0.35
$b_{\text{LS-level}}$	Normal	Systematic	1	0.26
$b_{\text{Mic-cal}}$	Normal	Systematic	1	0.21
b_{LTI}	Normal	Random	1	0.2
$b_{\text{LS-spec}}$	Normal	Systematic	1	0.16
$b_{\text{Mic-spec}}$	Normal	Systematic	1	0.15
b_{Filter}	Normal	Systematic	1	0.12
$b_{\text{Meteo-}\vartheta}$	Normal	Systematic	1	0.12
$b_{\text{Meteo-p}}$	Normal	Systematic	1	0.07
$b_{\text{Mic-dir}}$	Normal	Random	1	0.07
$b_{\text{Mic-field}}$	Normal	Random	1	0.011
		Combined standard uncertainty	$u_{\text{c}}(b_{\text{Equip}})$	0.71
		Coverage factor	k	2
		Expanded uncertainty (95 %)	$u_{\text{c, }k=2}(b_{\text{Equip}})$	1.42

10.2 Uncertainty of room acoustical quantities

The random type standard uncertainties in Table 10.1 are the relevant contributions to the combined standard uncertainty of a measured impulse response necessary to determine the uncertainty of room acoustical quantities (see Chapter 9.3.1). The uncertainty of the room acoustical quantities derived from each of the 420 470 RIRs collected through 26 measurement series (see Table 8.1) was calculated according the rules of the standard ISO Guide 98-3 (2008). The resulting range of standard uncertainties of room acoustical quantities is shown in Figures 6.2 to 6.12. From this standard uncertainty data, Table 10.2 shows the median standard uncertainty for each of the discussed room acoustical quantities. Since both smaller and significantly larger standard uncertainties can occur in individual cases, important quantiles are also listed, which allow deriving the 68 % coverage interval.

Table 10.2: Standard uncertainty of broadband room acoustical quantities based on more than 400 000 uncertain impulse response measurements. The quantiles indicate the range of uncertainties that occurred in the sample.

Room acoustical quantity	Standard uncertainty of room acoustical quantities		
	Quantiles		
	Median	15.9 %	84.1 %
T_{30}	3.8×10^{-5} s	3.3×10^{-5} s	4.8×10^{-5} s
EDT	1.6×10^{-4} s	1.2×10^{-4} s	2.5×10^{-4} s
C_{80}	5.9×10^{-2} dB	4.6×10^{-2} dB	8.4×10^{-2} dB
D_{50}	3.8×10^{-1} %	2.9×10^{-1} %	5.0×10^{-1} %
t_c	0.6 ms	0.5 ms	0.9 ms
G	3.0×10^{-2} dB	2.1×10^{-2} dB	5.3×10^{-2} dB

10.3 Uncertainty due to spatial fluctuations

The main results of this study are the uncertainties of room acoustical quantities due to the spatial variance of the sound field. Since general experience with these uncertainty contributions is not yet widespread, the results are presented in slightly more detail, in broadband and octave filtered form. Based on 26 measurement series, the uncertainty of room acoustical quantities is shown as a function of an uncertain measurement position.

The graphic representation in Figures 10.1 and 10.2 shows a solid blue line that indicates the mean expanded uncertainty for each of the investigated quantities. The x-axis indicates the expanded uncertainty of the measurement position - for the broadband results the uncertainty is given in absolute unit, i.e., meter, whereas for the band-filtered results the position uncertainty is given relative to the center frequencies' wavelength kd. The y-axis represents the room acoustical quantity's associated uncertainty. The shaded area marks the 2σ interval in which the expanded uncertainty curves of the 26 sets run. The dashed line results from the segment-wise linear regression of the mean uncertainty curve and forms the basis of the summary statistics given in Tables 10.3 and 10.4. In these tables, the second column lists the expanded uncertainty due to spatial fluctuations, and the third column shows the expanded position uncertainty, above which the uncertainties are fully pronounced.

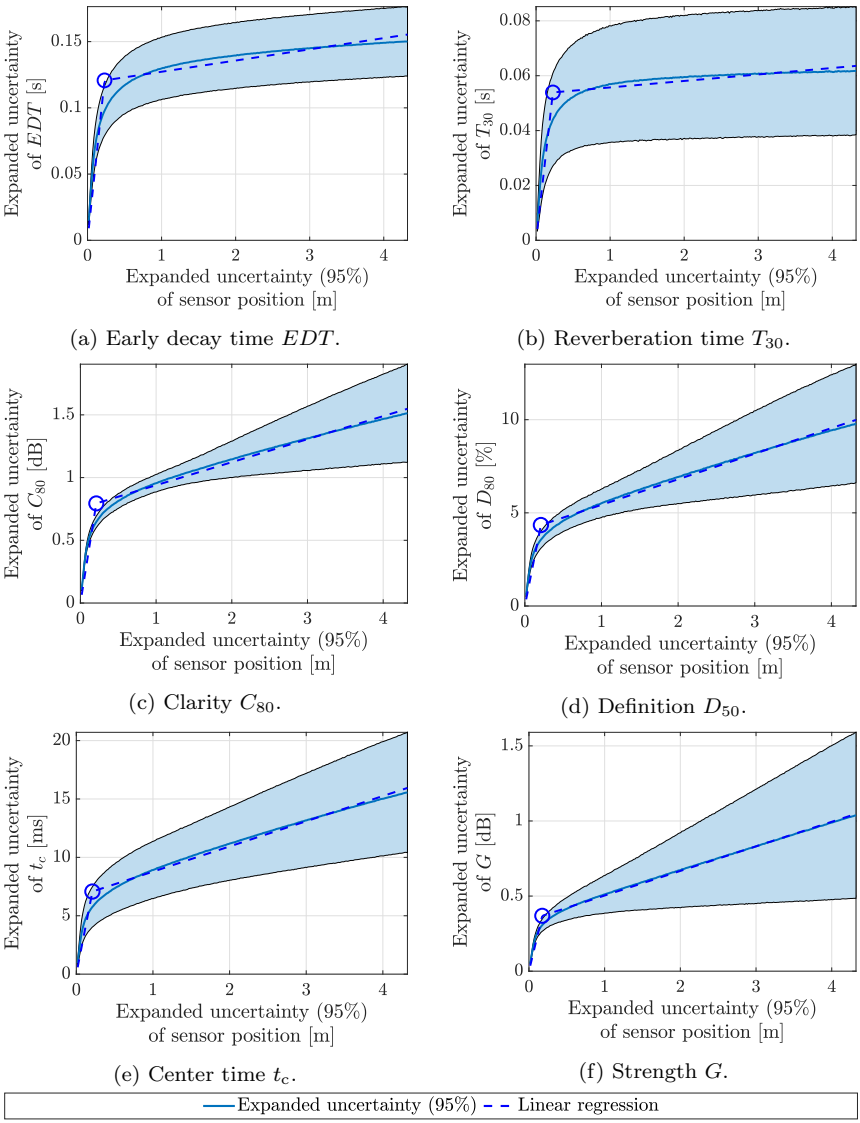

(a) Early decay time EDT.

(b) Reverberation time T_{30}.

(c) Clarity C_{80}.

(d) Definition D_{50}.

(e) Center time t_c.

(f) Strength G.

Figure 10.1: Expanded uncertainty of different broadband room acoustical quantities as a function of uncertainty of the sensor position with dashed parametrized curves. The shaded areas mark the standard deviation as spanned by the 26 measured sets.

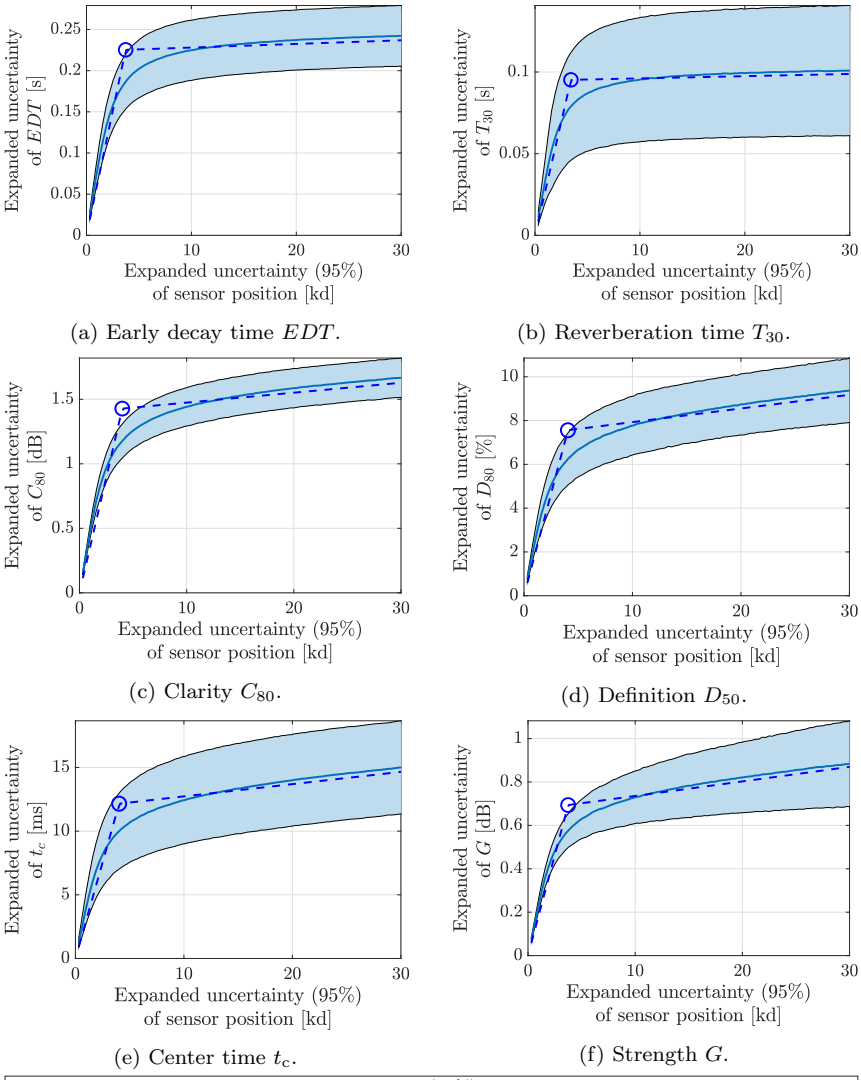

Figure 10.2: Expanded uncertainty of different full octave filtered room acoustical quantities as a function of uncertainty of the sensor position with dashed parametrized curves. The shaded areas mark the standard deviation as spanned by the 26 measured sets.

Table 10.3: Expanded uncertainty (95 %) of broadband room acoustical quantities and the expanded position uncertainty (95 %) above which the fluctuations are fully pronounced.

Room acoustical quantity	Expanded uncertainty (95 %) of room acoustical quantities due to spatial fluctuations	Expanded uncertainty (95 %) of position with fluctuations fully pronounced [m]
T_{30}	0.05 s	0.23 m
EDT	0.12 s	0.23 m
C_{80}	0.79 dB	0.21 m
D_{50}	4 %	0.21 m
t_c	7 ms	0.21 m
G	0.37 dB	0.18 m

Table 10.4: Expanded uncertainty (95 %) of full octave filtered room acoustical quantities at 1 kHz and the expanded position uncertainty (95 %) in kd above which the fluctuations are fully pronounced.

Room acoustical quantity	Expanded uncertainty (95 %) of room acoustical quantities due to spatial fluctuations	Expanded uncertainty (95 %) of position with fluctuations fully pronounced [kd]
T_{30}	0.09 s	3.41
EDT	0.23 s	3.73
C_{80}	1.43 dB	3.99
D_{50}	8 %	4.05
t_c	12 ms	4.03
G	0.69 dB	3.74

The uncertainty of room acoustical quantities due to spatial fluctuations changes by a factor of $1/\sqrt{2}$ from one octave band to the next higher. Relative to the uncertainties given in Table 10.4 (column 2) for the reference frequency $f_r = 1\,\text{kHz}$, the scaling factor x_f can be determined according to Equation 10.3.2 to yield the uncertainties due to spatial fluctuations at higher or lower octaves frequency bands.

$$u_{k=2}(f_\mathrm{m}) = x_f u_{k=2}(f_\mathrm{r}) \tag{10.3.1}$$

$$x_f = \sqrt{2}^{\,a} \text{ with } a = -\frac{10}{3}\log_{10}\frac{f_\mathrm{m}}{f_\mathrm{r}} \tag{10.3.2}$$

The uncertainty of the position when the fluctuations are fully pronounced changes by a factor of 1.25 from one octave band to the next higher. Relative to the position uncertainty given in Table 10.4 (column 3) for the reference frequency $f_\mathrm{r} = 1\,\mathrm{kHz}$, the scaling factor x_d can be determined according to Equation 10.3.4 to yield the position uncertainties at higher or lower octave frequency bands.

$$u_{\mathrm{pos},k=2}(f_\mathrm{m}) = x_d u_{\mathrm{pos},k=2}(f_\mathrm{r}) \tag{10.3.3}$$

$$x_\mathrm{d} \approx 1.25^{-a} \text{ with } a = -\frac{10}{3}\log_{10}\frac{f_\mathrm{m}}{f_\mathrm{r}} \tag{10.3.4}$$

The uncertainty of room acoustical quantities changes by a factor of $\sqrt{3}$ when third octave bands are analyzed instead of full octave bands.

11

General Discussion

The discussion of uncertainties is not yet part of the standard repertoire in the field of auditorium acoustics, probably due to the relative complexity of the problems discussed in this field. While generic questions can be addressed using mathematical closed-form solutions, more challenging scenarios often feature an abundance of input variables that can only be approached with simulation tools on a case-by-case basis. When the flow of information can only be determined in individual scenarios, it is difficult to identify higher-level influence factors and how they contribute to the output. At the same time, it is not uncommon that the many input quantities are not known down to the last detail. In such conditions, it tends to be challenging to distinguish the important aspects from the less relevant ones.

This discussion stresses the importance of recording and quantifying all contributing influence quantities to investigate the propagation of uncertainties. Referring to the previous discussion of Ishikawa diagrams, it is important to recall that identifying influence quantities is a qualitative process with no guarantee of reaching comprehensive results. Against this backdrop, it is important to move forward in a granular and diligent manner to minimize the likelihood of overlooking uncertainty contributions. This argument holds even if that means discussing contributions that turn out to be factors of lesser significance. At the same time, such a comprehensive approach allows adjusting existing uncertainty contributions or introducing new ones whenever new findings suggest a reassessment.

To ensure this generality and extendability, it is important to discuss the measurement uncertainty according to standardized and defined rules, such as the framework offered in ISO Guide 98-3 (2008). At the same time, it must be acknowledged that the intricacies of the GUM are its own field of research in metrology. The discussion in scientific journals highlights two aspects: First, there are matters that can only be described in a very approximate way using the standard tools of the GUM. Second, there are numerous examples where authors autonomously enhance the uncertainty framework, using good reason,

to allow a more precise discussion of specific uncertainty scenarios. This liberty was also claimed here, for example when interpreting the measurement function from a Bayesian perspective and implementing the Monte Carlo simulations in a two-step process.

11.1 Uncertainty of measured impulse responses

In this spirit, the uncertainty of measured room impulse responses was discussed. Guided by an extended root cause model of manufacturing reliability, a variety of possible uncertainty contributions were collected. These input quantities were then recognized in the uncertainty evaluation in different ways.

Some contributions are listed based on plausibility, however, that could not be recognized in the uncertainty budget. The reasons are manifold, but can be as mundane as in the following examples. The influence of the observer on measurements, for instance, is undisputed; however, its contribution can hardly be quantified. The same is true for environmental conditions that affect the results: Calculating the sound propagation in a non-homogeneous and non-stationary medium is highly complex and exceeds the scope of this study. Such factors must be investigated in detailed and tailored studies that are specifically designed for this purpose.

Other influences were included based on a rather basic and simple model of the measurement process. The intricacies of 2-Ch-FFT correlation techniques may serve as an example of how a focus was placed on steady state and energetic contributions to the measurement uncertainty. In order to discuss transient disturbances in specific measurements, reference must be made to other works, such as that of Eichstädt (2012).

A similar pragmatism is appropriate when discussing the uncertainty contribution measurement chain elements that couple directly to the sound field. Approaching this matter requires a model on sound propagation. For the sake of general applicability, the rather elementary concept of the diffuse sound field was adopted. Especially for early reflections and for typical sound fields in auditoria, however, this approach may be valid only with limitations.

Also, it has to be noted that the uncertainty model does not yet consider correlations of input quantities. It has to be discussed that correlations over time may exist between neighboring time samples of the impulse response. Also, correlations may exist when the same equipment, the same calibration normal or the same sensor is used in repeated or reproduced measurements. These factors can and should be recognized in dedicated future investigations.

Other contributions are recognized in the uncertainty budget based on experience from other fields of acoustics, e.g., building acoustics. In standardized

measurements in reverberation rooms to determine the radiated sound power or in wall testing facilities to determine the sound reduction index, uncertainties are regularly considered. Despite relying on this existing knowledge and implementing simple models, the uncertainty budget reported in Table 10.1 represents a step forward in combining different sources of knowledge and making the result available in architectural acoustics. The hierarchical listing of key uncertainty contributions to the measurement of room impulse responses provides a structure and context for open questions. For instance, the discussion about the measurement loudspeaker's directivity or the influence of nonlinearities can be put into context by relating their contribution to the combined uncertainty.

Depending on the individual setup and equipment used, adjustments to respective entries may be necessary. The procedure pursued in Section 4 to compile this table can serve as a practical example to quantify one's own measurement capabilities.

Finally, the shown data provides clear evidence for which influence quantities to target in order to have the greatest impact in affecting the combined measurement uncertainty.

11.2 Uncertainty of room acoustical quantities

The uncertainty in the measurement of room impulse responses was propagated through the algorithms to determine room acoustical quantities. The resulting uncertainties of the quantities are so small that one may well ask whether this meticulous effort is really justified. Of course, this objection is especially valid in that it is already known from ray tracing simulations (Vorländer, 2013) that many of the metrics can be determined quite accurately with very few sound particles.

As a rebuttal, it should be pointed out that, until now, a quantitative uncertainty estimate for room acoustical quantities was unavailable, and thus the presented findings add to the body of knowledge. This step forward holds, even if it were only to serve the conclusion that other, more prominent uncertainty contributions deserve more attention in future investigations.

It seems particularly important, however, to consider the quantities' intrinsic uncertainty as a benchmark for uncertainties due to spatial fluctuations. The magnitude of the fluctuations becomes quantitatively clear through this reference.

Finally, these findings also have a methodological value. Quite obviously, the uncertainty of room acoustical quantities is far below thresholds of perception. If this can be taken as a reason to accept larger uncertainties, then the uncertainty propagation can be reversed and the requirements on the measurement chain can be relaxed. As a result, alternative quasi-impulsive sound sources (such as fire-

crackers or popped balloons or paper bags) could be considered to determine room acoustical metrics. This could warrant a new validity to ad hoc measurements.

11.3 Uncertainty due to spatial fluctuations

The uncertainties of room acoustical quantities due to spatial fluctuations may be regarded as the most significant findings of this study. Compared to all other known sources of uncertainty, spatial fluctuation is by far the single most important one.

So far, knowledge about the sound field's spatial fluctuations is essentially based on the groundbreaking studies conducted when revising ISO 3382 (1997) in the early 1990s (e.g., Pelorson et al. (1992), J. S. Bradley and Halliwell (1988)), or the study by de Vries et al. (2001) in Concertgebouw Amsterdam that has brought new attention to the matter. The fundamentals of Kuttruff and Thiele (1954), Bodlund (1977) and Davy et al. (1979) provide a solid theoretical framework for discussing spatial variances in exponentially decaying sound fields.

This present study builds on the previous work and attempts to add to the existing state of knowledge. A major contribution is establishing the uncertainty due to spatial fluctuations as it depends on the uncertainty of the measurement position. This is a new finding compared to existing work both empirical and theoretical. The reasonable discussion of room acoustical quantities thus requires a sufficiently precise specification of the measurement location (source and receiver). This is important so that results can be reproduced in the presence of spatial fluctuations.

A second advance is the uncertainty of room acoustical quantities like clarity, definition, center time and strength that cannot be discussed based on theoretical considerations alone. The comparison of the different quantities indicates that they are affected differently by spatial fluctuations. Consequently, their uncertainties are not solely due to spatial variances in the sound field's exponential decay, but also due to changes in the early reflection patterns.

Relating empirical findings to theoretical predictions is of enormous importance, as their agreement places additional weight and confidence in the results' validity. The consistency in two aspects is particularly noteworthy: First, the linear rise in the uncertainties of EDT and T_{30} with longer average reverberation times is evident in both theory and empirical studies. Second, it is remarkable that the measured fluctuations' amplitude over frequency and bandwidth is in almost perfect agreement with theory. In addition, it was shown for the first time that the spatial fluctuations' dependence on frequency and bandwidth also holds for room acoustical quantities that focus on the early part of the room impulse response. The fact that these quantities cannot be modeled in the theoretical framework

stresses the need for empirical investigations. This is also true in light of the fact that it is not ensured that spatial fluctuations can be modeled with simulation tools of geometrical acoustics.

11.4 Critical aspects

In empirical studies, the question arises of whether the collected data is valid - translated to this study, whether the sample of surveyed auditoria is suitable and representative. When choosing the auditoria to survey, great care was taken to cover rooms that spanned a wide range of reverberation times and room shapes. With relatively small orchestra rehearsal rooms, large lecture halls, multi-purpose halls and full-size concert halls, this target was achieved. The covered range of clarity, definition and center time also suggests that a practical range of acoustic conditions has been covered.

Due to the design of the measurement apparatus, all halls had in common relatively flat floors. The results' relatively good agreement with theoretical predictions seems to confirm that the selection was appropriate. However, should additional factors exist that have an influence on spatial fluctuations, it is not guaranteed that the selected auditoria exhibit these influences sufficiently.

When looking at the measurement equipment used, it can be seen that the massive structure that forms the measurement device is, with an uncertainty of 0.35 dB, the second largest contributor to the uncertainty budget. Obviously, this has a negative influence on the collected impulse responses; however, the contribution has to be seen in context.

Interference by the trusswork is the second most important uncertainty contribution after the directivity of the sound source. The high-performance loudspeaker was meticulously designed to exhibit a directivity as homogeneous as possible. As a result, general ISO-3382 compliant sound sources show a much more pronounced directivity. This means that the influence of the measurement apparatus is smaller than disturbances that can normally be tolerated. Also, being the second most important uncertainty contribution, the setup used does not represent an outstanding uncertainty contribution relative to the other elements of the measurement chain. Finally, it was also shown that the equipment's influence on the uncertainty of room acoustical quantities is negligible compared to the uncertainty due to spatial fluctuations.

This assessment should not hide the fact that some aspects in the design of the array could have been better addressed. For the author, it is a painful experience to realize that decisions made in the past can have long-term effects. In this regard, the anisotropic sampling accuracy is a particularly fitting example. A supposedly straightforward decision made for reasons of austerity, the effects

could still be clearly demonstrated years later after several steps of data analysis. However, to be upfront, these effects are merely small factors that can only be detected by a targeted analysis, and they are ultimately rendered invisible through the mixing and smoothing of the Monte Carlo trials.

Another experience is that complicated measurements and large setups increase the likelihood of errors and failures, and eventually make them inevitable. As an example of this rendition of *Murphy's law*, it has happened that microphones dropped out at individual positions, or that areas remained unsampled after running out of time due to delays during setup. Enormous efforts were made to detect errors early on and to sort out invalid data. Ultimately, the uncertainty principle also applies here. A clear statement about the proportion of erroneous data cannot be made, as this data could otherwise be removed from the analysis. The good agreement of the results with theoretical predictions can be taken as an indication that flawed measurements did not have a significant influence.

11.5 Implications

This leads to the question of how meaningful the general results are and which interpretations are legitimate. As things stand today, spatial fluctuations certainly represent the largest contribution to the uncertainty in measurement of room acoustical quantities. Whether this uncertainty renders room acoustical quantities unusable needs to be seen in reference to appropriate just noticeable differences.

For reverberation times, uncertainties due to spatial fluctuations can be within the just noticeable difference of 5 %. This very general statement needs to be put into context: Disregarding local fluctuations, reverberation normally changes relatively little throughout the room, which is evident in the relatively flat *extended trend*. In light of Figure 9.18, it can be seen that the standard and expanded uncertainty of T_{30} is smaller than its JND even for large uncertainties in the measurement position. Consequently, for T_{30}, there is no evidence for an upper limit of the measurement position's uncertainty. This conclusion implies that it makes little sense to discuss measured reverberation times up to the second decimal digit. Of course, this assessment is not very new and stands on long experience, but is reconfirmed by the presented findings.

Because reverberation times are analyzed with smaller dynamic ranges (e.g., EDT), spatial fluctuations easily exceed their JNDs. For this quantity, a distinction between the regime of standard and expanded uncertainty needs to be made. When it needs to be ensured that it is 95 % unlikely that fluctuations in EDT exceed the JND, it becomes necessary to define the measurement position to an accuracy of about 10 cm. When the 68 % coverage interval is considered, fluctuations of EDT less frequently (< 32 % probability) exceed the JND even

for larger position uncertainties. Under the paradigm of expanded uncertainties, these findings seem to contradict the common experience that the perception of reverberance does not change over such small distances. Given that the established JND for reverberation (Seraphim, 1958) predates the concept of EDT (Jordan, 1970), it may be reasonable to investigate whether the difference limen can be confirmed using more modern techniques.

For other room acoustical quantities, the question becomes more delicate. Clarity or strength are significantly more dependent on the position in the auditorium, making it appropriate to document the measurement position anyway. For clarity, there are a number of studies that address the JNDs. Findings range from very high sensitivities of 1 dB under laboratory conditions (Cox et al. (1993)) to about 3 dB under real-life conditions (Höhne & Schroth, 1995). For the situations addressed here, Höhne and Schroth's results seem more appropriate, and thus JNDs seem larger than the uncertainty due to spatial fluctuations. The evidence is not equally conclusive for the other energy ratio parameters. But, as both definition and center time characterize similar sound field properties, a fundamentally different outcome would be surprising.

Since the spatial fluctuations in the broadband case are already fully pronounced after 25 cm, it seems reasonable to specify the measurement position with at least the accuracy of a seat (≈ 50 cm). Strictly speaking, this would still not be sufficient, so additional specifications such as "center" or "right armrest" may be helpful. With information of this nature, the uncertainty from Table 10.3 can be assumed. More accurate results require a more precise specification of the measurement location, and the exact requirements can be obtained from Figures 10.1 and 10.2 or by linear interpolation from the respective tables.

The same reasoning must apply to the band-limited case. Figure 10.2 shows that filtering increases the amplitude of spatial fluctuations significantly. Just as before, the resulting implications have to be discussed with reference to the applicable JNDs. As of today, however, JNDs at different octave bands are not yet available. As a result, important information is missing that would identify these fluctuations as detrimental to interpreting measurement results.

Based on the reciprocity principle, the uncertainty contribution due to spatial fluctuations applies independently to the sound source and to the microphone. This implication can also be independently confirmed by Equation 2.1.3, which notes how the source and receiver are independently coupled to the modes of the resonant system. Thus, if a measurement is to be reproduced completely, the uncertainty contribution for fluctuations must be taken into account for both the source and the receiver. Since these contributions are completely independent of each other, this means an increase of the uncertainty by a factor of $\sqrt{2}$ compared to the simple contribution.

12

General conclusions and outlook

12.1 General conclusions

Based on the results shown and the previous discussion, the following conclusions were drawn:

- A GUM conforming strategy was described according to which the main uncertainty contributions to the measurement of room impulse responses were discussed. The method allows considering additional factors or adjusting existing factors when new knowledge becomes available.

- A hierarchical listing of the most important uncertainty contributions to the measurement of room impulse responses was created. Based on this list, the effort for accurate measurements can be targeted to the most relevant influencing factors to improve the efficiency of measurements.

- The uncertainty of room acoustical quantities due to uncertain room impulse responses is very low and in most cases probably not a significant factor.

- Spatial fluctuations are by far the single most significant uncertainty contribution to room acoustical quantities. For many of the investigated quantities (i.e., T_{30}, EDT, C_{80}, D_{50}, t_c, G), this study marks the first time that spatial fluctuations have been studied with such precision.

- The uncertainty due to spatial fluctuations has to be recognized independently for the source and the receiver (reciprocity).

- In order to reasonably interpret room acoustical quantities, a sufficiently precise specification of the measurement location (source and receiver) is necessary.

- The uncertainty is quantified and reported in Section 10. The uncertainty is given in broadband but also filtered in full octaves and in third octave bands.
- For the investigated parts direct theoretical predictions are possible, the empirically determined uncertainties due to spatial fluctuations show very good agreement.
- In addition to theoretical predictions, spatial fluctuations are not only due to variances in the exponential decay of the sound field, but also due to changes in the early reflection patterns.
- The comparison of C_{80}, D_{50} and t_c shows that center time is least prone to spatial fluctuations.
- Theoretical predictions regarding the influence of frequency and bandwidth are not only valid for reverberation times, but also for other room acoustical quantities (i.e., C_{80}, D_{50}, t_c and G).

12.2 Outlook

In Chapter 4 (with reference to Appendix A), the uncertainty of room acoustical impulse response measurements was discussed. As a result, the sorted list of influences contributing to the combined uncertainty (Table 4.1) indicates how significant each individual influence is to the combined measurement uncertainty. These findings offer the potential to optimize room acoustical measurements. Either requirements on the most significant influences can be tightened to effectively reduce the combined uncertainty, or the demands on the least significant influences can be relaxed without deteriorating the overall result.

This argument also holds on an absolute scale as the uncertainty of impulse response measurements was used in Chapter 9.3.1 to determine the measurement uncertainty of room acoustical quantities. It was found that all quantities can be calculated very accurately compared to the uncertainty due to spatial fluctuations in Chapter 10. It makes little sense to impose excessive requirements on the measurement hardware when its influence is only noticeable in the fifth decimal place of the measured reverberation time. Future investigations could study the validity of ad hoc measurements to determine room acoustical quantities.

In Chapter 10, the uncertainty of room acoustical quantities was presented as a function of the measurement position's uncertainty. In reference to theoretic predictions, the influence of the filter's center frequency and bandwidth on the fluctuations was discussed. In addition, it was pointed out that there must be

other factors contributing to the spatial fluctuations. Future investigations could therefore target the analysis of variance (ANOVA) and investigate the relevance of the contributing factors. As a result, it may be possible to identify and understand the contributions that cannot be presently identified.

For the ANOVA, large data samples are necessary to ensure the possible range of acoustic environments is sufficiently covered. In order to reduce the reliance on measurements, it makes sense to investigate whether spatial fluctuations can be investigated using simulation tools. In this regard it is particularly important to study whether geometrical methods can correctly predict fluctuations when their rationale does not consider modal effects. First steps were already made by Witew, Dietrich, et al. (2013).

The measurement function established in Chapter 7.2 is suitable to discuss other questions of practical relevance. The question regularly arises of what resolution the sound field in auditoria must be surveyed at in order to capture the global trend across the room. This is synonymous with the question of which size an area a single measurement carries meaning for. The knowledge of how the sound field changes over the distance to a reference position is available through the measurement function. Depending on the shape of the discussed area, a distance distribution to the reference position can be established. Just like in Chapter 9, the measurement function can be sampled accordingly using a Monte Carlo method.

Based on the results of de Vries et al. (2001), the validity question regarding room acoustical measurements has already been raised. On the grounds of the results presented here, it is now evident how accurately measurement positions have to be defined to collect valid results. Depending on the room acoustical quantity and the properties of the filter, it is clear that the measurement positions usually have to be documented rather precisely. Ultimately, this conclusion is motivated by reference to perceptual thresholds. However, since JNDs depend on the test paradigm prevalent in the respective study, it seems reasonable to investigate these dependencies in future studies. This could provide a better understanding of how perceptible fluctuations of the sound field in auditoria actually are. Furthermore, little is known about the frequency dependence of perceptual thresholds.

In the present study, a clear focus was placed on standardized room acoustical quantities, even though this focus is not mandatory because of the collected measurement data. It would therefore be conceivable to reanalyze the data in a future study and investigate the influence of spatial fluctuations on individual time intervals of RIRs. This would permit a more detailed investigation of how the early reflections contribute to spatial fluctuations, and would set the foundation for a general discussion of other possible room acoustical quantities.

13

Acknowledgements

The findings of this investigation also due to support that cannot be listed adequately in the references. The author is deeply indebted to all contributors for their versatile and valuable help.

Special thanks go to **Michael Vorländer** for supervising this work by giving helpful advice, creating a friendly and constructive working environment at the *Institute of Technical Acoustics* and granting exceptional liberties and freedom to follow individual interests and strategies in pursuing scientific research. The versatility of the acoustical topics studied at the Institute is a valuable resource providing a research environment that makes it easy to look at acoustic research from different angles.

I would like to thank **Ferdinanda Ponci** for accepting the position of second reviewer and for taking the time to evaluate the reasoning of this thesis.

The author's appreciation also extends to his many colleagues. The author considers it a privilege to work with so many bright minds, and admires their willingness to engage in detailed discussions or simply help when needed. The long discussions and the helpful advice of the Institute's retired academic senior councilor **Gottfried Behler** are particularly appreciated. Special thanks go to the dear colleagues I shared the office with, for showing the amazing ITA-spirit and not shying away from long discussions about anything, namely **Tobias Lenz**, **Matthias Lievens**, **Markus Müller-Trapet**, **Xun Wang**, **Renzo Vitale**, **Rob Opdam**, **Christian Dreier** and **Josep Llorca Bofi**.

As a research assistant, the author had the chance to supervise many students in their bachelors' and masters' theses or during their time at the Institute during research projects. Their work has provided a valuable contribution to running research projects but also allowed learning in many nontechnical fields. In regard to this dissertation, **Jakob Hartl**, **Lennart Reich**, **Henry Hasti**, **David Kliesch** and **Florian Thevissen** are worth mentioning for their collaboration in operating measurements, cross-checking uncertainty analyses and preparing the software infrastructure. The experience and the work in the electrical and mechanical workshops of **Rolf Kaldenbach** and **Uwe Schlömer** (and his team)

are an essence that made it possible to design a measurement apparatus of this size from scratch.

In preparing the manuscript, special thanks go to colleagues and friends for their help in proofreading the text. The willingness of **Henry Hasti**, **Johannes Klein**, **Simon Kersten Christoph Höller**, **Marco Berzborn**, **Christian Dreier**, **Jonas Heck**, **Pascal Dietrich**, **Philipp Schäfer**, **David Kliesch**, **Markus Brinkmann** and **Josep Llorca Bofi** to spend time, engage in the presented line of argument and verbalize their critical and open feedback is a priceless support that has massively increased the quality of the presented work.

The measurements in *Eurogress Aachen*, *Aachen Symphony*'s *rehearsal room* and *Historische Stadthalle Wuppertal* were made possible through the kind and selfless support of the halls' technical directors and administration. Measurements in *Concertgebouw Amsterdam* were possible through kind support by *Peutz bv*'s **Margriet Lautenbach** and **Martijn Vercammen**.

Simulations were performed with computing resources granted by *RWTH Aachen University* under project *thes0745*.

Last but definitely not least I am indebted to my family and especially my parents for their support and emphasis on getting the best education possible.

Bibliography

Ahearn, M. J., Schaeffler, M. J., Celmer, R. D., & Vigeant, M. C. (2009). Investigation of the just noticeable difference of the clarity index for music, C_{80}. *J. Acoust. Soc. Am.*, *126*(4), 2288. doi:10.1121/1.3249382

Akama, T., Suzuki, H., & Omoto, A. (2010). Distribution of selected monaural acoustical parameters in concert halls. *Applied Acoustics*, *71*(2), 564–577. doi:10.1016/j.apacoust.2010.01.004

Ballio, F., & Guadagnini, A. (2004). Convergence assessment of numerical Monte Carlo simulations in groundwater hydrology. *Water Resources Research*, *40*(4), 1–5. doi:10.1029/2003WR002876

Barron, M. (1984). Impulse testing techniques for auditoria. *Applied Acoustics*, *17*(3), 165–181. doi:10.1016/0003-682X(84)90035-5

Barron, M. (1988). Subjective study of British symphony concert halls. *Acustica*, *66*(1), 1–14.

Barron, M. (2005). Using the standard on objective measures for concert auditoria, ISO 3382, to give reliable results. *Acoust. Sci. & Tech.*, *26*(2), 162–169. doi:10.1250/ast.26.162

Barron, M. (2009). *Auditorium acoustics and architectural design*. London, UK: Spon Press.

Barron, M., & Marshall, A. H. (1981). Spatial impression due to early lateral reflections in concert halls: The derivation of a physical measure. *J. Sound Vibr.*, *77*(2), 211–232. doi:10.1016/S0022-460X(81)80020-X

Behler, G. K., & Vorländer, M. (2018). An active loudspeaker point source for the measurement of high quality wide band room impulse responses. *Proc. IOA 2018, Hamburg*, *40*(3), 435–446.

Berkson, J. (1950). Are there two regressions? *J. Am. Stat. Ass.*, *45*(250), 164–180. doi:10.1080/01621459.1950.10483349

Berzborn, M., & Vorländer, M. (2019). A high order rigid spherical microphone array design using MEMS microphones. In *Proc. ICA 2019, Aachen* (Vol. 23). doi:10.18154/RWTH-CONV-239728

Bodlund, K. (1977). A normal mode analysis of the sound power injection in reverberation chambers at low frequencies and the effects of some response averaging methods. *J. Sound and Vibration*, *55*(4), 563–590. doi:10.1016/S0022-460X(77)81180-2

Bohn, D. A. (1988). Environmental effects on the speed of sound. *JAES*, *36*(4), 223–231.

Bork, I. (2000). A comparison of room simulation software – The 2nd round robin on room acoustical computer simulation. *Acta Acustica*, *86*(6), 943–956.

Bradley, E. (2017). *Reliability engineering : A life cycle approach*. Boca Raton, FL: CRC Press.

Bradley, J. S. (1994). Comparison of concert hall measurements of spatial impression. *J. Acoust. Soc. Am.*, *96*(6), 3525–3535. doi:10.1121/1.410612

Bradley, J. S. (1996). An international comparison of room acoustic measurement systems. *IRC Internal Report*, *714*(1), 1–130.

Bradley, J. S. (2005). Using ISO 3382 measures, and their extensions, to evaluate acoustical conditions in concert halls. *Acoust. Sci. & Tech.*, *26*(2), 170–178. doi:10.1250/ast.26.170

Bradley, J. S., Gade, A. C., & Siebein, G. W. (1993). Comparisons of auditorium acoustics measurements as a function of location in halls. *J. Acoust. Soc. Am.*, *93*(4), 2265–2266. doi:10.1121/1.406637

Bradley, J. S., & Halliwell, R. E. (1988). Accuracy and reproducibility of auditorium acoustics measures. *Proc. IOA*, *10*, 399–406.

Bradley, J. S., Reich, R., & Norcross, S. G. (1999). A just noticeable difference in C_{50} for speech. *Appl. Acoust.*, *58*, 99–108.

Bradley, J. S., & Soulodre, G. A. (1995a). The influence of late arriving energy on spatial impression. *J. Acoust. Soc. Am.*, *97*(4), 2263–2271. doi:10.1121/1.411951

Bradley, J. S., & Soulodre, G. A. (1995b). Objective measures of listener envelopment. *J. Acoust. Soc. Am.*, *98*(5), 2590–2597. doi:10.1121/1.413225

Bronstein, I. N., Semendyayev, K. A., Musiol, G., & Mühlig, H. (2015). *Handbook of mathematics* (6th ed.). Berlin, Heidelberg: Springer. doi:10.1007/978-3-662-46221-8

Brüel & Kjær. (1996). *Microphone handbook – Vol. 1: Theory – Technical documentation*. Naerum, Denmark: Brüel & Kjaer A/S.

Carroll, R. J., Ruppert, D., Stefanski, L. A., & Crainiceanu, C. M. (2006). *Measurement error in nonlinear models – A modern perspective* (2nd ed.). Boca Raton: Chapman and Hall / CRC Press.

Carter, G. C. (1987). Coherence and time delay estimation. *Proc. IEEE*, *75*(2), 236–255. doi:10.1109/PROC.1987.13723

Cat. No. 002280. (2005). *Data sheet KE 4-211-2 microphone capsule.* Wedemark, Germany: Sennheiser electronic GmbH.

Cook, R. K., Waterhouse, R. V., Berendt, R. D., Edelman, S., & Thompson Jr., M. C. (1955). Measurement of correlation coefficients in reverberant sound fields. *J. Acoust. Soc. Am.*, *27*(6), 1072–1077. doi:10.1121/1.1908122

Cox, T. J., Davies, W. J., & Lam, Y. W. (1993). The sensitivity of listeners to early sound field changes in auditoria. *Acustica*, *79*(1), 27–41.

Davy, J. L. (1980). The variance of impulse decays. *Acustica*, *44*(1), 51–56.

Davy, J. L. (1981). The relative variance of the transmission function of a reverberation room. *J. Sound Vibration*, *77*(4), 455–479. doi:10.1016/S0022-460X(81)80044-2

Davy, J. L., Dunn, I. P., & Dubout, P. (1979). The variance of decay rates in reverberation rooms. *Acustica*, *43*(1), 12–25.

de Vries, D., Hulsebos, E. M., & Baan, J. (2001). Spatial fluctuations in measures for spaciousness. *J. Acoust. Soc. Am.*, *110*(2), 947–954.

Dietrich, P. (2013). *Uncertainties in acoustical transfer functions* (PhD thesis). RWTH Aachen University, Aachen, Germany.

DIN SPEC 45660-1. (2014). *Guide for handling uncertainty in acoustics and vibration – Part 1: Uncertainty of acoustical quantities.* Berlin: Deutsches Institut für Normung e.V., Beuth Verlag.

Donaldson, J. R., & Schnabel, R. B. (1987). Computational experience with confidence regions and confidence intervals for nonlinear least squares. *Technometrics*, *29*(1), 67–82.

Eichstädt, S. (2012). *Analysis of dynamic measurements* (PhD thesis). Technische Universität Berlin, Berlin, Germany.

Eichstädt, S. (2015). Parameter identification and measurement uncertainty for dynamic measurement systems. *PTB-Mitteilungen*, *125*(2), 18–23.

Eichstädt, S., Link, A., Harris, P., & Elster, C. (2012). Efficient implementation of a Monte Carlo method for uncertainty evaluation in dynamic measurements. *Metrologia*, *49*(3), 401–410. doi:10.1088/0026-1394/49/3/401

Elster, C., Klauenberg, K., Walzel, M., Wübbeler, G., Harris, P., Cox, M., ... Pendrill, L. (2015). A guide to Bayesian inference for regression problems. *Deliverable of EMRP project NEW04 (Novel mathematical and statistical approaches to uncertainty evaluation)*, 1–69. doi:10.13140/RG.2.2.34414.25922

Evans, J. D. (1996). *Straightforward statistics for the behavioral sciences.* Pacific Grove, Ca., USA: Brooks/Cole Publishing Company.

Farina, A. (2007). Advancements in impulse response measurements by sine sweeps. In *Proc. AES convention* (Vol. 122).

Gade, A. C. (1982). *Subjective room acoustic experiments with musicians* (PhD thesis). Technical University of Denmark, DTU, Copenhagen, Denmark.

Gade, A. C. (2007). Chapter 9 – Acoustics in Halls for Speech and Music. In T. D. Rossing (Ed.), *Handbook of Acoustics* (pp. 301–350). New York, NY: Springer.

Gade, A. C., & Rindel, J. H. (1985). Die Abstandsabhängigkeit vom Schallpegel in Konzertsälen [The distance dependence of the sound level in concert halls]. In *Proc. DAGA 1985, Bad Honnef* (Vol. 11, pp. 435–438).

Genz, A. (1992). Numerical computation of multivariate normal probabilities. *J. Comp. Graph. Stat.*, *1*(2), 141–149. doi:10.1080/10618600.1992.10477010

Genz, A., & Kass, R. E. (1997). Subregion-adaptive integration of functions having a dominant peak. *J. Comp. Graph. Stat.*, *6*(1), 92–111. doi:10.1080/10618600.1997.10474729

Goertz, A. (2008). Chapter 8 – Elektroakustik II: Lautsprecher [Electroacoustics II: Loudspeakers]. In S. Weinzierl (Ed.), *Handbuch der Audiotechnik* (pp. 421–490). Berlin: Springer.

Grabe, M. (2010). *Generalized Gaussian error calculus* (1st ed.). Berlin, Heidelberg: Springer. doi:10.1007/978-3-642-03305-6

Griliches, Z., & Ringstad, V. (1970). Error-in-the-variables bias in nonlinear contexts. *Econometrica*, *38*(2), 368–370. doi:10.2307/1913020

Guski, M. (2015). *Influences of external error sources on measurements of room acoustic parameters* (PhD thesis). RWTH Aachen University, Aachen, Germany.

Guski, M., & Vorländer, M. (2014). Uncertainty of room acoustic parameters caused by air movement and temperature changes. In *Proc. DAGA 2014, Oldenburg* (Vol. 40, pp. 439–440).

Guski, M., & Vorländer, M. (2015). Impulsive noise detection in sweep measurements. *Acta Acustica u/w Acustica*, *101*(4), 723–730. doi:10.3813/AAA.918868

Hanes, P. (2001). *Comparison of measurement uncertainty budgets for calibration of sound calibrators: Euromet project 576 – NPL report CMAM 73.* Teddington, Middlesex: National Physical Laboratory,UK.

Harrell, F. E., & Davis, C. E. (1982). A new distribution-free quantile estimator. *Biometrika*, *69*(3), 635–640. doi:10.1093/biomet/69.3.635

Havelock, D., Kuwano, S., & Vorländer, M. (2008). *Handbook of signal processing in acoustics* (1st ed.). New York: Springer. doi:10.1007/978-0-387-30441-0

Hidaka, T., Beranek, L. L., & Okano, T. (1995). Interaural cross-correlation, lateral fraction, and low- and high-frequency sound levels as measures of acoustical quality in concert halls. *J. Acoust. Soc. Am.*, *98*(2), 988–1007. doi:10.1121/1.414451

Höhne, R., & Schroth, G. (1995). Zur Wahrnehmbarkeit von Deutlichkeits- und Durchsichtigkeitsunterschieden in Zuhörersälen [On the perceptibility of differences in clarity and transparency in auditoria]. *Acustica*, *81*(4), 309–319.

Huang, Y., Benesty, J., & Elko, G. W. (2000). Passive acoustic source localization for video camera steering. *Proc. IEEE Int. Conf. on Acoustics, Speech, and Signal Processing (Cat. No.00CH37100)*, *2*, II909-II912. doi:10.1109/ICASSP.2000.859108

IEC 60268-4. (2017). *Sound system equipment – Part 4: Microphones.* Geneva, Switzerland: International Electrotechnical Commission.

IEC 61260. (1995). *Electroacoustics – Octave-band and fractional-octave-band filters.* Geneva, Switzerland: International Electrotechnical Commission.

IEC 61260-1. (2014). *Electroacoustics – Octave-band and fractional-octave-band filters – Part 1: Specifications.* Geneva, Switzerland: International Electrotechnical Commission.

IEC 61672-1. (2013). *Electroacoustics – Sound level meters – Part 1: Specifications.* Geneva, Switzerland: International Electrotechnical Commission.

Ishikawa, K. (1996). *Guide to quality control* (13th ed.). Tokyo: Asian Productivity Organization.

ISO 140. (all parts). *Acoustics – Measurement of sound insulation in buildings and of building elements.* Geneva, Switzerland: International Organization for Standardization.

ISO 17497-1. (2004). *Acoustics – Sound-scattering properties of surfaces – Part 1: Measurement of the random-incidence scattering coefficient in a reverberation room.* Geneva, Switzerland: International Organization for Standardization.

ISO 18233. (2006). *Acoustics – Application of new measurement methods in building and room acoustics.* Geneva, Switzerland: International Organization for Standardization.

ISO 3382. (1975). *Acoustics – Measurement of reverberation time in auditoria.* Geneva, Switzerland: International Organization for Standardization.

ISO 3382. (1997). *Acoustics – Measurement of the reverberation time of rooms with reference to other acoustical parameters.* Geneva, Switzerland: International Organization for Standardization.

ISO 3382-1. (2009). *Acoustics – Measurement of room acoustic parameters – Part 1: Performance spaces.* Geneva, Switzerland: International Organization for Standardization.

ISO 354. (2003). *Acoustics – Measurement of sound absorption in a reverberation room.* Geneva, Switzerland: International Organization for Standardization.

ISO 3741. (2011). *Acoustics – Determination of sound power levels and sound energy levels of noise sources using sound pressure – Precision methods for reverberation test rooms.* Geneva, Switzerland: International Organization for Standardization.

ISO 3745. (2017). *Acoustics – Determination of sound power levels and sound energy levels of noise sources using sound pressure – Precision methods for anechoic rooms and hemi-anechoic rooms.* Geneva, Switzerland: International Organization for Standardization.

ISO 9613-1. (1993). *Acoustics – Attenuation of sound during propagation outdoors – Part 1: Calculation of the absorption of sound by the atmosphere.* Geneva, Switzerland: International Organization for Standardization.

ISO Guide 98-3. (2008). *Uncertainty of measurement – Part 3: Guide to the expression of uncertainty in measurement (GUM:1995)* (Vol. 98) (No. 3). Geneva, Switzerland: International Organization for Standardization.

ITU-R BS.468-4. (1986). *Measurement of audio frequency noise voltage level in sound broadcasting.* Geneva, Switzerland: ITU International Telecommunication Union.

Jankovic, M., Ciric, D. G., & Pantic, A. (2016). Automated estimation of the truncation of room impulse response by applying a nonlinear decay model. *J. Acoust. Soc. Am.*, *139*(3), 1047–1057. doi:10.1121/1.4941657

JCGM 101. (2008). *Evaluation of measurement data – Supplement 1 to the "Guide to the expression of uncertainty in measurement" – Propagation of distributions using a Monte Carlo method* (Vol. 101). Sèvres, France: Joint Committee for Guides in Metrology (JCGM).

JCGM 104. (2008). *Evaluation of measurement data – An introduction to the "Guide to the expression of uncertainty in measurement" and related documents* (Vol. 104). Sèvres, France: Joint Committee for Guides in Metrology (JCGM).

JCGM 200. (2012). *International vocabulary of metrology – Basic and general concepts and associated terms (VIM)* (Vol. 200). Sèvres, France: Joint Committee for Guides in Metrology (JCGM).

Johnson, N. L., Kotz, S., & Balakrishnan, N. (1994). *Continuous univariate distributions* (2nd ed., Vol. 1). New York [i.a.]: John Wiley and Sons, Inc.

Jordan, V. L. (1970). Acoustical criteria for auditoriums and their relation to model techniques. *J. Acoust. Soc. Am.*, *47*(2A), 408–412. doi:10.1121/1.1911535

Kacker, R., Sommer, K.-D., & Kessel, R. (2007). Evolution of modern approaches to express uncertainty in measurement. *Metrologia*, *44*(6), 9513–529. doi:10.1088/0026-1394/44/6/011

Katz, B. F. G. (2004). International round robin on room acoustical impulse response analysis software 2004. *Acoustics Research Letters Online*, *5*(4), 158–164. doi:10.1121/1.1758239

Kaune, R. (2012). Accuracy studies for TDOA and TOA localization. In *Proc. Int. Conf. on Information Fusion* (Vol. 15, pp. 408–415).

Klein, J. C. (2020). *Directional room impulse response measurement* (PhD thesis). RWTH Aachen University, Aachen, Germany.

Knüttel, T., Witew, I. B., & Vorländer, M. (2013). Influence of "omnidirectional" loudspeaker directivity on measured room impulse responses. *J. Acoust. Soc. Am.*, *134*(5), 3654–3662.

Kürer, R. (1969). Zur Gewinnung von Einzahlkriterien bei Impulsmessungen in der Raumakustik [On obtaining single-number criteria in impulse measurements in room acoustics]. *Acustica*, *21*, 370–372.

Kuttruff, H. (1954). *Unnamed diploma thesis* (Unpublished master's thesis). 3. Physikalisches Institut, Göttingen University.

Kuttruff, H. (2000). *Room acoustics* (4th ed.). London, New York: Taylor & Francis.

Kuttruff, H., & Thiele, R. (1954). Über die Frequenzabhängigkeit des Schalldrucks in Räumen [About the frequency dependence of the sound pressure in rooms]. *Acustica*, *4*(5), 614–617.

Lehmann, P. (1976). *Über die Ermittlung raumakustischer Kriterien und deren Zusammenhang mit subjektiven Beurteilungen der Hörsamkeit [On the determination of room acoustic quantities and their relation to subjective ratings of listening quality]* (PhD thesis). Technische Universität Berlin, Berlin, Germany.

Leishman, T. W., Rollins, S., & Smith, H. M. (2006). Uncertainties in measurement of spatial parameters in room acoustics. *J. Acoust. Soc. Am.*, *120*(3), 1411–1422. doi:10.1121/1.2221552

Lokki, T. (2013). Throw away that standard and listen: Your two ears work better. *Building Acoustics*, *20*(4), 283–293. doi:10.1260/1351-010X.20.4.283

Lundeby, A., Vigran, T. E., Bietz, H., & Vorländer, M. (1995). Uncertainties of measurements in room acoustics. *Acta Acustica*, *81*(4), 344–355.

Maritz, J. S., & Jarrett, R. G. (1978). A note on estimating the variance of the sample mean. *J. Am. Stat. Ass.*, *73*(361), 194–196. doi:10.2307/2286545

Marquardt, D. W. (1963). An algorithm for least-squares estimation of nonlinear parameters. *J. Soc. Ind. Appl. Math.*, *11*(2), 431–441. doi:10.1137/0111030

Massey, F. J. (1951). The Kolmogorov-Smirnov test for goodness of fit. *J. Am. Stat. Ass.*, *46*(253), 68–78.

Mechel, F. P. (2008). *Formulas of acoustics*. New York, NY: Springer.

Meyer, E., & Thiele, R. (1956). Räumliche Untersuchungen in zahlreichen Konzertsälen und Rundfunkstudios unter Anwendung neuerer Messverfahren [Spatial investigations in numerous concert halls and broadcasting studios using newer measurement methods]. *Acustica*, *6*, 425–444.

Mieke, S. (2014). Berechnung der Messunsicherheit nach GUM – Kurzfassung in 20 min [Calculation of measurement uncertainty according to the GUM – short version for 20 minutes]. In *PTB seminar "Berechnung der Messunsicherheit – Empfehlungen für die Praxis", Berlin* (Vol. 277, pp. 1–23).

Militello, C., & Buenafuente, S. R. (2007). An exact noniterative linear method for locating sources based on measuring receiver arrival times. *J. Acoust. Soc. Am.*, *121*(6), 3595–3601. doi:10.1121/1.2724241

Miyara, F. (2017). *Software-based acoustical measurements* (1st ed.). New York: Springer. doi:10.1007/978-3-319-55871-4

Mood, A. M., Graybill, F. A., & Boes, D. C. (1974). *Introduction to the theory of statistics* (3rd ed.). New York: McGraw-Hill.

Morse, P. M., & Ingard, M. U. (1968). *Theoretical acoustics* (1st ed.). New York [i.a.]: McGraw-Hill.

Müller, S., & Massarani, P. (2001). Transfer-function measurement with sweeps. *J. Audio Eng. Soc.*, *49*(1), 443–471.

Müller-Gronbach, T., Ritter, K., & E., N. (2012). *Monte Carlo-Algorithmen [Monte Carlo algorithms]* (1st ed.). Berlin, Heidelberg: Springer. doi:10.1007/978-3-540-89141-3

Müller-Trapet, M., & Höller, C. (2018). Measuring with noise? We can do better! *J. Acoust. Soc. Am.*, *144*(3), 1813–1813. doi:10.1121/1.5067999

Neal, M. T., & Vigeant, M. C. (2017). A concert hall database of US and European halls: Preliminary measurements and results. *J. Acoust. Soc. Am.*, *142*(4), 2717. doi:10.1121/1.5014911

Neu, T. (2010). Clock jitter analyzed in the time domain, Part 1. *TI-Analog Appl. J.*, *2010*(Q3), 5–9.

Nielsen, J. L., Halstead, M. M., & Marshall, A. H. (1998). On spatial validity of room acoustics measures. In *Proc. ICA 1998, Seattle* (Vol. 15, pp. 2121–2122).

Novak, A. (2009). *Identification of nonlinear systems in acoustics* (PhD thesis). Université du Maine, Le Mans, France and Czech Technical University, Prague, Czech Republic.

Okano, T., Beranek, L. L., & Hidaka, T. (1998). Relations among interaural cross-correlation coefficient ($IACC_E$), lateral fraction (LF_E), and apparent source width (ASW) in concert halls. *J. Acoust. Soc. Am.*, *104*(1), 255–265. doi:10.1121/1.423955

Payne, R. (2004). *Uncetainties associated with the use of sound level meters – NPL report DQL-AC 002*. Teddington, Middlesex: National Physical Laboratory,UK.

Pazen, D., Witew, I. B., & Vorländer, M. (2011). Unsicherheiten bei Richtcharakteristikmessungen [Uncertainties in directivity measurements]. In *Proc. DAGA 2011, Düsseldorf* (Vol. 37, pp. 721–722).

Pelorson, X., Vian, J.-P., & Polack, J.-D. (1992). On the variability of room acoustical parameters: Reproducibility and statistical validity. *Applied Acoustics*, *37*(3), 175–198. doi:10.1016/0003-682X(92)90002-A

Polack, J.-D. (1992). Modifying chambers to play billiards the foundations of reverberation theory. *Acustica*, *76*(6), 257–272.

Pollow, M., Dietrich, P., Krechel, B., & Vorländer, M. (2011). Unidirektionale mehrkanalige Audioübertragung über Ethernet [Unidirectional multi-channel audio transmission via ethernet]. In *Proc. DAGA 2011, Düsseldorf* (Vol. 37). doi:10.1121/1.4800303

Rasmussen, K. (1999). The static pressure and temperature coefficients of laboratory standard microphones. *Metrologia*, *36*(4), 265–273. doi:10.1088/0026-1394/36/4/4

Rayleigh, J. W. S. (1880). On the resultant of a large number of vibrations of the same pitch and of arbitrary phase. *Philosophical Magazine*, *5*(10), 73–78.

Reich, L. (2018). *Spatial variation of the acoustic field in auditoria* (Unpublished bachelor's thesis). Institute of Technical Acoustics, RWTH Aachen University, Aachen, Germany.

Reichardt, W., Abdel Alim, O., & Schmidt, W. (1974). Abhängigkeit der Grenzen zwischen brauchbarer und unbrauchbarer Durchsichtigkeit von der Art des Musikmotives, der Nachhallzeit und der Nachhalleinsatzzeit [Dependence of the transition between usable and unusable transparency on the type of musical motif, the reverberation time and the onset of reverberation]. *Appl. Acoust.*, *46*(4), 243–164. doi:10.1016/0003-682X(74)90033-4

Reichardt, W., & Schmidt, W. (1967). The detectability of changes in sound field parameters for music. *Acustica*, *18*(5), 274–282.

Rossing, T. D. (2007). Chapter 2 – A Brief History of Acoustics. In T. D. Rossing (Ed.), *Handbook of Acoustics* (pp. 9–24). New York, NY: Springer.

Sabine, W. C. (1922). *Collected papers on acoustics*. London, Humphrey, Milford: Harvard University Press.

Sackett, D. L. (1979). Bias in analytic research. *J. Chron. Dis.*, *32*(1), 51–63. doi:10.1016/0021-9681(79)90012-2

San Martin, R., Witew, I. B., Arana, M., & Vorländer, M. (2007). Influence of the source orientation on the measurement of acoustic parameters. *Acta Acustica*, *93*(3), 387–397.

Schau, H., & Robinson, A. (1987). Passive source localization employing intersecting spherical surfaces from time-of-arrival differences. *IEEE Transactions on Acoustics, Speech, and Signal Processing*, *35*(8), 1223–1225. doi:10.1109/TASSP.1987.1165266

Schmidt, H. (2003). Warum GUM? [Why GUM?]. *zfv – Zeitschrift für Geodäsie*, *128*(5), 303–312. doi:10.1088/1742-6596/13/1/052

Schneider, M. (2008). Chapter 8 – Elektroakustik I: Mikrophone [Electroacoustics I: Microphones]. In S. Weinzierl (Ed.), *Handbuch der Audiotechnik* (pp. 313–419). Berlin: Springer.

Schröder, M. R. (1954). Die statistischen Parameter der Frequenzkurven in grossen Räumen [The statistical parameters of frequency curves in large rooms]. *Acustica*, *4*(5), 594–600.

Schroeder, M. R. (1962). Frequency-correlation functions of frequency responses in rooms. *J. Acoust. Soc. Am.*, *34*(12), 1819–1823. doi:10.1121/1.1909136

Schroeder, M. R. (1965). New method of measuring reverberation time. *J. Acoust. Soc. Am.*, *37*(3), 409–412. doi:10.1121/1.1909343

Sekiguchi, K., & Hanyu, T. (1998). Study on acoustic index variations due to small changes in the observation point. In *Proc. ICA 1998, Seattle* (Vol. 15, pp. 947–954).

Seraphim, H.-P. (1958). Untersuchungen über die Unterschiedsschwelle exponentiellen Abklingens von Rauschimpulsen [Investigations on the difference limen of exponential decay of noise pulses]. *Acustica*, *8*(4), 280–108.

Smith, J., & Abel, J. (1987). Closed-form least-squares source location estimation from range-difference measurements. *IEEE Transactions on Acoustics, Speech, and Signal Processing*, *35*(12), 1661–1669. doi:10.1109/TASSP.1987.1165089

Sommer, K.-D., & Siebert, B. R. L. (2004). Praxisgerechtes Bestimmen der Messunsicherheit nach GUM [Practical evaluation of the measurement uncertainty according to the GUM]. *Technisches Messen*, *71*(2), 52–66.

Sommer, K.-D., Weckenmann, A., & Siebert, B. R. L. (2005). A systematic approach to the modelling of measurements for uncertainty evaluation. *Journal of Physics: Conference Series*, *13*, 224–227. doi:10.1088/1742-6596/13/1/052

Squires, G. L. (2001). *Practical Physics*. Cambridge, UK: Cambridge University Press.

Thevissen, F. (2015). *Eine Messeinrichtung zur Abtastung von Schallfeldern in Räumen [A measurement apparatus to sample the sound field in rooms]* (Unpublished master's thesis). Institute of Technical Acoustics, RWTH Aachen University, Aachen, Germany.

Torrieri, D. J. (1984). Statistical theory of passive location systems. *IEEE Transactions on Aerospace and Electronic Systems*, *AES-20*(2), 183–198. doi:10.1109/TAES.1984.310439

Vigeant, M. C., Celmer, R. D., Jasinski, C. M., Ahearn, M. J., Schaeffler, M. J., Giacomoni, C. B., ... Ormsbee, C. I. (2015). The effects of different test methods on the just noticeable difference of clarity index for music. *J. Acoust. Soc. Am.*, *138*(1), 476–491. doi:10.1121/1.4922955

Vorländer, M. (1995). International round robin on room acoustical computer simulations. In *Proc. ICA 1995, Trondheim* (Vol. 15, pp. 689–692).

Vorländer, M. (2013). Computer simulations in room acoustics: Concepts and uncertainties. *J. Acoust. Soc. Am.*, *133*(3), 1203–1213.doi:10.1121/1.4788978

Vorländer, M., & Kuttruff, H. (1985). Die Abhängigkeit des Seitenschallgrades von der Form und der Flächengestaltung eines Raumes [The dependence of the lateral fraction on the shape and surface design of a room]. *Acustica*, *58*(3), 118–129.

Vorländer, M., & Witew, I. (2004). Uncertainties in measurement of spatial parameters in room acoustics. *J. Acoust. Soc. Am.*, *116*(4), 2483. doi:10.1121/1.4784918

Vorländer, M., & Witew, I. (2020). Chapter B7 – Raumakustik und Beschallungstechnik [Room acoustics and public address systems]. In N. A. Fouad (Ed.), *Bauphysik-Kalender 2020* (pp. 499–538). Berlin: Wilhelm Ernst & Sohn.

Weinzierl, S. (2017). The perceptual evaluation of acoustical environments I: Simulated environments. *J. Acoust. Soc. Am.*, *141*(5), 3932. doi:10.1121/1.4988894

Weinzierl, S., & Vorländer, M. (2015). Room acoustical parameters as predictors of room acoustical impression: What do we know and what would we like to know? *Acoustics Australia*, *43*(1), 41–48. doi:10.1007/s40857-015-0007-6

Wenmaekers, R. H. C., & Hak, C. C. J. M. (2015). The sound power as a reference for sound strength (G), speech level (L) and support (ST): Uncertainty of laboratory and in situ calibration. *Acta Acustica*, *101*(5), 892–907. doi:10.3813/AAA.918884

Wiese, K., & Wöger, K. (1999). *Messunsicherheit und Messdatenauswertung [Measurement uncertainty and data analysis]*. Weinheim, Germany: Wiley-VCH.

Wilcox, R. R. (2005). *Introduction to robust estimation and hypothesis testing* (2nd ed.). Amsterdam: Elsevier/Academic Press.

Wilkens, H. (1977). Mehrdimensionale Beschreibung subjektiver Beurteilungen der Akustik von Konzertsälen [Multidimensional description of subjective evaluations of the acoustics of concert halls]. *Acustica*, *38*(1), 10–23.

Witew, I. B. (2006). Is the perception of listener envelopment in concert halls affected by clarity? In *Proc. DAGA 2006, Braunschweig* (Vol. 32, pp. 699–700).

Witew, I. B., & Behler, G. K. (2003). Der Einfluß der Mikrophonrichtcharakteristik auf den Lateral Fraction-Parameter [The influence of the microphone's directivity on the lateral fraction quantity]. In *Proc. DAGA 2003, Aachen* (Vol. 29, pp. 664–665).

Witew, I. B., & Behler, G. K. (2005). Uncertainties in measurement of single number parameters in room acoustics. In *Proc. FA 2005, Budapest* (Vol. 4, pp. 2291–2295).

Witew, I. B., Behler, G. K., & Vorländer, M. (2004). Spatial variation of lateral measures in different concert halls. In *Proc. ICA 2004, Kyoto* (Vol. 18, pp. 2949–2952).

Witew, I. B., & Dietrich, P. (2007). Assessment of the uncertainty in room acoustical measurements. In *Proc. ICA 2007, Madrid* (Vol. 19).

Witew, I. B., Dietrich, P., de Vries, D., & Vorländer, M. (2010). Uncertainty of room acoustic measurements – How many measurement positions are necessary to describe the conditions in auditoria? In *Proc. ISRA 2010, Melbourne.*

Witew, I. B., Dietrich, P., Pelzer, S., & Vorländer, M. (2013). Comparison of strategies to model spatial fluctuations of room acoustic single number quantities. In *Proc. ISRA 2013, Toronto.*

Witew, I. B., Dietrich, P., & Vorländer, M. (2010). Error and uncertainty of IACC measurements introduced by dummy head orientation using Monte Carlo simulations. In *Proc. ICA 2010, Sydney* (Vol. 20).

Witew, I. B., Knuettel, T., & Vorländer, M. (2012). A model to predict measurement uncertainties due to loudspeaker directivity and its validation. *J. Acoust. Soc. Am.*, *131*(4), 3244. doi:10.1121/1.4708108

Witew, I. B., Lindau, A., van Dorp Schuitman, J., Vorländer, M., Weinzierl, S., & de Vries, D. (2010). Uncertainties of IACC related to dummy head orientation. In *Proc. DAGA 2010, Berlin* (Vol. 36).

Witew, I. B., Lindau, A., van Dorp Schuitman, J., Vorländer, M., Weinzierl, S., & de Vries, D. (2013). Uncertainties of IACC related to dummy head orientation. In *Proc. DAGA 2013, Rotterdam* (Vol. 35, pp. 664–665).

Witew, I. B., Müller-Giebeler, M., & Vorländer, M. (2014). Evaluation and improvement of a model to predict the measurement uncertainty due to the directivity of room acoustical sound sources. *J. Acoust. Soc. Am.*, *135*(4), 2236. doi:10.1121/1.4877313

Witew, I. B., & Vorländer, M. (2011). Uncertainties of room acoustical measurements – Influence of the exact source and receiver position. *Proc. IOA*, *33*(2), 23–26.

Witew, I. B., & Vorländer, M. (2018). Wave field analysis in concert halls using large scale arrays. In *Proc. IOA* (Vol. 40, pp. 319–326).doi:10.18154/RWTH-2018-228715

Witew, I. B., Vorländer, M., & Xiang, N. (2017). Sampling the sound field in auditoria using large natural-scale array measurements. *J. Acoust. Soc. Am.*, *141*(3), EL300–EL306.

Wittstock, V. (2007). On the uncertainty of single-number quantities for rating airborne sound insulation. *Acta Acustica*, *93*(3), 375–386.

Wittstock, V. (2015). Determination of measurement uncertainties in building acoustics by interlaboratory tests. Part 1: Airborne sound insulation. *Acta Acustica*, *101*(1), 88–98. doi:10.3813/AAA.918807

Wittstock, V. (2018). Personal communication.

Wittstock, V., & Bethke, C. (2005). On the uncertainty of sound pressure levels determined by third-octave band analysers in a hemianechoic room. In *Proc. FA 2005, Budapest* (Vol. 4, pp. 1301–1306).

Xiang, N., Alamuru, A., Witew, I. B., & Vorländer, M. (2018). Experimental investigations on sound energy propagation in acoustically coupled volumes using a high-spatial resolution scanning system. *J. Acoust. Soc. Am.*, *143*(6), EL437–EL442. doi:10.1121/1.5040886

Xiang, N., Escolano, J., Navarro, J. M., & Jing, Y. (2013). Investigation on the effect of aperture sizes and receiver positions in coupled rooms. *J. Acoust. Soc. Am.*, *133*(6), 3975–3985.

Zwillinger, D. (2003). *CRC standard mathematical tables* (28th ed.). Boca Raton: Chapman & Hall / CRC Press.

A

Detailed discussion of uncertainties in room impulse response measurements

A.1 Introduction

This entire study relies on auditorium impulse response measurements that are analyzed to investigate spatial fluctuations of the sound field. This leads directly to the question of uncertainty in these measurements due to the acoustical measurement chain used and due to other influences on the acoustic conditions that haven an effect on the uncertainty. This appendix closely follows the stages of uncertainty evaluation outlined in the "Guide to the expression of uncertainty in measurement" (GUM) ISO Guide 98-3 (2008) and its introductory document JCGM 104 (2008) to address this question. Essentially, this argument divides the uncertainty evaluation into the *formulation stage* of the measurement scenario and actually *calculating the uncertainty*. Even though a clear focus is placed on the equipment used in this study, the presented method may serve as a blueprint for other studies to evaluate the capabilities of their own measurement chains.

A.2 Formulation stage

A.2.1 The output quantity

The *measurement problem* is identified as determining the acoustic transmission channel of a given source-receiver combination in a room, i.e., the room impulse response (RIR), $h(t)$. This makes the RIR the primary output measurand. Room acoustical parameters such as the reverberation time T, the clarity index C_{80} or difinition D_{50}, etc., are derived output measurands that will be subject to an independent discussion in Section 6.2.

In light of the fundamental discussion about the measurement principle of two channel FFT methods in Section 2.2.1, it becomes clear that the primary output quantity is derived from secondary quantities, i.e., the systems' respective input

and output sound pressure signals $s(t)$ and $g(t)$ that are divided in frequency domain to yield the transfer function $H(\omega)$. According to Dietrich (2013), who refers to Havelock et al. (2008); Kuttruff (2000); Miyara (2017), there are some finer details to consider when choosing the locations to pick up these signals from. In practice, however, the inputs and outputs of the software are usually understood as best estimates for $s(t)$ and $g(t)$.

A.2.2 The input quantities

With the measurement problem defined, the various influence factors can now be identified and characterized. JCGM 104 (2008)[6.1] suggests the use of available knowledge to determine influence quantities. In measurement problems, where the output quantity is determined through sophisticated simulations or through highly simplified models, the significance of individual influencing factors cannot be determined precisely. Identifying uncertainty contributions thus becomes a creative process in which potential influence factors are collected through brainstorming sessions, a process that is difficult to control since the participants' contributions cannot be operationalized. To organize the search, the factors contributing to quality management (Ishikawa, 1996) can be used as a starting point. As an extension to Ishikawa's original "5M" approach (see Figure 2.5) from the manufacturing industry, an "8M" model (e.g., E. Bradley (2017),Ch. 5) can be used to structure the search for uncertainty contributions. Not all of the eight manufacturing categories seem to relate to questions of measurement uncertainty; however, the available explanations identify the basic idea behind the grouping and, thus, an adaptation to the concepts in measurement uncertainty is possible. A list of potential uncertainty categories is shown in Table A.1.

Assigning the last category of *calibration* in Table A.1 to the *measurement equipment*-group, an Ishikawa diagram with seven categories as shown in Figure A.1 emerges. The elements of the measurement chain (Figure 2.3) are referenced in the *classical measurement equipment* category. Properties of the propagation medium and acoustic noise sources are summarized in the group dealing with *environmental conditions*. The device under test and its properties as they influence the measurand are discussed as part of the item *auditorium*. The influence factors that can be attributed to the algorithm that calculates the measurand from the collected data are summarized in the *measurement method*. This category includes properties of the 2-Ch-FFT method, but also the calculation of ISO3382 parameters. Influence factors due to the organizational sequence of steps are discussed under the umbrella term *measurement procedure*. Here, aspects such as reproducibility, repeatability, the duration of measurement series or even the choice of measurement locations in the auditorium play a role. The human factor

Table A.1: Root causes of manufacturing reliability according to an Ishikawa (1996)-inspired 8 category model and their interpretation in an (acoustical) measurement uncertainty context.

Tautogram	Clarification	Translation to measurement uncertainty
Man	Human resources	Observer
Machine	Technology	Equipment I (Measurement chain)
Method	Process	Measurement method (logic)
Milieu	Environment	Environmental conditions
Materials	Raw material Consumables Information	Measurement object (Documentation)
Mission	Purpose	Equipment II (Special measurement objective)
Management	Leadership	Measurement procedure (Organization)
Maintenance		Calibration

in measurements is covered in *observer*-related aspects. Influence factors that are characteristic of specialized measurement surveys requiring special infrastructure are discussed as part of another *measurement equipment* category. As far as this specific study is concerned, this category includes the special infrastructure of the large measurement array. Implications regarding measurement uncertainty of large arrays are discussed in the methodology Section 5 and Appendix B.

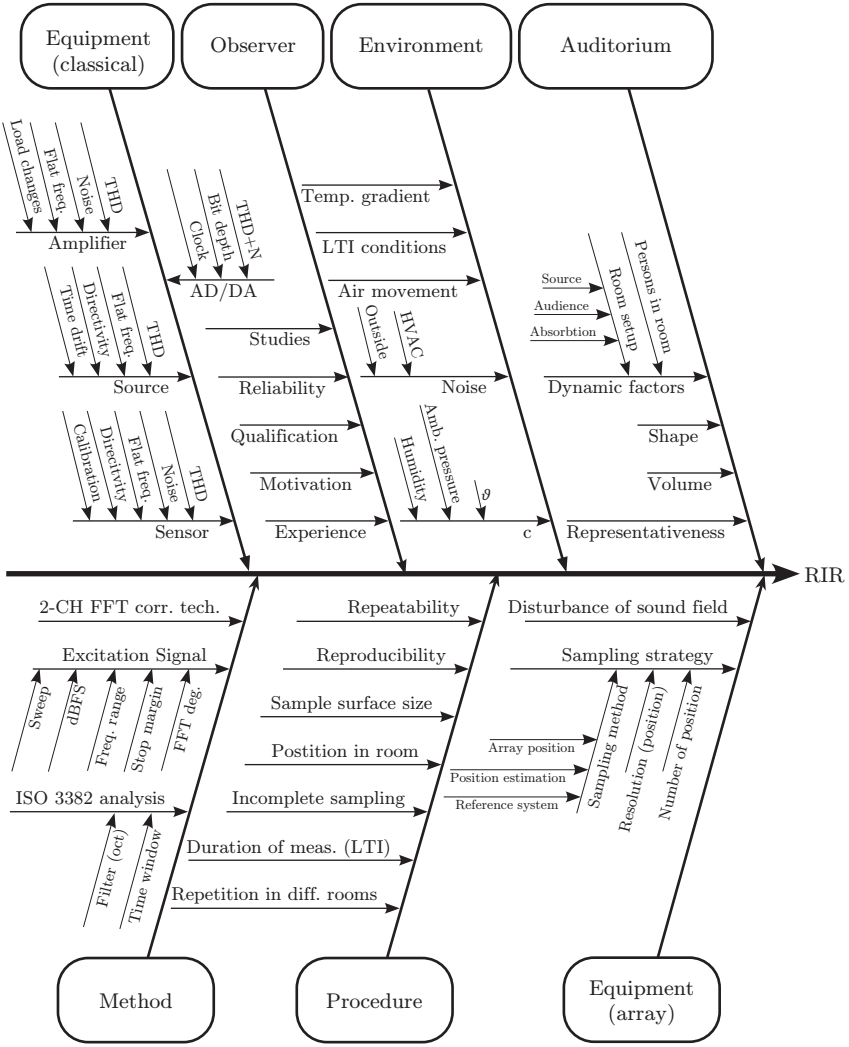

Figure A.1: Ishikawa Diagram of a generic measurement process.

A.2.3 The measurement model

Basic considerations

Dynamic measurements in the presence of noise

Figure A.2: Systematic drawing of the measurement chain. Elements that are shaded are referred to in this paragraph.

Measurements using 2-Ch-FFT correlation techniques are widespread, are a standardized approach (ISO 18233, 2006) and are considered extremely reliable and robust against disturbances (Müller & Massarani, 2001; Müller-Trapet & Höller, 2018). Discussing the associated uncertainty is challenging as the classical GUM method requires establishing an algebraic relation between the system's stationary input and output quantities. 2-Ch-FFT methods, however, are dynamic measurements as the impulse response is calculated from a microphone's time domain signal, whose value at a given time instant depends on the excitation's time domain signal at previous instants in time. The FFT is not an algebraic relation in the GUM sense, and thus does not suit the basic GUM approach (Eichstädt, 2015).

For the individual case of a specific measurement, Eichstädt (2012) developed a mathematical method to establish the uncertainty propagation in a dynamic measurement. Since the input and output quantities are multi-dimensional vectors ($s(t)$ and $g(t)$), determining the uncertainty due to a transient disturbance becomes complex and computationally demanding. Guski (2015) and Farina (2007) discuss how impulsive disturbances affect impulse response measurements in architectural acoustics, providing useful considerations when investigating the uncertainty of already existing measurement results. For large data sets or for general evaluations on generic measurements, however, these methods reach their limits. In situations where sources of uncertainty can be identified as constant or quasi-stationary during the measurement process, existing strategies that align with the classical tools of the ISO Guide 98-3 (2008) can be used.

Wittstock and Bethke (2005) discuss the uncertainty of ISO 3741 (2011)-compliant sound level/power measurements: In the presence of stationary background noise L_{noise} a correction term $\mathrm{b}_{\mathrm{noise}}$ can be applied to the noise-impaired signal L'_{signal} to have an estimate of the intended measurand L_{signal}.

$$\mathrm{b_{noise}} = -10\log_{10}\left(1 - 10^{-\frac{L'_{\mathrm{signal}} - L_{\mathrm{noise}}}{10}}\right) \tag{A.2.1}$$

$$u(\mathrm{b_{noise}}) = \frac{10^{-\frac{L'_{\mathrm{signal}} - L_{\mathrm{noise}}}{10}}}{1 - 10^{-\frac{L'_{\mathrm{signal}} - L_{\mathrm{noise}}}{10}}} \sqrt{u^2(L'_{\mathrm{signal}}) + u^2(L_{\mathrm{noise}})} \tag{A.2.2}$$

Since Equations A.2.1 and A.2.2 do not hold exclusively for averaged sound pressure levels, Wittstock and Bethke's approach can also be used for individual samples of a recorded sound pressure signal such as $g(t)$. Thus, according to Equation A.2.2, determining the uncertainty of the correction term requires knowledge of the prevailing signal-to-noise ratio, the uncertainty of the recorded signal, and the variance of the noise.

Provided that the AWGN[3]-assumption is appropriate for the background noise, and the amplitude spectrum of the excitation signal $s(t)$ is flat, the signal-to-noise ratio depends on how the measurement chain's dynamic range is utilized, and so follows the established experience with 2-Ch-FFT correlation measurements (Dietrich, 2013; Müller & Massarani, 2001)[4]. On these grounds, Equation A.2.2 applies not only to the recorded signal $g(t)$, but also to the calculated impulse response $h(t)$.

Under suitable conditions, the variance of the noise level could be determined empirically from the measured impulse response. If the noise level follows a $10\log_{10}(|\mathcal{N}(\mu = 0, \sigma^2)|)$ distribution, its variance does not depend on σ^2 and is thus $u^2(L_{\mathrm{noise}}) \approx 23.27\,\mathrm{dB}$. When deterministic excitation signals are used, $u(L'_{\mathrm{signal}})$ indicates the standard uncertainty that the elements of the measurement chain introduce. When $u^2(L'_{\mathrm{signal}}) \ll u^2(L_{\mathrm{noise}})$, the variance of the signal can be neglected in the square root of Equation A.2.2.

To make the results of this discussion more tangible, the correction term $\mathrm{b_{noise}}$ and its uncertainty $u(\mathrm{b_{noise}})$ (based on JCGM 101 (2008) Monte Carlo simulations) are shown in Figure A.3 for different output-signal-to-noise ratios. The red line gives an account that the correction term decreases double exponentially for increasing output signal to noise ratios. The corresponding uncertainty of the correction term is shown in green. Both the correction term and its standard uncertainty very quickly assume negligibly small values, i.e., $\mathrm{SNR} \gtrsim 10\,\mathrm{dB}$

For systems whose impulse responses decay over time, the uncertainty due to noise is therefore not constant, but inversely related to the SNR of the impulse

[3] Additive white Gaussian noise

[4] In practical measurements, a headroom of 10 dB has proven to be sufficient. The maximum possible dynamic range is further reduced by the crest factor of the excitation signal (3 dB for sine sweeps).

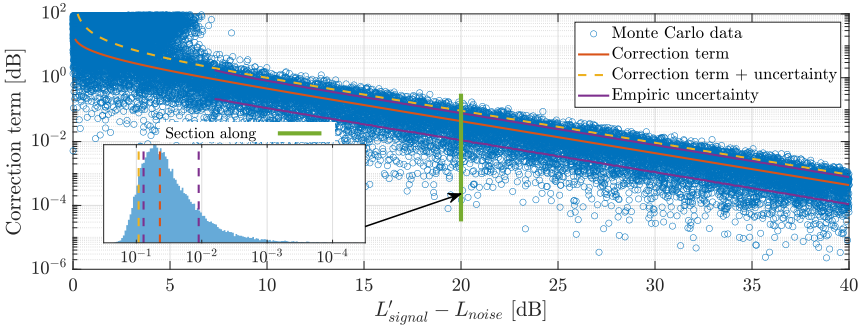

Figure A.3: Correction term and its associated uncertainty according to Equation A.2.1. Based on standard uncertainties of 0 dB for the measured sound pressure level L'_{signal} and 4.8 dB for the background noise level L_{noise}. The results from Monte Carlo simulations are shown in blue.

response (e.g., see Figure A.4). It remains therefore a valid observation that the uncertainty due to background noise is negligible for SNRs larger than 10 dB.

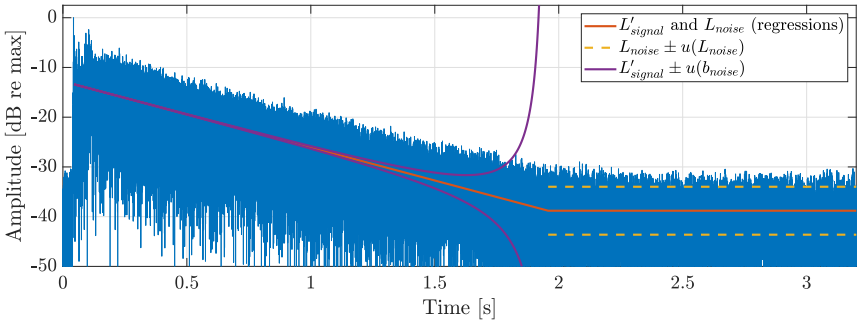

Figure A.4: Measured room impulse response including the measurement uncertainty due to noise.

Nonlinear systems

Figure A.5: Systematic drawing of the measurement chain. Elements that are shaded are referred to in this paragraph.

Deviations from the linearity of the measurement system's characteristic curve pose a problem that may lead to errors when using correlation techniques to measure impulse responses (ISO 18233, 2006). Dietrich (2013)(Ch. 3) and Novak (2009) dedicate a substantial investigation to the effects of such nonlinearities on the measurement of transfer functions. Their modeling is based on the decomposition of the measurement system's characteristic curve into a Taylor polynomial series (Bronstein et al., 2015, 7.3.3.3) and trigonometric power series (Zwillinger, 2003) to quantify the system's distortion. This perspective is extremely helpful to understand how odd-ordered harmonics contribute energy to the fundamental signal. The potentially unknown leakage into the fundamental signal may be detrimental to the correct acquisition of the impulse response's amplitude. To this date, there is no estimate of this uncertainty contribution.

Expressing the odd orders of the power series as in Equation A.2.3 shows how the sum's $k = n$ term potentially scatters into the fundamental system output.

$$\cos^{2n+1}[x] = \sum_{k=0}^{n} C_{n,k} \cos[(2n+1-2k)x], \text{ with } C_{n,k} = \frac{1}{4^n}\binom{2n+1}{k} \quad \text{(A.2.3)}$$

When fixed rate exponential sine sweeps are used to excite the system it is generally possible to easily identify any 3^{rd} order responses at the end of the measured impulse response. These contributions are given in the $k = n - 1$ summation term in Equation A.2.3. It is evident from Equation A.2.4 that the disturbing 1^{st} order harmonic can be estimated to have an amplitude of up to 5 dB above the 3^{rd} order response.

$$C_{n,\text{rel}} = \frac{C_{n,k=n}}{C_{n,k=n-1}} = \frac{n+2}{n} \leq 3 \approx 5\,\text{dB} \quad \text{(A.2.4)}$$

The quintessence of Equations A.2.2 and A.2.1 holds even when harmonic distortions are deterministic and the AWGN-assumption may not be fully valid. When fundamental disturbances have an amplitude more than 10 dB below that of the linear system response the correction term b_{noise} becomes negligibly small. Compared to random noise deterministic disturbances have a lower variance

($u^2(L_{\text{noise}})$) which leads to a lower uncertainty of the correction term. Both factors suggest that provisions should be made to prevent third-order harmonics from reaching amplitudes exceeding levels of 15 dB below the linear system response.

Calibration and equalization of the measurement chain

Figure A.6: Systematic drawing of the measurement chain. Elements that are shaded are referred to in this paragraph.

The elements of the measurement chain are usually discussed under the realm of system theory and characterized through their transfer functions. Following the principles of the GUM, deviations from ideally flat transfer function can be separated into systematic and random components (ISO Guide 98-3, 2008, 3.2.1). Systematic influences can be compensated using a correction term $\mathrm{b}_{x_i}(\omega)$, while random influences directly contribute to the uncertainty $u\big(x_i(\omega)\big)$ (ISO Guide 98-3, 2008, 3.2.3). Calibration can therefore be understood as a measurement process to determine the correction term $\mathrm{b}_{x_i}(\omega)$. Of course, this measurement has uncertainty, i.e., $u\big(\mathrm{b}_{x_i}(\omega)\big)$. A calibration is therefore only useful when $u\big(\mathrm{b}_{x_i}(\omega)\big) \ll \mathrm{b}_{x_i}(\omega)$

The electrical elements of the measurement chain can be calibrated relatively easily in a short circuit measurement. If close to the full dynamic range has been used and there is sufficient SNR, the uncertainty of the electrical calibration measurement usually plays a minor role. The correction of acoustic measurement sources and microphones, however, cannot be determined in situ in the same way. Both transducers are subject to the sound field under test, which permits no access to a sound pressure that characterizes solely the transducer. As a result, separate measurements that are more complex and introduce a larger uncertainty are required (e.g., the sound power calibration in a reverberation room or a pistonphone calibration).

Classical measurement equipment

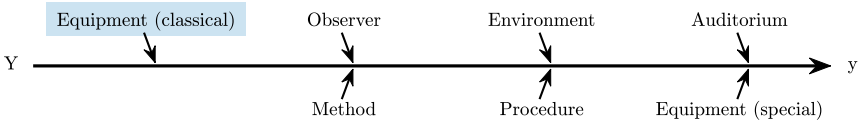

Figure A.7: Ishikawa drawing with shaded category this section refers to.

D/A converters - Quantization

Figure A.8: Systematic drawing of the measurement chain. Elements that are shaded are referred to in this paragraph.

The audio interface or sound card feeds the output signal into the measurement chain. In many cases such devices use the *MADI*, *ADAT* or comparable protocols to convey the signal data. This investigation used a *RME MADIface XT*, that provides the audio signal at a (chosen) word depth of $Q = 24$bit at a sampling frequency of 44.1 kHz to the connected digital-analog-converter. The quantization adds noise to the measurement: the maximum possible SNR can be determined through basic formulas (Havelock et al., 2008, Ch. 45)

$$L_{\text{quant, SNR}} = 20\log_{10}(2^{-Q}) - 1.76\,\text{dB} = -146.2\,\text{dB}. \tag{A.2.5}$$

As this is the introduction of the signal into the measurement chain, $u(L'_{\text{signal}}) = 0$ and $u(L_{\text{quant-SNR}}) = 4.8\,\text{dB}$. Based on an effective SNR of 133 dB, Equation A.2.2 yields an uncertainty due to quantization noise of

$$u(\text{b}_{\text{SNR-quant}}) = 2.3{\times}10^{-13}\,\text{dB}. \tag{A.2.6}$$

Practical D/A converters present a piecewise constant voltage signal as a sequence of rect(t)-functions that hold the amplitude coded in the incoming 24-bit words for the duration of the sampling period. Aliasing that is introduced through the side bands of the rect(t)-function are attenuated through low pass filters.

This study used a *RME ADI-8 QS* DA/AD converter that features eight output and eight input channels. The manufacturer specifies the conversion's signal-to-noise ratios as the level difference between the highest convertible amplitude

(full scale level) and the amplitude of the total harmonic distortions (THD). Oftentimes the total harmonic distortions and noise will be summarized as the THD+N-level.

$$\mathrm{SNR}_{\mathrm{THD,\ D/A\text{-}conversion}} = -104\,\mathrm{dB} \tag{A.2.7}$$

$$\mathrm{SNR}_{\mathrm{THD+N,\ D/A\text{-}conversion}} = -102\,\mathrm{dB}. \tag{A.2.8}$$

This information does not perfectly correspond to the presented model for background noise or harmonic distortions. Nonetheless, based on the previous headroom discussion (e.g., see footnote 3), the resulting effective signal-to-noise ratios can be estimated to be greater than 90 dB for both scenarios. In line with the previous discussions this yields an uncertainty of

$$u(\mathrm{b_{D/A\text{-}SNR}}) \approx u(\mathrm{b_{D/A\text{-}THD}}) \lesssim 1{\times}10^{-8}\,\mathrm{dB}. \tag{A.2.9}$$

The manufacturer specifies the output channels' frequency response to be flat within a range of -0.5 dB between 5 Hz and 22 kHz. This information could be included in the uncertainty budget as a GUM type B uncertainty. However, since a compensation of the frequency response is possible without major effort (and has been carried out), this uncertainty contribution is not to considered.

The accuracy of the analog-digital and digital-analog conversion depends in part on the accuracy of the sampling clock and its jitter. Inaccuracies in the times at which samples are taken result in errors in the amplitude of the sampled signal that can be interpreted as introduced noise. This suggests that the familiar tools for evaluating background noise can be used. Clock jitter creates larger amplitude error for signals that have higher slopes. For a sinusoidal signal $\sin(\omega t)$ the slope is highest at $t = 0$ and can be quantified (by taking the signal's derivative) as $2\pi f$. From the GUM-framework, the uncertainty of the signal's voltage amplitude $u(v_{\mathrm{Amplitude}}) = cu(t_{\mathrm{Jitter}})$, with the sensitivity coefficient $c = 2\pi f$. The manufacturer specified the used hardware's jitter $u(t_{\mathrm{Jitter}})$ to be less then 1 ns. The introduced noise due to clock jitter rises by 6 dB with each doubling of the frequency and can be determined using Equation A.2.10 (Neu, 2010). The resulting SNRs are given in Table A.2 for different octave bands.

$$\mathrm{SNR}_{\mathrm{Jitter}} = -20\log_{10}(2\pi f_{max} t_{Jitter}) \tag{A.2.10}$$

The signal-to-noise ratios given in Table A.2 are much smaller than what practical experience would suggest, possibly because in current circuitry it is common practice to implement approaches which increase the SNR even further, and, hence, contribute even less to the uncertainty (Pollow, Dietrich, Krechel, &

Table A.2: SNR for different octave bands due to clock jitter of $t_{Jitter} = 1\,\text{ns}$.

Octave band	[Hz]	63	125	250	500	1000	2000	4000
$\text{SNR}_{\text{Jitter}}$	[dB]	-125	-119	-113	-107	-101	-95	-89

Vorländer, 2011). Still, the lowest SNR in Table A.2 indicates that uncertainty due to clock jitter can be conservatively estimated to be

$$u(\text{b}_{\text{clock jitter}}) \lesssim 1{\times}10^{-8}\,\text{dB}. \tag{A.2.11}$$

Amplifiers (of the excitation signal)

Figure A.9: Systematic drawing of the measurement chain. Elements that are shaded are referred to in this paragraph.

In the next stage, the analog signal is fed to a power amplifier to provide the energy needed to drive the sound source. Generally, amplifiers are considered to have properties sufficient for today's acoustical measurement tasks: linearity, flat frequency response and noise suppression. In this study a *Stage Line STA-1508* 8-channel amplifier was used. Within the frequency range from 12 Hz to 60 kHz, the transfer function is constant within the limits of $\pm 0.75\,\text{dB}$. These specifications can be used to establish a GUM type B uncertainty, but this deterministic deviation from the ideal transfer function also can be compensated.

The manufacturer's quotes for the signal-to-noise ratio and the THD level is

$$\text{SNR}_{\text{Amp-SNR}} = 80\,\text{dB and} \tag{A.2.12}$$

$$\text{SNR}_{\text{Amp-THD}} \approx 60\,\text{dB}. \tag{A.2.13}$$

Thus, the associated uncertainty due to the power amplifier is likely to be on the order of

$$u(\text{b}_{\text{Amp-SNR}}) \lesssim 1{\times}10^{-6}\,\text{dB and} \tag{A.2.14}$$

$$u(\text{b}_{\text{Amp-THD}}) \lesssim 1{\times}10^{-4}\,\text{dB}. \tag{A.2.15}$$

Electroacoustic sound sources

Figure A.10: Systematic drawing of the measurement chain. Elements that are shaded are referred to in this paragraph.

The next element in the measurement chain is the electroacoustic loudspeaker that actually feeds the excitation signal into the room. As with the previously discussed elements, sound sources introduce uncertainties to the measurement either due to nonlinearities that lead to harmonic distortions, or due to their nonflat transfer functions. In addition, there are some factors that are specifically characteristic of electroacoustic sound transducers, such as the directivity or the long-term stability.

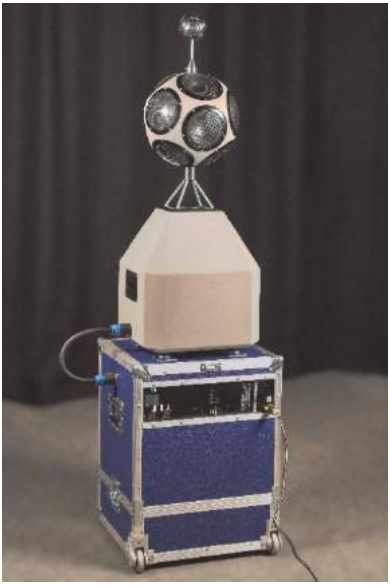

Figure A.11: Measurement loudspeaker designed at ITA set up as a broadband omnidirectional source.

The loudspeaker system used here is described in detail by Behler and Vorländer (2018). As shown in Figure A.11, the system consists of three parts: a bass cabinet to radiate the lowest frequencies up to the 125 Hz-octave, a 30 cm sphere with 12

membranes to excite the octave bands ranging from 250 Hz to 1 kHz and a high frequency tweeter that is designed for the octave bands above 2 kHz.

Influence of the sound power calibration For loudspeakers in general, determining the transducer constant (in $\mathrm{V/m^3/s^2}$) is of some importance. The basic idea does not entirely differ from the existing considerations on the equalization of the amplifier's or D/A converter's transfer functions. An essential difference, however, is that loudspeakers change the signal domain from electrical to acoustical, introducing uncertainties.

Wenmaekers and Hak (2015) have shown that determining the level of the direct sound in situ, i.e., in the (vaguely controlled) reverberant conditions of an auditorium, is prone to significant errors. Such reference measurements are thus best conducted under the controlled laboratory conditions of an (hemi-)anechoic room. It is not too surprising that such measurements are also uncertain. Wittstock and Bethke (2005) have shown that the sound power measurement of a sound source in a hemi-anechoic room introduces an uncertainty of $u(\mathrm{b_{LS\text{-}Level}}) \approx 0.45\,\mathrm{dB}$ to the uncertainty budget. This value is due to the uncertainty contributions shown in Table A.3.

Wittstock and Bethke (2005) refer to ISO 3745 (2017) measurements to determine the sound power levels of noise sources in (hemi-)anechoic rooms. In such scenarios the sound sources are generally uncorrelated to the measurement equipment. In the measurement chain discussed here, however, the sound source is a loudspeaker, which means that not all of the original aspects in Table A.3 contribute to the uncertainty to the same extent. Of the most notable differences, the uncertainty due to filtering can be omitted, since the targeted sound power calibration is applied as a function of frequency across the entire bandwidth. Furthermore, the contribution of background noise is significantly reduced in correlation measurements. Finally, the influence of the microphone calibration can be revised due to the discussion in one of the following paragraphs. All of these revisions are due to differences between the general measurement procedure Wittstock and Bethke (2005) discuss and the detailed implementation used in this study. The juxtaposition of both views leads to a revised uncertainty budget in Table A.3, and consequently to the combined uncertainty of

$$u(\mathrm{b_{LS\text{-}Level}}) \approx 0.26\,\mathrm{dB}. \tag{A.2.16}$$

To evaluate the relevance of this uncertainty contribution, the intended use of the collected data (Chapter 7) needs to be considered. Generally, calibration measurements serve two goals: They determine the transducer constant, and they determine the average sensitivity of the sound source over frequency. Thus,

Table A.3: Uncertainty budget for sound level measurements according to Wittstock and Bethke (2005) and with revised contributions.

Contribution	Uncertainty				
	Wittstock et al. (2005)		Revised		
Filter	0.34	dB	0	dB	
Calibration	0.25	dB	0.21	dB	
Microphone frequency response	0.1	dB	0.15	dB	
Background noise	0.1	dB	$\ll$0.01	dB	(SNR >30 dB)
Positioning	0.05	dB	0.05	dB	
Display resolution	0.03	dB	0	dB	
Changes in sound emission	$\approx$0	dB	0	dB	
Averaging time	$\approx$0	dB	0	dB	
Angel of sound incidence	$\approx$0	dB	$\approx$0	dB	
Combined uncertainty	0.45	dB	0.26	dB	

calibration is necessary to determine measurands absolutely. In contrast, most room acoustical quantities (e.g., reverberation time or clarity) evaluate energy ratios within the RIR or the decay process over time. These metrics are independent of the RIR's absolute amplitude. Other quantities (e.g., sound strength or listener envelopment), however, require by definition a sound level calibration. If, as in Chapter 7, room acoustical quantities are placed in direct comparison to each other, a sound power calibration becomes obsolete as long as the collected quantities were determined during the same measurement series in which the measurement chain's amplification remained unchanged. As a result, the sound power calibration is optional for any of the room acoustical metrics examined here. Consequently, in this study, the calibration's uncertainty contribution can be neglected regardless of whether the calibration was carried out or not.

Influence of spectral characteristics Sound sources behaving (approximately) as point sources have to work against the radiation impedance, which is a function of frequency. At low frequencies, the sound source displaces the

medium without compression. At these frequencies sound cannot be radiated, and so the sensitivity of the source is reduced. At higher frequencies, the size of the membrane and the proximity of the individual drivers (both relative to the wavelength) lead to interference effects that reduce the overall radiated sound power. Figure A.12 shows the sensitivity as a function of frequency for four different dodecahedron loudspeakers (Witew & Behler, 2005).

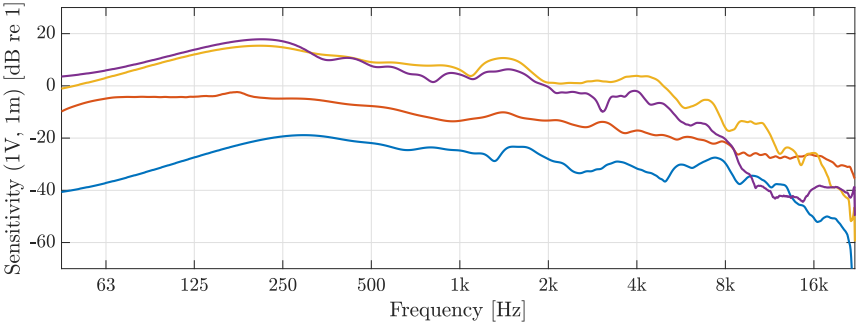

Figure A.12: Sensitivity as a function of frequency for different dodecahedron loudspeakers.

The sensitivity of the sound source can be determined under controlled laboratory conditions in a setup very similar to the one used for sound power calibration. Thus, essentially the same input variables contribute to the uncertainty. However, since the spectral equalization is only relative, a pistonphone calibration is not necessary. This reduces the combined uncertainty in Table A.3 for the loudspeaker equalization to

$$u(\mathrm{b}_{\text{LS-spec}}) = 0.16\,\mathrm{dB}. \tag{A.2.17}$$

The uncertainty contributions given in Equations A.2.16 and A.2.17 need only be considered once in the uncertainty budget, obviously depending on the investigations line of argument. In the measurements discussed here, compensating the spectral characteristics of the source (i.e., without calibration) is sufficient.

Influence of harmonic distortions Loudspeakers are often identified as the "weak link" that is especially prone to introducing nonlinearities into the measurement chain. This is because loudspeakers used in professional applications are regularly operated near their load limits (Goertz, 2008) and so harmonic distortions characterize their acoustic behavior considerably.

Since the distortion's contribution depends strongly on the signal amplitude, or the power fed into the system, it is common to characterize loudspeakers through the sound pressure levels (measured 1 m away from the speaker) at which the total harmonic distortions (THDs) provide a defined percentage to the total level. THD ratios of 1 %, 3 % and 10 % correspond to respective THD levels of −40 dB, −30 dB and −20 dB relative to the fundamental signal. For the measurement source used in this study (see Figure A.11), the results of such a maximum level measurement can be seen in Figure A.13. From left to right, the maximum levels for the bass cabinet, the mid-frequency dodecahedron and the high-frequency tweeter are shown. The orange, green and magenta lines indicate the THD ratios of 1 %, 3 % and 10 %.

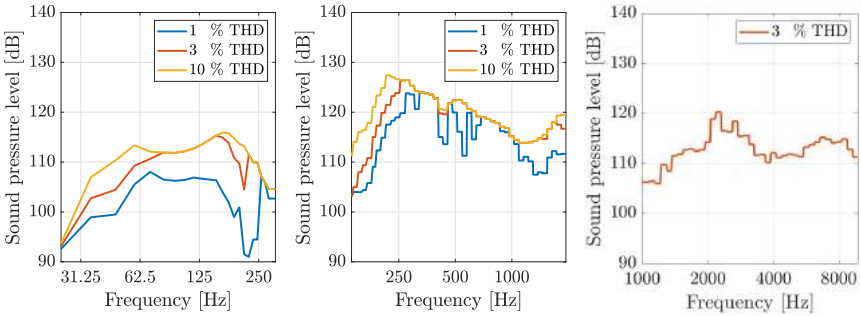

(a) Low, $P_{\max} = 500\,\mathrm{W}$. (b) Mid, $P_{\max} = 2800\,\mathrm{W}$. (c) High, $P_{\max} = 160\,\mathrm{W}$.

Figure A.13: Maximum sound pressure level, for the different parts of the loudspeaker system at different distortion limits. Measurements were performed under anechoic conditions and calculated for a distance of 1 m from the loudspeaker (from Behler and Vorländer (2018)).

From a formal point of view, in order to make the best use of the information shown in Figure A.13 it is necessary to calibrate the sound sources and so ensure beyond doubt that the loudspeaker operates at a known level. Obviously, this comes at the cost of introducing the uncertainty of 0.26 dB to the budget, but if measurements of strength parameters were planned, this calibration would not involve additional effort.

For the research question discussed here, however, a power calibration is not necessary. Furthermore, the influence of the harmonic distortions in the measurement chain can be identified in the measured impulse response. Even if a high 3^{rd} order THD level of −40 dB relative to the RIRs maximum were assumed, an uncertainty of

$$u(\mathrm{b_{LS\text{-}THD}}) \approx 1{\times}10^{-3}\,\mathrm{dB} \tag{A.2.18}$$

would have to be recognized. With the given sound source it is not particularly problematic to conduct measurements with harmonic distortions of less then $-80\,\mathrm{dB}$. The actual influence of loudspeaker THDs can be much less than the number in Equation A.2.18.

Influence of the directivity The uncertainty contribution due to the loudspeaker's directivity is very similar to the influence of the transfer function's flatness, except that the additional variable of "radiation angle" is introduced to the spectral characteristics. The strategies to quantify this factor are diverse.

ISO 3382-1 (2009) specifies a measurement method to characterize dodecahedron sources and to evaluate their suitability for measurements in rooms based on a single number value. This method requires sampling the sound power distribution over a great circle of one of the source's enveloping concentric spheres and calculating an angular average. This pragmatic approach has it's roots in standards of building acoustics and fundamental research, e.g., Pelorson et al. (1992). This ISO 3382-1 (2009) directivity parameter is clearly related to the directivity of measurement sound sources and, hence, can be seen as a valid metric to compare different sound sources to each other. On the other hand, however, this single-number characteristic is defined in a rather abstract manner, making it meaningful only in reference to the measurement method. Conclusions regarding the expected measurement uncertainty based on the ISO 3382 directivity metric are not evident.

To bridge this gap and establish a relation between the ISO 3382-1 (2009) directivity metric and the uncertainty in measurements, Witew and Behler (2005) discuss a measurement method that is based on dodecahedron loudspeakers placed on a turntable and repeated measurements with the source turned in steps. Such measurements show how quantities describing the acoustics in auditoria (e.g., $\mathrm{C_{80}}$, etc.) vary due to the sources' directivity. Later, in a follow-up, San Martin et al. (2007) were able to put these results on a broader foundation and discuss uncertainties of different room acoustical parameters due to the directivity of sound sources. The value of this approach needs to be discussed in a differentiated manner. On the one hand, it is a useful result to know the expected uncertainties when common measurement loudspeakers are used. On the other hand, it would be even better if the source properties were documented in a way that permitted establishing a clear functional relationship showing how increasing deviations from omni-directionality translated to an increasing variance of room acoustical parameters.

In an investigation that studied which loudspeaker shapes are most suitable to achieve the best possible omni-directional sound radiation, Leishman et al. (2006) free themselves from the limitations of the ISO 3382-1 (2009) directivity metric. On the basis of numerous free field measurements in different directions they calculate the area-weighted standard deviation of the radiated sound energy as a metric to quantify a source's directivity. Provided that the ray tracing paradigm and the concept of the source's radiation into a diffuse sound field are valid Leishman et al. (2006)'s weighted standard deviation is identical to the uncertainty of individual reflections in an impulse response. This approach has the benefit that the source characterization coincides with a metric that is directly usable for the measurement uncertainty discussion. It may be taken with a grain of salt that the concepts of "individual reflections" and the "diffuse sound field" cannot be perfectly combined.

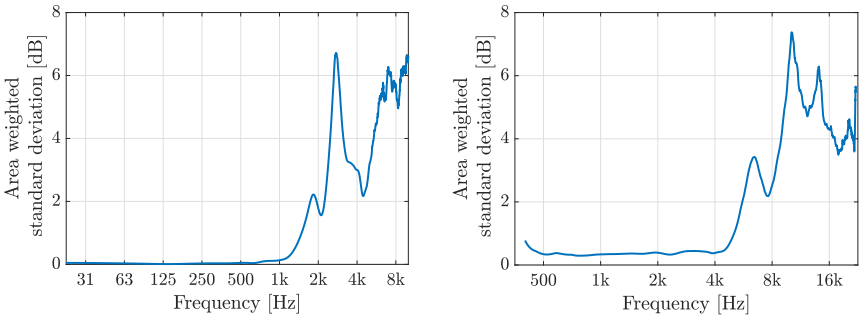

(a) Mid frequency sphere.

(b) High frequency tweeter.

Figure A.14: Area weighted standard deviation of the dodecahedron loudspeaker shown in Figure A.11

For the sound source depicted in Figure A.11, Figure A.14 shows the standard deviation of the radiated sound intensity level. The underlying data is based on the sound radiation over a 4π solid angle sampled in a 5° resolution. Hence, it can be assumed that the uncertainty contribution of measurements due to source directivity, conducted with this source in this study, is about $u(\mathrm{b}_{\text{LS-dir}}) = 0.35\,\mathrm{dB}$.

Instead of blindly accepting this uncertainty, the uncertainty of the measurement method leading to the area weighted standard deviation needs to be taken into account as well. Due to the automated measurement procedure used at the Institute of Technical Acoustics, many of the most significant contributions Wittstock and Bethke (2005) identfies (e.g., pistonphon calibration, filtering, etc.) are not applicable in this special case (Pazen, Witew, & Vorländer, 2011). As a result,

it is reasonable to estimate the measurement method's uncertainty contribution to $u(\mathrm{b}_{LS-spec}) = 0.16\,\mathrm{dB}$, yielding a combined directivity uncertainty of

$$u(\mathrm{b}_{\text{LS-dir}}) = 0.38\,\mathrm{dB}. \tag{A.2.19}$$

As part of an upfront critical discussion it is important to indicate potential limitations that may exist:

- Using the loudspeakers' area weighted standard deviation of the radiated sound energy to determine the uncertainty in the measured RIR relies on the concept of the perfectly diffuse sound field. Gade and Rindel (1985) have shown, however, that the perfectly diffuse sound field is a rare condition in auditoria.

- The implied model suggests a constant uncertainty contribution over the running time of the impulse response. Using a very large data collection, Witew et al. (2014) have shown that the uncertainty of the impulse response due to the source's directivity changes over the running time of the impulse response. The very early parts of the impulse response show a significantly higher uncertainty compared to the later parts of the (diffuse) exponential decay.

- The implied model also suggests that other (secondary) influences cannot contribute to the uncertainty. Witew et al. (2012) have shown on the same data set, however, that the uncertainty due to the primary factor "directivity" depends on secondary factors such as "room volume", "surface scattering" and "surface absorption", as well as the interactions of these factors.

These findings could be taken as evidence that the "mixing" of the sound field, and aspects of "averaging" due to the rising reflection density over time, play a role in continuously reducing the uncertainty as the running time of the RIR increases. In contrast to that perception, Knüttel et al. (2013) have shown that despite the high number of reflections arriving in late parts of the RIR, the influence of the sources' directivity was proven beyond doubt. Due to the complex way the various influences are linked to each other, it is difficult to establish a clear relationship between deviance from omni-directionality and the measurement uncertainty of RIRs. Resorting on the uncertainty given in Equation A.2.19 therefore represents a pragmatic approach, while potential refinements are a question of ongoing research.

Microphones

Figure A.15: Systematic drawing of the measurement chain. Elements that are shaded are referred to in this paragraph.

IEC 60268-4 (2017) lists 48 parameters that can be used to describe the technical properties of microphones. Generally, not all of the parameters are available from the manufacturer's data sheet, and not all are relevant factors contributing to the uncertainty in measurement. Payne (2004) and Wittstock and Bethke (2005) discuss the uncertainties associated with sound level meters and provide helpful information about the factors contributing to the uncertainty in measurements in general and also to factors associated with microphones.

In the present study, 32 Sennheiser KE 4-221-2 pre-polarized, back-electret condenser microphone capsules have been used. The manufacturer's data sheet (Cat. No. 002280, 2005) quotes sensor characteristics that are similar to the loudspeaker and amplifier properties that have been discussed before. As a result, the same strategy to recognize these contributions can be used.

Influence of harmonic distortions Sennheiser publishes the maximum sound pressure levels while not exceeding THD-values of 1 % and 3 % at the output as 130 dB and 140 dB respectively. As before, this information cannot contribute directly to the uncertainty discussion because the prevailing signal-to-noise ratio during the measurement is unknown for the time being. Considering a THD level of at least 100 dB, however, implies an uncertainty of less than

$$u(\mathrm{b_{Mic\text{-}THD}}) \lesssim 1{\times}10^{-9}\,\mathrm{dB}. \tag{A.2.20}$$

Influence of inherent noise The noise in the microphone's output voltage due to the acoustic, mechanical and electric parts of the microphone (Schneider, 2008) is regularly published in the microphone's data sheet as the equivalent noise level in dB(A) or as the CCIR rating according to ITU-R BS.468-4 (1986). This property plays a central role in direct acoustical measurements. In correlation measurements, however, the microphone's intrinsic noise only contributes to the background noise, in conjunction with the properties of the excitation signal and the utilization of the dynamic range. Thus, determining the (combined) noise level from the measured impulse response a posteriori is justified. For the

measurements performed here, a peak-to-noise ratio of 70 dB can be taken as a reference. This yields

$$u(\mathrm{b_{Mic\text{-}SNR}}) \lesssim 1{\times}10^{-6}\,\mathrm{dB}. \tag{A.2.21}$$

This strategy overestimates the uncertainty contribution of the microphone's intrinsic noise as the analyzed noise level can be composed from many sources. Compared to the already discussed uncertainties of up to 0.38 dB, contributions in the order of 10^{-6} dB should not play a significant role.

Influence of the microphone-altered sound field The presence of the microphone distorts the sound field and thus has an effect on the prevailing sound pressure. According to Payne (2004), manufacturers of microphones and sound level meters do not provide any indication of the magnitude of associated uncertainties. In Payne's study about sound level analyzers in (hemi) free field conditions, correction terms ranging from 0.04–0.11 dB and an uncertainty of

$$u(b_{\mathrm{Mic\text{-}Field}}) = 0.011\,\mathrm{dB} \tag{A.2.22}$$

has been determined.

Since the disturbance of a scattering body in the sound field is wavelength-dependent, and since 1/2 inch (12.7 mm) microphone capsules of average sound level meters and the 5 mm diameter of a KE 4 capsule are different in size, it is evident that the uncertainty estimation in Equation A.2.22 exceeds the effect that can be anticipated in this study. Since the wavelength of a 4 kHz tone is more than one order of magnitude larger than the dimensions of the sensor, the effect of the microphone on the measured sound pressure is considered negligible in this study for the discussed frequency range. In order to clearly distinguish this influence factor from others, it is noted that the disturbance of the sound field discussed here only concerns the sensor and its support in the immediate vicinity. Any positioning mechanisms that may play a role in this investigation are deferred to a later discussion.

Influence of the frequency response Wittstock and Bethke (2005) investigated the free field sensitivity of five high-quality 1/2 inch microphones and amplifier cartridges as a function of frequency to determine the uncertainty of published sensitivity data in calibration charts. They determine the uncertainty of a measurement microphone's frequency response to be as shown in Table A.4a.

Based on unpublished reference measurements by Lukas Aspöck in 2017, the frequency responses of the 32 KE 4-221-2 microphones are available. From this data, the correction terms $\mathrm{b_{Mic\text{-}spec}}$ and their uncertainties $u(\mathrm{b_{Mic\text{-}spec}})$ can be

Table A.4: Uncertainty due to the microphone frequency response.

Frequency range [Hz]	Uncertainty $u(b_{Mic\text{-}spec})$ [dB]
20 – 80	0.15
100 – 5000	0.10
6300 – 10 000	0.15
12 500 – 20 000	0.20
–	–
–	–
–	–
–	–
–	–

(a) From Wittstock and Bethke (2005).

Frequency band [Hz]	Correction $b_{Mic\text{-}spec}$ [dB]	Uncertainty $u(b_{Mic\text{-}spec})$ [dB]
62.5	−0.44	0.15
125	−0.07	0.10
250	−0.13	0.08
500	−0.18	0.08
1000	−0.19	0.07
2000	−0.09	0.13
4000	−0.35	0.46
8000	0.73	1.57
16 000	5.33	3.94

(b) Based on differences between 32 KE 4 microphones.

determined. The results shown in Table A.4b give evidence that the microphones used in this study introduce a measurement uncertainty into the measurement chain that is comparable to the "high-quality up-to-date instruments" used by Wittstock and Bethke (2005). Only for the highest frequency bands (i.e., 4–16 kHz-octaves) is the uncertainty well above typical measurement grade microphones. As these bands are excluded from the analysis in this present investigation, the uncertainty introduced due to the microphones' frequency response can be given as a single number quanitity:

$$u(b_{Mic\text{-}spec}) = 0.15\,\text{dB}. \tag{A.2.23}$$

Influence of the directivity Similarly to the radial pattern of the sound source, the directivity of the microphone is a source of uncertainty as well. Payne (2004) considers the uncertainty resulting from sound incidence at angles diverging up to 20° from that which the instrumentation has been calibrated for. Assuming an excitation with a flat frequency spectrum he determines the uncertainty of the A-weighted level to be 0.14 dB.

Wittstock and Bethke (2005) provides more detailed data based on directivity measurements and an assumed uncertainty of 5° in the direction of the incident sound. They determine the uncertainty to narrow band sound level measurements as shown in Table A.5a.

Table A.5: Uncertainty due to the directivity of the microphone.

Frequency band [Hz]	Uncertainty $u(\mathrm{b}_{\text{Mic-dir}})$ [dB]
16 – 2000	0.05
4000	0.10
8000	0.20
16 000	0.50
–	–
–	–
–	–
–	–

(a) From Wittstock and Bethke (2005).

Frequency band [Hz]	Uncertainty $u(\mathrm{b}_{\text{Mic-dir}})$ [dB]
125	0.07
250	0.02
500	0.01
1000	0.02
2000	0.06
4000	0.19
8000	0.48
16 000	0.96

(b) For a KE 4 microphones.

These results, however, cannot be directly applied to the situation discussed here, because Wittstock and Bethke's free field conditions do not apply in auditoria. In regard to Payne (2004), the A-weighted levels do not quite relate to measured impulse responses.

For this reason, directivity measurements of the KE 4 microphones by Markus Müller-Trapet from 2012 were re-analyzed and the area-weighted standard deviation (see Chapter A.2.3 and Leishman et al. (2006)) was calculated as an estimate for the uncertainty contribution. The results are shown in Table A.5b. It can be seen that the uncertainty for omni-directional sound incidence at mid frequencies is well below the reference values determined under free field conditions. At higher frequencies, however, there are significant deviations in the directivity and therefore larger uncertainty contributions. The slowly rising measurement uncertainty at lower frequencies is surprising and cannot be clearly explained. As this increase in uncertainty is rather subtle, however, it needs not be of concern. To merge these results in a single number value, the uncertainty is expressed through

$$u(\mathrm{b}_{\text{Mic-dir}}) = 0.07\,\mathrm{dB}. \tag{A.2.24}$$

The limitations of this approach were already discussed in the context of the uncertainty due to the sound source's directivity. Due to reciprocity, they apply for microphones as well.

Influence of the calibration During calibration, a known sound pressure level is produced at the diaphragm of the measurement microphone and the resulting signal is propagated through the receiving part of the measurement chain. As a result, the relevant uncertainty contributions of the measurement chain in Equation A.2.25 must be taken into account when determining the combined uncertainty of the calibration.

$$u_c(\mathrm{b_{Mic\text{-}cal}}) = \sqrt{u^2(L_{\mathrm{Cal}}) + u^2(\mathrm{b_{calibrator}}) + u^2(\mathrm{b_{Mic\text{-}spec}}) + u^2(\mathrm{b_{Amp\text{-}THD}})} \tag{A.2.25}$$

Hanes (2001) compares voltage calibration data from 13 national metrological institutions, and determines the uncertainty of sound pressure levels produced by calibrated pistonphones to be $u(\mathrm{b_{calibrator}}) = 0.035\,\mathrm{dB}$. Hanes concludes that the uncertainty of the calibrator is the greatest contribution to the overall calibration uncertainty. In contrast, Payne (2004), from the same laboratory, rates the uncertainty contribution of the calibration to be $u(\mathrm{b_{calibrator}}) = 0.025\,\mathrm{dB}$, based on his investigation of 22 sound level meters. Compared to Wittstock and Bethke (2005) these uncertainties seem rather low, as they determine the uncertainties of the sinusodial calibration level to be $u(L_{\mathrm{Cal}}) = 0.09\,\mathrm{dB}$, and of the pistonphone to be $u(\mathrm{b_{calibrator}}) = 0.09\,\mathrm{dB}$. The reason for this discrepancy may be the accuracy of different calibration methods (Brüel & Kjær, 1996, Ch. 6.6). According to the B&K Microphone Handbook, the combined uncertainty $u_c(\mathrm{b}_{cal})$ of pistonphones may range from 0.035 to $0.15\,\mathrm{dB}$.

Adopting Wittstock and Bethke (2005)'s result and including the remaining open uncertainty contributions in Equation A.2.25 (i.e., $u(\mathrm{b_{Mic\text{-}spec}}) = 0.15\,\mathrm{dB}$ and $u(\mathrm{b_{Amp\text{-}THD}}) \approx 1{\times}10^{-4}\,\mathrm{dB}$) yields the combined uncertainty of

$$u_c(\mathrm{b_{Mic\text{-}cal}}) = 0.21\,\mathrm{dB}. \tag{A.2.26}$$

Finally, it should be mentioned that the previous discussion on calibration disregards possible correlation of the uncertainty contributions, as they may exist through use of the same equipment or the same calibration normal. Correlation effects are not considered by Payne (2004), Wittstock and Bethke (2005) or Hanes (2001) either.

Amplifiers (of the microphone signal)

Figure A.16: Systematic drawing of the measurement chain. Elements that are shaded are referred to in this paragraph.

At the receiving side of the measurement chain, the microphone signal is amplified twice before quantization. Although the first step is actually to convert the capacitor's charge separated by the diaphragm and the backplate into a stable voltage (and current), it can still be interpreted as an amplification. The second cascade of the amplification is to make best use of the transmission channel and amplify the microphone signal so that it (reasonably) covers the A/D converter's full dynamic range.

The linearity of the reference range of sound level meters is an important criterion for type ratings specified in IEC 61672-1 (2013). The acceptance limits for level linearity are measured with electrical signals that are fed to the sound level meters through the input of the microphone preamplifier. Payne (2004) investigated 22 different sound level meter types and determined the uncertainty due to nonlinearities in the (pre)amplifier's characteristic curve to

$$u(\mathrm{b}_{\text{Pre-Amp-lin}}) = 0.10\,\mathrm{dB} \tag{A.2.27}$$

in the reference range. In other ranges, i.e., when the signal is amplified a second time to fall within the range of the sound level meter's A/D-converter, the combined uncertainty of

$$u_c(\mathrm{b}_{\text{Amp-lin}}) = 0.17\,\mathrm{dB} \tag{A.2.28}$$

was determined.

The interpretation of these findings on amplifiers presents some challenges to the critical reader. Payne (2004) determined that the uncertainty contribution due to nonlinearities in amplifiers' critical curves on the receiving side is about seven orders of magnitudes higher than what is determined reasonable on the transmitting side. To further substantiate these doubts, the series of comparative measurements by Müller and Massarani (2001) using MLS and sweep excitation give little indication that such disturbances in 2-Ch-FFT correlation measurements are to be expected. As a result, the question of whether differences in the respective measurement methods could be reason for the diverging assessments needs to be considered. Since this question cannot be answered on the basis of the information available here, greater weight is given to Müller and Massarani

(2001), Dietrich (2013) and own experience from acoustical measurements in auditoria in which $u(\mathrm{b_{Amp\text{-}THD}})$ for the transmitting side is valid for the microphone amplification side, too.

A/D converters

Figure A.17: Systematic drawing of the measurement chain. Elements that are shaded are referred to in this paragraph.

At the end of the acoustical measurement chain is the A/D converter, which feeds the received signal back to the computer for calculation of the impulse response. The discussion of this element's uncertainty contributions mirrors the example of the D/A-conversion almost identically. This leads to uncertainties due to the prevailing SNR, THDs and the quantization of

$$u(\mathrm{b_{A/D,\ THD}}) \lesssim 1{\times}10^{-9}\,\mathrm{dB}. \tag{A.2.29}$$

Environmental conditions

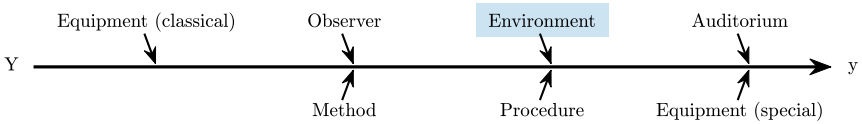

Figure A.18: Ishikawa drawing with shaded category this section refers to.

This section discusses the properties of the acoustic environment, extending beyond purely meteorological influences and including the acoustic properties of the measurement environment as well. Noise sources related to the measurement object that impair the result serve as a significant example in this regard.

Noise sources In room acoustical measurements, background noise is a factor that is introduced to the measurement not only through the elements of the measurement chain (as discussed in the previous section), but also through other sources that radiate sound into the auditorium. Such sources can include technical equipment (e.g., stage elevators, lighting or equipment cooling) or the flow noise from the hall's heating and ventilation system (HVAC). Structure-borne sound

that originates from sources outside the auditorium can be a factor as well. For a quantitative discussion of noise the reader is referred to the this section's basic considerations. In this study the combined influence of noise sources was determined a posteriori through analysis of the collected impulse responses. The contribution to the combined uncertainty can be neglected.

Meteorological conditions It is almost obvious that the meteorological conditions prevailing during a measurement affect the result. The room that serves as the device under test is filled with air whose acoustic properties change with temperature ϑ, humidity h and the ambient pressure p. The environmental conditions, however, do not only affect the properties of the propagation medium, but also the microphone sensitivity.

Influence on the microphone sensitivity Based on a mechano-electrical equivalent parameter network, Rasmussen (1999) discusses how the air enclosed in the microphone's back cavity affects the total acoustic impedance of the microphone. Below the lowest resonance frequency, the back cavity behaves as a parallel resonance circuit in series with a low-frequency compliance. All the elements of the resonance circuit are associated to the air's compliance, mass (density) and viscosity, which in turn depend on the environmental variables:

$$\text{compliance} \propto \frac{1}{p}, \tag{A.2.30}$$

$$\text{mass} \propto \frac{p}{\vartheta} \text{ and} \tag{A.2.31}$$

$$\text{viscosity} \propto \sqrt{\vartheta}. \tag{A.2.32}$$

Rasmussen (1999) shows that regardless of how these effects are combined, the microphone sensitivity changes linearly with the ambient pressure p and temperature ϑ. The effect of changes in humidity is comparable to changes in the density of air. Hence, a change in relative humidity of 30 % is equivalent to a change in temperature of 1 K.

Payne (2004) conducted comparative measurements between 22 different sound level meters and determined a temperature coefficient of $0.002 - 0.015\,\mathrm{dB\,K^{-1}}$ and a pressure coefficient of $0.0015 - 0.019\,\mathrm{dB\,kPa^{-1}}$. Based on a valid temperature rage (in auditoria) from $15 - 31\,^{\circ}\mathrm{C}$ and an ambient atmospheric pressure range of $975 - 1051\,\mathrm{hPa}$, Payne (2004) determines an uncertainty of

$$u(\mathrm{b}_{\text{Meteo-}\vartheta}) = 0.12\,\mathrm{dB} \text{ and} \tag{A.2.33}$$

$$u(\mathrm{b}_{\text{Meteo-p}}) = 0.0722\,\mathrm{dB}. \tag{A.2.34}$$

Assuming a plausible range for the relative humidity in buildings of about 30 – 60 % yields an associated uncertainty in the microphone sensitivity of

$$u(\mathrm{b}_{\text{Meteo-rh}}) = 0.0075\,\mathrm{dB}. \tag{A.2.35}$$

Influence on the propagation medium The prevailing meteorologic conditions also influence the properties of the propagation medium. Two driving properties can be identified, namely a change in the speed of sound and a change in attenuation due to atmospheric absorption. A change in the propagation speed will manifest in a compression or a dilatation of the running time of the RIR. The basic discussion of the speed of sound and its driving properties (e.g., Rossing (2007), Ch. 2.3, Bohn (1988)) indicates that a change in air temperature by 1 K leads to a scaling of the RIR's time axis of 0.18 %.

While the influence of water vapor (humidity) on the speed of sound is generally considered to be small (for regularly encountered conditions), the attenuation due to atmospheric absorption is significant. ISO 9613-1 (1993) quotes formulas to determine the sound attenuation that suggest that the driving meteorological factors are understood reasonably well and their influences on the measured impulse response can be predicted with some confidence. Guski and Vorländer (2014) have investigated how a changes in humidity and temperature affect the measured reverberation times and other room acoustical measurement parameters. While they found that model predictions are satisfactory at very high frequencies ($> 2\,\mathrm{kHz}$), performance drops significantly for lower frequencies when other (unknown and uncontrolled) larger effects overlay the results. Such findings cast doubt on the assumption that measurements can be reproduced provided that humidity and temperature are constant within the means of simple documentary measurements.

In ISO 3382-1 (2009), the air temperature needs to be determined with an accuracy of $\pm 1\,^{\circ}\mathrm{C}$ and relative humidity $\pm 5\%$. Based on the underlying general physical relationships, this notion is understandable. On the other hand, however, the benefit of meticulously documenting environmental conditions is difficult to recognize, since this information provides little direct gain towards deriving the measurement uncertainty or compensating the meteorological influences. Instead, limiting temperature and humidity to close bounds can be thought of creating classes of measurement conditions within which reproducibility is possible.

Another practical question to address is the assumption that the measured temperature and humidity at a single position adequately represents the conditions in the entire auditorium. Oftentimes measurements can only be scheduled for the summer break when there are no regular concerts. During this period the

HVAC-Systems are regularly not operating, leading to a noticeable temperature gradient within the hall. As smallest changes in the RIR can be measured in impulse responses, from a metrological point of view, such deviations from the ideal are undoubtedly evident in the measured result. There is still little evidence of whether such deviations are of any relevance.

Changes during measurement series The previous discussion raises the question of what changes in meteorological parameters are to be expected. During measurements conducted in Berlin Philharmonic Hall (August 2006), Amsterdam Concertgebouw (July 2018) and a small community hall in Dorsten (July 2006), meteorological conditions were documented repeatedly as shown in Tables A.6 and A.7.

The shown standard deviations indicate that the changes in temperature and humidity during measurement sessions between 7 and 18 hours long are relatively small. When comparing measurements conducted in subsequent days (e.g., Table A.6), it becomes evident that the changes in humidity can be larger. In this light, documenting the temperature and the relative humidity appears reasonable. How often these measurements need to be repeated cannot be determined conclusively from this sparse data, but it can be supposed that as long as conditions are not known to be transient measuring, the temperature and the relative humidity every once in a while is sufficient.

Table A.6: Change in meteorological conditions during measurements in Berlin Philharmonic Hall (Witew & Dietrich, 2007).

Time [h:min]	Temp. [°C]	rel. Humidity [%]	Time [h:min]	Temp. [°C]	rel. Humidity [%]
16 : 46	30.8	42	17 : 25	31.6	33
20 : 01	31.1	41	18 : 47	32.0	34
21 : 16	32.0	41	19 : 50	32.1	34
22 : 48	32.1	41	20 : 12	32.3	34
23 : 32	32.2	40	22 : 28	32.3	34
00 : 55	32.3	40	23 : 43	32.4	35
-	-	-	00 : 55	32.5	35
Standard Deviation	0.64	0.81	Standard Deviation	0.30	0.72

Table A.7: Change in meteorological conditions during measurements in Concertgebouw Amsterdam (left) and Dorsten (right) [Dorsten data from Witew and Dietrich (2007)].

Time [h:min]	Temp. [°C]	rel. Humidity [%]	Time [h:min]	Temp. [°C]	rel. Humidity [%]
13 : 15	24.0	44	11 : 46	24.7	54
14 : 30	24.0	45	12 : 16	25.3	54
19 : 50	25.5	41	13 : 32	24.3	55
00 : 25	25.7	41	14 : 05	24.4	55
07 : 00	25.1	45	14 : 30	24.6	55
-	-	-	20 : 01	25.0	56
Standard Deviation	0.81	2	Standard Deviation	0.38	0.64

Air movement Guski and Vorländer (2014) investigated how time variances due to air movement contribute to the measurement uncertainty. They demonstrated that running a ventilation system introduced an added variance to acoustical measurements. The effect is more prominent at higher frequencies and for room acoustical quantities with smaller evaluation ranges (e.g., T_{20} vs. T_{30}). Although an introduced uncertainty of less than 1 % is hardly relevant for room acoustical metrics, the effect may play a more pronounced role for measurements in which the phase information is relevant.

For repeated array measurements it seems to be a practical conclusion to avoid operating ventilation systems as more stable results were achieved without air circulation. Based on the behavior during the transition periods, there is evidence showing that it takes a room about 15 min after turning off the ventilation system to become acoustically stable.

LTI conditions Violations of the paradigm of linear and time-invariant system conditions are a serious impediment to acoustical measurements. For a detailed discussion the reader is referred to Müller and Massarani (2001), Dietrich (2013) or Farina (2007).

Auditorium/Room

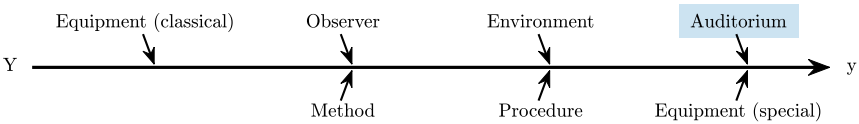

Figure A.19: Ishikawa drawing with shaded category this section refers to.

The geometry of the auditorium determines the sound field through the waves' interaction with the walls. This makes the room part of the measurement chain and so it influences how uncertainties propagate from the transmitting to the receiving side. According to the rules of the ISO Guide 98-3 (2008), theoretical modeling or empirical surveys are possible tools to quantify the uncertainty propagation.

In auditorium acoustics, theory covers the fields of statistical room acoustics, geometrical acoustics, or the solution of the elementary wave equation. Each of these methods requires different input data and predicts different aspects of the resulting sound field. Ultimately, these methods map a four-dimensional space (3-D sound propagation over time) onto the two-dimensional space of an impulse response. Since this involves a loss of information, the significance of individual influences cannot always be quantified down to the last detail.

To address this aspect, ISO 3382-1 (2009) requires that the hall's condition during the measurement be documented. From a GUM point of view, this strategy aims at reducing the uncertainty of input quantities through determining their values during the measurement. When all influences are sufficiently controlled, the deterministic nature of sound propagation ensures that acoustical measurements are repeatable and reproducible. This leads to the general question of how precisely the influence factors must be determined in order to enable sufficiently accurate measurements. As far as it concerns the measurement position, this question is exactly this study's central research target.

Shape and volume Based on the above considerations, the room acts as a secondary influence quantity on the uncertainty of room acoustical measurements. This can be illustrated using the studies by Witew et al. (2012) and Witew et al. (2014) as examples. In extensive measurement series, the influence of the loudspeaker directivity on measured room impulse responses was investigated. In these series the volume of the model scale room, the wall absorption, the scattering properties of the surfaces and the source-receiver distance were varied and thus examined as influence factors. The test setup is shown in Figure A.20.

Figure A.20: Setup to investigate the influence of the sound source's directivity on room acoustical measurements. The walls' absorptive and scattering properties were changed in a large number of measurement series.

Data analysis showed that the influence of the directivity is not constant over the running time of the RIR. In the early part[5] of the impulse response, the directivity's influence varied a lot from time interval to time interval, while in later parts differences got evened out. The influence of the room became apparent when the other variables were investigated in subgroups. The analysis shows that the early part of the RIR lasts much longer in large rooms, as sound takes more time to reach the bounding surfaces of the room and get reflected back to the microphone. Likewise, it becomes evident that the increased sound-scattering properties of the walls enhance the mixing of the sound field, which, in turn, reduces the length of the early part of the RIR.

The exact and sole contributions of the influence factors "room shape" and "volume" cannot currently be quantified in the uncertainty budget, and should be investigated in the context of other influences.

Variable room setup The influence of variable (acoustic) elements or the presence of an audience during the measurement has an influence on the measurement result that is quite similar to the shape of the auditorium. As the present state of knowledge does not yet provide the foundation to answer such complex problems conclusively, it remains necessary to carry out measurement or simulation series in which the influence of the variable room element is studied in a controlled manner.

Representativeness of auditorium When measurements are taken to answer a research question, care must be taken to ensure that the object under test is

[5] This paragraph's notion of earliness refers to a general sequence in time rather than to a fixed time window.

suitable for and representative of the research objective. On the other hand, it is necessary to survey a suitable range of auditoria to make sure that the results remain meaningful for different types of rooms that are used for the same given purpose (Weinzierl & Vorländer, 2015).

An earlier discussion on the representativeness of surveyed rooms is conducted by Barron (1988) when investigating how his findings on the sound perception in concert halls could not reproduce earlier findings by Wilkens (1977) in all nuances. Barron considers his selection of British concert halls (with a relatively high clarity index) as a possible cause. This problem can be easily translated to the uncertainty discussion when relevant influence factors are limited in range or cover atypical values. Due to the high number of influencing factors and the complexity of their interaction, this uncertainty contribution can so far only be assessed qualitatively.

Measurement method

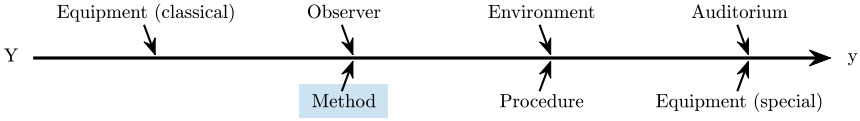

Figure A.21: Ishikawa drawing with shaded category this section refers to.

The rationale behind a measurement method has a significant influence on the result and its uncertainty. This becomes obvious when considering that different measurement strategies go hand in hand with differences in signal processing, and therefore also with differences in uncertainty propagation. Determining the reverberation time in rooms using the interrupted noise method compared to strategies employing the reverse-time integration of the squared impulse response is a suitable example where the different input data leads to different analyses and thus different uncertainties.

Different measurement methods should become subject to a thorough uncertainty investigation; however, it is beyond the scope of this work to discuss all conceivable methods. This is because the room acoustical measurements of this study serve as a tool to investigate the uncertainty contribution of the measurement position. Consequently, a focus is placed on the methods used here, but some of the following results may be valid to alternative measurement methods as well.

ISO 3382 standardization Defining a procedure of measurement and analysis is a significant contribution to the uncertainty discussion as it makes the uncertainty evaluation possible in the first place. When the procedure allows alternative methods or is defined unspecifically, however, new sources of uncertainty are introduced. Examples are the orientation of directional microphones such as artificial heads (Witew, Dietrich, & Vorländer, 2010; Witew, Lindau, et al., 2010) or the sequence of filtering and time windowing (Lundeby et al., 1995; Witew & Behler, 2005). These studies quickly reach the conclusion that the significance of these uncertainty contributions depends a lot on the individual case and can hardly be quantified from only a small sample size.

This study attempts to reduce the uncertainty due to an unspecific definition of the measurement scenario by explaining the conditions under which the results were collected. This may come with the disadvantage that some of the results may not be completely generalizable when other conditions are of interest.

Filtering The requirements on filters and their tolerances are specified in IEC 61260 (1995). Wittstock and Bethke (2005) derive the uncertainties due to filtering based on these standardized tolerances regarding linearity, relative response, the pass-band attenuation for a sinusodial input signal and the effective bandwidth (or integrated impulse response) for a broadband input signal. In the time since Wittstock and Bethke (2005) was published, IEC 61260 (1995) was revised and replaced by IEC 61260-1 (2014). While many of the underlying concepts went through the revision without change, the classification and the tolerances for filters were modified. This relatively small update makes it straightforward to update the uncertainty based on the same rationale that Wittstock and Bethke (2005) utilized.

In contrast to Wittstock and Bethke's original calculations, the contribution of the relative filter response was slightly modified in this study. Instead of determining the uncertainty based on the smallest tolerance at the filter's center frequency, the average tolerance was determined using

$$\overline{\Delta A_{\mathrm{diff}}} = \frac{1}{G^{0.5} - G^{-0.5}} \int_{\Omega=G^{-0.5}}^{G^{0.5}} \Delta A_{\max}(\Omega) - \Delta A_{\min}(\Omega) \mathrm{d}\Omega, \qquad \text{(A.2.36)}$$

with the relative frequency $\Omega = G^{x/b}$. For class 1 filters, $\overline{\Delta A_{\mathrm{diff}}} = 1.76\,\mathrm{dB}$, and for class 2 filters, $\overline{\Delta A_{\mathrm{diff}}} = 2.23\,\mathrm{dB}$. The associated uncertainty is $u(\mathrm{b_{rel\ resp}}) = \overline{\Delta A_{\mathrm{diff}}}/\sqrt{12}$ when the input distribution is uniform. This leads to the revised combined uncertainties as shown in Table A.8.

When critically discussing the lineup in Table A.8, one may wonder if the filter's linearity is an aspect that still plays a role in modern digital filter implementations.

Table A.8: Uncertainty due to filtering, based on contributions from IEC 61260-1 (2014).

	Limits in dB		Uncertainty in dB	
Filter class	1	2	1	2
Relative response	IEC 61260-1 (2014)		0.51	0.64
Linearity	±0.7	±0.9	0.40	0.52
Effective bandwidth / pass-band attenuation	±0.4	±0.6	0.23	0.35
$u(\mathrm{b_{Filter}})$			0.68	0.90

This leads to the question of whether this aspect should have the same weight as the other uncertainty contributions in Table A.8.

The juxtaposition of the *effective bandwidth* and the *relative response*, as part of the same critical discussion, casts doubt on whether both can be seen independently. Both contributions seem to target characteristics of the filter's shape over frequency. While the *relative response* addresses the deviation from the ideally flat, attenuation-free frequency response, the IEC 61260-1 (2014) definition of the *effective bandwidth* could be understood to characterize the match of adjacent filters in the frequency domain when they are added. The latter characteristic can be very important for hand-held sound level meters, but plays a minor role in room acoustical measurements where the analysis is regularly based on genuine impulse responses.

In a discussion with Wittstock (2018) through personal communication, to better understand the relationships between filter properties and their uncertainty, it was determined that practical reasons motivated Wittstock and Bethke's recognizing the three uncertainty contributions as equally weighted and independent. This exchange of ideas highlighted that the "conditions of use" are an important part of the uncertainty discussion. When nothing is known about the filters being used except for their normative class, the uncertainties given in Table A.8 seem quite large but appropriate. This perspective is very much in line with Wittstock and Bethke (2005).

When the special circumstances of this study are recognized, it can and should be considered that in this study, known 10^{th} order Butterworth filters are used that meet the class 1 IEC 61260-1 (2014) requirements. Figure A.22 shows the filter attenuation over frequency in red, which yields a mean pass-band attenuation of 0.41 dB. The amplitude linearity does not seem to play a significant role

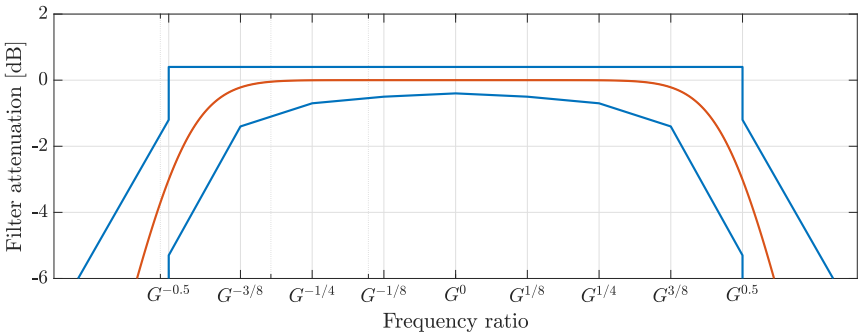

Figure A.22: Class 1 filter tolerances from IEC 61260-1 (2014).

with the modern digital filters used, leading to the assumption that this contribution has no effect on the uncertainty. Likewise, the context of this study gives no indication that the filter's *effective bandwidth* contributes to the uncertainty. Quantitatively, this leads to the following correction term and uncertainty due to filtering:

$$\begin{aligned} \mathrm{b_{Filter}} &= -0.205\,\mathrm{dB} \text{ and} \\ u(\mathrm{b_{Filter}}) &= \frac{0.41\,\mathrm{dB}}{\sqrt{12}} = 0.12\,\mathrm{dB}. \end{aligned} \tag{A.2.37}$$

Measurement procedure

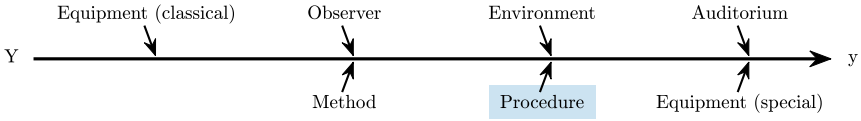

Figure A.23: Ishikawa drawing with shaded category this section refers to.

Sampling - Choice of measurement position Impulse responses in auditoria are regularly considered to depend strongly on the source and receiver positions. A poor choice of measurement positions can therefore be insufficiently complete to comprehensively survey the acoustic conditions. The resulting uncertainty is certainly not the same for all room acoustical quantities: While changes in the early part of the impulse response with dominant individual reflections

vary from one position to the next, the decay constant of the late reverberation is generally assumed to be the same in the entire auditorium (within the limits Davy et al. (1979) indicated). For the latter to hold, the presence of a diffuse sound field is required. Obviously, both conditions cannot simultaneously be met in both the early and late part of a specific impulse response. The transition to the diffusely reverberant part of the impulse response can be determined by the mixing time according to Polack (1992).

In light of Gade and Rindel (1985), this puristic viewpoint is oftentimes only an approximation of conditions encountered in practice. Accordingly, the discussion by Barron (2005) and J. S. Bradley (2005) is relevant as it indicates which characteristics carry meaning when discussed as an average property over the entire auditorium. Other metrics hence require an analysis that includes the measurement position.

These considerations are part of a qualitative discussion that is not intended to yield a quantitative result that could be interpreted as an uncertainty. Instead, it emphasizes the need to clearly identify the target of an investigation and determine a suitable and clearly defined measurement objective and procedure that recognize the natural variation of the sound field from one position to another. Under circumstances that recognize the natural variation as a statistical distribution it is necessary to consider the factor of required sample size.

Sample size - Number of measurement positions Due to the extensive studies by Barron (1984); J. S. Bradley, Gade, and Siebein (1993); Pelorson et al. (1992), specifications exist in ISO 3382-1 (2009) that target the required sample size for measurements in auditoria. This may proove towards an awareness that a sufficient sample is required for meaningful measurements. At the same time, the uncertainty target these provisions are linked to remain open. As Vorländer and Kuttruff (1985) have shown, the distribution of room acoustical quantities depends on the auditorium's geometry and, thus, no unique relation between the number of samples and how they cover the range of the sound field exists.

(Akama et al., 2010) approached this problem from a statistical perspective and investigated the distribution functions of room acoustical quantities when sampling at all seats in different auditoria. The collected distributions diverge from normality and suggest individual nonparametric distributions in different rooms. As such morphologies cannot be adequately described by their means or variances, the center of attention shifts to quantiles. According to Maritz and Jarrett (1978) (and similarly by Harrell and Davis (1982)), the standard uncertainty of quantiles $Q_f(p)$ can be estimated based on the sample size n distribution function $F(x)$. As $F(x)$ depends on the auditorium's geometry, the uncertainty of $Q_f(p)$ can only be determined after measurements have been

conducted. Also, the uncertainty of extreme quantiles increases for "tail-heavy" distributions, thus requiring larger sample sizes.

Documentation of the measurement position The need to determine the measurement location with sufficient precision is addressed in the introduction to this study and represents the central research question. Section 6 presents a method to determine the sensor position through acoustical multilateration methods and Section 10 presents the findings of this study.

Duration of measurement In situations where the time invariance of supposed LTI systems cannot be fully ensured, the data collected during an extended series of measurements may be inconsistent. Similar to curve fitting or numerical optimization problems, this leads to a residual due to a mismatch between the collected data and the underlying measurement model. This difference or inconsistency can be understood as uncertainty in measurements due to uncontrolled changing conditions in combination with the measurement's duration. Reasonable candidates for such uncontrolled influences are contributions that were previously summarized as environmental conditions. Following the terminology of ISO Guide 98-3 (2008), these uncertainties can be associated with the umbrella term of "incomplete knowledge". This classification, however, does not particularly help in assessing how large this uncertainty contribution may be.

This study relies on measurement series that took a relatively long period of time. It is thus reasonable to take this uncertainty contribution into consideration. In order to have an estimate on the order of magnitude of this influence factor, measurements in the Historic Town Hall of Wuppertal and the Berlin Philharmonic Hall in July and August 2006, respectively, were re-evaluated. In these measurement series, impulse responses were collected repeatedly in regular intervals over a long period of time at night. In between these measurements, there was no controlled change in the conditions of the auditorium. In particular, this means that the measurements were carried out completely automatically and no person was in the room during the measurement series. In the case of the Berlin Philharmonic Hall, measurements were collected every 3 min 13 s over a period of about 2 h. In Wuppertal, the repeatability of acoustical measurements was investigated over a period of almost 10 h through measurements every 13 min.

To investigate how the impulse response changed with the progressing measurement time, first the impulse start was determined according to ISO 3382-1 (2009). Next, the signal energy of the impulse response was summarized in fixed Hanning/raised-cosine time windows that had a length of 10 ms and an overlap of 5 ms. This summary provides the energy distribution over the running time of the impulse response in steps of 5 ms. To show the average change in the impulse

responses' energy over the time between two measurements (and over the running time of the RIR), all collected impulse responses in a measurement series were compared. Taking the example of the Berlin measurements, this means that all impulse responses, which were taken integer multiples of 193 s apart, would be compared to each other. For the Wuppertal-data the same was done, except that the time between measurements was integer multiples of 780 s. In each hall three microphone positions were analyzed.

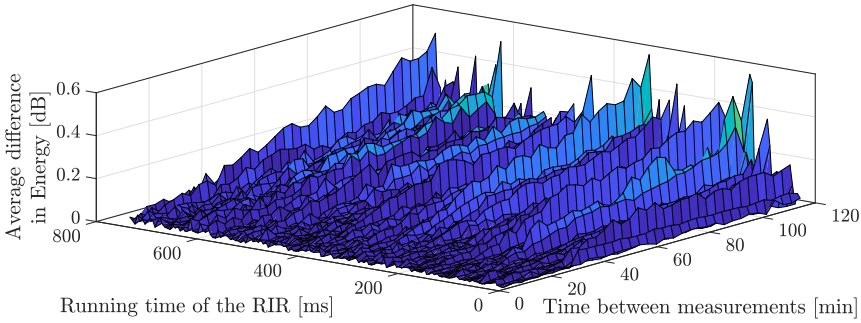

Figure A.24: Change of the RIR as a function of time between measurements.

This analysis leads to results that are shown in Figure A.24 for the example of the first microphone position in Berlin Philharmonic Hall. The axis in the horizontal plane shown to the left indicates the running time of the room impulse response. The time between repeated measurements is depicted in the same plane along the axis to the right. Due to the fixed length in time of this measurement series, the number of pairs N to be compared to each other decreases linearly; for a time of 193 s in between measurements, 36 pairs are available. The vertical axis shows the average difference in level $\overline{\Delta L}(t_{\mathrm{RIR}}, t_{\mathrm{pause}})$ according to Equation A.2.38. $E_i(t_{\mathrm{RIR}})$ refers to the energy in the i^{th} RIR that is collected by the Hamming window at the running time t_{RIR}.

$$\overline{\Delta L}(t_{\mathrm{RIR}}, t_{\mathrm{pause}}) = \sum_{i=1}^{N} \frac{1}{N} \left| 10 \log_{10} \frac{E_i(t_{\mathrm{RIR}})}{E_{i+t_{\mathrm{pause}}}(t_{\mathrm{RIR}})} \right| \tag{A.2.38}$$

With

$$E_i(t_{\mathrm{RIR}}) = \int_{t_{\mathrm{RIR}}-5\,\mathrm{ms}}^{t_{\mathrm{RIR}}+5\,\mathrm{ms}} \sin^2\left(\pi \frac{t+5\,\mathrm{ms}}{10\,\mathrm{ms}}\right) h_i^2(t)\mathrm{d}t \tag{A.2.39}$$

In general, it can be seen (as in Figure A.24) that the differences in the impulse responses become larger with increasing time between measurements. These differences are not of the same order of magnitude for all time windows (along the running time of the RIR). Some time windows in particular show consistently larger average differences, compared to others that show a relatively small variation. Figure A.25 shows the overall trend of the average energy level difference, over the time between measurements t_{pause}, based on all time windows, for both halls, respectively. The blue lines show the measurements in Berlin and Wuppertal. The red lines show the respective 16 % and 84 % quantiles, i.e., the 68 % coverage interval.

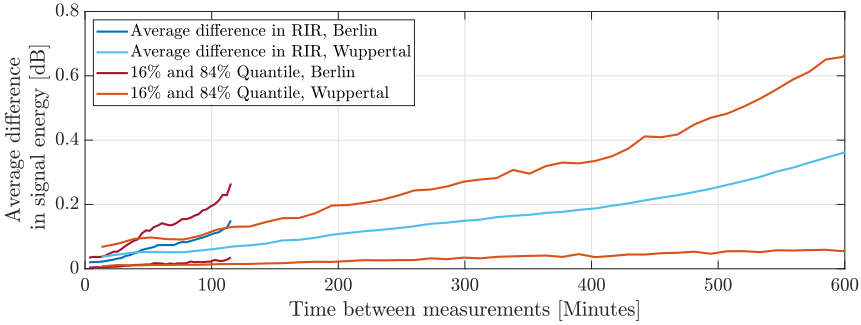

Figure A.25: Change of the RIR as a function of time between measurements.

Figure A.26 shows the average difference over the running time of the impulse response t_{RIR} for measurements in Berlin. Aside from a very moderate increase over t_{RIR}, the graphs show the relatively strong variance between samples of t_{RIR}. This variance is the major factor contributing to the relatively large coverage interval shown in Figure A.25.

Due to the limited sample size of just two measurement series, this data does not warrant final conclusions. Nevertheless, in the absence better data, a first estimate of this uncertainty contribution seems beneficial: From the data shown in Figure A.25, it is evident that the uncertainty increases with longer time intervals in between measurements.

In order not to overinterpret the existing data and thus to limit the complexity, a simple global estimate of this uncertainty contribution is taken. Based on the (arbitrarily chosen) maximum time of 200 min between measurements, an uncertainty of

$$u(\mathrm{b}_{\text{LTI/incomplete knowledge}}) \approx 0.2\,\mathrm{dB} \tag{A.2.40}$$

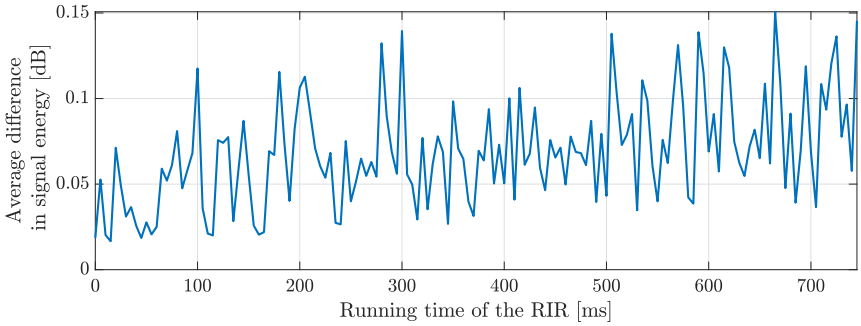

Figure A.26: Change of the RIR as a function of time between measurements.

can be read from Figure A.25.

In a related aspect, the change of the uncertainty over the running time of the impulse response in Figure A.26 seems to be relatively small compared to the uncertainties shown in Figure A.25. Since proving the significance of relatively small effects requires a relatively large sample size, doubts are justified that the uncertainty over the running time of the RIR can be determined accurately from the presented data. In light of the relatively small uncertainty contribution and the open question of validity, this uncertainty contribution will not be recognized in the uncertainty budget. In future investigations a database can be collected that addresses this uncertainty contribution in depth.

Reproducibility According to (ISO Guide 98-3, 2008, B.2.16), reproducibility is the "closeness of the agreement between results of measurements of the same measurand carried out under changed conditions of measurements." This definition raises the question of whether reproducibility can be considered as an independent contribution to the measurement uncertainty at all. When a measurement is defined to the last detail, the uncertainty is expected to approach zero. So, in contrast, if "changed conditions" are considered as possible sources of uncertainty, this either means targeting tolerances in defining the measurement procedure, or discussing uncertainties in implementing the measurement scenario's strict definitions. Against this backdrop, the different reproducibility conditions must be investigated as independent uncertainty factors.

Observer

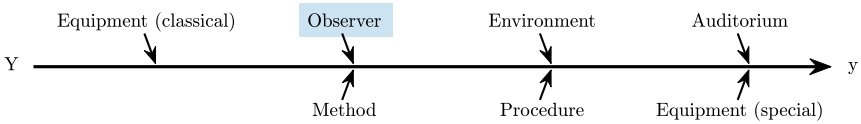

Figure A.27: Ishikawa drawing with shaded category this section refers to.

The "observer-expectancy effect" is a researcher's cognitive bias that influences the outcome of an experiment. Sackett (1979) compiled a catalog of biases he considers relevant in psychological investigations, such as the *literature review*, the *study sample*, the *measurement*, the *analysis*, the *interpretation* and the *publishing* of results as possible biases. The full set of these concepts can be applied to technical investigations, too. A researcher's different experience or background could lead to a different uncertainty inventory compared to those presented in this chapter. The selection of auditoria (study sample) has been addressed before. Since measurements in this context are not limited to psychophysical experiments, it is appropriate to recognize the influence of the observer in technical measurements as well.

The observer bias takes effect wherever the investigator has to make decisions about the further steps of the study. Ishikawa's (1996) model on quality management recognizes the root cause "Man (people)" and identifies observer traits such as *experience*, *qualification*, *reliability* and *motivation* that govern decisions.

It does not require a strong imagination to align this perspective with the process of acoustical impulse response measurements. The immediate interpretation of collected data is required to identify potential problems with the measurement (e.g., to adjust the usable dynamic range in measurements or to fine-tune the excitation signal). Actions to address these shortcomings are occasionally based on rules of thumb or on practical experience. When these relations have a physical/technological foundation but can only be grasped qualitatively, such uncertainty influences are particularly prone to bias and misinterpretation by the observer. Even though these contributions seem intuitively plausible, they cannot be quantified easily.

Ultimately, humility on the author's part seems appropriate in realizing that the present investigation is also subject to uncertainties due the observers and his bias.

Special measurement equipment used in this investigation

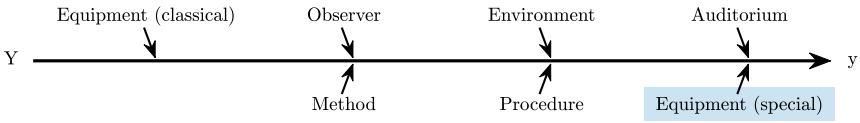

Figure A.28: Ishikawa drawing with shaded category this section refers to.

The discussion of uncertainty contributions has to this point focused mainly on factors that affect the "elementary" measurement problem (i.e., measuring a RIR). When a specific investigation builds on particular measurement tasks, recognizing influences that are characteristic to the pursued strategy becomes necessary.

The methodology described in Section 3 refers to the sampling of sound fields over a large area with an automated setup. The detailed properties of this array are discussed in Section 5. Using a larger apparatus, however, raises the question of how such structures disturb the sound field being measured. Additionally, the validity and the properties of the sampling strategy need to be investigated.

Disturbance of the sound field The measurement apparatus requires two elements: a structure that is capable of supporting the mass of the microphones, and actuators that permit moving the receivers automatically. This structure introduces surfaces and bodies into the sound field that reflect and scatter the sound. As a rule of thumb, scattering needs to be considered when the structure assumes dimensions that are comparable to those of the wavelength in question. It makes sense to consider this uncertainty component at a later stage in the uncertainty budget, since the measurement device is custom-made and cannot be considered part of the established measurement repertoire. In Chapter 5, the detailed characteristics of the measurement setup are presented. Its influence on the measurement uncertainty is quantitatively investigated with reference to Appendix B using analytical and empirical methods. This uncertainty will amend the uncertainty budget in Chapter 5.

Sampling strategy The topic of sampling needs to be illuminated from different sides and at different scales. From a statistical perspective, sampling is related to the task of selecting a representative subset from a global population. This choice must be made both within the spectrum that different auditoria span, and within the sound field of an individual room. The uncertainty resulting from

the choice of the sampled sound fields is difficult to quantify, but an honest and critical discussion can possibly help to identify relevant factors.

In signal processing, sampling refers to transforming a continuous signal into a discrete signal. When aspects of signal theory are considered in the discussion about sampling, the measurement position of individual microphones becomes important. Based on the spatial Nyquist-Shannon sampling theorem, a relation between the highest spatially resolvable frequency and the minimum distance between microphone positions can be devised. For frequencies up to and including the 2 kHz-octave band, a sampling resolution of 5 cm is sufficient for an error-free synthesis of the sound field. This order of magnitude must be taken as a guiding rail, even if synthesizing the sound field is not the aim of this study.

In this context, the properties of possible sampling patterns must be observed, too: Their suitability and potential uncertainty have to be discussed in regard to the intended analysis. As an example: a regular and rectangular sampling grid may lends itself to synthesis, yet may introduce preferential directions when other analyses are pursued. These aspects are investigated in Section 5.

Finally, the implementation of the sampling also plays a role, i.e., how uncertain the targeted sampling location is. Section 6.3 discusses how the measurement position can be determined through an acoustical multilateration method. Based on this data the actual measurement position and its associated uncertainty can be determined. As far as it concerns a regression or a synthesis problem, the uncertainty due to inaccurate measurement positions can be described using the standard Berkson error model (Berkson, 1950; Carroll et al., 2006). As long as the position error is small compared to the surveyed sampling area, the introduced uncertainty can be neglected.

Correlations

According to the GUM framework ISO Guide 98-3 (2008) it is necessary to consider correlations between individual uncertainty contributions, as such correlations can significantly increase the combined measurement uncertainty. Equation 2.3.3 gives a mathematical account of how the uncertainty contribution's mixed terms of covariances add to the uncertainty of the uncorrelated individual terms.

Wittstock and Bethke (2005) discuss the same measurement equipment and the same calibration normal or the same measurement sensors as candidates for such correlated influences. These may be relevant to this investigation as well. Another factor is that the acoustic propagation model assumes a diffuse field, which rarely exists in real sound fields. The model that adjacent samples (in the time domain) of the measured impulse response are subject to uncorrelated

uncertainties seems a strong simplification. This knowledge can potentially serve as a basis to refine the underlying models in future studies and thus provide more accurate estimates of the measurement uncertainty in room acoustics. In this study correlation terms are not considered, matching the approach taken by Wittstock and Bethke (2005).

A.3 Results - Calculation stage

The combined uncertainty is determined according to ISO Guide 98-3 (2008), using Equation 2.3.3. Based on the previous discussion, correlations between input quantities are not considered, which simplifies Equation 2.3.3 to Equation 2.3.2. As a result, the combined uncertainty of the measured impulse response is the root mean square (rms) of the individual influence quantities' uncertainty.

Uncertainty Budget for classical measurement equipment

The full budget of all the discussed influences in this chapter is given in Table A.9. The uncertainty inventory is sorted, starting with the largest uncertainty contribution.

Table A.9: Measurement uncertainty budget for a basic measurement problem

Symbol b_i	Uncertainty source	Knowledge base	Uncertainty contribution $u(b_i)$ [dB]
$b_{\text{LS-dir}}$	Directivity	Behler and Vorländer (2018)	0.38
$b_{\text{LS-level}}$	Calibration measurement	Wittstock and Bethke (2005) with revised contributions	(0.45) 0.26
$b_{\text{Mic-cal}}$	Pistonphon calibration	Wittstock and Bethke (2005)	0.21
b_{LTI}	Long term repeatability	Measurements in two auditoria	0.2
$b_{\text{LS-spec}}$	Equalization measurement	Revised contributions based on Wittstock and Bethke (2005)	0.16

Table A.9: (continued)

Symbol b_i	Uncertainty source	Knowledge base	Uncertainty contribution $u(b_i)$ [dB]
$b_{\text{Mic-spec}}$	Flatness of microphone freq. response	32 measurements (LAS)	0.15
b_{Filter}	Octave-band filtering	Wittstock and Bethke (2005) with revised contributions	(0.68) 0.12
$b_{\text{Meteo-}\vartheta}$	Change in temperature	Payne (2004)	0.12
$b_{\text{Meteo-p}}$	Change in athm. pressure	Payne (2004)	0.07
$b_{\text{Mic-dir}}$	Directivity	measurements in 3° resolution (MMT)	0.07
$b_{\text{Mic-field}}$	Sound field distortion	Payne (2004)	0.011
$b_{\text{Meteo-rh}}$	Change in rel. humidity	Payne (2004)	7.5×10^{-3}
$b_{\text{LS-THD}}$	Loudspeaker nonlinearities	Behler and Vorländer (2018)	$\approx 1\times10^{-3}$
$b_{\text{Amp-THD}}$	Power amplification	Manufacturer's specifications	$\approx 1\times10^{-4}$
$b_{\text{Mic-amp}}$	Amplification linearity	Payne (2004) own experience	(0.17) $\approx 1\times10^{-4}$
$b_{\text{Amp-SNR}}$	Amplification noise	Technical documentation	$\approx 1\times10^{-6}$
$b_{\text{Mic-SNR}}$	Microphone noise	Technical documentation	$\approx 1\times10^{-6}$

Table A.9: (continued)

Symbol b_i	Uncertainty source	Knowledge base	Uncertainty contribution $u(b_i)$ [dB]
$b_{\text{D/A-SNR}}$	D/A noise	Technical documentation	$\approx 1\times10^{-8}$
$b_{\text{D/A-THD}}$	Digital-Analog distortion	Manufacturer's specifications	$\approx 1\times10^{-8}$
$b_{\text{clock jitter}}$	clock jitter	Neu (2010)	$\approx 1\times10^{-8}$
$b_{\text{Mic-THD}}$	Microphone nonlinearities	Manufacturer's specifications	$\approx 1\times10^{-9}$
$b_{\text{A/D-THD}}$	Analog-digital conversion	Manufacturer's specifications	$\approx 1\times10^{-9}$
$b_{\text{quant-SNR}}$	Quantization noise	Havelock et al. (2008), specifications	$\approx 1\times10^{-12}$
$u_c(b_{\text{Equip}})$	Combined uncertainty		0.62
$U(b_{\text{Equip}})$	Expanded uncertainty	k=2	1.24

The combined uncertainty given in the last row of Table A.9 can be calculated according to Equation A.3.1 with all significant (larger than 1×10^{-2} dB) contributions included. Influences that introduce a background noise to the measurement are not recognized.

$$\begin{aligned} u_c(b_{\text{Equipment}}) = [&u^2(b_{\text{LS-dir}}) + u^2(b_{\text{LS-level}}) + u^2(b_{\text{LTI}}) + \\ &+ u^2(b_{\text{LS-spec}}) + u^2(b_{\text{Mic-spec}}) + \\ &+ u^2(b_{\text{Mic-cal}}) + u^2(b_{\text{Filter}}) + \\ &+ u^2(b_{\text{Meteo-}\vartheta}) + u^2(b_{\text{Meteo-p}}) + \\ &+ u^2(b_{\text{Mic-dir}}) + u^2(b_{\text{Mic-field}})]^{\frac{1}{2}} \end{aligned} \tag{A.3.1}$$

This leads to a combined standard uncertainty of

$$u_c(\mathrm{b_{Equip}}) = 0.62\,\mathrm{dB}, \tag{A.3.2}$$

which reduces to

$$u_c(\mathrm{b_{Equip}}) = 0.56\,\mathrm{dB} \tag{A.3.3}$$

when not considering the sound power calibration, and to

$$u_c(\mathrm{b_{Equip}}) = 0.52\,\mathrm{dB} \tag{A.3.4}$$

when neither the sound power nor the pistonphon calibration are taken into account.

For a breakdown between systematic and random effects the reader is referred to Section 6.2.1. When discussing the uncertainty of most room acoustic quantities, contributions that systematically affect all time samples of the measured impulse responses in the same way do not have to be considered.

A.4 Discussion

The practical uncertainty discussion comes with fundamental challenges that can be discussed effectively using the influence of octave band filters. In this case the uncertainty contribution has been determined based on literature considering unfavorable scenarios, leading to a significant increase of Wittstock and Bethke's original uncertainty budget. This increase in uncertainty is partially based on revised IEC 61260-1 (2014) specifications, but also on revised calculation principles. However, this modification is not to be misunderstood as ignoring the experience behind Wittstock and Bethke (2005)'s initial assessment: In personal correspondence with Wittstock in February 2018, the rationale behind the 2005 review was discussed. It was determined that, oftentimes, pragmatic approaches are necessary to determine initial uncertainty estimates. Secondly, the acceptable range of values specified in standards is regularly set large enough to cover a wide range of conceivable applications. Without additional knowledge, these limits are definitely a useful basis for determining uncertainties. When it can be argued in good faith, however, that these general boundaries overestimate the common practice or do not represent a specific measurement situation, it is necessary to revise the general uncertainties.

Despite this faithful revision, the uncertainty discussion of the filter contributions still appears incomplete. With the general correction term of $-0.2\,\mathrm{dB}$, an equalization was pursued that would still not brutally force the filter to an ideal rectangular shape. This strategy avoids overshooting the discrete and low-pass

filtered rect-function in the frequency domain and the considerable decay times of the sinc function in the time domain. The latter aspect highlights that, so far, the time domain behavior of filters finds no consideration in the relevant standards. As a result, this aspect is not part of the uncertainty discussion even though the distribution of energy over the RIR's running time is a crucial argument in architectural acoustics.

Uncertainties in the time domain also play a role in the uncertainty due to changes in the speed of sound (i.e., through a change in temperature) that will show in the RIR through scaling of the time axis. Brute force methods would yield enormous uncertainties when phase relationships (i.e., small shifts in energy over time) are not discussed using sensible tools. Here, further investigations are required to illuminate open questions.

In other cases, the data to determine the uncertainty is relatively sparse, too. In such cases it is reasonable to develop a first uncertainty assessment based on small data samples. Such a first estimate presents an advance compared to the lack of knowledge in the absence of any data at all, even when this first ad hoc estimate may have to be revised later once better data becomes available. The investigations to determine the LTI properties of auditoria may be a valid example in this regard.

The largest uncertainty contribution relates to the normalized radiated power of the sound source. This aspect needs to be seen relative to the loudspeaker's directivity and frequency response. Determining the radiated sound power is a relatively complex measurement problem and taxing it with an uncertainty influence of 0.45 dB (Wittstock & Bethke, 2005) is reasonable. In architectural acoustics, however, this information is only of interest when individual measurements of sound strength are investigated. As a result, in many cases recognizing this uncertainty contribution may not be necessary.

At the same time, however, the directivity and spectral properties of the sound source are quite significant, and knowing these characteristics of the source is important. The source's sound power is almost a coincidental byproduct of spectral directivity measurements, and thus it is not entirely clear how these uncertainty contributions should and could be kept separate. Correlation effects almost certainly play a role with these three uncertainty contributions.

Automated goniometric devices are an important tool for directivity measurements that may reduce that uncertainty significantly. It would be interesting and meaningful to look at this aspect in further detail and add to the work of Pazen et al. (2011).

A differentiating discussion also becomes necessary when different sources seemingly contradict each other in their uncertainty assessments. Oftentimes this is due to seemingly similar measurement problems that differ enough from each

other that a plain comparison is simply no longer valid. An example may be the uncertainty due to the linearity of the microphone's amplifier. The specifics of hand-held sound level meters may not be transferable to other measurement environments and may thus require their own assessments.

Further down the list of contributing uncertainties are the influences of the system's nonlinear behavior, which have been studied by many investigators. Based on the uncertainty discussion here, it seems, once basic rules of good measurement practice are adhered to, nonlinearities do not play a significant role in (relatively) simple measurement problems.

Two final perspectives are worth discussing: Numerous influences have been subject to a qualitative discussion in order to point out general relationships. Many of these contributions feature staggeringly high degrees of freedom, which makes a proper uncertainty discussion still unfeasible. Approaching this challenge requires additional studies that may have to place a stronger emphasis on the properties of dynamic measurement systems. Here, the dynamic nature of room impulse response measurements (in architectural acoustics) has not been investigated at the level that may become necessary in the future.

A.5 Conclusions

This section discusses the intrinsic uncertainty of room acoustical measurements. To follow an organized approach, quality management principles using a cause-and-effect perspective were used to identify and group different uncertainty contributions. Based on the GUM framework more than 20 influence factors were discussed quantitatively and reasonable uncertainties were determined that characterize the properties of the measurement environment.

As a result, the expected uncertainty of individual time samples in measured room impulse responses due to the used equipment is

$$u_c(\mathrm{b}_{\mathrm{Equipment}}) = 0.52\,\mathrm{dB}. \tag{A.5.1}$$

This uncertainty will be used in this study's main line of argument to determine the uncertainty of room acoustical single number quantities (see Section 6.2).

B

Influence of the measurement apparatus on the sound field

B.1 Introduction

The question of how the array setup affects the acoustical measurement was already raised in Chapter 5, but was only considered phenomenologically there. Introducing sensors and other equipment may alter sound propagation and thus disturb the original sound field with additional reflected or scattered sound. The issue of the measurand being affected by the measurement setup is an important factor in measurements in general, but is considered here in the context of acoustics.

For a more detailed discussion, the question is approached from two directions: First, computational solutions are considered from the theoretical point of view. This has the advantage that the disturbance can be examined without secondary influences. The disadvantage, however, is that the geometry may have to be simplified in order to build on closed-form solutions. Thus, there is a risk that the analytical solution does not correctly represent the targeted scenario.

In a second strategy, the influence of the measurement setup is empirically investigated. This has the advantage that the properties of the measuring apparatus actually being used serve as a basis. In the wide range of influences that can affect the uncertainty of measurements, there is sometimes a danger that subtle disturbances will be difficult to detect. The findings from the first scenario's analytical predictions may prove helpful in this regard, as they identify measurement locations which are particularly vulnerable to the disturbance. By combining both strategies, the plausibility of the results can be evaluated.

B.2 Analytical approach

B.2.1 Methodology

The profound starting point for the calculation of sound scattering is Huygens's principle and its quantification by Kirchhoff, Fresnel and Helmholtz (Morse & Ingard, 1968, p. 400 ff.). Although this theory is generally suitable to describe the scattered sound field for arbitrary incident waves and arbitrary scattering bodies, the resulting surface integrals can become very complicated to solve: It is not guaranteed that a closed form solution to these integrals is known at all. For this reason it makes sense to simplify the geometry of the scattering body and the incident wave in a suitable way so that the complexity of the problem is reduced to a point where known solutions are available.

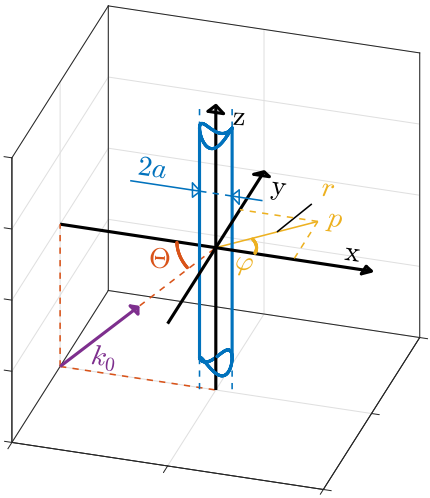

Figure B.1: Geometry of Mechel's case E.1 scenario: A plane wave in the xz-plane, at an oblique incident angle Θ that is scattered at an infinitely long cylinder of diameter $2a$. The observation point p is in the xy-plane.

For this specific measurement setup, this translates into three simplifications: The distance between the sound source and the experimental setup (in relation to the dimensions of the supporting trusses) is recognized to be large. This means that the incident wave can be considered planar. Second, the detailed geometry of the trusses, with their triangular cross-section and the small stiffening struts, is simplified into a single infinitely long cylinder. Ultimately, this simplification

is justified on pragmatic grounds due to the apparent similarity in geometry and the availability of relatively simple analytical solutions to calculate the scattered sound field. Third, the difference in impedance between the propagation medium and the material of the scattering body (i.e., air and aluminum) is assumed to be very large. This means the scattering body's inner sound field can be neglected and the body's admittance G is zero.

These assumptions reduce the sound field to a plane wave at an oblique incident angle Θ that is scattered at an infinitely long cylinder of a diameter $2a$ (Mechel, 2008, Case E.1). Figure B.1 defines the geometric parameters. The total exterior sound field is the sum of the incident plane wave and the scattered wave as shown in Equation B.2.1.

$$\begin{aligned} p(r,\varphi,z) &= p_{\text{incident}} + p_{\text{scattered}} \\ &= e^{-jk_0 z\sin\Theta}\Big[J_0(k_0 r\cos\Theta) + D_0 H_0^{(2)}(k_0 r\cos\Theta) + \\ &\quad + 2\sum_{m=1}^{\infty}(-j)^m\cos(m\varphi)\Big(J_m(k_0 r\cos\Theta) + D_m H_m^{(2)}(k_0 r\cos\Theta)\Big)\Big] \end{aligned} \tag{B.2.1}$$

with

$$D_m = -\frac{\frac{m}{k_0 a}J_m(k_0 a\cos\Theta) - \cos\Theta J_{m+1}(k_0 a\cos\Theta)}{\frac{m}{k_0 a}H_m^{(2)}(k_0 a\cos\Theta) - \cos\Theta H_{m+1}^{(2)}(k_0 a\cos\Theta)}$$

for the admittance $G = 0$, with Bessel functions $J_m(z)$ and Hankel functions of the second kind $H_m^{(2)}(z)$.

Essentially, in Mechel's E.1 case the impeding wave can be understood as a superposition of two plane waves propagating in the z-direction and in the x-direction. The wave traveling along the z-axis does not interact with the scattering body, as the wave's particle velocity normal to the rigid cylinder's surface is zero. In Equation B.2.1, $e^{-jk_0 z\sin\Theta}$ describes this plane wave propagating along the z-axis with unit amplitude. $k_0\sin\Theta = k_z$ can be understood as the projection of k_0 onto the z-axis, which means that the angle of incidence Θ defines the period of the wave traveling along the cylinder. Apart from the oscillation in the z-domain, the amplitude of the total sound field is not affected by the exponential term. As a result, this term can be omitted when discussing how much the sound field is altered by the scattered body.

For the second component, i.e., the plane wave in the x-direction, the inner terms of the Bessel and Hankel function ($k_0 a\cos\Theta$ and $k_0 r\cos\Theta$) are important. Similarly, $k_0\cos\Theta = k_x$ is the projection of k_0 on the x-axis. Thus, when interested in the scattered sound field, two core aspects emerge:

- The size of the scattering body ($2a$) relative to the impeding wave's (projected) wavelength ($2\pi/k_x$).
- The distance r between the investigated field point $P(r, \varphi)$ and the scattering body, in relation to the impeding wave's (projected) wavelength ($2\pi/k_x$).

In this light it becomes clear that the initial approach given through Equation B.2.1 can be further simplified using Mechel's case E.2 with k_x as the x-component of k_0, yielding Equation B.2.2:

$$p(r,\varphi) = J_0(k_x r) + D_0 H_0^{(2)}(k_x r) + 2\sum_{m=1}^{\infty}(-j)^m \cos(m\varphi)[J_m(k_x r) + D_m H_m^{(2)}(k_x r)] \tag{B.2.2}$$

with

$$D_m = -\frac{\frac{m}{k_x a}J_m(k_x a) - J_{m+1}(k_x a)}{\frac{m}{k_x a}H_m^{(2)}(k_x a) - H_{m+1}^{(2)}(k_x a)} \text{ for the admittance } G = 0$$

In the next steps, Equation B.2.2 is evaluated numerically and the results are discussed from different perspectives. This is done with the aim to determine the largest expected disturbance to the sound field by the cylindrical scattering body.

B.2.2 Results

Angular variation

In Equation B.2.2 it can be seen that the angular dependence (φ) essentially arises from the sum and particularly from the contained cosine weighting of the Bessel and Hankel functions. Since both J_m and $H_m^{(2)}$ can assume positive and negative values, there is no obvious argument that hints at how this sum converges. Based only on energetic considerations, it could be suggested that the sum of potentially incoherent terms in Equation B.2.2 becomes extreme for $\varphi = \pi$.

Figure B.2 shows the results of Equation B.2.2's numerical evaluation of the total field. The amplitude $|p(r, \varphi)|$ is shown in logarithmic scale relative to the unit amplitude of the impeding wave for $f = 1\,\text{kHz}$ and $2a = 35\,\text{mm}$. Since f and a scale the result along r in cylindrical coordinates, Figure B.2 is evidence that the assumption that disturbances become extreme for $\varphi = \pi$ is correct. The strongest disturbance of the sound field by a cylindrical scattering body is

therefore to be expected at the side facing the incident wave. Disturbances in the "shadow zone" are much smaller and more homogeneous.

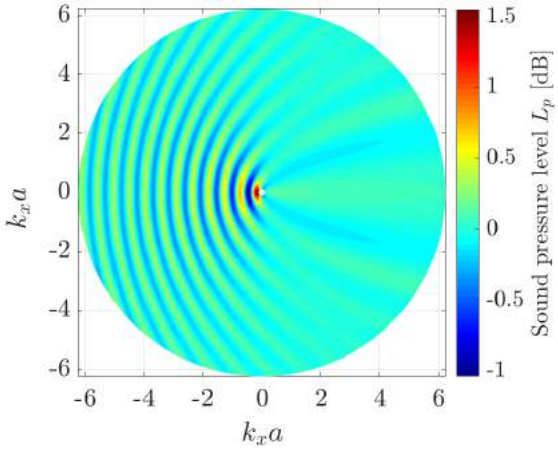

Figure B.2: Mechel case E.1 - Total SPL scattered around a rigid cylinder.

Variation over frequency and distance

The next step is to add the frequency as a variable. Since we are interested in the largest possible disturbance of the sound field, it is sufficient to consider only $\varphi = \pi$ as a function of distance r to the origin.

Figure B.3 shows the amplitude of the total field (SPL) at different frequencies and at different distances from the scattering body. The left edge of the diagram shows the sound pressure level at the surface of the body. The white line marks the locations of the disturbance's largest absolute value as a function of frequency.

It can be seen that the oscillation has a longer spatial period with decreasing frequency. The maximum disturbances are fairly small at low frequencies, but they reach relatively large distances from the scattering body. At higher frequencies, the interference becomes stronger while the absolute maximum moves closer to the scattering body.

At higher frequencies, there are indications that it may not be sufficient to focus solely on the greatest disturbance at a given frequency. There are numerous local extremes in absolute value that extend relatively far into the sound field and thus may be relevant as well. This raises the question of how close a microphone can be placed to the scattering body without exceeding a given upper limit of the disturbance. This question can of course be answered for a given distance

$r_{\min}$ and frequency f based on the data shown in Figure B.3 by determining the largest absolute value of the disturbance for all distances between $r_{\min}$ and ∞:

$$\arg\max_{r \geq r_{\min}} |L_p(f, r)|. \tag{B.2.3}$$

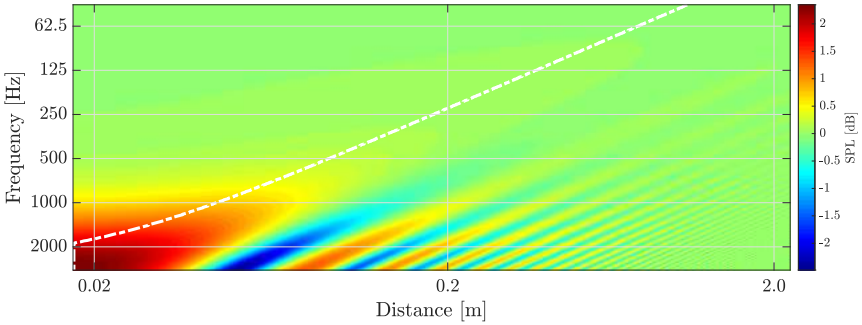

Figure B.3: Mechel case E.2: Disturbance of the sound field relative to the impeding plane wave of unit amplitude as a function of frequency and distance to the scattering cylinder.

These minimal distances are shown as a function of frequency in Figure B.4. The color indicates the maximum absolute value of the disturbance according to Equation B.2.3.

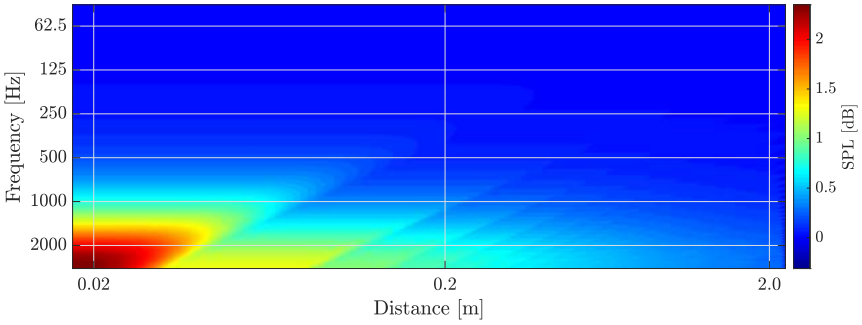

Figure B.4: Mechel case E.2: Maximum absolute value disturbance to the sound field over frequency at a given minimum distance from a scattering cylinder

Since color gradients are generally difficult to quantify, it makes sense to com-

press the data from Figure B.4 even further and plot the disturbance's maximum absolute value over frequency as a function of distance according to Equation B.2.4, as shown in Figure B.5. For the frequency range between the 62.5 Hz and 2 kHz octaves, it can now be determined that, to avoid disturbances exceeding 0.85 dB, microphones may not be placed closer than 20 cm to a scattering cylinder with a diameter of 3.5 cm. At distances greater than 30 cm, the maximum disturbance is 0.74 dB. This assumes a sinusoidal excitation at a single frequency.

$$\underset{\frac{62.5\,\mathrm{Hz}}{\sqrt{2}} \le f \le \sqrt{2}\,2\,\mathrm{kHz}}{\arg\max} \left(\underset{r \ge r_{\min}}{\arg\max} \, |L_p(f, r)| \right). \tag{B.2.4}$$

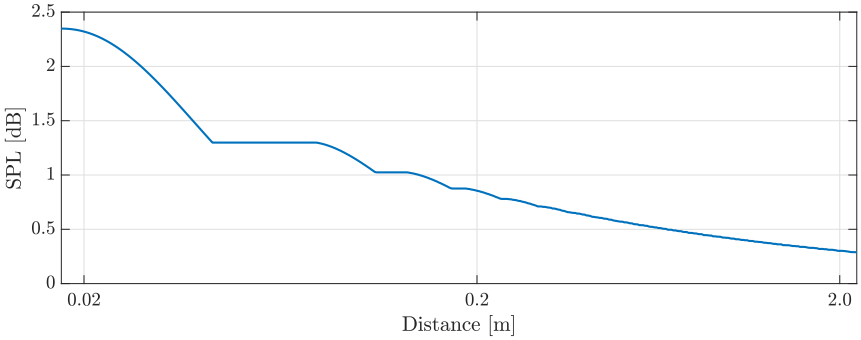

Figure B.5: Mechel case E.2: Maximum absolute value disturbance to the sound field at a given minimum distance from a scattering cylinder.

The influence of the disturbance on an incident plane wave appears relatively large compared to what practical experience would suggest. The main reason for this discrepancy may be the calculation's paradigm of vertical sound incidence on the scattering cylinder. Additionally, the data compression that led to Figures B.3 and B.4 considered only regions directly in front of the scattering body. It is easy to see that this represents a worst-case scenario that overestimates the sound field interference under realistic conditions.

Scattering from a cylinder in the diffuse sound field

With a reflection density increasing towards later times in the impulse response, theory suggests a transition to the diffuse sound field (Kuttruff, 2000). Due to the rotational symmetry around the z-axis, it can be seen that Θ and φ are evenly distributed in the interval between 0 to π and 0 to 2π, respectively. The sound

pressure level $\overline{p(r)}$ in the diffuse sound field can be determined as a function of distance according to Equation B.2.5

$$\overline{p(r)} = \frac{1}{2\pi^2} \int_0^{\pi} \int_0^{2\pi} |p(r, \varphi, \Theta, z)| \, \mathrm{d}\varphi \, \mathrm{d}\Theta \tag{B.2.5}$$

Figure B.6 shows $\overline{p(r)}$ at 1 kHz in logarithmic scale. It can be seen that the disturbance to the diffuse field is below 0.04 dB for reasonable distances from the scattering body. These values are one order of magnitude lower compared to the single plane wave case. Based on previous findings, it can be expected that the trend shown in Figure B.6 stretches along distance and reduces in amplitude as the frequency decreases.

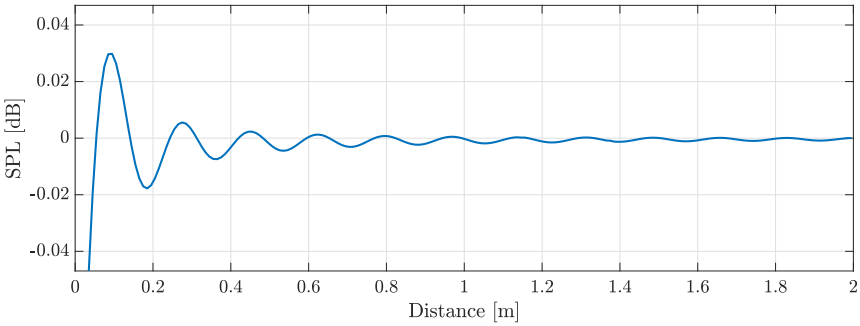

Figure B.6: Mechel case E.2: Scattering in the diffuse field at 1 kHz

Reference to the actual measurement situation

In the measurement setup, the microphones are suspended rigidly from the carbon truss by the approximately 1 m-long carbon tubes. Both the carbon truss and the aluminum frame structure are therefore at least 1 m away from the sampling locations. Figure B.5 shows that under the most unfavorable (and therefore less realistic) conditions, an interference of up to 0.42 dB may be expected.

However, the four supports, which carry the weight of the entire array, are closer to the sampling grid. The corner positions of the measurement surface are the most critical locations, as these are only up to 30 cm away from the vertical pillars. Figure B.5 shows the largest possible interference to be up to 0.74 dB. In the diffuse sound field, the interference still appears negligible.

Analytical closed-form solutions reach their limits when the scattering body is no longer assumed to be a simple cylinder, but rather a truss that consist of three

cylinders. It can be argued that the scattered field of the truss can be determined in a first-order approximation by superposition of the fields from three individual cylinders. Mathematically, however, the concept is challenging to implement. First, the incident plane wave reaches each individual cylinder at a different phase. Second, for the transmission path from the scatterer to the receiving point P, a translation must be taken into account either on the sending or receiving side. In either case, this will makes the expressions in Equations B.2.1 and B.2.2 much more complex as Bessel and Hankel functions are solutions to the wave equation for rotationally symmetric cases.

For these reasons, it makes sense to also investigate the scattered sound field empirically.

B.3 Empirical approaches

B.3.1 Methodology

Matching analytical and empirical approaches

In the previous section on analytical approaches, a joint perspective of telecommunications and theoretical acoustics was taken that recognized the sound field as the sum of an incident plane wave (signal) and an interfering scattered wave (noise). This was essentially done for reasons of mathematical simplicity and to build on existing solutions. This perspective - and the normalization to the unit amplitude of the incident plane wave - made it relatively easy to identify the disturbance as a deviation from 0 dB.

While these theoretical concepts are understood as simplifications of the real-life scenario encountered in measurements, the findings from theory cannot be seen as final results. At the same time, the data does highlight spatial regions of interest and lines of argument of where and how measured data can be analyzed to evaluate the disturbance. Nevertheless, it is not self-evident how scattered sound from the supporting structure can be identified in the presence of a complex sound field featuring direct sound, reflections and reverberation.

In Chapter 5, specifically Figure 5.6 (left), it was discussed how the scattering from the apparatus could be identified in the empty hall right after the direct sound. In a simplified view, following the mirror image source model, the impulse response could be understood as the sum of many sound events, including the direct sound. This interpretation is not very far from the signal/noise approach that was considered when following the analytical approach. In fact, because of the superposition principle, the energetic SNR for the entire RIR is equal to the SNR of the direct sound and its scattered wave:

$$L_{\mathrm{SNR}} = 20 \log_{10} \frac{|\bar{p}_{\mathrm{scatter}}|}{|\bar{p}_{\mathrm{direct}}|}. \tag{B.3.1}$$

In this reasoning, the direction of sound incidence is not correctly recognized for most of the reflections and the reverberation. Therefore, the presented idea should be understood as a pragmatic approach in the absence of a more accurate concept.

Analysis of the direct sound

In implementing this approach, the first challenge is determining the energy of an isolated wave front. Figure B.7a shows the first 10 ms of a measured impulse response. In contrast to idealized concepts, due to the band limitation during the measurement, the direct sound does not resemble a perfect delta dirac function. Instead, it consists of a sequence of oscillations with about three local extremes. In addition, the direct sound and the reflection at the floor in *Eurogress Aachen* are so close to each other in the time domain that the two wave trains partially overlap.

The appreciation that these are two sound events, nevertheless, results from the inspection of this impulse response's initial part measured at different distances to the source. This detailed observation is not discussed here in depth since this separation into individual sound events is not essential to the line of argument. Even when the "useful" signal consists of a number of signal components that are difficult to separate, the resulting scattered "noise" consists of the same number of signals as well. As long as the signal and noise components can be identified unambiguously, and as long as both parts are the result of the same sum, their ratio can be determined.

The start of the impulse response can be determined very easily and reliably from the definition in ISO 3382-1 (2009) with a reduced threshold of −9 dB. The inspection of different impulse responses of different distances to the sound source shows that the first two sound events have a maximum length of 2.2 ms in the time domain. The signal energy in this time interval can be seen as the best estimate of the energy of the direct sound and the floor reflection. The energy is plotted in Figure B.7b over the entire sampling area relative to the maximum occurring energy.

The geometry of the measurement setup is known, and therefore it is possible to determine the time window in which the direct sound passes the four supporting pillars. These vertical trusses are also the origin of the cylindrical scattered waves, and thus for each measurement location a time window can be calculated at which the scattered sound travels through the sampling area. Due to the dimensions

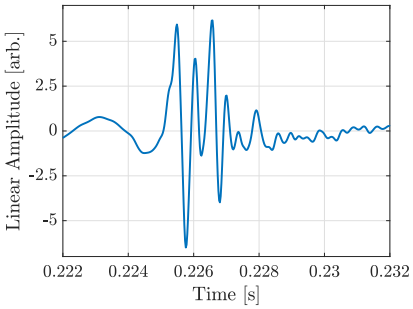

(a) The first 10 ms of a measured impulse response in Eurogress Aachen without chairs.

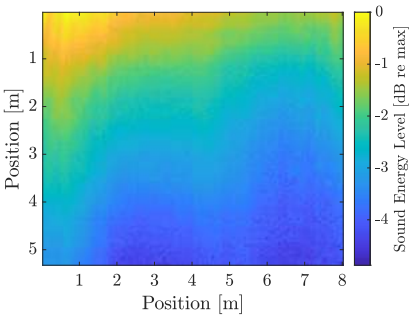

(b) Energy of the direct sound in the sampling area relative to the maximum encountered direct sound energy.

Figure B.7: Analysis of measured impulse responses.

of the columns, this time window for the scattered sound is slightly longer (i.e., 2.4 ms) than the time window for the direct sound. The energy of the scattered sound can be determined in the same way that the energy of the direct sound was calculated.

B.3.2 Results

Figures B.8a and B.8b show the level of the scattered sound from the two columns closest to the sound source relative to the direct sound (Equation B.3.1). Many regions show relatively low levels (in blue and green colors), whereas the areas directly behind the supports show much higher levels (in yellow). The latter suggests that the scattered sound has almost the same energy as the initial wave. Upon close reflection it becomes clear that the direct and the scattered sound waves pass the sensor at almost the same time, and are thus inseparable using only simple geometric considerations. In other regions of the sampling area the two signal components are readily distinguished, and it can be seen that the scattered waves carry at least 20 dB less energy compared to the direct sound. In both graphs, narrow-striped regions are evident that show a lower signal-to-noise ratio in greenish colors. Such a reduction in SNR occurs when tertiary reflections exist in the evaluation interval of the scattered sound. As an example, the green region ranging from the top center to the bottom left (1 m in Figure B.8a is due to the scattering of both frontal pillars interfering with each other. Other reflections may be due to scattering from the frame above.

Figure B.8c and B.8d show the energy level of the scattered sound from columns

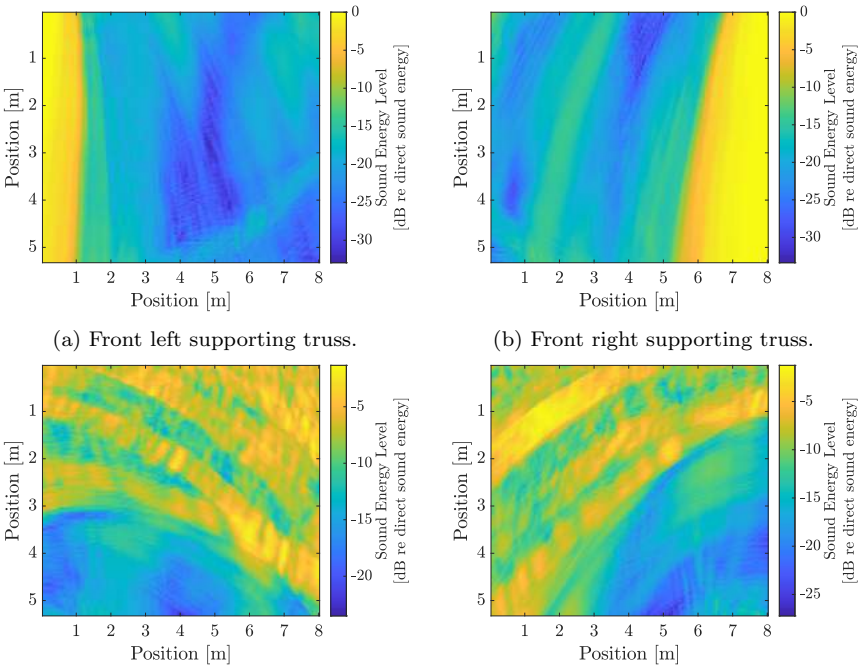

(a) Front left supporting truss.

(b) Front right supporting truss.

(c) Rear left supporting truss.

(d) Rear right supporting truss.

Figure B.8: Energy level L_{SNR} of the scattered sound from the supporting pillars relative to the direct sound.

that are located behind the sampling area (as seen from the sound source). In the regions close to the supports the signal-to-noise ratio is about $-15\,\mathrm{dB}$, which is shown in blue and turquoise colors. The upper (frontal) part of the sampling area, however, is dominated by yellow color tones showing narrow regions of very low SNRs. These isolated areas occur when the scattered waves from the columns coincide with high amplitude reflections from the hall's large surfaces. Since these reflections have significantly more signal energy than the scattered sound, it is no longer possible to determine a reliable signal-to-noise ratio.

In summary, it can be said that at each measurement location four scattered waves are to be expected. Reflections from the columns "in front" of the sampling field are likely to have amplitudes of about $-20\,\mathrm{dB}$, whereas reflections from the supports "behind" the sampling area are likely to have amplitudes of around $-15\,\mathrm{dB}$. Adding these four signals incoherently to the direct sound (with a level of $0\,\mathrm{dB}$) yields a total level of $0.35\,\mathrm{dB}$.

B.4 Discussion

Theory

The question of how strongly the measurement setup affects the measurand was investigated in two stages. In the first step, the scattered sound field of a cylindrical body, irradiated by a plane wave, was discussed on the grounds of available analytical solutions. From these considerations, it was possible to identify regions around the scattering body that are particularly affected by the backscattering. In the reference system of the incoming wave, the zones in front of the scatterer are of particular relevance to study the adverse effects of the measurement setup. In the zones behind the cylinder, the scattered sound field has a significantly lower amplitude.

Based on a worst case scenario, considering the disturbance in front of scattering bodies, an uncertainty of 0.74 dB can be expected in the frequency range from the 62.5 Hz to 2000 Hz octaves. In the diffuse sound field, i.e., when averaging all possible directions of sound incidence, a disturbance of the sound field of up to 0.04 dB at 1 kHz is possible.

The presented approach comes with known shortcomings. First, the calculated model represents a possibly significant simplification of the measurement array's actual geometry. The supposed plane wave sound incidence is also a simplification compared to the curved first wave front shown in Figure 5.7. Second, the worst case scenario considered is likely to overestimate the disturbance since the critical sampling area is on the side away from the sound, where disturbances are considerably lower. Since this factor cannot be quantified, it cannot be included in the worst case assessment. It may be possible, however, to come back to this argument when comparing the analytical predictions with actual measurements.

Measurements

When evaluating the measurement data, potentially critical imponderables exist. These arise mainly due to the fact that, in measurements, theoretical assumptions are rarely met in their purest form, which leads to uncertainties. Prominent examples are wavefronts which should exist as dirac delta functions according to pure theory, but instead are extended wave forms due their band-limited excitation or the mechanical properties of the loudspeaker. As a further factor, wall reflections and reverberation occur in the complex sound fields of real auditoria. These partially obscure the phenomena that are of actual interest, and thus renders them invisible at some locations. Figures B.8a to B.8d are graphical representations of this problem.

Nevertheless, it was possible to identify measurement locations where the different sound events could be separated adequately to measure the disturbance caused by scattered sound. In other regions of the sampling area, the scattered wave is masked by other sound. Since abrupt discontinuities are unreasonable in the amplitude of propagating cylindrical waves, the results from regions where the "signal" and "noise" part are clearly separable can be transferred to other regions as well.

Comparison of both strategies

When comparing the theoretical prediction to the measured data, two aspects stand out: The sampling locations "in front" of scattering bodies were identified as particularly susceptible to interference by scattered sound, both in calculations and in measurements. At the same time, however, the amplitudes of the calculated and actually measured scattering are quite different. While uncertainty in a worst case scenario was determined to be 0.74 dB in the theoretical case, (this corresponds to an SNR level of about -7.3 dB) the comparison to the measured data suggests a much lower SNR of -15 dB that leads to an empirical uncertainty of about 0.35 dB.

In this light, it is of course necessary to consider which perspective and which result should be prioritized. The theoretical approach may represent a pathological worst case that is based on strong simplifications. On the other hand, individual factors may have been uncontrolled in the empirical approach, which could imply not having considered a particularly critical case.

Since the empirically investigated case is quite similar to the other measurement series carried out in different auditoria, there is good reason to assume that the selected *Eurogress* case is representative for the other 25 series. Against this hypothesis, it is not obvious why the simplified numerical solution could yield more robust predictions of the scattered sound. It is therefore determined that the analyzed measurement represents a relevant reference scenario, and that the theoretical discussion serves as a foundation that shows the overall scenario and identifies critical regions that need to be investigated empirically using special care.

Diffuse sound field

The previous discussion makes it clear that the measurements and the available analysis tools cannot provide evidence for the disturbance of the diffuse reverberation. Nevertheless, the calculations show that the impairment of the late reverberation due to scattering from the measurement device is much less than the scattering's detrimental effect to the early reflections. Thus, the uncertainty

due to scattering from the measurement device interfering with reverberation would take one of the lower positions in the uncertainty budget in Table A.9. With this in mind, such influence factors would not provide relevant contributions to the combined uncertainty. In this context, the estimated measurement uncertainty of 0.35 dB may even appear as an exaggeration of the actually encountered measurement uncertainty.

B.5 Conclusions

- Based on the detailed investigation of a measurement series, the influence of the measurement setup on the measurand was determined to be

$$u(b_{\mathrm{Setup}}) = 0.35\,\mathrm{dB}. \tag{B.5.1}$$

- The uncertainty contribution due to the measurement setup's disturbance of the sound field increases the combined uncertainty from 0.62 dB (from Table A.9, based on Equation A.3.1) to

$$u_{\mathrm{c}}(b_{\mathrm{Equip}}) = 0.71\,\mathrm{dB}. \tag{B.5.2}$$

C

Uncertainty propagation for room acoustical quantities

In this appendix, the analytical discussion of uncertainty propagation is presented in more detailed than would be appropriate in the main body of this study. The equations listed here make it possible to trace how the uncertainties of room acoustical quantities arise. In the bigger picture of this studies overall rationale, it is mainly this appendix's final result that is relevant.

C.1 Energy decay curve

The energy decay curve is the starting point for many room acoustical quantities. Its discrete notation, the backward integrated impulse response is given in Equation 6.2.4:

$$E(s_j) = 10 \log_{10} \left(1 - \frac{\sum_{k=1}^{j} p^2(s_k)}{\sum_{k=1}^{\infty} p^2(s_k)} \right). \tag{C.1.1}$$

For relatively complex functions, through which the uncertainties are propagated according to Equation 2.3.2, there is a risk that the results become convoluted when the entire measurement function is derived with respect to all variables at the same time. For this reason, it makes sense to perform the uncertainty propagation step-by-step, in a top-down approach. The main function in Equation C.1.1 is the logarithm, and so the uncertainty of the energy decay curve can be represented in the first step as

$$u^2\big(E(s_j)\big) = \left(\frac{\partial E(s_j)}{\partial p(s_j)}\right)^2 u^2\left(p(s_j)\right)$$
$$= \left(\frac{10}{\log_e(10)} \frac{\sum_{k=1}^{\infty} p^2(s_k)}{\sum_{k=j+1}^{\infty} p^2(s_k)}\right)^2 u^2 \left(1 - \frac{\sum_{k=1}^{j} p^2(s_k)}{\sum_{k=1}^{\infty} p^2(s_k)}\right). \qquad \text{(C.1.2)}$$

The next step is to investigate how the ratio of sums contributes to the propagation of uncertainty. This step of the discussion should not be taken lightly. If the focus is solely limited to the ratio of the two sums, there is the risk of missing that many of the individual samples of the impulse response appear in the denominator and, depending on j, in the numerator as well. This is why the combined uncertainty of the fraction is a sum of two parts with different partial derivatives.

$$u^2 \left(\frac{\sum_{k=1}^{j} p^2(s_k)}{\sum_{k=1}^{\infty} p^2(s_k)}\right) = \sum_{k=1}^{\infty} \left(\frac{\partial}{\partial p^2(s_k)} \frac{\sum_{k=1}^{j} p^2(s_k)}{\sum_{k=1}^{\infty} p^2(s_k)}\right)^2 u^2\left(p^2(s_k)\right)$$
$$= \sum_{k=1}^{j} \left(-\frac{\sum_{l=j+1}^{\infty} p^2(s_l)}{\left(\sum_{l=1}^{\infty} p^2(s_l)\right)^2}\right)^2 u^2\left(p^2(s_k)\right) +$$
$$+ \sum_{k=j+1}^{\infty} \left(\frac{\sum_{l=1}^{j} p^2(s_l)}{\left(\sum_{l=1}^{\infty} p^2(s_l)\right)^2}\right)^2 u^2\left(p^2(s_k)\right) \qquad \text{(C.1.3)}$$

Since the running variable of the outer sums, k, is not part of the squared derivatives, the terms in brackets can be factored out.

$$u^2\left(\frac{\sum_{k=1}^{j} p^2(s_k)}{\sum_{k=1}^{\infty} p^2(s_k)}\right) = \left(\frac{\sum_{l=j+1}^{\infty} p^2(s_l)}{\left(\sum_{l=1}^{\infty} p^2(s_l)\right)^2}\right)^2 \sum_{k=1}^{j} u^2\left(p^2(s_k)\right) + \\ + \left(\frac{\sum_{l=1}^{j} p^2(s_l)}{\left(\sum_{l=1}^{\infty} p^2(s_l)\right)^2}\right)^2 \sum_{k=j+1}^{\infty} u^2\left(p^2(s_k)\right) \qquad \text{(C.1.4)}$$

The uncertainty of the individual samples of the impulse response can be stated based on Equation 6.2.5 following the same principles (Equation 2.3.2):

$$\begin{aligned} u^2\left(p^2(s_k)\right) &= \left(\frac{\partial p^2(s_k)}{\partial b_\mathrm{r}}\right)^2 u^2\left(b_\mathrm{r}\right) \\ &= \left(\frac{\log_\mathrm{e}(10)}{5} p_x^2(s_k) \underbrace{10^{0.2 b_\mathrm{r}}}_{=1}\right)^2 u^2\left(b_\mathrm{r}\right) \\ &= \left(\frac{\log_\mathrm{e}(10)}{5}\right)^2 p_x^4(s_k) u^2\left(b_\mathrm{r}\right). \end{aligned} \qquad \text{(C.1.5)}$$

The terms in Equations C.1.2 to C.1.5 can be combined into a single expression:

$$u^2\left(E(s_j)\right) = 4\left(\frac{1}{\sum_{k=j+1}^{\infty} p^2(s_k) \times \sum_{k=1}^{\infty} p^2(s_k)}\right)^2 \times \\ \times \left[\left(\sum_{k=j+1}^{\infty} p^2(s_k)\right)^2 \sum_{k=1}^{j} p_x^4(s_k) + \left(\sum_{k=1}^{j} p^2(s_k)\right)^2 \sum_{k=j+1}^{\infty} p_x^4(s_k)\right] \times \\ \times u^2\left(b_\mathrm{r}\right). \qquad \text{(C.1.6)}$$

C.2 Reverberation times

The energy decay curve is approximated by a linear regression (Bronstein et al., 2015, 16.3.4.2), and the reverberation time is reciprocal to the regression's slope m:

$$T_{\mathrm{RT}} = \frac{60}{m} \tag{C.2.1}$$

with

$$m = \frac{\sum_{j=1}^{n} (s_j - \overline{s})(E(s_j) - \overline{E})}{\sum_{j=1}^{n} (s_j - \overline{s})^2} = \frac{\sum_{j=1}^{n} \mu_1 \mu_2}{\sum_{j=1}^{n} \mu_1^2}. \tag{C.2.2}$$

Linear regression is a common analysis tool in research and technology. The uncertainty discussion of both regression parameters is considered an introductory problem in metrology (Wiese and Wöger (1999)[Ch. 5], Squires (2001)[App. C]). But, however trivial regression may allegedly be, there are a multitude of sophisticated strategies each addressing the specifics of the individual perspective on the problem. Squires (2001), for example, assumes that the uncertainties of the amplitudes are independent of the expected value, and takes advantage of algebraic simplifications which lead to a very compact notation for the regression uncertainty. Looking beyond the classical Gaussian least-square method, maximum-likelihood-(bootstrap) approaches or numerical Monte Carlo simulations are available to recognize additional available knowledge. Relatedly, there are recent efforts to extend the GUM framework to include Bayesian inference methods (Elster et al., 2015) to overcome some of the disadvantages of the classic least-squares method. These problems include (a) indefinite equation systems when the number of observations are smaller than the number of regression parameters, (b) uncertainties that are not to be treated only in first-order approximations or (c) input variables that are not normally distributed and cause some basic assumptions to no longer be met (Wiese & Wöger, 1999, Ch. 6.5.1).

Since these disadvantages are not significant relative to the reasonably pursuable depth of discussion (i.e., the number of samples is significantly larger than the number of regression parameters and the input uncertainties are available only as first-order estimates and, hence, normal), the procedure of least-square linear regression can be discussed with the basic GUM tools. Once further knowledge about the input quantities' distribution becomes available, it may make sense to revise the uncertainty models and investigate how more complex approaches benefit the uncertainty discussion. Since the uncertainty of the energy decay curve is not constant during the decay process, the previously discussed simplification of Squires (2001) cannot be adopted without modification.

On these grounds, it is appropriate to refer to Equation 2.3.2 and discuss the uncertainty of the slope m in Equation C.2.2. To make the discussion easier to

follow, the uncertainties of the individual factors $\mu_{1,j}$ and $\mu_{2,j}$ for the j^{th} element of the sum are determined first:

$$u^2\left(\mu_{1,j}\right) = \left(\frac{\partial \mu_1}{\partial s_j}\right)^2 u^2\left(s_j\right) = \left(1 - \frac{1}{n}\right)^2 u^2\left(s_j\right) \tag{C.2.3}$$

and likewise

$$u^2\left(\mu_{2,j}\right) = \left(1 - \frac{1}{n}\right)^2 u^2\left(E(s_j)\right). \tag{C.2.4}$$

According to Equation C.2.2, the slope m depends on the variables $\mu_{1,j}$ and $\mu_{2,j}$, which leads to:

$$u^2\left(m\right) = \sum_{j=1}^{n}\left(\frac{\partial m}{\partial \mu_{1,j}}\right)^2 u^2\left(\mu_{1,j}\right) + \sum_{j=1}^{n}\left(\frac{\partial m}{\partial \mu_{2,j}}\right)^2 u^2\left(\mu_{2,j}\right) \tag{C.2.5}$$

In cases where clock jitter plays a role, the first part of the sum can be developed further. It was shown in Section 4 that the sampling time's uncertainty $u\left(s_j\right)$ is in the order of a few nanosenconds, which is small compared to the analysis periods (of EDT). As a result, the uncertainty contribution related to $u\left(\mu_{1,j}\right)$ can be neglected (Carroll et al., 2006, Ch. 3).

The partial derivative of m with respect to $\mu_{2,j}$ yields

$$\frac{\partial m}{\partial \mu_{2,j}} = \frac{\mu_{1,j}}{\sum\limits_{k=1}^{n} \mu_{1,k}^2}, \tag{C.2.6}$$

and thus the variance

$$\begin{aligned} u^2\left(m\right) &= \sum_{j=1}^{n}\left(\frac{\mu_{1,j}}{\sum\limits_{k=1}^{n} \mu_{1,k}^2}\right)^2 u^2\left(\mu_{2,j}\right) \\ &= \sum_{j=1}^{n}\left(\frac{s_j - \overline{s}}{\sum\limits_{k=1}^{n}\left(s_k - \overline{s}\right)^2}\frac{n-1}{n}\right)^2 u^2\left(E(s_j)\right). \end{aligned} \tag{C.2.7}$$

As a final result, the uncertainty of the reverberation time can be given through

$$u^2(T_{\mathrm{RT}}) = \left(-\frac{60}{m^2}\right)^2 u^2(m). \tag{C.2.8}$$

Recognizing the previous results from Equations C.2.1, C.2.2 and C.2.7 yields:

$$\begin{aligned} u^2(T_{\mathrm{RT}}) &= \sum_{j=1}^{n} \left(T_{\mathrm{RT}} \frac{\sum\limits_{k=1}^{n} (s_k - \overline{s})^2}{\sum\limits_{k=1}^{n} (s_k - \overline{s})(E(s_k) - \overline{E})} \frac{s_j - \overline{s}}{\sum\limits_{k=1}^{n} (s_k - \overline{s})^2} \frac{n-1}{n} \right)^2 u^2\left(E(s_j)\right) \\ &= \sum_{j=1}^{n} \left(\frac{T_{\mathrm{RT}} \left(s_j - \overline{s}\right)}{\sum\limits_{k=1}^{n} (s_k - \overline{s})(E(s_k) - \overline{E})} \frac{n-1}{n} \right)^2 u^2\left(E(s_j)\right) \\ &= \left(\frac{n-1}{n} \frac{T_{\mathrm{RT}}}{\sum\limits_{k=1}^{n} (s_k - \overline{s})^2} \right)^2 \sum_{j=1}^{n} \left(s_j - \overline{s}\right)^2 u^2\left(E(s_j)\right). \end{aligned} \tag{C.2.9}$$

The sampling times s_j in the denominator's sum are multiples of the reciprocal sampling rate n_{SR}. This common term can be factored out with a negligible error ($< 1/2n_{\mathrm{SR}}$) for $\overline{s}$. The remaining elements of the sum represent a discrete quadratic function symmetrical to $n/2$ which is the equivalent to a finite geometric sum. Based on Bernoulli or Faulhaber (Bronstein et al., 2015, Ch. 1.2.4), this sum can be replaced and further simplified by substituting $n/2 = l$:

$$\sum_{j=1}^{n} (s_j - \overline{s})^2 \approx \frac{1}{n_{\mathrm{SR}}^2} \sum_{j=1}^{n} \left(j - \frac{n}{2}\right)^2 = \frac{2}{n_{\mathrm{SR}}^2} \sum_{j=1}^{l} j^2 = \frac{2}{n_{\mathrm{SR}}^2} \frac{l(l+1)(2l+1)}{6}. \tag{C.2.10}$$

With n being the number of samples that fit into the reverberation time's evaluation period, l can be expressed as a function of the evaluated dynamic range ΔL:

$$l = \frac{n}{2} = \frac{1}{2} T_{\mathrm{RT}} \frac{\Delta L}{60} n_{\mathrm{SR}}. \tag{C.2.11}$$

This leads to a revised expression for the reverberation time's uncertainty:

$$u^2(T_{\mathrm{RT}}) = T_{\mathrm{RT}}^2 \left(\frac{2l-1}{2l} \frac{3n_{\mathrm{SR}}^2}{l(l+1)(2l+1)} \right)^2 \frac{1}{n_{\mathrm{SR}}^2} \sum_{j=1}^{2l} (j-l)^2 \, u^2 \left(E(s_j) \right)$$

$$= \left(\frac{2l-1}{2l} \frac{360}{\Delta L(l+1)(2l+1)} \right)^2 \sum_{j=1}^{2l} (j-l)^2 \, u^2 \left(E(s_j) \right). \qquad \text{(C.2.12)}$$

C.3 Clarity

The starting point for the uncertainty discussion of the clarity metric is its definition in Equation 6.2.9.

$$C_{t_{\mathrm{e}}} = 10 \log_{10} \frac{\int_0^{t_{\mathrm{e}}} p^2(t) \mathrm{d}t}{\int_{t_{\mathrm{e}}}^{\infty} p^2(t) \mathrm{d}t} \widehat{=} 10 \log_{10} \frac{\sum_{j=1}^{n_{\mathrm{e}}} p^2(s_j)}{\sum_{j=n_{\mathrm{e}}}^{\infty} p^2(s_j)} = 10 \log_{10} \frac{\sum_{j=1}^{n_{\mathrm{e}}} p^2(s_j)}{\sum_{j=n_{\mathrm{e}}}^{n_{\mathrm{cp}}} p^2(s_j) + E_{\mathrm{comp}}} \qquad \text{(C.3.1)}$$

$$= 10 \log_{10} \frac{E_{\mathrm{early}}}{E_{\mathrm{late}} + E_{\mathrm{comp}}}$$

The sound pressures in the time-discrete notation $p(s_j)$ contain, as before, the correction factors for random and systematic effects. As β_{s} can be separated from both sums and canceled from the fraction entirely, systematic effects will not have an influence on the clarity metric's uncertainty.

Determining the "late" energy and its uncertainty in the denominator's sum poses some practical difficulties, since measured impulse responses fall below the noise floor after some point in time, meaning all subsequent samples have an infinitely large uncertainty. Lundeby et al. (1995) suggested a solution through an algorithm which determines the energy of the noise floor and replaces it with a compensation term that represents the energy of the "hidden" decay. To recognize this approach, the definition of the clarity metric can be modified by introducing two new variables to Equation C.3.1, namely the time sample corresponding to the cross point n_{cp}, where the decaying impulse response falls beneath the noise floor, and the compensation energy E_{comp}. Both variables are uncertain as well, and thus have an influence on $u\left(C_{t_{\mathrm{e}}}\right)$.

Following a top-down approach entails investigating how the uncertainties propagate through Equation 6.2.9 according to Equation 2.3.2.

$$
\begin{aligned}
u^2\left(C_{t_\mathrm{e}}\right) &= \left(\frac{\partial C_{t_\mathrm{e}}}{\partial E_\mathrm{early}}\right)^2 u^2\left(E_\mathrm{early}\right) + \left(\frac{\partial C_{t_\mathrm{e}}}{\partial E_\mathrm{late}}\right)^2 u^2\left(E_\mathrm{late}\right) + \left(\frac{\partial C_{t_\mathrm{e}}}{\partial E_\mathrm{comp}}\right)^2 u^2\left(E_\mathrm{comp}\right) \\
&= \left(\frac{10}{\log_e(10)}\frac{E_\mathrm{late}+E_\mathrm{comp}}{E_\mathrm{early}}\right)^2 \frac{1}{\left(E_\mathrm{late}+E_\mathrm{comp}\right)^2}\times \\
&\quad \times\left(u^2\left(E_\mathrm{early}\right) + \left(\frac{E_\mathrm{early}}{E_\mathrm{late}+E_\mathrm{comp}}\right)^2\left(u^2\left(E_\mathrm{late}\right)+u^2\left(E_\mathrm{comp}\right)\right)\right)
\end{aligned}
\tag{C.3.2}
$$

In view of Equation C.3.2, it becomes evident that the mathematical representations of uncertainties tend to become increasingly complex as the discussion advances. It is therefore reasonable to establish the uncertainties of the individual energy components separately. The uncertainty of a sum results from the sum of the partial derivatives with respect to each summand, and thus the uncertainty of the energy in the early part of the impulse response is given through

$$
u^2\left(E_\mathrm{early}\right) = \left(\frac{\log_\mathrm{e}(10)}{5}\right)^2 \sum_{j=1}^{n_\mathrm{e}} p_x^4(s_j) u^2(b_\mathrm{r}). \tag{C.3.3}
$$

The same holds for the Energy in the late part of the impulse response

$$
u^2\left(E_\mathrm{late}\right) = \left(\frac{\log_\mathrm{e}(10)}{5}\right)^2 \sum_{j=n_\mathrm{e}}^{n_\mathrm{cp}} p_x^4(s_j) u^2(b_\mathrm{r}). \tag{C.3.4}
$$

Next, the focus will be on the uncertainty discussion of E_comp. The original description of Lundeby et al. (1995) discusses an iterative approach and a regression based on a stepwise averaged impulse response. For the sake of simplicity, it is assumed that the iterative optimization has already been completed, and therefore a good estimate for the crosspoint n_cp is available. In addition, the stepwise averaging is not applied, and instead the regression line is determined directly from the logarithmic impulse response without influence on the uncertainty.

First, the noise floor, i.e., the root-mean-square noise level, needs to be determined, with

$$
L_\mathrm{noise} = 10\log_{10}\tilde{p}^2_\mathrm{noise} \tag{C.3.5}
$$

and

$$u^2\left(L_{\text{noise}}\right) = \left(\frac{20}{\log_e(10)}\right)^2 \frac{u^2\left(p_{\text{noise}}\right)}{\sum_{j=n_{\text{cp}}}^{n_{\text{end}}} p^2_{\text{noise}}(s_j)}. \tag{C.3.6}$$

The cross point corresponds to the time from which the regression line, with the slope m and the y-axis section a, falls below the noise level L_{noise}:

$$t_{\text{cp}} = \frac{L_{\text{noise}} - a}{m} \tag{C.3.7}$$

and the associated uncertainty

$$u^2(t_{\text{cp}}) = \frac{1}{m^2}(u^2(L_{\text{noise}}) + u^2(a)) + \left(\frac{L_{\text{noise}} - a}{m^2}\right)^2 u^2(m) \tag{C.3.8}$$

The uncertainties of the slope $u(m)$ and the noise level $u(L_{\text{noise}})$ are already available through Equations C.2.2 and C.3.6. The y-axis section a and its uncertainty can be determined on the same grounds (Bronstein et al., 2015, 16.3.4.2):

$$a = \bar{L}_p - m\bar{s} \tag{C.3.9}$$

with the associated uncertainty

$$u^2(a) = u^2(\bar{L}_p) + \bar{s}^2 u^2(m) + m^2 u^2(\bar{s}). \tag{C.3.10}$$

The last term of this sum can be neglected as long as the assumption that the clock jitter is insignificant holds. To calculate the average energy level, the raw impulse response is evaluated, in which systematic effects continue to play a role.

$$\begin{aligned} u^2(a) &\approx \frac{1}{n_{\text{cp}}^2} \sum_{i=1}^{n_{\text{cp}}} u^2\left(L_p\right) + \bar{s}^2 u^2(m) \\ &= \frac{4}{n_{\text{cp}}} \left(u^2(b_{\text{r}}) + u^2(b_{\text{s}})\right) + \bar{s}^2 u^2(m). \end{aligned} \tag{C.3.11}$$

The determined slope m and the y-axis section a are exactly the parameters that characterize the supposed exponential decay that is then used to calculate the compensation term E_{comp}:

$$E_{\text{comp}} = \int_{t_{\text{cp}}}^{\infty} 10^{0.1a} \mathrm{e}^{\frac{\ln(10)}{10} mt} \mathrm{d}t = -\frac{10}{\ln(10)} \frac{10^{0.1a}}{m} \mathrm{e}^{\frac{\ln(10)}{10} mt_{\text{cp}}} \tag{C.3.12}$$

with the associated uncertainty

$$u^2(E_{\text{comp}}) = \left(\frac{10}{\ln(10)} 10^{0.1a} \mathrm{e}^{\frac{10}{\ln(10)} m t_{\text{cp}}}\right)^2 \times \\ \times \left(\frac{u^2(a)}{4m^2} + \left(\frac{m t_{\text{cp}} - \frac{\ln(10)}{10}}{m^2}\right)^2 u^2(m) + u^2(t_{\text{cp}})\right)$$

During the analysis of measured impulse responses, it turned out that the transition time t_{cp} is determined exactly by the Lundeby algorithm down to the sample, so that this uncertainty contribution can be neglected. This leads to the following uncertainty of the compensation energy.

$$E_{\text{comp}} = \left(\frac{10}{\ln(10)} 10^{0.1a} \mathrm{e}^{\frac{10}{\ln(10)} m t_{\text{cp}}}\right)^2 \left(\frac{u^2(a)}{4m^2} + \left(\frac{t_{\text{cp}}}{m} - \frac{\ln(10)}{10m^2}\right)^2 u^2(m)\right) \tag{C.3.13}$$

The uncertainties of the energy fractions in Equations C.3.3, C.3.4 and C.3.13 can be introduced into the uncertainty of Equation C.3.2 to determine the global uncertainty of the clarity parameter. Since the fully spelled out equation is somewhat convoluted and bulky, it will not be explicitly shown here.

Bisher erschienene Bände der Reihe

Aachener Beiträge zur Akustik

ISSN 1866-3052
ISSN 2512-6008 (seit Band 28)

1	Malte Kob	Physical Modeling of the Singing Voice ISBN 978-3-89722-997-6 40.50 EUR
2	Martin Klemenz	Die Geräuschqualität bei der Anfahrt elektrischer Schienenfahrzeuge ISBN 978-3-8325-0852-4 40.50 EUR
3	Rainer Thaden	Auralisation in Building Acoustics ISBN 978-3-8325-0895-1 40.50 EUR
4	Michael Makarski	Tools for the Professional Development of Horn Loudspeakers ISBN 978-3-8325-1280-4 40.50 EUR
5	Janina Fels	From Children to Adults: How Binaural Cues and Ear Canal Impedances Grow ISBN 978-3-8325-1855-4 40.50 EUR
6	Tobias Lentz	Binaural Technology for Virtual Reality ISBN 978-3-8325-1935-3 40.50 EUR
7	Christoph Kling	Investigations into damping in building acoustics by use of downscaled models ISBN 978-3-8325-1985-8 37.00 EUR
8	Joao Henrique Diniz Guimaraes	Modelling the dynamic interactions of rolling bearings ISBN 978-3-8325-2010-6 36.50 EUR
9	Andreas Franck	Finite-Elemente-Methoden, Lösungsalgorithmen und Werkzeuge für die akustische Simulationstechnik ISBN 978-3-8325-2313-8 35.50 EUR

10	Sebastian Fingerhuth	Tonalness and consonance of technical sounds ISBN 978-3-8325-2536-1 42.00 EUR
11	Dirk Schröder	Physically Based Real-Time Auralization of Interactive Virtual Environments ISBN 978-3-8325-2458-6 35.00 EUR
12	Marc Aretz	Combined Wave And Ray Based Room Acoustic Simulations Of Small Rooms ISBN 978-3-8325-3242-0 37.00 EUR
13	Bruno Sanches Masiero	Individualized Binaural Technology. Measurement, Equalization and Subjective Evaluation ISBN 978-3-8325-3274-1 36.50 EUR
14	Roman Scharrer	Acoustic Field Analysis in Small Microphone Arrays ISBN 978-3-8325-3453-0 35.00 EUR
15	Matthias Lievens	Structure-borne Sound Sources in Buildings ISBN 978-3-8325-3464-6 33.00 EUR
16	Pascal Dietrich	Uncertainties in Acoustical Transfer Functions. Modeling, Measurement and Derivation of Parameters for Airborne and Structure-borne Sound ISBN 978-3-8325-3551-3 37.00 EUR
17	Elena Shabalina	The Propagation of Low Frequency Sound through an Audience ISBN 978-3-8325-3608-4 37.50 EUR
18	Xun Wang	Model Based Signal Enhancement for Impulse Response Measurement ISBN 978-3-8325-3630-5 34.50 EUR
19	Stefan Feistel	Modeling the Radiation of Modern Sound Reinforcement Systems in High Resolution ISBN 978-3-8325-3710-4 37.00 EUR
20	Frank Wefers	Partitioned convolution algorithms for real-time auralization ISBN 978-3-8325-3943-6 44.50 EUR

21	Renzo Vitale	Perceptual Aspects Of Sound Scattering In Concert Halls ISBN 978-3-8325-3992-4 34.50 EUR
22	Martin Pollow	Directivity Patterns for Room Acoustical Measurements and Simulations ISBN 978-3-8325-4090-6 41.00 EUR
23	Markus Müller-Trapet	Measurement of Surface Reflection Properties. Concepts and Uncertainties ISBN 978-3-8325-4120-0 41.00 EUR
24	Martin Guski	Influences of external error sources on measurements of room acoustic parameters ISBN 978-3-8325-4146-0 46.00 EUR
25	Clemens Nau	Beamforming in modalen Schallfeldern von Fahrzeuginnenräumen ISBN 978-3-8325-4370-9 47.50 EUR
26	Samira Mohamady	Uncertainties of Transfer Path Analysis and Sound Design for Electrical Drives ISBN 978-3-8325-4431-7 45.00 EUR
27	Bernd Philippen	Transfer path analysis based on in-situ measurements for automotive applications ISBN 978-3-8325-4435-5 50.50 EUR
28	Ramona Bomhardt	Anthropometric Individualization of Head-Related Transfer Functions Analysis and Modeling ISBN 978-3-8325-4543-7 35.00 EUR
29	Fanyu Meng	Modeling of Moving Sound Sources Based on Array Measurements ISBN 978-3-8325-4759-2 44.00 EUR
30	Jan-Gerrit Richter	Fast Measurement of Individual Head-Related Transfer Functions ISBN 978-3-8325-4906-0 45.50 EUR
31	Rhoddy A. Viveros Muñoz	Speech perception in complex acoustic environments: Evaluating moving maskers using virtual acoustics ISBN 978-3-8325-4963-3 35.50 EUR
32	Spyros Brezas	Investigation on the dissemination of unit watt in airborne sound and applications ISBN 978-3-8325-4971-8 47.50 EUR

33	Josefa Oberem	Examining auditory selective attention: From dichotic towards realistic environments ISBN 978-3-8325-5101-8 43.00 EUR
34	Johannes Klein	Directional Room Impulse Response Measurement ISBN 978-3-8325-5139-1 41.00 EUR
35	Lukas Aspöck	Validation of room acoustic simulation models ISBN 978-3-8325-5204-6 57.00 EUR
36	Florian Pausch	Spatial audio reproduction for hearing aid research: System design, evaluation and application ISBN 978-3-8325-5461-3 49.50 EUR
37	Ingo Witew	Measurements in room acoustics. Uncertainties and influence of the measurement position ISBN 978-3-8325-5529-0 63.00 EUR

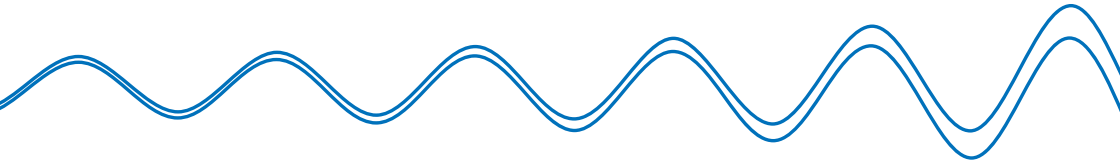

Regardless of the field, measurements are essential for validating theories and making well-founded decisions. A criterion for the validity and comparability of measured values is their uncertainty. Still, in room acoustical measurements, the application of established rules to interpret uncertainties in measurement is not yet widespread. This raises the question of the validity and interpretability of room acoustical measurements.

This work discusses the uncertainties in measuring room acoustical single-number quantities that complies with the framework of the "Guide to the Expression of Uncertainty in Measurement"(GUM). Starting point is a structured search of variables that potentially influence the measurement of room impulse responses. In a second step, this uncertainty is propagated through the algorithm that determines single-number quantities.

A second emphasis is placed on the investigation of spatial fluctuations of the sound field in auditoria. The spatial variance of the sound field in combination with an uncertain measurement position marks a major contribution to the overall measurement uncertainty. In extended measurement series, the relation between changes in the sensor location and the corresponding changes in measured room acoustical quantities is investigated.

This study shows how precisely a measurement position must be defined to ensure a given uncertainty of room acoustical quantities. The presented methods form a foundation that can be easily extended in future investigations to include additional influences on the measurement uncertainty.

λογος

ISSN 2512-6008
ISBN 978-3-8325-5529-0

Logos Verlag Berlin